1974

A second-order method of characteristics for two-dimensional unsteady flow with application to turbomachinery cascades

Robert Anthony Delaney
Iowa State University

A second-order method of characteristics for two-dimensional unsteady flow with application to turbomachinery cascades

by

Robert Anthony Delaney

A Dissertation Submitted to the
Graduate Faculty in Partial Fulfillment of
The Requirements for the Degree of
DOCTOR OF PHILOSOPHY

Departments: Mechanical Engineering
Engineering Science and Mechanics
Co-majors: Mechanical Engineering
Engineering Mechanics

Approved:

Signature was redacted for privacy.

In Charge of Major Work

Signature was redacted for privacy.

For the Major Departments

Signature was redacted for privacy.

For the Graduate College

Iowa State University
Ames, Iowa
1974

TABLE OF CONTENTS

LIST OF FIGURES

LIST OF TABLES

NOTATIONS

A	amplification matrix; matrix of polynomial coefficients in system of equations for least squares polynomial coefficients
A_{ij}	elements of amplification matrix A; coefficients of quadratic terms in equation of a cone
A^*_{ij}	cofactors of A_{ij}
A^{-1}_{ij}	coefficients of quadratic terms in equation of a reciprocal cone
A_ν	coefficients of derivatives in L_i direction in general form of wave surface compatibility relation ($\nu = 1,2,\ldots,n$) (see Eq. 11.19)
a	acoustic speed
a'	normalized acoustic speed, $(\gamma p'/\rho')^{\frac{1}{2}}$
$a_{\mu\nu}$	least squares polynomial coefficients ($\mu = 1,2,\ldots, 6$; $\nu = 1,2,\ldots,4$)
$a_{\mu\nu i}$	derivative coefficients in a general system of first-order partial differential equations ($\mu,\nu = 1,2,\ldots,n$; $i = 1,2,3$)
B	term in general form of wave surface compatibility relation (see Eq. 11.19)
$B_1,\ldots,B_4$	coefficients in system of difference equations for pressure and velocity components at solution point (see Eq. 3.29)
b_μ	nonhomogeneous terms in a general system of first-order partial differential equations
C	Courant number; blade chord
C_x	axial chord
C_ν	coefficients of derivatives in M_i direction in general form of wave surface compatibility relation ($\nu = 1,2,\ldots,n$) (see Eq. 11.19)

$C_1,\ldots,C_4$	coefficients in system of difference equations for pressure and velocity components at solution point (see Eq. 3.29)
$F_1,\ldots,F_4$	nonhomogeneous terms in system of difference equations for pressure and velocity components at solution point (see Eq. 3.29)
I	identity matrix; frequency index (defined in Eqs. 13.45 and 13.91)
L	characteristic length; duct length
L_i	tangent vector to a bicharacteristic
M	Mach number
M_i	vector in a characteristic wave surface transverse to bicharacteristic direction L_i
m_i	unit vector tangent to the intersection of a characteristic wave surface and the physical plane
m	frequency index (see Eq. 13.20)
N	magnitude of N_i
N_i	characteristic surface normal vector
n_i	unit normal vector
n	order of system of partial differential equations; frequency index (see Eq. 13.20)
P	function of t in Fourier series solution for $\tilde{p}$ (see Eq. 13.20)
p	static pressure
p'	normalized static pressure, p/p_{01}
p_0	stagnation pressure
q	magnitude of velocity vector
r	radius
r_{min}	minimum distance to convex hull of difference scheme
S	coefficient matrix in system of equations for least squares polynomial coefficients; blade spacing

S_i	vector tangent to particle path
S_ν	sum of squares of differences between u_ν^i and $u_\nu^{i'}$ ($\nu = 1,2,3,4$; $i = 1,2,\ldots,9$)
s	specific entropy
s_i	vector tangent to intersection of the physical plane and a characteristic flow surface
T	static temperature
T'	normalized static temperature, T/T_{01}
$\bar{T}$	vector with components U_1, U_2, P
T_0	stagnation temperature
T_ν	components of $\bar{T}$ ($\nu = 1,2,3$)
t	time
U	matrix in system of equations for least squares polynomial coefficients
U_1	function of t in Fourier series solution for $\tilde{u}_1$ (see Eq. 13.20)
U_2	function of t in Fourier series solution for $\tilde{u}_2$ (see Eq. 13.20)
U_i	vector with physical component u_i and tangent to particle path
$\bar{U}$	vector with components $\tilde{u}_1$, $\tilde{u}_2$, $\tilde{p}$
u	x coordinate velocity component
u_i	velocity vector ($i = 1,2$)
u_ν	dependent variables in a general system of first order partial differential equations ($\nu = 1,2,\ldots,n$); dependent variables in least squares interpolating polynomial ($\nu = 1,2,3,4$)
u_ν^i	cell point data u_ν in least squares interpolation ($i = 1,2,\ldots,9$)

$u_\nu^{i'}$	interpolated u_ν at cell points (i = 1,2,...,9)
u_1'	normalized u_1 velocity component, $u_1/(p_{01}/\rho_{01})^{\frac{1}{2}}$
u_2'	normalized u_2 velocity component, $u_2/(p_{01}/\rho_{01})^{\frac{1}{2}}$
v	y coordinate velocity component
v_r	radial velocity
w_μ	left eigenvector (μ = 1,2,...,n) (see Eq. 10.3)
x, y	rectangular cartesian coordinates
x_i	rectangular coordinates (i = 1,2,3) corresponding to {x, y, t}
α_i, β_i	orthonormal reference vectors (i = 1,2)
γ	ratio of specific heats
$\gamma°$	blade stagger angle
δ_{ij}	kronecker delta
η	frequency parameter (see Eq. 13.57)
θ	flow angle; bicharacteristic parameter
κ_1	blade leading edge mean camber angle
κ_2	blade trailing edge mean camber angle
λ	eigenvalue
λ_i, μ_i, ν_i	reference vectors in bicharacteristic equation (see Eq. 11.2)
μ	Mach angle
ν	Prandtl-Meyer angle
ξ	frequency parameter (see Eq. 13.56)
ρ	static density; spectral radius of amplification matrix A
ρ'	normalized static density, ρ/ρ_{01}

ρ_0	stagnation density
τ	variable of integration along bicharacteristic in general numerical method
ϕ	polar angle
ϕ_i	frequency parameter (i = 1,2,3,4) (see Eqs. 13.33-13.36, 13.43, 13.44, 13.70, 13.71)
ψ	angle between reference vector α_i and x_1 axis

Subscripts

a	ambient state
L	bicharacteristic direction
U	particle path direction
0	stagnation state
1	uniform state upstream of cascade
2	uniform state downstream of cascade

Superscripts

-	average value or transformed variable
~	small perturbation

I. INTRODUCTION

A. Statement of the Problem

In recent years aircraft gas turbine engines have been reduced in size and weight by incorporating fewer, but more highly loaded compressor and turbine stages. Relative flow velocities near the tip sections of these blade rows have been pushed well into the transonic regime. In this case, blade profile design or selection becomes more critical than in conventional subsonic machines; slight variations in blade profiles can induce strong shock waves. Also, the use of highly cambered blades for increased blade loading may lead to boundary layer separation on the blade suction surface. In contrast to subsonic experience, a smooth blade profile in transonic or supersonic flow does not guarantee smooth blade-surface pressure distributions. Thus, the designer is faced with the problem of solving for the blade-to-blade flow in determining aerodynamically efficient blade designs.

The purpose of this study was to develop an accurate numerical method for solution of steady, inviscid transonic blade-to-blade flow in turbine cascades. In the particular turbine cascade cases of interest, shock losses are generally small; thus capability of the analysis method to predict strong shocks was not considered important. Also, it is generally true in transonic cascade flows that the Reynolds number is

sufficiently large so that viscous effects may be neglected, and that inviscid flow solutions will yield acceptable results.

B. Solution Methods for Flow Problems in Gas Dynamics

The equations of motion for two-dimensional steady inviscid flow are not easily solved in the transonic regime. In steady subsonic flow, the system of equations is elliptic, and the solution at a point in the flow field depends on all boundary data (jury problem). In steady supersonic flow, however, the system of equations is hyperbolic, and the flow solution depends only on upstream data (initial-value problem). Hence, a single numerical method does not exist for the solution of the flow in both the subsonic and supersonic regimes. A number of solution methods based on approximations to the physical flow model have been used for mixed-flow analysis (e.g. method of integral relations (ref. 1) and streamline curvature methods (ref. 2, 3); however, the accuracy of these methods may be questioned on the basis of the mathematical model used.

An alternate approach for solution of steady transonic flows is available if one considers the steady flow as the asymptotic limit in time of a transient flow. With the addition of time as a third independent variable in two-dimensional flow, the equations of motion become hyperbolic regardless of flow regime. The analysis problem is then an

initial-value or Cauchy problem. Due to the advent of high-speed digital computers, time-dependent techniques have received much attention in computational fluid dynamics in recent years and hold considerable promise for cascade flow analysis.

The numerical solution methods for hyperbolic systems of partial differential equations in three independent variables can be classified as; (1) finite-difference methods, and (2) characteristic methods. Finite-difference methods involve replacement of the derivatives in the system of equations by finite-differences, followed by solution of the difference equations. In characteristic methods, the original system of equations is first replaced by an equivalent system of compatibility relations written on characteristic surfaces. The system of compatibility relations is then written in finite-difference form for numerical solution.

Variations on the finite-difference methods include methods utilizing artificial viscosity (ref. 4, 5). In these methods, extra terms are added to the difference equations to simulate viscous terms in the Navier-Stokes equations. These added terms stabilize the numerical solution in regions of large property gradients and allow a direct accounting of embedded shock waves in transonic flows. A major problem encountered with finite-difference methods is incurred in devising accurate boundary point calculations at surfaces which

are not coordinate planes. At these points, extrapolations or interpolations must be used. Even if the boundaries are coordinate planes, loss of accuracy results because derivatives normal to the boundaries can only be replaced by one-sided differences.

A number of investigators have developed cascade analyses based on finite-difference methods. Gopalakrishnan and Bozzola (6, 7) have used MacCormack's scheme (8) for solution of transonic flows in turbine and compressor cascades. Unfortunately, they presented no experimental data to verify the computed results. McDonald (9) has also developed a finite-difference scheme in which numerical representations of the equations of motion in integral form are employed. This scheme, called the "finite area" method, was applied by McDonald to transonic flows in turbine cascades; good comparisons of his computed results with experimental data were obtained.

Characteristic methods are, in general, more accurate than finite-difference methods because they adhere closely to the physical flow model. In particular, the differential domain of dependence of the solution point is considered. Another advantage of characteristic methods is that accurate numerical solution procedures can be devised at flow field boundaries. A disadvantage is the complexity of the formulation and programming tasks. It is for this reason, perhaps,

that characteristic methods have not been applied to the cascade problem.

Since the objective of this study was to develop an accurate numerical method for solution of steady transonic flows in cascades, the method of characteristics was employed. Rigorous treatment of the differential domain of dependence which lies upstream of solution points in transonic flows is necessary to obtain accurate solutions. Also, the advantage in accuracy afforded by characteristic methods at boundary points is extremely important in the cascade application where a large number of complex boundary conditions exist.

Many numerical integration schemes for the method of characteristics have been proposed and used for solution of flow problems in gas dynamics involving three independent variables. These various schemes are based on different numerical integration networks formed from combinations of characteristic surfaces. Although most of these schemes have been specifically developed for two-dimensional unsteady flow or three dimensional steady supersonic flow, they apply equally well to either of these flow problems. Two infinite families of characteristic surfaces exist in either of these flow problems. One family of surfaces (flow surfaces) is tangent to the particle path or streamline and the other family of surfaces (wave surfaces) is locally tangent to the characteristic cone, which in two-dimensional unsteady flow is the

sonic cone and in three-dimensional steady supersonic flow is the Mach cone. An infinite number of combinations of characteristic surfaces may be used for numerical solution, thus explaining why the many different numerical integration networks have been proposed in various characteristic solution methods.

C. Numerical Integration Networks for the Method of Characteristics

1. General

A survey of the literature on numerical integration networks for the method of characteristics is presented in the following sections. Similar surveys have been given by Fowell (10), Chushkin (11), Sauerwein (12), Strom (13), and Ransom (14). Prior to the discussions of the various schemes, however, a few remarks regarding construction, accuracy, stability and computation time required in the different types of characteristic networks are appropriate.

The characteristic networks, as presented here, are divided into characteristic surface networks and bicharacteristic line networks. Characteristic surface networks utilize the mutual intersections of characteristic surfaces, or the intersections of characteristic surfaces with noncharacteristic reference planes. In bicharacteristic line networks, the generators of the characteristic cone are employed. In general, characteristic surface schemes are more efficient

because of the simplicity of the network. On the other hand, schemes based on bicharacteristic line networks are usually more accurate due to the more rigorous treatment of the differential domain of dependence.

Characteristic networks can be further subdivided on the basis of direct or inverse schemes. In direct schemes, the network lines are projected forward from known base points in the initial data surface to locate the solution point. In inverse schemes, the base points are located by projecting the network lines back from a predetermined solution point, and base point flow properties are then determined by interpolation. Inverse schemes allow the solution to advance in parallel planes, thus simplifying the global solution algorithm. However, direct schemes require fewer interpolations, thus increasing accuracy and decreasing computation time.

All numerical solution schemes for hyperbolic systems of partial differential equations must be examined for stability before implementation. Many criteria exist for testing stability, and an extensive discussion of these criteria is given by Richtmyer and Morton (15). All the stability criteria are based on linear difference equations. For the case of nonlinear difference equations, the approach taken is to linearize the difference equations and to apply these same criteria locally. Courant, Friedrichs, and Lewy (16) have shown that a necessary condition for stability is that the domain of dependence of the

system of differential equations must be contained within the convex hull of the differencing scheme defined as the polygon formed by connecting the outermost points used in the differencing scheme on the initial data surface. For two-dimensional unsteady flow, the differential domain of dependence is the region enclosed by the intersection of the sonic cone, whose vertex lies at the solution point, with the initial data surface. This geometric stability test, called the Courant-Friedrichs-Lewy (CFL) stability criterion, is particularly useful for preliminary evaluation of proposed networks.

In the numerical solution incorporating these schemes, finite-difference approximations of the compatibility relations are written along the network lines between base points on the initial data surface and the solution point. The minimum number of compatibility relations employed is equal to the number of dependent variables appearing in the system of equations. In first-order accuracy schemes, the coefficients in the difference equations are evaluated on the initial data surface, and the solution is determined using a single predictor step. More accurate schemes are obtained by supplementing this procedure with a corrector step wherein the coefficients in the difference equations are updated with average values between the base point and solution point. Many schemes use multiple corrector steps.

In order to develop second-order accuracy schemes, cross derivatives appearing in the wave surface compatibility relations (i.e. derivatives along a direction transverse to the network lines) must be either evaluated or eliminated at the solution point. In some characteristic surface networks, the solution point is coupled to a previously determined neighboring point in the solution plane, and the cross derivatives at the solution point are approximated by simple differences between the points. However, it does not appear that second-order accuracy is achieved with these schemes because the differential domain of dependence is not rigorously considered. In bicharacteristic line networks, the cross derivatives can only be calculated if the entire solution plane is solved and the solution repeated using derivatives calculated from the first solution. Butler (17), in his integration scheme utilizing the pentahedral bicharacteristic line network, eliminated cross derivative terms at the solution point in the system of difference equations by introducing one additional wave surface compatibility relation and a noncharacteristic relation.

There is an infinite number of bicharacteristics passing through the solution point from which to choose for construction of inverse bicharacteristic line networks. Butler (17) and Chu (18) have devised schemes which incorporate any number of the infinite family of bicharacteristics. In these schemes, the finite-difference form of the bicharacteristic compatibility

relations are integrated around the circumference of the differential domain of dependence. While the accuracy of these methods increases with the number of bicharacteristics, the computational time also increases due to extensive interpolations required at the base points to evaluate the integrals.

Practical schemes have been developed using more than the minimum number of finite-difference relations required for a determined system. This redundant solution approach has been used by Pridmore Brown and Franks (19), Powers, Niemann and Der (20), and Chu (21) where an overdetermined system of four wave surface compatibility relations was solved for three dependent variables in a least squares sense. Sauerwein (22) and Strom (13) determined multiple solutions using the minimum number of relations required for a determinant system and subsequently averaged the results.

2. Characteristic surface networks

a. Network of intersections of reference planes with characteristic surfaces The network of intersections of reference planes with characteristic surfaces, as discussed by Ferrari (23), Moeckel (24), and Sauer (25) for solution of three-dimensional supersonic flow, is a direct scheme utilizing intersections of characteristic surfaces with orthogonal coordinate planes. As shown in Figure 1.1, the solution is advanced on constant-x_1 planes. The solution point (8) lies at the intersection of two characteristic wave surfaces and the

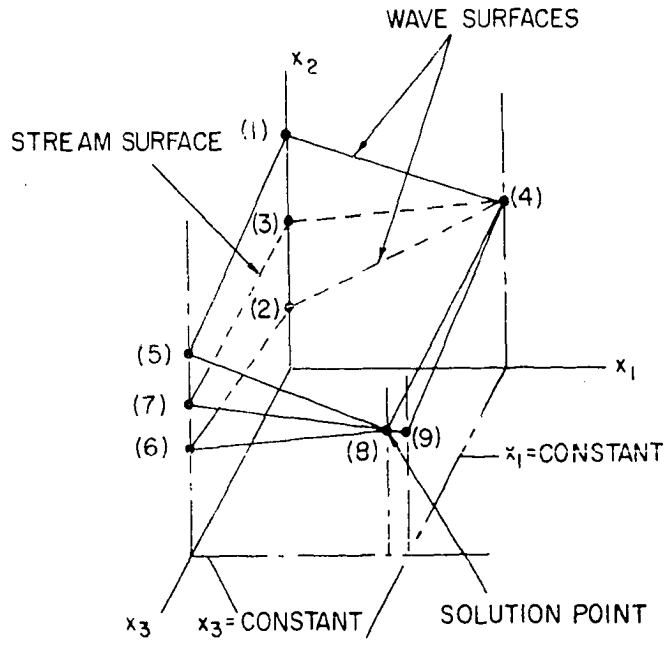

Figure 1.1. Network of intersections of reference planes with characteristic surfaces

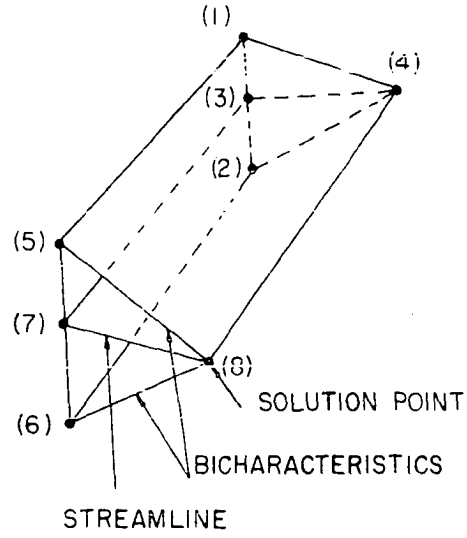

Figure 1.2. Prismatic characteristic surface network

reference plane, x_3 = constant. Initial data points (1), (2), (5), and (6) lie along the lines of intersection of the initial data plane and the planes, x_3 = constant. Point (4) is a previous solution point. The wave surface compatibility relations are written along line (5) - (8) and (6) - (8) with cross derivative terms evaluated along the wave surface intersection (4) - (8). A compatibility relation written along the streamline projection (7) - (8) is used as an additional equation for solution of nonhomentropic flows. Following the solution at point (8), the solution at point (9), lying in the plane x_1 = constant, is predicted using interpolation or extrapolation along one of the characteristic surfaces.

The major disadvantage of this network is that the CFL stability criterion is violated whenever the initial data points do not include the differential domain of dependence of the solution point. Also, the accuracy of the scheme is reduced due to interpolations required to maintain the solution on parallel planes (x_1 = constant). A further difficulty in applying this scheme is that additional end conditions on the constant-x_3 planes are required to initiate calculations on the solution plane. If planes of symmetry do not exist, an iterative procedure is required to obtain closure of the solution between end planes.

b. Prismatic characteristic surface network Holt (26) developed a network based upon the works of Coburn and Dolph (27) and Titt (28). This network was later named the prismatic characteristic surface network by Fowell (10). The network, shown in Figure 1.2, is similar to the network of intersections of reference planes with characteristic surfaces, except that the end planes are meridional planes through the characteristic cone defined by two bicharacteristics and the streamline. As pointed out by Heie and Leigh (29), this scheme violates the CFL stability criterion. This method shares the same disadvantages as the network of intersections of reference planes and characteristic surfaces regarding interpolation to maintain the solution on parallel planes, and regarding initiation and closure of the solution on end planes. Apparently, no attempts have been made to use this scheme.

c. Near characteristics network The near characteristics network, shown in Figure 1.3, is formed by the intersections of two characteristic wave surfaces and one characteristic flow surface with a single reference plane. An inverse approach is used in which the near characteristics are projected back into the initial data surface from the fixed solution point (4). Flow properties at base points (1), (2), and (3) are determined by simple univariate interpolations along the intersection of the initial data surface and the reference plane. Cross derivatives in the wave surface compatibility relations are evaluated only on the initial data surface.

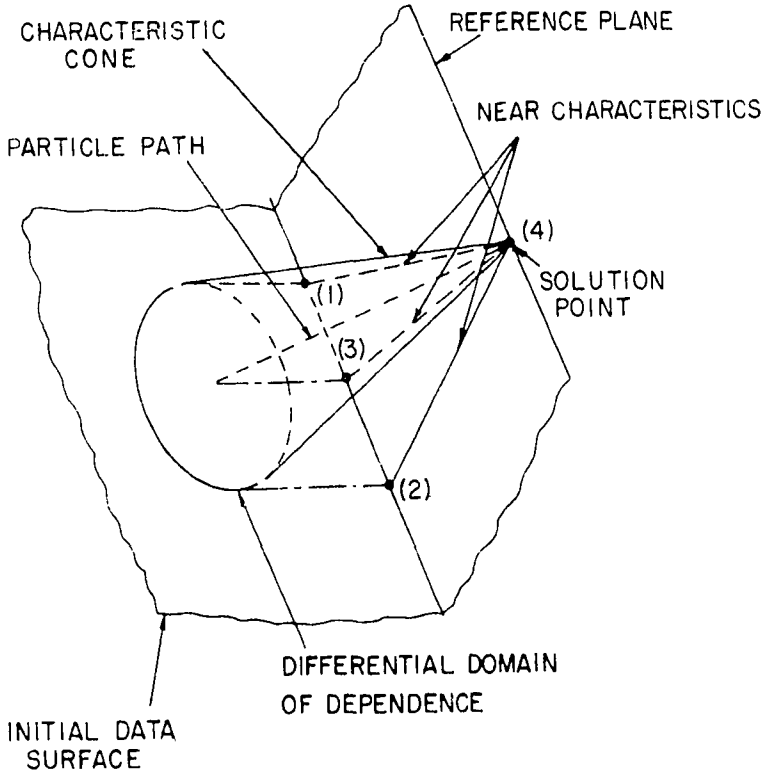

Figure 1.3. Near characteristics network

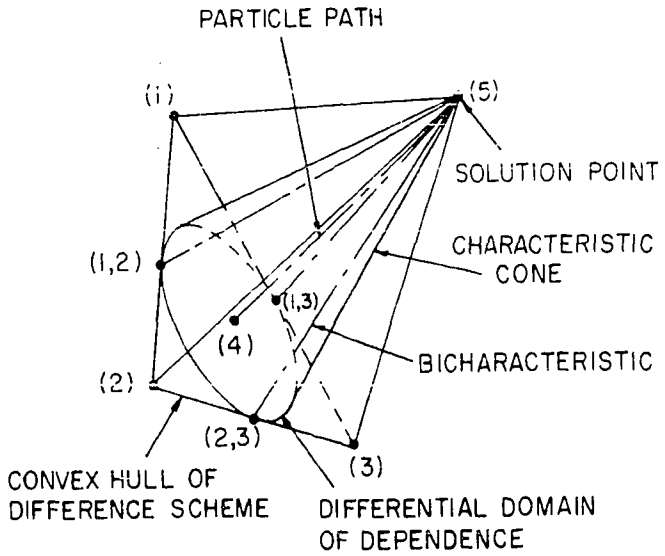

Figure 1.4. Tetrahedral characteristic surface network

Originally, the method was developed by Sauer (30) and Holt (31) for two-dimensional unsteady flows; however, it has been applied to three-dimensional supersonic flow field calculations by Moretti (32, 33), Rakich (34, 35), and Katskova and Chushkin (36). Recently, the method has been proposed and/or used at boundaries in hybrid time-dependent calculations incorporating finite-difference procedures at interior points, by Moretti and Abbett (37), D'Souza, Molder and Moretti (38), Serra (39, 40), Kentzer (41), Porter and Coakley (42), and Gopalakrishnan (43).

The main advantage of the near characteristics scheme is its simplicity. Only three near characteristics are used, and base point flow properties are determined by simple univariate interpolations. The scheme has been shown to be particularly well suited to three-dimensional steady supersonic flows about axisymmetric bodies where the reference planes are meridional planes through the body axis. However, it is not apparent that the method can be applied with equal success to the general two-dimensional unsteady flow problem where cross flow normal to reference planes can result in the base points, as shown in Figure 1.3, lying completely outside the differential domain of dependence.

d. Tetrahedral characteristic surface network The tetrahedral characteristic surface network is a direct scheme originally proposed by Thornhill (44). In this network, shown in Figure 1.4, the solution point (5) is located at the mutual

intersection of three characteristic wave surfaces through lines (1) - (2), (1) - (3), and (2) - (3), where points (1), (2), and (3) are known initial data points. Bicharacteristics (1,2) - (5), (1,3) - (5), and (2,3) - (5) are located as lines of tangency between the characteristic cone and the three characteristic planes. The particle path or streamline (4) - (5), projected from the solution point back to the initial data surface, provides a fourth characteristic line. Flow properties at base points (1,2), (1,3), and (2,3) are determined by linear interpolation along lines (1) - (2), (1) - (3), and (2) - (3), respectively. As shown in Figure 1.4, the CFL stability criterion is satisfied; hence a stable scheme is expected. Tsung (45) used this method to solve the three-dimensional steady flow past a conical boattail and a delta wing at an angle of attack. Reed (46, 47, 48) also used this method for solving three-dimensional supersonic rotational flow in nozzles.

The main disadvantage of this scheme is the large number of different interpolations required for base point data; i.e., three linear interpolations at points (1,2), (1,3), and (2,3) and bivariate interpolation at point 4. Interpolation or extrapolation is also required in the direction of integration if the solution is to be advanced on parallel planes.

3. Bicharacteristic line networks

a. Tetrahedral bicharacteristic line network Another direct scheme proposed by Thornhill (44) is the tetrahedral bicharacteristic line network shown in Figure 1.5. In this network, the solution point (5) is located at the mutual intersection of characteristic cones with vertices at the known initial data points (1), (2), and (3). Lines (1) - (5), (2) - (5), and (3) - (5) are straight line approximations of bicharacteristics through point (5). The particle path (4) - (5) is projected from the solution point back to the initial data surface.

The main advantage of this scheme is that base points (1), (2), and (3) remain fixed during the solution; thus no interpolation is required for the flow properties at these points. However, interpolation is required at point (4). An apparent disadvantage with this scheme, as with all direct schemes, is that there is no direct control over the location of the solution point. The major disadvantage of the scheme, however, is that it is unstable due to violation of the CFL stability criterion seen in Figure 1.5 where the differential domain of dependence lies partially outside the convex hull of the difference scheme. This fact was discovered by Sauerwein (12) in attempting to apply the technique to unsteady flow problems. Fowell (10) developed numerical procedures based on this network for analysis of supersonic flow over wing-body

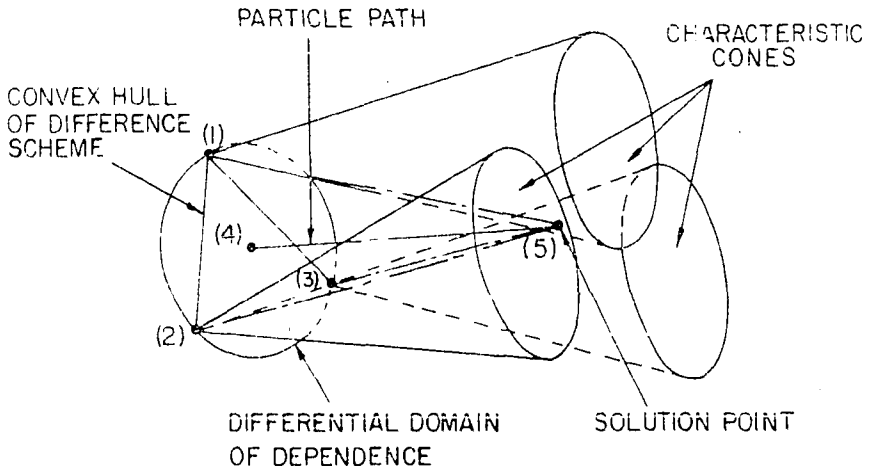

Figure 1.5. Tetrahedral bicharacteristic line network

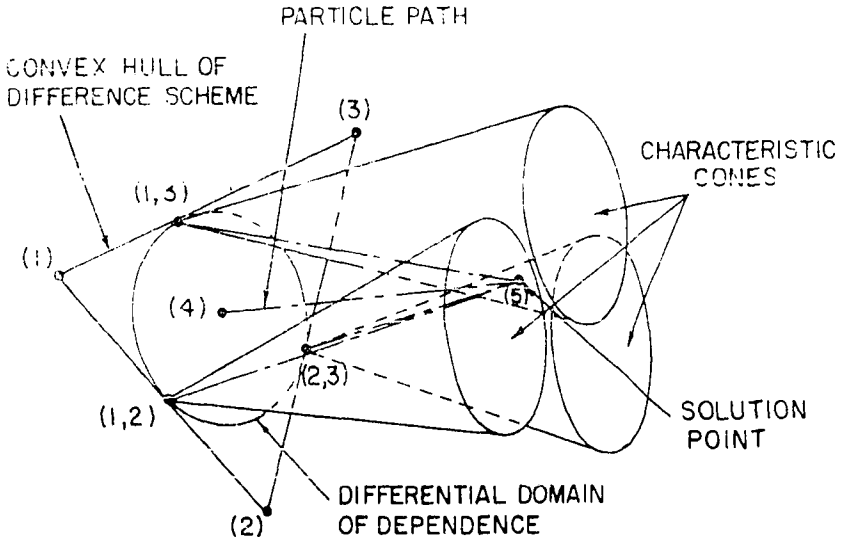

Figure 1.6. Modified tetrahedral bicharacteristic line network

configurations. However, he made only a few hand calculations with the method, and apparently did not discover the instability of the method.

b. Modified tetrahedral bicharacteristic line network Sauerwein (12) proposed a modified version of the tetrahedral bicharacteristic line network in order to satisfy the CFL stability criterion. In this network, shown in Figure 1.6, a triangle is drawn connecting initial data points (1), (2), and (3). Points of tangency of the triangle and an inscribed circle [points (1,2), (1,3), and (2,3)] are used as base points for the tetrahedral bicharacteristic line network. Linear interpolations along the sides of the triangle are used to determine the flow properties at the base points. This scheme satisfies the CFL criterion and was found to be stable by Sauerwein. This network closely resembles the tetrahedral characteristic surface network and also shares the same advantages and disadvantages.

c. Network of intersections of streamlines and reference planes Strom (13) developed an indirect scheme, shown in Figure 1.7, which he called the network of intersections of streamlines and reference planes. In the network construction, the solution point (6) is located first by projecting the streamline forward from the initial data point (5). Four equally spaced bicharacteristics are then projected from the solution point back to the initial data surface. Bivariate

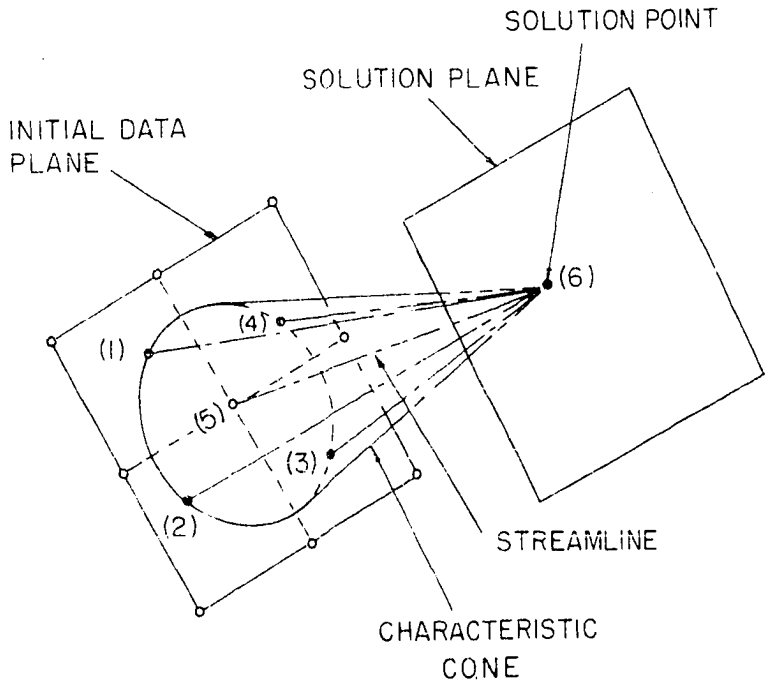

Figure 1.7. Network of intersections of streamlines and reference planes

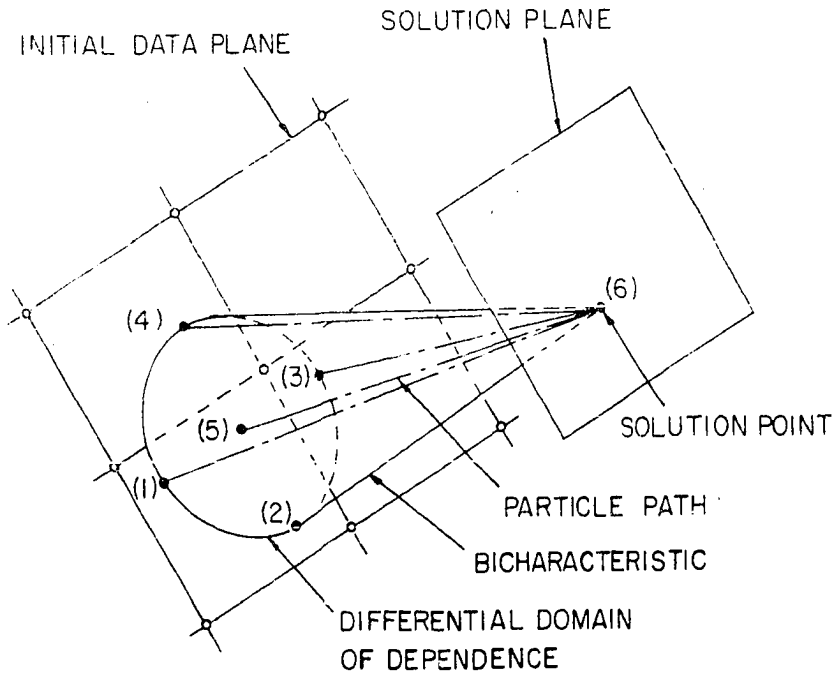

Figure 1.8. Pentahedral bicharacteristic line network

interpolating polynomials fitted to point (5) and eight neighboring points are used to determine the flow properties at base points (1) - (4). The cross derivative terms in the wave surface compatibility relations are ignored at the solution point. Multiple solutions are determined using sets of three bicharacteristics with the results subsequently averaged.

One advantage of this network, over previous inverse schemes, is that streamlines are followed in the solution. Streamline tracing is especially desirable in chemically reacting flows. Also, according to Strom, the use of a single bivariate interpolating polynomial for calculating each dependent variable at all base points is desirable from the standpoint of computational time required.

Strom (13) used this scheme to predict the three-dimensional supersonic flow field over blunt conical bodies. Chu et al. (49, 50) used a version of this scheme to solve a number of three-dimensional supersonic flow problems.

d. Pentahedral bicharacteristic line network Butler (17) developed the pentahedral bicharacteristic line network shown in Figure 1.8. In this scheme, second order accuracy is clearly maintained. As originally proposed, the scheme involves integration of the wave surface difference equations over the infinite family of bicharacteristics passing through a point. In practice, however, the integrals are replaced by summations over four equally spaced bicharacteristics around

the characteristic cone. The scheme is unique in that cross derivatives are eliminated at the solution point. Butler proposed an inverse scheme in which the solution point (6) is fixed, and the bicharacteristics and particle path are projected back into the initial data surface. Base point flow properties are determined using bivariate polynomials fitted to known initial data points. Talbot (51) has applied this method to unsteady shock-thermal layer interaction problems. Also, Elliott (52) and Richardson (53) used this scheme with modifications for solution of unsteady flow fields about detonated cylindrical bodies.

Ransom et al. (14, 54, 55, 56) and Cline and Hoffman (57, 58) developed a modified version of Butler's scheme for solution of chemically reacting, supersonic nozzle flows. In this scheme, streamlines are traced in the same manner as in the network of intersections of streamlines and reference planes. A degree of freedom in the choice of the four bicharacteristics was also introduced in this scheme. Good comparisons of numerical solutions and experimental data are presented by Ransom et al. (56) for supersonic flow in super-elliptical contour nozzles. Cline and Hoffman (57) have made comparisons of the pentahedral bicharacteristic line network and two inverse versions of the tetrahedral bicharacteristic line network. The pentahedral bicharacteristic line network was found to be the best overall scheme in terms of accuracy and computation

time required.

D. The Present Numerical Method for Solution of Cascade Flows

The numerical method developed in this study for solution of steady transonic flows in turbine cascades is based on the method of characteristics for two-dimensional unsteady flow. Steady cascade flows are computed as the asymptotic limit in time of a transient solution.

The present method is based on the pentahedral bicharacteristic line network developed by Butler (17). Butler's scheme was chosen because it is the only characteristic method in which second-order accuracy is clearly maintained. Improvements, some of which are due to Ransom (14), have been incorporated into the scheme. For completeness, Butler's general numerical method incorporating the infinite family of bicharacteristics is developed in Appendix B. Supporting material on the general theory of hyperbolic partial differential equations is included in Appendix A. The general numerical method presented in Appendix B, although not essential to the development of the numerical scheme for two-dimensional unsteady flow, has been included for the reader interested in extending the method.

II. CHARACTERISTIC RELATIONS

In this chapter the characteristic relations for plane two-dimensional unsteady flow of an inviscid fluid are developed. The characteristic property used in these developments is that particular linear combinations of the equations produce interior differential operators, called compatibility relations, on characteristic surfaces in the space formed by the two physical space coordinates and the time axis. A discussion of this characteristic property as applied to a general hyperbolic system of first-order partial differential equations is presented in Appendix A. For the comprehensive theory of hyperbolic systems of partial differential equations in three independent variables the reader is referred to Courant and Hilbert (59).

A. Equations of Motion

The equations of motion for unsteady adiabatic flow of an inviscid fluid in two dimensions are the two Euler momentum equations, the continuity equation and the isentropic relation. These equations are

$$\rho\left(u_1 \frac{\partial u_1}{\partial x_1} + u_2 \frac{\partial u_1}{\partial x_2} + \frac{\partial u_1}{\partial t}\right) + \frac{\partial p}{\partial x_1} = 0 \tag{2.1}$$

$$\rho\left(u_1 \frac{\partial u_2}{\partial x_1} + u_2 \frac{\partial u_2}{\partial x_2} + \frac{\partial u_2}{\partial t}\right) + \frac{\partial p}{\partial x_2} = 0 \tag{2.2}$$

$$\rho\left(\frac{\partial u_1}{\partial x_1} + \frac{\partial u_2}{\partial x_2}\right) + u_1 \frac{\partial \rho}{\partial x_1} + u_2 \frac{\partial \rho}{\partial x_2} + \frac{\partial \rho}{\partial t} = 0 \qquad (2.3)$$

$$u_1 \frac{\partial s}{\partial x_1} + u_2 \frac{\partial s}{\partial x_2} + \frac{\partial s}{\partial t} = 0 \qquad (2.4)$$

where u_1 and u_2 are the velocity components along the x_1 and x_2 Cartesian coordinate directions, respectively, p is the static pressure, ρ is static density, s is specific entropy and t is time. Equation 2.4 states that entropy is conserved along a particle path. From the definition of acoustic speed, a,

$$a^2 = \left.\frac{\partial p}{\partial \rho}\right|_s \qquad (2.5)$$

an expression equivalent to Eq. 2.4 is

$$u_1 \frac{\partial p}{\partial x_1} + u_2 \frac{\partial p}{\partial x_2} + \frac{\partial p}{\partial t} - a^2\left(u_1 \frac{\partial \rho}{\partial x_1} + u_2 \frac{\partial \rho}{\partial x_2} + \frac{\partial \rho}{\partial t}\right) = 0 \qquad (2.6)$$

In the derivation of the characteristic relations consider the time axis as directed normal to the physical plane; also introduce the notation $x_3 = t$. Any vector A_i in the space (x_1, x_2, x_3) can be represented as the sum of two vectors, one lying in the physical plane and the other directed along the time axis, i.e.,

$$A_i = a_i + \{0, 0, A_3\} \qquad (2.7)$$

where

$$a_i = \{A_1, A_2, 0\} \tag{2.8}$$

The vector a_i (lower case letter) is the physical component of A_i. Let $U_i = \{u_1, u_2, 1\}$; then the physical component $u_i = \{u_1, u_2, 0\}$ is the velocity vector. With this notation, the equations of motion, Eqs. 2.1-2.3, and 2.6 in matrix form are

$$\begin{bmatrix} \rho U_i & 0 & \delta_{1i} & 0 \\ 0 & \rho U_i & \delta_{2i} & 0 \\ \rho\delta_{1i} & \rho\delta_{2i} & 0 & U_i \\ 0 & 0 & U_i & -a^2 U_i \end{bmatrix} \begin{bmatrix} \frac{\partial u_1}{\partial x_i} \\ \frac{\partial u_2}{\partial x_i} \\ \frac{\partial p}{\partial x_i} \\ \frac{\partial \rho}{\partial x_i} \end{bmatrix} = 0 \tag{2.9}$$

where the repeated indices imply summation over the range 1 to 3. (The elements of the coefficient matrix in Eq. 2.9 correspond to the coefficients $a_{\mu\nu i}$ in Eq. 10.1 of Appendix A.)

B. Characteristic Surfaces

Hyperbolic systems of partial differential equations in three independent variables have the property that particular linear combinations of the equations yield relations involving

differentiation in only two independent directions (see Appendix A). These two independent directions locally define a surface called a characteristic surface. A linear combination of the equations written on a characteristic surface is called a compatibility relation.

The characteristic surfaces for the system of equations, Eq. 2.9, are obtained by solving for the left eigenvector which will reduce the system of equations to an interior operator on a surface. Multiplication of Eq. 2.9 by the left eigenvector w_μ ($\mu = 1,2,3,4$) yields the single equation

$$\rho(U_i w_1 + \delta_{1i} w_3) \frac{\partial u_1}{\partial x_i} + \rho(U_i w_2 + \delta_{2i} w_3) \frac{\partial u_2}{\partial x_i}$$

$$+ (\delta_{1i} w_1 + \delta_{2i} w_2 + U_i w_4) \frac{\partial p}{\partial x_i} + (U_i w_3 - a^2 U_i w_4) \frac{\partial \rho}{\partial x_i} = 0 \tag{2.10}$$

The coefficients of the derivatives in Eq. 2.10 are vectors of directional differentiation (W_ν in Eq. 10.6). Equation 2.10 reduces to an interior operator on a surface if the coefficient vectors are coplanar, or equivalently, if the scalar products of the coefficient vectors and a vector N_i normal to the characteristic surface vanish, i.e.,

$$\rho(U_i w_1 + \delta_{1i} w_3) N_i = 0 \tag{2.11}$$

$$\rho(U_i w_2 + \delta_{2i} w_3) N_i = 0 \tag{2.12}$$

$$(\delta_{1i}w_1 + \delta_{2i}w_2 + U_i w_4)\ N_i = 0 \tag{2.13}$$

$$(U_i w_3 - a^2 U_i w_4)\ N_i = 0 \tag{2.14}$$

The physical component of the characteristic surface normal is taken to be unity. Hence,

$$n_i n_i = 1 \tag{2.15}$$

The system of equations, Eqs. 2.11-2.14, provides four equations for the four components of the left eigenvector, w_μ, and can be written in matrix form as

$$\begin{bmatrix} \rho U_i N_i & 0 & \rho\delta_{1i}N_i & 0 \\ 0 & \rho U_i N_i & \rho\delta_{2i}N_i & 0 \\ \delta_{1i}N_i & \delta_{2i}N_i & 0 & U_i N_i \\ 0 & 0 & U_i N_i & -a^2 U_i N_i \end{bmatrix} \begin{bmatrix} w_1 \\ w_2 \\ w_3 \\ w_4 \end{bmatrix} = 0 \tag{2.16}$$

A nontrivial solution for w_μ exists if the determinant of the coefficient matrix in Eq. 2.16 vanishes. Expansion of the determinant of the coefficient matrix yields the characteristic equation for the original system of equations, Eq. 2.9, as

$$(U_i N_i)^2 \{[U_i U_j - a^2 (\delta_{1i} \delta_{1j} + \delta_{2i} \delta_{2j})] N_i N_j\} = 0 \quad (2.17)$$

The two distinct factors in Eq. 2.17 correspond to two different families of characteristic surfaces with normals N_i (Appendix A).

1. Characteristic flow surfaces

Characteristic flow surface normals, N_i, satisfy the equation obtained by setting the first factor in Eq. 2.17 equal to zero, i.e.,

$$U_i N_i = 0 \quad (2.18)$$

Equations 2.15 and 2.18 are two equations for the three components of the normal N_i. The remaining condition needed to determine N_i is arbitrary. Therefore, rather than a uniquely determined normal, N_i, an infinite family of normals exists.

Simultaneous solution of Eqs. 2.15 and 2.18 yields the locus of endpoints of the normals N_i. Equation 2.18 is the equation of a plane passing through the origin (see Eq. 16.6 in Appendix G) whose orientation depends on the velocity components at a point, and Eq. 2.15 is that of a cylinder of unit radius whose axis lies along the x_3 axis. Therefore, the locus of endpoints of N_i is the elliptic curve of intersection of the plane and cylinder shown in Figure 2.1. Since the plane of normals passes through the origin, all normals are

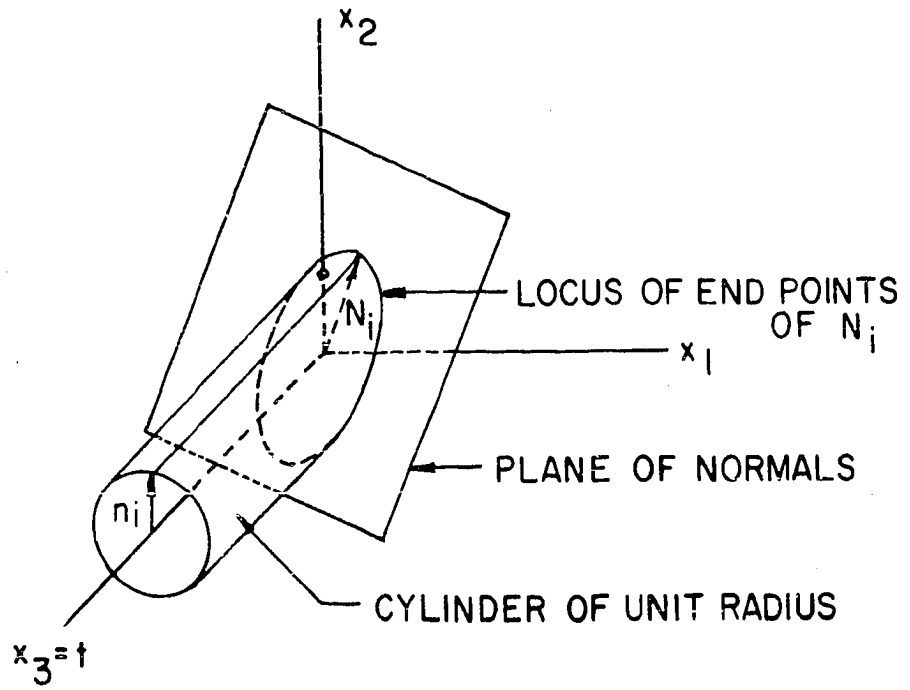

Figure 2.1. Characteristic flow surface normals in two-dimensional unsteady flow

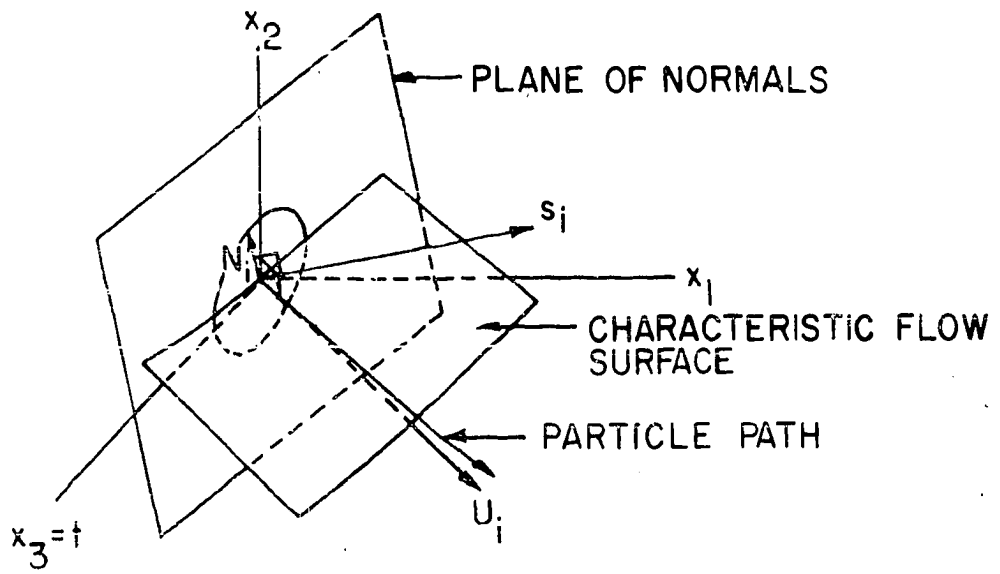

Figure 2.2. Characteristic flow surface geometry in two-dimensional unsteady flow

coplanar.

At a point in space there exists an infinite number of characteristic flow surfaces corresponding to the infinite family of normals N_i satisfying Eq. 2.18. The condition expressed by Eq. 2.18 is that the normals N_i are orthogonal to the vector U_i, as shown in Figure 2.2. Therefore, all characteristic flow surfaces contain U_i, and the envelope of these surfaces is a degenerate surface or a curve locally tangent to U_i. Let $dS_i = \{dS_1, dS_2, dS_3\}$ be a differential element of this curve; then according to Eq. 2.18

$$dS_i N_i = ds_i n_i + N_3 dS_3 = 0 \tag{2.19}$$

where $ds_i = \{dS_1, dS_2, 0\}$ is the physical component of dS_i. If Eq. 2.19 is divided by dS_3 and the resulting coefficients of n_i are set equal to the coefficients of n_i in the expanded form of Eq. 2.18, we get

$$\frac{dS_1}{dS_3} = u_1 \tag{2.20}$$

$$\frac{dS_2}{dS_3} = u_2 \tag{2.21}$$

Elimination of dS_3 from Eqs. 2.20 and 2.21 gives

$$\frac{dS_2}{dS_1} = \frac{u_2}{u_1} \tag{2.22}$$

The condition expressed by Eqs. 2.20, 2.21 and 2.22 is that the vector dS_i lies along the particle path. Thus, the particle path, shown in Figure 2.2, is the envelope of the infinite family of characteristic flow surfaces.

2. Characteristic wave surfaces

Normals N_i to characteristic wave surfaces satisfy the vanishing of the second factor in Eq. 2.17, i.e.,

$$\{U_i U_j - a^2 (\delta_{1i} \delta_{1j} + \delta_{2i} \delta_{2j})\} N_i N_j = 0 \qquad (2.23)$$

Equation 2.23 is of the general form

$$A_{ij} N_i N_j = 0 \qquad (A_{ij} = A_{ji}) \qquad (2.24)$$

which is the equation of a cone (cone of normals) with the vectors N_i directed along the generators (see Appendix G). Summation on repeated subscripts in Eq. 2.23 and substitution of Eq. 2.15 yields a quadratic equation in $U_i N_i$ with roots

$$U_i N_i = \pm a \qquad (2.25)$$

where the choice of the positive or negative root is arbitrary. The sign in Eq. 2.25 merely fixes the direction of N_i along the generators of the cone of normals.

The locus of endpoints of the characteristic wave surface normals is determined by simultaneous solution of Eqs. 2.15 and 2.25. Equation 2.25 is the equation of a plane

whose orientation in space depends on the magnitudes of the velocity components and acoustic speed at a point. With the normalization condition on the physical component of N_i, Eq. 2.15, the endpoints of N_i lie on the elliptic curve of intersection of the plane, Eq. 2.25, and the unit cylinder, as shown in Figure 2.3.

At any point in the (x_1, x_2, x_3) space there exist an infinite number of characteristic wave surfaces with normals N_i satisfying Eq. 2.23. This family of surfaces forms a curved conical envelope which is called the characteristic conoid. The conoid is locally tangent to the characteristic cone which is the reciprocal cone to the cone of normals. Tangent loci of the characteristic wave surfaces and the characteristic conoid are called bicharacteristics (see Appendix A).

A differential element of the characteristic conoid is represented by the quadratic relation (Eq. 10.14 in Appendix A)

$$A_{ij}^{-1}\, dx_i dx_j = 0 \qquad (2.26)$$

The differential vectors dx_i satisfying Eq. 2.26 are locally tangent to the bicharacteristics and lie along the generators of the characteristic cone. The coefficients A_{ij}^{-1} in Eq. 2.26 are obtained by constructing the matrix A with elements A_{ij} from Eq. 2.24 and determining the inverse matrix A^{-1}. After considerable manipulation, the elements of A^{-1} can be written

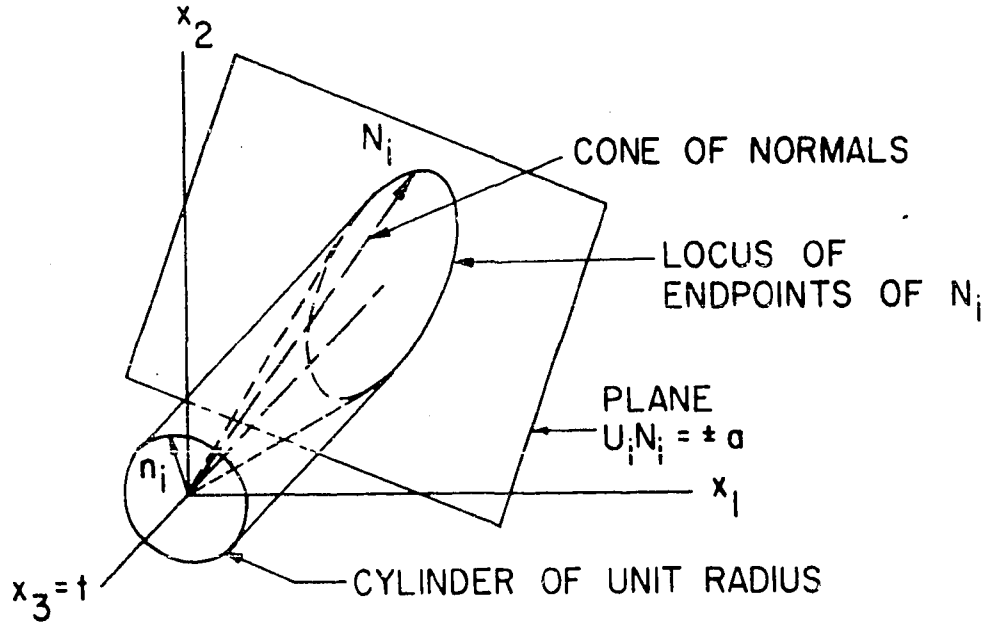

Figure 2.3. Characteristic wave surface normals in two-dimensional unsteady flow

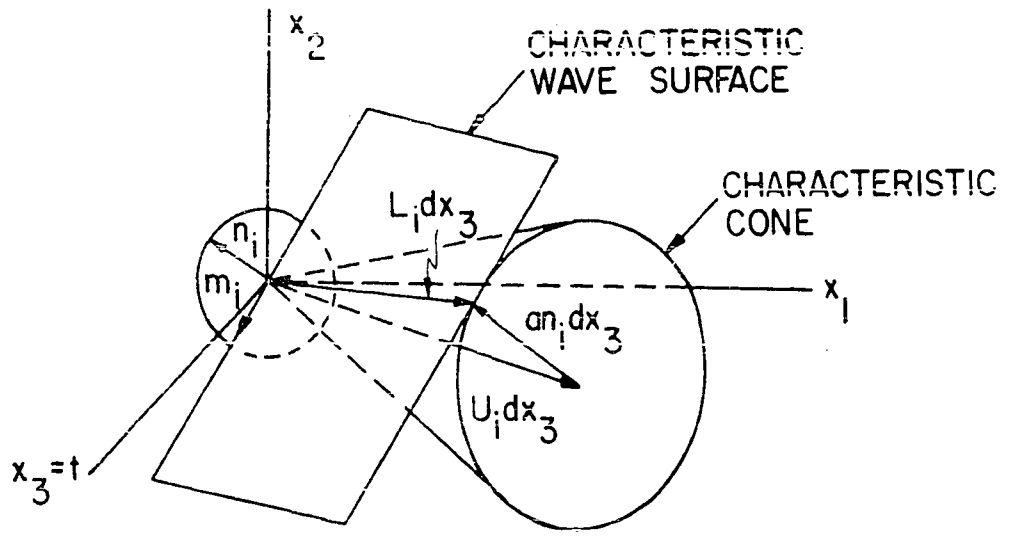

Figure 2.4. Characteristic wave surface geometry in two-dimensional unsteady flow

in the form

$$A_{ij}^{-1} = \frac{1}{a^2}\{U_iU_j - U_kU_k\delta_{ij} + (u_1\delta_{2i} - u_2\delta_{1i})(u_1\delta_{2j} - u_2\delta_{1j}) + a^2\,\delta_{3i}\delta_{3j}\} \tag{2.27}$$

Substitution of this result into Eq. 2.26 for A_{ij}^{-1} and summation on repeated subscripts yields

$$(dx_1 - u_1dx_3)^2 + (dx_2 - u_2dx_3)^2 = a^2dx_3^2 \tag{2.28}$$

which is the equation of the real oblique cone shown in Figure 2.4. The base of the cone in the plane dx_3 = constant is a circle of radius adx_3 centered about the point $\{u_1dx_3, u_2dx_3, dx_3\}$. This cone is the sonic cone and represents the local path of propagation of a disturbance generated at the origin.

C. Compatibility Relations

The compatibility relation, Eq. 2.10, is an interior operator on a characteristic surface and is determined by a linear combination of the equations of the original system, Eq. 2.9. For a particular characteristic surface, the components of the left eigenvector w_μ used in forming the linear combination are determined from Eq. 2.16 with appropriate conditions on the characteristic surface normal N_i. Since Eq. 2.16 is homogeneous, the left eigenvector is

determined only to within an arbitrary scalar multiplier. The number of independent solutions for w_μ is determined from the rank of the coefficient matrix in Eq. 2.16.

1. Flow surface compatibility relations

The vectors N_i normal to a characteristic flow surface satisfy Eq. 2.18. Thus Eq. 2.16 for this case reduces to

$$\begin{bmatrix} 0 & 0 & \rho N_1 & 0 \\ 0 & 0 & \rho N_2 & 0 \\ N_1 & N_2 & 0 & 0 \\ 0 & 0 & 0 & 0 \end{bmatrix} \begin{bmatrix} w_1 \\ w_2 \\ w_3 \\ w_4 \end{bmatrix} = 0 \qquad (2.29)$$

The coefficient matrix in Eq. 2.29 is rank 2; therefore, two linearly independent solutions for w_μ exist for each flow surface normal, yielding two linearly independent compatibility relations. From Eq. 2.29, w_3 vanishes for both solutions, and the value of w_4 is arbitrary. The most obvious two independent solutions for w_μ are one with w_4 finite and the remaining components zero, and the other with w_3 and w_4 zero and w_1, w_2 satisfying the equation, $w_1N_1 + w_2N_2 = 0$. Since the system of equations Eq. 2.29 is homogeneous, we can write for the first solution

$$w_\mu = \{0,\ 0,\ 0,\ 1\} \tag{2.30}$$

For the second solution, if we let $w_1 = S_1$ and $w_2 = S_2$, where $s_i = \{S_1,\ S_2,\ 0\}$ is normal to n_i ($n_i s_i = 0$), then

$$w_\mu = \{S_1,\ S_2,\ 0,\ 0\} \tag{2.31}$$

The vector s_i lies in the characteristic flow surface and is directed along the curve of intersection of the surface with the physical plane, as shown in Figure 2.2.

The compatibility relations corresponding to the left eigenvectors w_μ, Eqs. 2.30 and 2.31, are obtained by forming the coefficient vectors of the derivatives in Eq. 2.10 or by taking the linear combination of the equations of the original system, Eq. 2.9, with multipliers equal to the components of w_μ. Hence, the compatibility relation associated with the eigenvector given by Eq. 2.30 is simply the last equation of the original system, Eq. 2.6. In directional differential notation, this equation is written as

$$d_U p - a^2 d_U \rho = 0 \tag{2.32}$$

where U denotes the particle path direction, U_i. The compatibility relation corresponding to the eigenvector given by Eq. 2.31 is

$$\rho\, S_1 U_i \frac{\partial u_1}{\partial x_i} + \rho\, S_2 U_i \frac{\partial u_2}{\partial x_i} + s_i \frac{\partial p}{\partial x_i} = 0 \tag{2.33}$$

or, in directional differential notation

$$\rho\, S_1 d_U u_1 + \rho\, S_2 d_U u_2 + d_s P = 0 \qquad (2.34)$$

where s denotes the s_i direction. Equation 2.32 involves differentiation in a single direction, U_i, while Eq. 2.34 involves differentiation in two independent directions, U_i and s_i.

2. Wave surface compatibility relations

The vectors N_i normal to characteristic wave surfaces satisfy Eq. 2.25, i.e.

$$U_i N_i = -a \qquad (2.35)$$

where the negative root is arbitrarily chosen. In this case, Eq. 2.16 reduces to

$$\begin{bmatrix} -\rho a & 0 & \rho N_1 & 0 \\ 0 & -\rho a & \rho N_2 & 0 \\ N_1 & N_2 & 0 & -a \\ 0 & 0 & -a & a^3 \end{bmatrix} \begin{bmatrix} w_1 \\ w_2 \\ w_2 \\ w_4 \end{bmatrix} = 0 \qquad (2.36)$$

The coefficient matrix in Eq. 2.36 is rank 3; therefore, only one solution for w_μ exists for each wave surface normal N_i. If we let $w_4 = 1$, then solution for the remaining components w_μ in Eq. 2.36 gives

$$w_\mu = \{aN_1,\ aN_2,\ a^2,\ 1\} \tag{2.37}$$

The wave surface compatibility relation from Eq. 2.10 then becomes

$$\rho a(N_1 U_i + a\,\delta_{1i})\,\frac{\partial u_1}{\partial x_i} + \rho a(N_2 U_i + a\,\delta_{2i})\,\frac{\partial u_2}{\partial x_i}$$

$$+\ (aN_1\delta_{1i} + aN_2\delta_{2i} + U_i)\,\frac{\partial p}{\partial x_i} = 0 \tag{2.38}$$

The fact that this equation involves directional derivatives within the wave surface can be verified by taking scalar products of the coefficient vectors of the derivatives and the wave surface normal N_i. With incorporation of Eq. 2.35 these scalar products vanish, ensuring that Eq. 2.38 can be rewritten in terms of derivatives in only two independent directions.

Equation 2.38 can be rewritten in terms of directional derivatives in two arbitrary independent directions in a characteristic wave surface. For the two directions we choose first, as shown in Figure 2.4, the bicharacteristic direction, locally tangent to the vector L_i,

$$L_i = U_i + an_i \tag{2.39}$$

and second the direction m_i,

$$m_i = n_j(\delta_{1j}\,\delta_{2i} - \delta_{2j}\,\delta_{1i}) \tag{2.40}$$

locally tangent to the intersection of the characteristic wave surface and the physical plane. Note that the scalar products of the vectors L_i and m_i with the wave surface normal N_i vanish, and that the vectors n_i and m_i are orthogonal.

Equation 2.38 can be rewritten in a more compact form as

$$\rho a(n_j U_i + a\delta_{ij}) \frac{\partial u_j}{\partial x_i} + (U_i + a n_i) \frac{\partial p}{\partial x_i} = 0 \qquad (2.41)$$

where the subscripts on δ_{ij} take values 1 and 2, only. If the term $\rho a^2 n_j n_i \frac{\partial u_j}{\partial x_i}$ is added to and subtracted from Eq. 2.41, then

$$\rho a n_j (U_i + a n_i) \frac{\partial u_j}{\partial x_i} + (U_i + a n_i) \frac{\partial p}{\partial x_i} + \rho a^2 (\delta_{ij} - n_j n_i) \frac{\partial u_j}{\partial x_i} = 0 \qquad (2.42)$$

The first two terms of Eq. 2.42 involve differentiation in the bicharacteristic direction, L_i. After considerable algebraic manipulation, the product $m_i m_j$, according to Eq. 2.40, can be expressed as

$$m_i m_j = \delta_{ij} - n_j n_i \qquad (2.43)$$

Hence, the wave surface compatibility relation, Eq. 2.42, can be written as

$$\rho a n_j (U_i + a n_i) \frac{\partial u_j}{\partial x_i} + (U_i + a n_i) \frac{\partial p}{\partial x_i} + \rho a^2 m_j m_i \frac{\partial u_j}{\partial x_i} = 0 \qquad (2.44)$$

or, in directional differential notation, as

$$\rho a n_j \, d_L u_j + d_L p + \rho a^2 m_j \, d_m u_j = 0 \qquad (2.45)$$

where L and m denote the bicharacteristic L_i and the m_i directions, respectively.

D. Interdependence of the Compatibility Relations

There exists a double infinity of compatibility relations at a point in space written on two infinite families of characteristic surfaces. Since any compatibility relation is a linear combination of the four equations of motion in Eq. 2.9, the maximum number of independent compatibility relations is four. Also, in forming a complete set of compatibility relations, a minimum of four relations must be considered. Many combinations of four compatibility relations can be formed. However, the interdependence of these combinations must be examined in order to obtain a complete set of independent relations.

To examine the interdependence of any set of four compatibility relations, it is necessary to write out the matrix

$$w_\mu^j = \{w_1^j, w_2^j, w_3^j, w_4^j\} \quad (j = 1,2,3,4) \qquad (2.46)$$

whose rows are the left eigenvectors associated with the particular compatibility relations considered. The number of

linearly independent compatibility relations is equal to the rank of the matrix described by Eq. 2.46. The rows of the matrix yielding the highest order nonzero determinant show which compatibility relations are independent.

In order to determine the maximum number of linearly independent wave surface compatibility relations of the form of Eq. 2.45, we determine the rank of the matrix

$$w_{\mu}^{j} = \{aN_1^j,\ aN_2^j,\ a^2,\ 1\} \quad (j = 1,2,3,4) \tag{2.47}$$

whose rows are the left eigenvectors given by Eq. 2.37 for four different wave surface normals, N_i^j $(j = 1,2,3,4)$. Since the last two columns of this matrix are dependent, the rank is at most three; therefore, we examine the reduced matrix

$$\begin{bmatrix} aN_1^1 & aN_2^1 & a^2 \\ aN_1^2 & aN_2^2 & a^2 \\ aN_1^3 & aN_2^3 & a^2 \end{bmatrix} \tag{2.48}$$

If the rows of this matrix are dependent, then the endpoints of the vectors n_i^j $(n_i = \{N_1, N_2, 0\})$ lie on a straight line (i.e., the two difference vectors obtained by subtracting two rows of the matrix from the remaining row are collinear). However, from Eq. 2.15, the endpoints of n_i^j lie on a circle of unit radius. Therefore, the rows of the matrix are independent and three linearly independent wave surface compatibility

relations exist.

Since only three wave surface compatibility relations are independent, a complete set of four equations must include at least one flow surface relation. The particle path relation, Eq. 2.32, is the only compatibility relation involving derivatives of the density, ρ. Hence, Eq. 2.32 is independent of the other relations and must be included in any complete set of compatibility relations.

It is now clear that a complete system of four compatibility relations can be formed from three wave surface relations and the particle path relation. This particular combination of compatibility relations is of interest in the development of the numerical integration scheme to be discussed in Chapter III. Other combinations of the compatibility relations can be used to form complete systems of equations. For a discussion of these combinations see Delaney and Kavanagh (60).

III. SECOND-ORDER NUMERICAL INTEGRATION SCHEME

A. General

Second-order accuracy is not easily achieved in the application of the method of characteristics to the numerical integration of hyperbolic systems of partial differential equations in three independent variables. That this is the case is because the compatibility relations, in general, involve differentiations in two independent directions on the characteristic surfaces. Thus, second-order finite-difference approximations to the compatibility relations, obtained by differencing along network lines in the numerical integration network, inherently contain cross-derivative terms at the solution point. Evaluation of these terms to maintain second-order accuracy necessarily involves an outer iteration in which the entire solution surface is calculated a number of times, with cross-derivatives at the solution points updated after each iteration. The usual approach, however, as stated previously in the discussion of the characteristic numerical integration networks in Chapter I, has been to neglect the cross-derivatives at the solution point and to accept the attendant decrease in accuracy.

Second-order accuracy is maintained in Butler's scheme (17) by elimination of cross-derivatives at the solution point.

In the original scheme proposed by Butler, the infinite family of bicharacteristics is employed and the cross-derivatives eliminated by weighted integration of the wave surface compatibility relations around the differential domain of dependence (Appendix B). In practical application, however, four wave surface compatibility relations corresponding to four equally spaced bicharacteristics are used in combination with the particle path compatibility relation and a non-characteristic relation. In the system of difference relations, the cross-derivatives at the solution point appear in two terms common to all the equations. The cross-derivatives are eliminated by taking appropriate linear combinations of the equations.

In this chapter, numerical solution procedures are developed for two-dimensional unsteady flow based on Butler's method. The development closely parallels that given by Ransom (14) for three-dimensional steady supersonic flow. Frequent reference is also made to the general numerical method contained in Appendix B.

B. Parameterization of Bicharacteristics

In the numerical scheme, the bicharacteristic direction is parameterized by introducing the following representation for the physical component of the wave surface normal vector:

$$n_i = \cos\theta\ \alpha_i + \sin\theta\ \beta_i \quad (i = 1,2) \tag{3.1}$$

where α_i and β_i are orthonormal reference vectors lying in the physical plane at the vertex of the characteristic conoid. In Eq. 3.1, the parameter θ is the polar angle measured from the α_i direction, as shown in Figure 3.1. The angle θ has the range $0 \leq \theta < 2\pi$. With this form for n_i, the generators of the sonic cone lie along the directions (see Eq. 2.39)

$$L_i = U_i + a\cos\theta\ \alpha_i + a\sin\theta\ \beta_i \quad (i = 1,2,3) \tag{3.2}$$

where the vector U_i is locally tangent to the particle path, and a is the local acoustic speed. The parametric representation of a differential element of a bicharacteristic curve is thus

$$dx_i = (U_i + a\cos\theta\ \alpha_i + a\sin\theta\ \beta_i)\ dt \tag{3.3}$$

$$(i = 1,2,3)$$

where t is the time of travel of a disturbance along the bicharacteristic. The equation of a differential element of the particle path is found from Eq. 3.3 with the last two terms set equal to zero, i.e.,

$$dx_i = U_i dt \quad (i = 1,2,3) \tag{3.4}$$

Equation 3.3 is the parametric representation of the bicharacteristics proposed by Butler. Butler fixed the

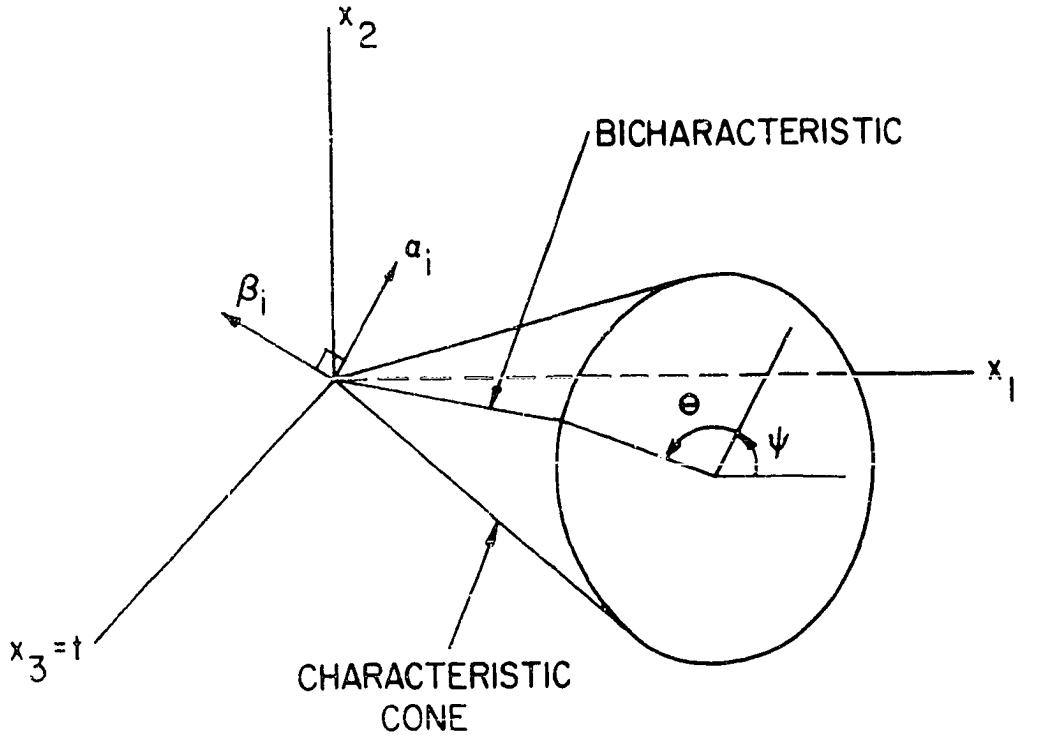

Figure 3.1. Characteristic cone, bicharacteristic parameter θ, reference vectors α_i, β_i, and degree of freedom, ψ, in orientation of the reference vectors in the x_1, x_2 plane

directions of α_i and β_i along the x_1, x_2 coordinate axes, respectively, and allowed θ to vary along the bicharacteristics. The approach used here, however, is that due to Ransom in which the degree of freedom in the rotation of the reference vectors α_i, β_i (the angle ψ in Figure 3.1) is used to maintain θ constant along the bicharacteristics. Ransom's approach results in a significant simplification of the numerical solution procedures.

The particular choice of U_i, α_i, and β_i as reference vectors in the bicharacteristic parameterization, Eq. 3.3, ensures that the quadric equation of the differential conoid, Eq. 2.26, is satisfied. The conditions which must be satisfied by the reference vectors correspond to Eqs. 11.4 and 11.5 in Appendix B with $\lambda_i = U_i$, $\mu_i = a\alpha_i$, and $\nu_i = a\beta_i$. With these substitutions, Eqs. 11.4 and 11.5 yield

$$A_{ij}^{-1} U_i \alpha_j = A_{ij}^{-1} U_i \beta_j = A_{ij}^{-1} \alpha_i \beta_j = 0 \tag{3.5}$$

and

$$-A_{ij}^{-1} U_i U_j = a^2 A_{ij}^{-1} \alpha_i \alpha_j = a^2 A_{ij}^{-1} \beta_i \beta_j \tag{3.6}$$

where the coefficients A_{ij}^{-1} are given by Eq. 2.27. Substitution of A_{ij}^{-1} from Eq. 2.27 into Eqs. 3.5 and 3.6 with α_i and β_i written as

$$\alpha_i = \cos\psi\ \delta_{1i} + \sin\psi\ \delta_{2i} \tag{3.7}$$

$$\beta_i = -\sin\psi\ \delta_{1i} + \cos\psi\ \delta_{2i} \tag{3.8}$$

where ψ is the angle between α_i and the x_1 axis, shows that Eqs. 3.5 and 3.6 are satisfied.

One other condition must be satisfied by the reference vectors to ensure that the curve obtained by integrating Eq. 3.3 for a particular value of θ is the tangent locus between the characteristic wave surface and the characteristic conoid (i.e., the definition of the bicharacteristic). This condition is called the "bicharacteristic tangency condition" and is obtained from the general form, Eq. 11.15, with substitution from Eqs. 2.27, 3.7 and 3.8. The result is

$$(\alpha_i \cos\theta + \beta_i \sin\theta)\ \frac{\partial x_i}{\partial \theta} = 0 \quad (i = 1,2) \tag{3.9}$$

Equation 3.9 is used to determine the orientation of α_i and β_i at any point along a bicharacteristic relative to a fixed reference at the vertex of the conoid.

The wave surface compatibility relation, Eq. 2.44, can now be written in terms of the bicharacteristic parameter θ. If the orthonormal properties of the vectors m_i and n_i are employed, m_i can be expressed as

$$m_i = -\sin\theta\alpha_i + \cos\theta\beta_i \qquad (i = 1,2) \tag{3.10}$$

Substitution of Eqs. 3.1 and 3.10 into Eq. 2.44 for n_i and m_i, and utilization of the definition of the directional differential along the bicharacteristic direction yields the relation

$$d_L p + \rho a (\cos\theta\, \alpha_j + \sin\theta\, \beta_j)\, d_L u_j$$

$$= -\rho a^2 (-\sin\theta\, \alpha_j + \cos\theta\, \beta_j)(-\sin\theta\, \alpha_i + \cos\theta\, \beta_i) \frac{\partial u_j}{\partial x_i} dt \qquad (3.11)$$

where the subscript L denotes the bicharacteristic direction. This particular form of the wave surface compatibility relation has the property that when written for $\theta = 0, \pi/2, \pi$, and $3\pi/2$, the derivatives of the dependent variables on the right-hand side of the equation appear in either one of the two groups of terms, $\alpha_j\alpha_i \frac{\partial u_j}{\partial x_i}$ or $\beta_j\beta_i \frac{\partial u_j}{\partial x_i}$. The fact that Eq. 3.11 has this property is used in the numerical solution to eliminate the cross-derivative terms at the solution point.

C. Difference Network

The difference network (pentahedral bicharacteristic line network) consists of four equally spaced bicharacteristics corresponding to $\theta = 0, \pi/2, \pi$, and $3\pi/2$ and the particle path. As shown in Figure 3.2, a completely inverted scheme is used in which the solution point (S) is fixed in the new time plane,

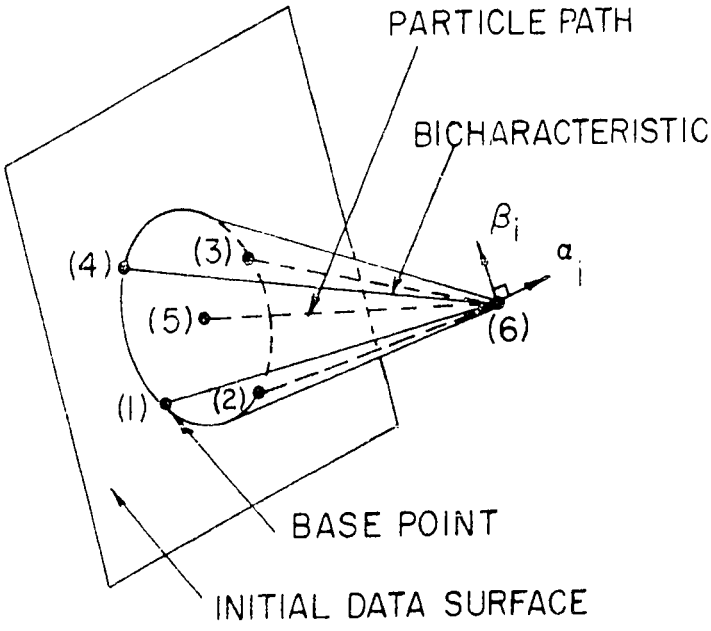

a. View showing bicharacteristics, particle path, and initial data surface

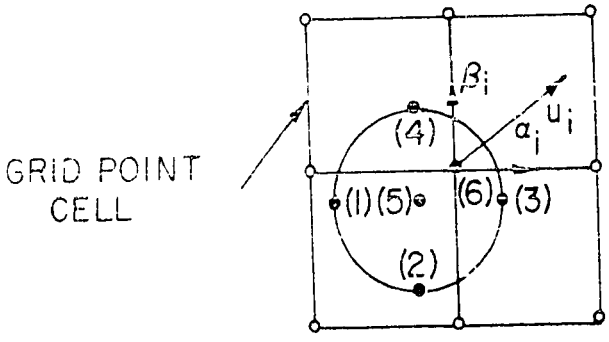

b. Projection onto initial data surface showing differential domain of dependence and grid point cell

Figure 3.2. Interior or field point network

and the bicharacteristics and particle path are projected back to the initial data plane. Base points (1), (2), (3), and (4) lie at the intersections of the bicharacteristics corresponding to $\theta = 0, \pi/2, \pi$, and $3\pi/2$, respectively, and the initial data plane. Point (5) is the intersection of the particle path and the initial data plane.

Base points are located by employing the finite-difference form of the appropriate direction equations. The finite-difference form of the particle path equation, Eq. 3.4, using the modified Euler scheme (ref. 61), is

$$x_i(5) = x_i(6) - \tfrac{1}{2}\{u_i(6) + u_i(5)\}\,\Delta t \quad (i = 1,2) \tag{3.12}$$

where the numbers in parentheses denote evaluation of the variables at corresponding points in the difference network, and Δt is the time increment between the initial data plane and the solution point, point (6). Similarly, the coordinates of points (1) through (4) are found from Eq. 3.3 written as

$$\begin{aligned} x_i(k) = x_i(6) - \tfrac{1}{2}\{&u_i(6) + a(6)\cos\theta(k)\,\alpha_i(6) \\ &+ a(6)\sin\theta(k)\,\beta_i(6) + u_i(k) + a(k)\cos\theta(k)\,\alpha_i(k) \\ &+ a(k)\sin\theta(k)\,\beta_i(k)\}\,\Delta t \quad (i = 1,2) \end{aligned} \tag{3.13}$$

where k takes values 1, 2, 3, and 4. Initial estimates for the values of the dependent variables at points (1) through (6) appearing in Eqs. 3.12 and 3.13 are taken as those at solution

point on the initial data surface.

The reference vectors α_i, β_i which appear in Eq. 3.13 must be established at point (6) and at the base points (1), (2), (3), and (4). The bicharacteristic tangency condition, Eq. 3.9, is used to establish the reference vectors $\alpha_i(k)$ and $\beta_i(k)$ ($k = 1,2,3,4$), relative to the fixed reference at point (6). Because of the length, the development of the finite-difference form of this condition is omitted here, but has been included in Appendix C. The results for the tangency condition are the following two equations for the components of $\alpha_i(k)$ ($k = 1,2,3,4$) obtained from Eqs. 12.35 and 12.36:

$$\alpha_1(k) = D(\theta)\ \beta_1(6)\ \Delta t + \alpha_1(6)\ [1 - D^2(\theta)\ \Delta t^2]^{\frac{1}{2}} \qquad (3.14)$$

$$\alpha_2(k) = D(\theta)\ \beta_2(6)\ \Delta t + \alpha_2(6)\ [1 - D^2(\theta)\ \Delta t^2]^{\frac{1}{2}} \qquad (3.15)$$

where

$$\begin{aligned} D(\theta) = {} & [\alpha_i(6)\ \cos\theta + \beta_i(6)\ \sin\theta] \\ & \times [\beta_j(6)\ \cos\theta - \alpha_j(6)\ \sin\theta]\ \frac{\partial u_i(6)}{\partial x_j} \\ & + [\beta_j(6)\ \cos\theta - \alpha_j(6)\ \sin\theta]\ \frac{\partial a(6)}{\partial x_j} \end{aligned} \qquad (3.16)$$

and where θ takes values 0, $\pi/2$, π, and $3\pi/2$ corresponding to $k = 1,2,3$, and 4, respectively. The derivatives $\frac{\partial u_i(6)}{\partial x_j}$ and

$\frac{\partial a(6)}{\partial x_j}$ appearing in Eq. 3.16 are computed to sufficient order of accuracy at the solution point (6) location on the initial data surface (see Appendix C). The derivatives $\frac{\partial a(6)}{\partial x_j}$ are evaluated in terms of derivatives of pressure and density from the property relation, in functional form,

$$a = a(p,\rho) \tag{3.17}$$

Differentiation of Eq. 3.17 according to the chain rule yields

$$\frac{\partial a(6)}{\partial x_i} = \frac{\partial a}{\partial p}\frac{\partial p(6)}{\partial x_i} + \frac{\partial a}{\partial \rho}\frac{\partial \rho(6)}{\partial x_i} \tag{3.18}$$

Following the solution for $\alpha_i(k)$, the components $\beta_i(k)$ are determined using the orthonormal properties of the reference vectors α_i and β_i, i.e.,

$$\alpha_i(k)\beta_i(k) = 0 \quad (i = 1,2) \tag{3.19}$$

$$\beta_i(k)\beta_i(k) = 1 \quad (i = 1,2) \tag{3.20}$$

Equations 3.19 and 3.20 provide two conditions for the two components of $\beta_i(k)$.

Once the base points (1) through (5) have been located, the dependent variables at these points are determined using bivariate interpolations on the initial data surface. For this purpose, second-order polynomials are fitted by the method of least squares to a nine-point cell consisting of the solution

point and eight neighboring points.

D. System of Difference Equations

The system of differential equations, which is the basis of the finite-difference integration scheme, consists of four wave surface compatibility relations, Eq. 3.11 written for $\theta = 0, \pi/2, \pi$, and $3\pi/2$, the particle path compatibility relation, Eq. 2.32, and a non-characteristic relation. From the previous discussion on the interdependence of compatibility relations in Section II.D, this system of six equations would appear to be overdetermined. However, in the numerical integration scheme the differential relations are replaced by finite-difference equations in which two terms involving derivatives of the velocity components at the solution point are treated as additional unknowns. Thus, in forming the difference equations from the differential relations, the order of the system is increased from four to six, and the resulting difference equations form a complete set of six equations.

The noncharacteristic relation involved in the system of difference equations is obtained by eliminating the derivatives of density from the continuity equation, Eq. 2.3, and the isentropic relation, Eq. 2.6, the result being

$$d_U p + \rho a^2 \left(\frac{\partial u_1}{\partial x_1} + \frac{\partial u_2}{\partial x_2}\right) dt = 0 \qquad (3.21)$$

where U denotes the particle path direction, U_i. Equation 3.21 can be written in an equivalent form involving the reference vectors α_i, β_i as

$$d_U p + \rho a^2 (\alpha_j \alpha_i + \beta_j \beta_i) \frac{\partial u_j}{\partial x_i} dt = 0 \qquad (3.22)$$

This noncharacteristic relation is used to eliminate the terms $\alpha_j \alpha_i \frac{\partial u_j(6)}{\partial x_i}$ and $\beta_j \beta_i \frac{\partial u_j(6)}{\partial x_i}$ which appear in the system of difference equations.

The system of difference equations is obtained by writing the differential relations in Eqs. 2.32, 3.11 and 3.22 in finite-difference form using the modified Euler scheme. The wave surface compatibility relation, Eq. 3.11, is written in finite-difference form along the bicharacteristic direction as

$$\begin{aligned}
&2[p(6) - p(k)] + \{\rho(6)\, a(6)[\cos\theta(k)\, \alpha_i(6) + \sin\theta(k)\, \beta_i(6)] \\
&\quad + \rho(k)\, a(k)\, [\cos\theta(k)\, \alpha_i(k) + \sin\theta(k)\, \beta_i(k)]\}[u_i(6) - u_i(k)] \\
&= -\{\rho(6)\, a^2(6)[-\sin\theta(k)\, \alpha_j(6) + \cos\theta(k)\, \beta_j(6)][-\sin\theta(6)\, \alpha_i(6) \\
&+ \cos\theta(k)\, \beta_i(6)] \frac{\partial u_j(6)}{\partial x_i} + \rho(k)\, a^2(k)\, [-\sin\theta(k)\, \alpha_j(k) \\
&+ \cos\theta(k)\, \beta_j(k)][-\sin\theta(k)\, \alpha_i(k) + \cos\theta(k)\, \beta_i k)] \frac{\partial u_j(k)}{\partial x_i}\}\Delta t
\end{aligned} \qquad (3.23)$$

where k (k = 1,2,3,4) denotes the base point at the intersection of the bicharacteristic and the initial data plane. With substitution of $\theta(k)$ values of 0, $\pi/2$, π, and $3\pi/2$ into Eq. 3.23 and rearrangement to put unknowns at point (6) on the left side of the equation, we obtain the following four wave surface compatibility relations:

$$
\begin{aligned}
&2\,p(6) + [\rho(6)\,a(6)\,\alpha_1(6) + \rho(1)\,a(1)\,\alpha_1(1)]\,u_1(6) \\
&\qquad + [\rho(6)\,a(6)\,\alpha_2(6) + \rho(1)\,a(1)\,\alpha_2(1)]\,u_2(6) \\
&\qquad + \rho(6)\,a^2(6)\,\beta_j(6)\,\beta_i(6)\,\frac{\partial u_j(6)}{\partial x_i}\,\Delta t \\
&= 2\,p(1) + [\rho(6)\,a(6)\,\alpha_1(6) + \rho(1)\,a(1)\,\alpha_1(1)]\,u_1(1) \\
&\qquad + [\rho(6)\,a(6)\,\alpha_2(6) + \rho(1)\,a(1)\,\alpha_2(1)]\,u_2(1) \\
&\qquad - \rho(1)\,a^2(1)\,\{\beta_1(1)[\beta_1(1)\,\frac{\partial u_1(1)}{\partial x_1} + \beta_2(1)\,\frac{\partial u_1(1)}{\partial x_2}] \\
&\qquad + \beta_2(1)\,[\beta_1(1)\,\frac{\partial u_2(1)}{\partial x_1} + \beta_2(1)\,\frac{\partial u_2(1)}{\partial x_2}]\}\,\Delta t
\end{aligned}
\tag{3.24}
$$

$$2\,p(6) + [\rho(6)\,a(6)\,\beta_1(6) + \rho(2)\,a(2)\,\beta_1(2)]\,u_1(6)$$

$$+ [\rho(6)\,a(6)\,\beta_2(6) + \rho(2)\,a(2)\,\beta_2(2)]\,u_2(6)$$

$$+ \rho(6)\,a^2(6)\,\alpha_j(6)\,\alpha_i(6)\,\frac{\partial u_j(6)}{\partial x_i}\,\Delta t$$

$$= 2\,p(2) + [\rho(6)\,a(6)\,\beta_1(6) + \rho(2)\,a(2)\,\beta_1(2)]\,u_1(2)$$

$$+ [\rho(6)\,a(6)\,\beta_2(6) + \rho(2)\,a(2)\,\beta_2(2)]\,u_2(2)$$

$$- \rho(2)\,a^2(2)\,\{\alpha_1(2)\,[\alpha_1(2)\,\frac{\partial u_1(2)}{\partial x_1} + \alpha_2(2)\,\frac{\partial u_1(2)}{\partial x_2}]$$

$$+ \alpha_2(2)\,[\alpha_1(2)\,\frac{\partial u_2(2)}{\partial x_1} + \alpha_2(2)\,\frac{\partial u_2(2)}{\partial x_2}]\}\,\Delta t \qquad (3.25)$$

$$2\,p(6) - [\rho(6)\,a(6)\,\alpha_1(6) + \rho(3)\,a(3)\,\alpha_1(3)]\,u_1(6)$$

$$- [\rho(6)\,a(6)\,\alpha_2(6) + \rho(3)\,a(3)\,\alpha_2(3)]\,u_2(6)$$

$$+ \rho(6)\,a^2(6)\,\beta_j(6)\,\beta_i(6)\,\frac{\partial u_j(6)}{\partial x_i}\,\Delta t$$

$$= 2\,p(3) - [\rho(6)\,a(6)\,\alpha_1(6) + \rho(3)\,a(3)\,\alpha_1(3)]\,u_1(3)$$

$$- [\rho(6)\,a(6)\,\alpha_2(6) + \rho(3)\,a(3)\,\alpha_2(3)]\,u_2(3)$$

$$- \rho(3)\,a^2(3)\,\{\beta_1(3)\,[\beta_1(3)\,\frac{\partial u_1(3)}{\partial x_1} + \beta_2(3)\,\frac{\partial u_1(3)}{\partial x_2}]$$

$$+ \beta_2(3)\,[\beta_1(3)\,\frac{\partial u_2(3)}{\partial x_1} + \beta_2(3)\,\frac{\partial u_2(3)}{\partial x_2}]\}\,\Delta t \qquad (3.26)$$

$$2\,p(6) - [\rho(6)\,a(6)\,\beta_1(6) + \rho(4)\,a(4)\,\beta_1(4)]\,u_1(6)$$

$$- [\rho(6)\,a(6)\,\beta_2(6) + \rho(4)\,a(4)\,\beta_2(4)]\,u_2(6)$$

$$+ \rho(6)\,a^2(6)\,\alpha_j(6)\,\alpha_i(6)\,\frac{\partial u_j(6)}{\partial x_i}\,\Delta t$$

$$= 2\,p(4) - [\rho(6)\,a(6)\,\beta_1(6) + \rho(4)\,a(4)\,\beta_1(4)]\,u_1(4)$$

$$- [\rho(6)\,a(6)\,\beta_2(6) + \rho(4)\,a(4)\,\beta_2(4)]\,u_2(4)$$

$$- \rho(4)\,a^2(4)\,\{\alpha_1(4)\,[\alpha_1(4)\,\frac{\partial u_1(4)}{\partial x_1} + \alpha_2(4)\,\frac{\partial u_1(4)}{\partial x_2}]$$

$$+ \alpha_2(4)\,[\alpha_1(4)\,\frac{\partial u_2(4)}{\partial x_1} + \alpha_2(4)\,\frac{\partial u_2(4)}{\partial x_2}]\}\,\Delta t \qquad (3.27)$$

The finite-difference form of the noncharacteristic relation, Eq. 3.22, written along the particle path with unknowns at point (6) on the left side of the equation is

$$2\,p(6) + \rho(6)\,a^2(6)\,\alpha_j(6)\,\alpha_i(6)\,\frac{\partial u_j(6)}{\partial x_i}\,\Delta t$$

$$+ \rho(6)\,a^2(6)\,\beta_j(6)\,\beta_i(6)\,\frac{\partial u_j(6)}{\partial x_i}\,\Delta t$$

$$= 2\,p(5) - \rho(5)\,a^2(5)\,[\frac{\partial u_1(5)}{\partial x_1} + \frac{\partial u_2(5)}{\partial x_2}] \qquad (3.28)$$

Examination of Eqs. 3.24-3.28 reveals a total of five unknowns considered: $p(6)$, $u_1(6)$, $u_2(6)$, $\rho(6)a^2(6)\beta_j(6)\beta_i(6)\dfrac{\partial u_j(6)}{\partial x_i}\Delta t$, $\rho(6)a^2(6)\alpha_j(6)\alpha_i(6)\dfrac{\partial u_j(6)}{\partial x_i}\Delta t$. Therefore Eqs. 3.24-3.28 comprise a complete system of five nonlinear difference equations for the five unknowns. The system of equations is displayed below as a matrix equation with an abbreviated notation for the coefficients:

$$\begin{bmatrix} 2 & B_1 & C_1 & 0 & 1 \\ 2 & B_2 & C_2 & 1 & 0 \\ 2 & B_3 & C_3 & 0 & 1 \\ 2 & B_4 & C_4 & 1 & 0 \\ 2 & 0 & 0 & 1 & 1 \end{bmatrix} \begin{bmatrix} p(6) \\ u_1(6) \\ u_2(6) \\ \rho(6)\ a^2(6)\ \alpha_j(6)\ \alpha_i(6)\ \dfrac{\partial u_j(6)}{\partial x_i}\Delta t \\ \rho(6)\ a^2(6)\ \beta_j(6)\ \beta_i(6)\ \dfrac{\partial u_j(6)}{\partial x_i}\Delta t \end{bmatrix} = \begin{bmatrix} F_1 \\ F_2 \\ F_3 \\ F_4 \\ F_5 \end{bmatrix} \tag{3.29}$$

The last two unknowns, involving cross-derivatives of the velocity components at the solution point, are of no interest in the solution. These two terms are eliminated by taking appropriate linear combinations of the equations in Eq. 3.29, with the result

$$\begin{bmatrix} 0 & B_1-B_3 & C_1-C_3 \\ 0 & B_2-B_4 & C_2-C_4 \\ 4 & B_1+B_2+B_3+B_4 & C_1+C_2+C_3+C_4 \end{bmatrix} \begin{bmatrix} p(6) \\ u_1(6) \\ u_2(6) \end{bmatrix} = \begin{bmatrix} F_1-F_3 \\ F_2-F_4 \\ F_1+F_2+F_3+F_4-2F_5 \end{bmatrix} \tag{3.30}$$

Solution for the primative variables $u_1(6)$, $u_2(6)$, and $p(6)$ is easily obtained from Eq. 3.30.

Finally, the density, $\rho(6)$, is determined from the particle path compatibility relation, Eq. 2.32, which when put into finite-difference form and solved for $\rho(6)$ is

$$\rho(6) = 2[p(6) - p(5)]/[a^2(6) + a^2(5)] + \rho(5) \tag{3.31}$$

where the acoustic speed, a, is determined from Eq. 3.17.

E. Iteration Scheme

A predictor-corrector iterative scheme is used in the numerical solution. In the predictor step, the solution at point (6) is computed using estimates for the unknowns which appear in the coefficients of the difference equations. For this purpose, the values of the dependent variables at all points in the difference network are assigned the values at the solution point on the initial data surface. Subsequently, the solution is corrected using the predicted values of the dependent variables at point (6) and interpolated values of the dependent variables at the base points (1) through (5) in the

difference equations. The corrector step is repeated until successive values of the dependent variables at point (6) agree to within a specified tolerance. This technique yields a solution in which the local truncation error is third order in time step.

The reference vectors $\alpha_i(k)$, $\beta_i(k)$ $(k = 1,2,3,4)$ are determined relative to their assumed orientation at point (6) from Eqs. 3.14-3.20. Note that these relations do not depend on data at points in the difference network but are solely functions of the dependent variables and their derivatives at the solution point on the initial data surface. Hence, the reference vector calculations are performed first in the numerical algorithm and are not involved in the iterative part of the solution.

In each iteration step, the base points (1) through (5) are located using the direction equations, Eqs. 3.12 and 3.13. The values of the dependent variables, u_1, u_2, p, and ρ and the derivatives $\frac{\partial u_1}{\partial x_1}$, $\frac{\partial u_1}{\partial x_2}$, $\frac{\partial u_2}{\partial x_1}$, and $\frac{\partial u_2}{\partial x_2}$ at the base points in the initial data plane, as needed in the difference equations, Eqs. 3.24-3.28, are then evaluated using bivariate interpolations (Appendix H). Finally, the values of the dependent variables $u_1(6)$, $u_2(6)$, $p(6)$, and $\rho(6)$ are obtained from Eqs. 3.30 and 3.31.

F. Accuracy Studies

Studies were undertaken to determine the order of accuracy of the numerical method. Since rigorous analytical methods do not exist for determining the order of nonlinear difference schemes, the order of the truncation error and, hence, the order of accuracy of the method was estimated numerically.

The truncation error order was estimated by comparing the results of the method at different time increments with exact solutions for: (1) steady source flow, and (2) Prandtl-Meyer flow over a cylinder. Since these flows were steady, any change in the transient solution with time was attributed to round-off and truncation errors. To minimize round-off error, all check cases were computed to 16 significant digits.

In setting up the transient solution, a square cell of nine points was constructed in the flow field with the solution point at the midpoint of the cell. The grid spacing was determined by using the smallest spacing allowed by the Courant-Friedrichs-Lewy stability criterion for a given time increment (see Appendix D). The dependent variables at the cell points on the initial data surface were determined from the exact solutions for steady source flow and Prandtl-Meyer flow over a cylinder presented in Appendix E.

The order of the truncation error was determined by doubling the time increment and comparing the ratio of the

time increments raised to the assumed order of the method. The local truncation error in the numerical method was assumed to be third-order in time step; thus, if the time increment were doubled, the theoretical truncation error would grow by a factor of 8. The process of doubling the time increment is shown schematically in Figures 3.3 and 3.4 for the source flow and Prandtl-Meyer flow, respectively, where the cell points and the differential domains of dependence are shown for three time increments.

1. Source flow accuracy study

In the source flow accuracy study, the Mach number along the upstream circular arc with radius r_1 in Figure 3.3 was $M_1 = 1.2$, and the solution point was located as shown at $r/r_1 = 1.25$. The results of the study are presented in Table 3.1 in terms of percent error and relative error in the static pressure for three time increments. The results indicate that the order of the method is greater than the assumed second-order. Similar results were obtained for different orientations of the initial data cell in the flow field obtained by rotations about the solution point. The computed higher order accuracy compared to that assumed in the method is due to the relatively small property gradients which exist in this one-dimensional flow case.

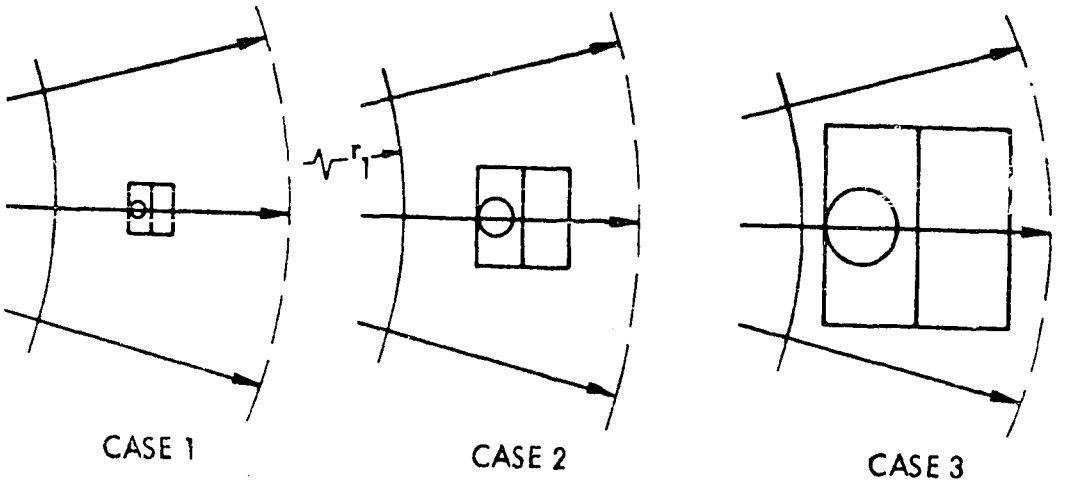

Figure 3.3. Steady source flow accuracy study

Different time increments showing grid point cell, differential domain of dependence, and upstream reference station, r_1. $M_1 = 1.2$; solution point location, $r/r_1 = 1.25$

Table 3.1. Results of steady source flow accuracy study

Case	(1)	(2)	(3)
Relative time increment	1	2	4
Error in static pressure (%)	0.0023	0.0331	0.6440
Relative error (ratio to case 1)	1	14.53	283.02
Theoretical relative error	1	8	64

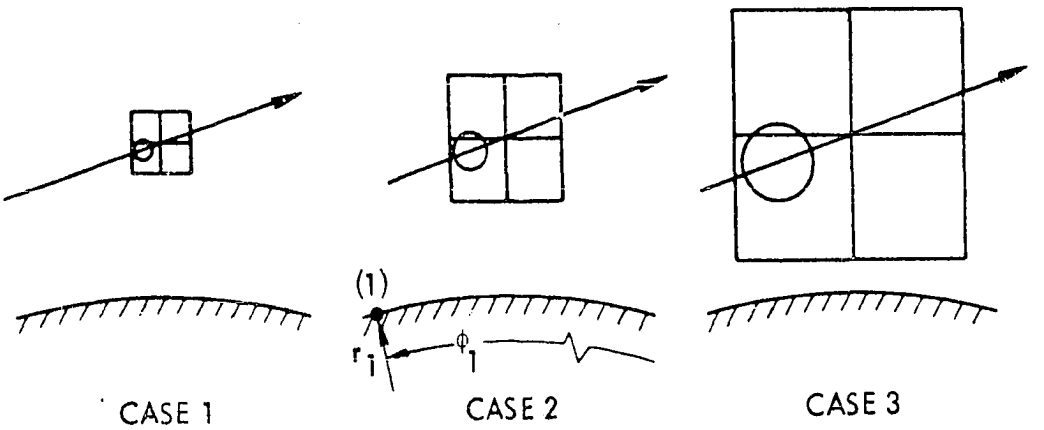

Figure 3.4. Prandtl-Meyer flow accuracy study

Different time increments showing grid point cell, differential domain of dependence, and cylinder surface. $M_1 = 1.2$, $\phi_1 = 3\pi/4$; solution point location, $r/r_1 = 1.25$, $\phi = \pi/2$

Table 3.2. Results of Prandtl-Meyer flow accuracy study

Case	(1)	(2)	(3)
Relative time increment	1	2	4
Error in static pressure (%)	0.0404	0.3213	5.4021
Relative error (ratio to case 1)	1	7.96	64.91
Theoretical relative error	1	8.00	64.00

2. Prandtl-Meyer flow accuracy study

Prandtl-Meyer flows have highly two-dimensional spatial character and, hence, provide a more severe test than source flows regarding the accuracy of the numerical method.

In the accuracy study for Prandtl-Meyer flow over a cylinder, the Mach number at an upstream reference point (1) on the cylinder with polar angle $\phi_1 = 3\pi/4$ was $M_1 = 1.2$ (see Appendix E for a description of reference point (1) location). The solution point was located, as shown in Figure 3.4, at $r/r_1 = 1.25$, $\phi = \pi/2$, where r_1 is the radius of the cylinder. The results of the accuracy study are presented in Table 3.2. In this example, the results indicate third-order truncation error. Again, comparable results were obtained with the initial data cell rotated to various positions in the flow field about the solution point.

G. Numerical Stability Studies

In the numerical solution of hyperbolic systems of partial differential equations, the possibility of numerical instability always exists. Numerical instability refers to the unbounded growth of errors in the numerical solution. In Appendix D, two stability criterion; (1) the Courant-Friedrichs-Lewy criterion, and (2) the von Neumann criterion are applied to the numerical method.

The Courant-Friedrichs-Lewy (CFL) stability criterion states that the differential domain of dependence must lie within the convex hull of the difference scheme. In the present scheme, the convex hull is the outer boundary of the nine point cell, shown in Figure 3.2, used for interpolation in the initial data plane. The CFL criterion limits the maximum allowable time step which can be taken between solution planes and is a necessary condition for stability which must be satisfied at all solution points.

The numerical scheme was found to be stable by the von Neumann criterion which states that a numerical scheme is stable only if there is a finite limit to the amplification of any Fourier component of the initial data. This condition requires that the spectral radii, $\rho(A)$, of the amplification matrix, A, for the difference equations satisfy the inequality

$$\rho(A) \leq 1 + 0(\Delta t) \tag{3.32}$$

for all possible combinations of Fourier components of the initial data. The von Neumann criterion is a sufficient condition for stability of linear difference equations. For the case of nonlinear difference equations, the sufficiency of this condition is not guaranteed; however, the approach taken is to linearize the equations and to apply the same criterion locally.

IV. CASCADE BOUNDARY POINT NUMERICAL PROCEDURES

A. General

Developed next are the numerical procedures for calculation at boundary points in the solution of cascade flows. These procedures, used for solution at blade surface boundary points, upstream boundary points, downstream boundary points and blade trailing-edge points, are special adaptations of the interior point calculation developed in Chapter III. In the following discussions, a basic understanding of cascade geometry and aerodynamics on the part of the reader is assumed; see Glassman (62).

The cascade configuration of interest consists of an infinite number of blades. Identical flow fields exist in each blade passage, and the flows upstream and downstream of the cascade are periodic with a period equal to one blade space. Accordingly, the cascade flow problem is solved by considering the flow through one blade passage with periodic flow boundary conditions imposed upstream and downstream of the cascade.

The cascade solution grid, shown in Figure 4.1, consists of uniformly spaced parallel panels of grid points in the x_1-direction. The bounding panels A-B upstream and G-H downstream are located sufficiently far from the cascade that uniform distributions of flow properties along these boundaries may be assumed. The spacing of panels is selected such that the leading and trailing edge planes of the cascade, C-D and

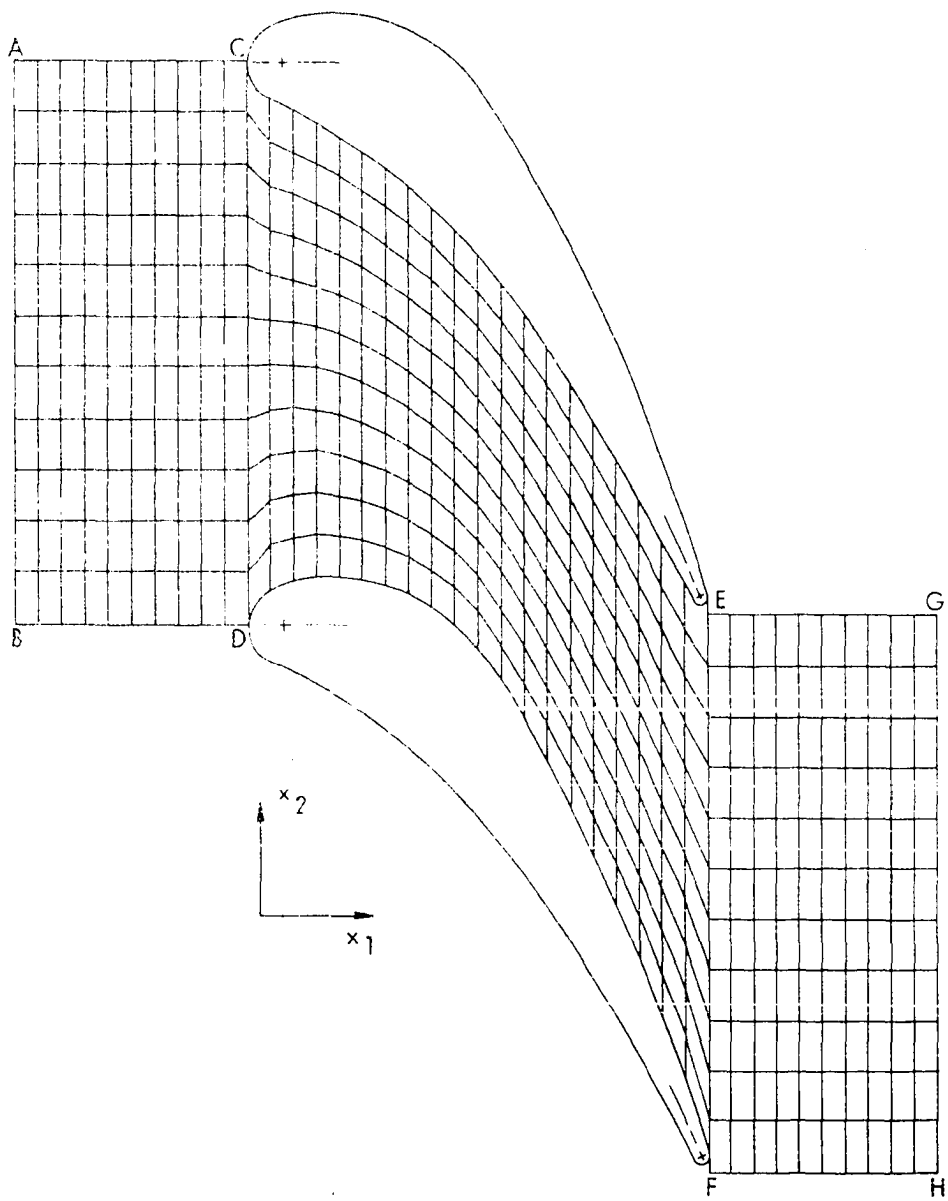

Figure 4.1. Cascade solution grid

E-F, respectively, are constant-x_1 panels. Points C and D in Figure 4.1 are points of tangency of the blade profiles and the cascade leading edge plane; points E and F are the intersections of the blade mean camber line and the trailing edge plane of the cascade. Uniform spacing of grid points along constant-x_1 panels is assumed between bounding constant-x_2 panels A-C, B-D upstream and F-H, E-G downstream, and between the blade surfaces inside the blade passage.

The boundary point calculation schemes were developed with the objective of modeling the transient phenomena for developing flow in cascades. The inviscid fluid assumption is used in body point calculations at points on the blade profile, i.e., the flow is assumed tangent to the blade surface. In the upstream boundary point calculation, specification of the stagnation state and u_2 velocity component (whirl) distribution along the boundary A-B in Figure 4.1 is assumed. This calculation can be applied to either subsonic inlet flow, or supersonic inlet flow with subsonic axial velocity component, u_1. In the downstream boundary point calculation, the static pressure distribution along the boundary G-H in Figure 4.1 is assumed known. This condition sets the flow through the cascade analogous to the physical situation in which a throttle valve is positioned downstream of the cascade. The blade trailing edge point calculation is applied at points E and F in Figure 4.1 and, as described later, is based on an approximate model of the blade wake.

The cascade flow periodicity requirement for points upstream and downstream of the cascade is enforced along the constant-x_2 panels A-C, B-D, E-G, and F-H in Figure 4.1. Calculations at grid points along these panels (excluding the endpoints) employ the interior point scheme developed in Chapter III. The periodic flow condition, however, requires special treatment of the grid point cells used for initial data interpolations; discussion of these cells is deferred until Chapter V where the overall solution algorithm is presented.

In all the boundary point calculation schemes, the differential domain of dependence lies partially outside the solution space with at least one of the bicharacteristics in the usual interior point scheme missing. This results in fewer compatibility relations available for solution for the dependent variables u_1, u_2, p, and ρ at the boundary points. Solutions at the boundary points are obtained, therefore, by supplementing the compatibility relations with the specified boundary conditions and orienting the reference vectors α_i, β_i at the solution point to position particular bicharacteristics in the solution space.

In the following discussions of the boundary point schemes, only the solution of the compatibility relations and the noncharacteristic relation for the dependent variables u_1, u_2, p, and ρ is covered. Base points are located in the same manner as the interior point scheme using the particle path direction

equation, Eq. 3.12, and the appropriate forms of the bicharacteristic direction equation, Eq. 3.13. Also reference vectors α_i, β_i at bicharacteristic base points are determined from Eqs. 3.14-3.20. The characteristic network point numbering system is the same as in the interior point scheme with bicharacteristic base points (1), (2), (3), and (4) corresponding to the parameterizations $\theta = 0$, $\pi/2$, π, and $3\pi/2$, respectively; the particle path base point is again point (5), and the solution point is point (6).

Finally, the perfect gas assumption was used in the development of the upstream boundary point calculation. This assumption was not needed in the development of the remaining boundary point calculations. However, in the actual cascade flows investigated, a perfect gas was assumed.

B. Body Point Calculation

The solution point (6) of the body point difference network lies in the body surface (blade profile), as shown in Figure 4.2. Three bicharacteristics and the particle path, with base points (1), (2), (3), and (5) in the initial data surface, are used in the finite-difference solution. At the solution point (6), the reference vectors $\alpha_i(6)$, $\beta_i(6)$ are oriented with $\beta_i(6)$ assigned the direction of the body surface inward normal $n_i(6)$ to give three bicharacteristic base points in the solution space.

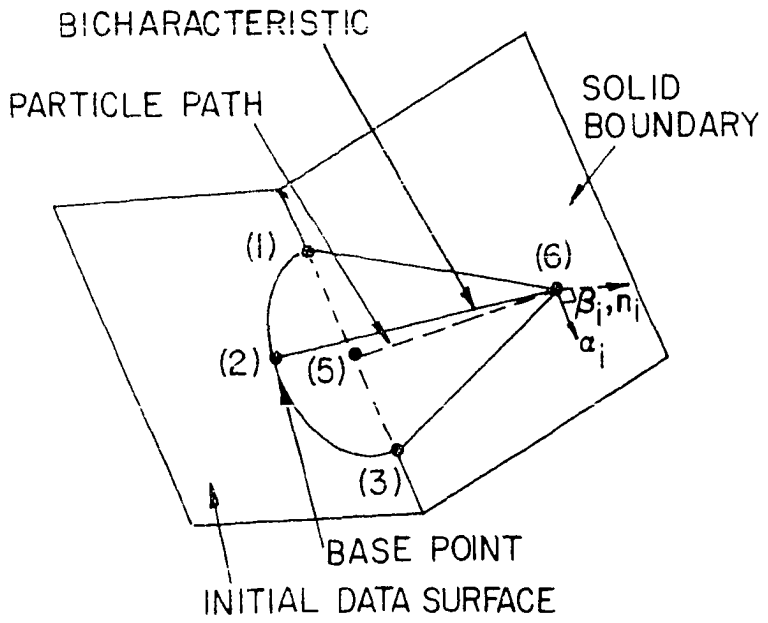

a. View showing bicharacteristics, particle path, solid boundary, and initial data surface

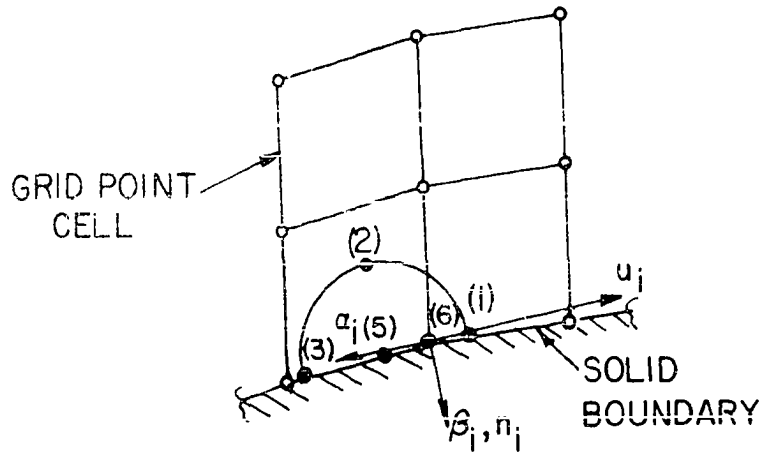

b. Projection onto initial data surface showing differential domain of dependence and grid point cell

Figure 4.2. Body point network

The system of difference equations used to determine the dependent variables $u_1(6)$, $u_2(6)$ and $p(6)$ includes the three wave surface compatibility relations, Eqs. 3.24-3.26, and the noncharacteristic relation, Eq. 3.28. The relation needed in addition to these is the flow tangency condition at the solution point (6), i.e.,

$$u_i(6)n_i(6) = 0 \tag{4.1}$$

This system of equations can be written as a matrix equation, similar to Eq. 3.29, as

$$\begin{bmatrix} 2 & B_1 & C_1 & 0 & 1 \\ 2 & B_2 & C_2 & 1 & 0 \\ 2 & B_3 & C_3 & 0 & 1 \\ 0 & B_4 & C_4 & 0 & 0 \\ 2 & 0 & 0 & 1 & 1 \end{bmatrix} \begin{bmatrix} p(6) \\ u_1(6) \\ u_2(6) \\ \rho(6)\ a^2(6)\ \alpha_j(6)\ \alpha_i(6)\ \dfrac{\partial u_j(6)}{\partial x_i}\Delta t \\ \rho(6)\ a^2(6)\ \beta_j(6)\ \beta_i(6)\ \dfrac{\partial u_j(6)}{\partial x_i}\Delta t \end{bmatrix} = \begin{bmatrix} F_1 \\ F_2 \\ F_3 \\ 0 \\ F_5 \end{bmatrix} \tag{4.2}$$

in which the fourth equation is now the flow tangency condition. Elimination of the last two unknowns, involving derivatives at the solution point, from Eq. 4.2 yields the system

$$\begin{bmatrix} 0 & B_1-B_3 & C_1-C_3 \\ 4 & B_1+2B_2+B_3 & C_1+2C_2+C_3 \\ 0 & B_4 & C_4 \end{bmatrix} \begin{bmatrix} p(6) \\ u_1(6) \\ u_2(6) \end{bmatrix} = \begin{bmatrix} F_1-F_3 \\ F_1+2F_2+F_3-2F_5 \\ 0 \end{bmatrix} \qquad (4.3)$$

From Eq. 4.3, the solutions for $p(6)$, $u_1(6)$, and $u_2(6)$ can easily be obtained. Density, $\rho(6)$, is obtained from the isentropic relation, Eq. 3.31, written along the particle path.

C. Upstream Boundary Point Calculation

The upstream boundary point calculation is employed along the panel A-B in Figure 4.1. In the difference network, consistent with the body point calculation, the reference vector pair $\alpha_i(6)$, $\beta_i(6)$ is oriented with $\beta_i(6)$ along the outward normal, $n_i(6)$, to the solution space, as shown in Figure 4.3.

In the cascade flow applications investigated here, subsonic inlet flow is assumed. In this case, the differential domain of dependence for point (6) lies partially upstream of the inlet boundary, and the particle path projects outside the solution space, as shown in Figure 4.3. Point (2) in the usual interior point scheme is the only base point lying inside the solution space, and, therefore, only one wave surface compatibility relation is available in the solution. The remaining conditions needed are supplied as boundary conditions.

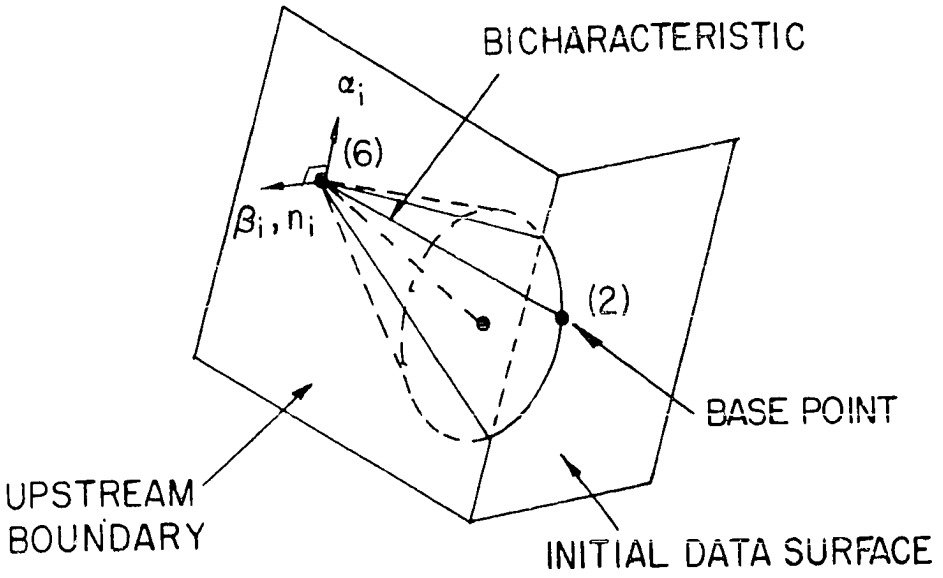

a. View showing bicharacteristics, particle path, upstream boundary, and initial data surface

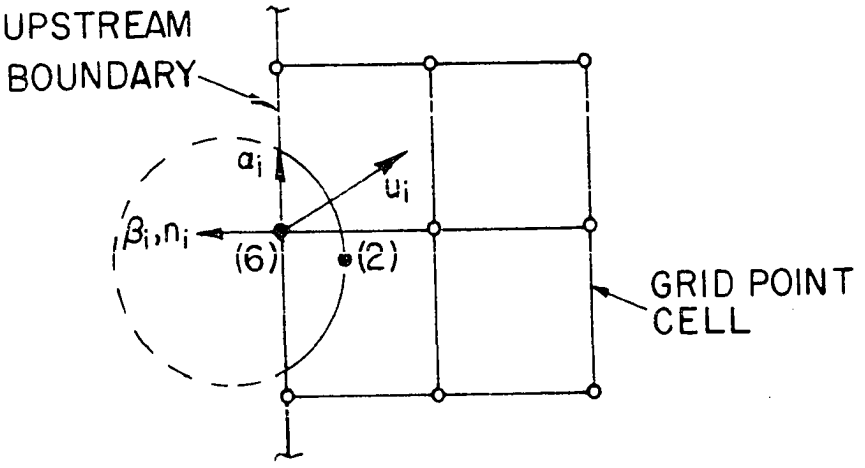

b. Projection onto initial data surface showing differential domain of dependence and grid point cell

Figure 4.3. Upstream boundary point network

In the present scheme, it is assumed that the stagnation pressure, p_0, stagnation temperature, T_0, and the u_2 velocity component distributions along the upstream boundary are given. Thus, the remaining primative variables $u_1(6)$, $p(6)$, $\rho(6)$ are determined in the solution.

The applicable wave surface compatibility relation for the single bicharacteristic with base point (2) is Eq. 3.25. Substitution of $\alpha_i(6) = \{0,1\}$, and $\beta_i(6) = \{-1,0\}$ into Eq. 3.25, followed by rearrangement to put unknowns on the left side of the equation yields

$$
\begin{aligned}
&2\,p(6) + [\rho(2)\,a(2)\,\beta_1(2) - \rho(6)\,a(6)]\,u_1(6) \\
&= 2\,p(2) + [\rho(2)\,a(2)\,\beta_1(2) - \rho(6)\,a(6)]\,u_1(2) \\
&\quad + \rho(2)\,a(2)\,\beta_2(2)[u_2(2) - u_2(6)] - \rho(6)\,a^2(6)\,\frac{\partial u_2(6)}{\partial x_2}\,\Delta t \\
&\quad - \rho(2)\,a^2(2)\,\{\alpha_1(2)[\alpha_1(2)\,\frac{\partial u_1(2)}{\partial x_1} + \alpha_2(2)\,\frac{\partial u_1(2)}{\partial x_2}] \\
&\quad + \alpha_2(2)[\alpha_1(2)\,\frac{\partial u_2(2)}{\partial x_1} + \alpha_2(2)\,\frac{\partial u_2(2)}{\partial x_2}]\}\,\Delta t \qquad (4.4)
\end{aligned}
$$

The derivative $\frac{\partial u_2(6)}{\partial x_2}$ in Eq. 4.4 is treated as a known quantity on the right side of the equation and is obtained from the given distribution of u_2 along the upstream boundary.

From the definitions of stagnation pressure and temperature, and acoustic speed, we are able to write for a perfect gas that

$$a_0^2(6) = a^2(6) + \frac{\gamma-1}{2}\left[u_1^2(6) + u_2^2(6)\right] \tag{4.5}$$

and

$$p_0(6) = p(6)\left[1 + \frac{\gamma-1}{2}\left(\frac{u_1^2(6) + u_2^2(6)}{a^2(6)}\right)\right]^{\frac{\gamma}{\gamma-1}} \tag{4.6}$$

In Eq. 4.7, $a_0(6)$ is the acoustic speed based on stagnation temperature. Both $p_0(6)$ and $a_0(6)$ are known from the given inlet stagnation conditions. Density, $\rho(6)$, is found from the perfect gas relation

$$\rho(6) = \frac{\gamma p(6)}{a^2(6)} \tag{4.7}$$

Equations 4.4, 4.5, and 4.6 comprise a system of three equations for the unknowns $u_1(6)$, $a(6)$, and $p(6)$.

Alternative to specification of inlet u_2 distribution, the distribution of inlet flow angle (i.e., the ratio u_2/u_1) has been frequently prescribed in cascade flow solutions (ref. 9). However, in the case of finite location of the upstream boundary, it appears more reasonable to prescribe the whirl velocity (u_2) distribution, and to solve for the resultant axial velocity (u_1) distribution. Also, in the case of supersonic flow with subsonic axial velocity component, specification of inlet flow angle would violate the unique incidence principle (ref. 63).

Finally, for supersonic inlet flow with supersonic axial velocity component the differential domain of dependence lies entirely upstream of the boundary. In this case no boundary points can be computed, and the distributions along the boundary of all the dependent variables u_1, u_2, p and ρ must be specified.

D. Downstream Boundary Point Calculation

The downstream flow boundary is specified as the panel G-H in Figure 4.1. At a solution point (6) on the boundary, reference vectors $\alpha_i(6)$, $\beta_i(6)$ are orientated with $\beta_i(6)$ along the outer normal to the solution space.

The exit flow condition of interest is that with subsonic axial velocity component. As shown in Figure 4.4, the domain of dependence for the solution point (6) positions itself with base points (1), (2), (3), and (5) within the solution space upstream of the boundary. With one bicharacteristic of the usual interior point scheme missing, a boundary condition must be specified. Hence, in the downstream boundary point calculation the distribution of static pressure along the downstream boundary is assumed known.

The compatibility relations are Eqs. 3.24-3.26, and the noncharacteristic relation is Eq. 3.28. Rewriting Eqs. 3.24-3.26 with $\alpha_i(6) = \{0,-1\}$, $\beta_i(6) = \{1,0\}$, and rearranging to put the unknowns on the left side of the equations, we obtain

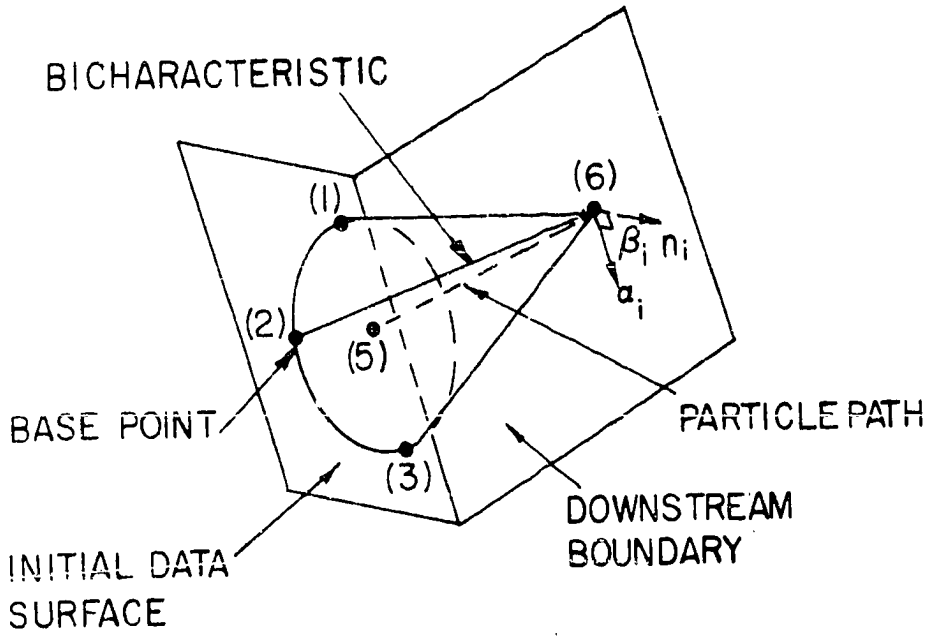

a. View showing bicharacteristics, particle path, downstream boundary, and initial data surface

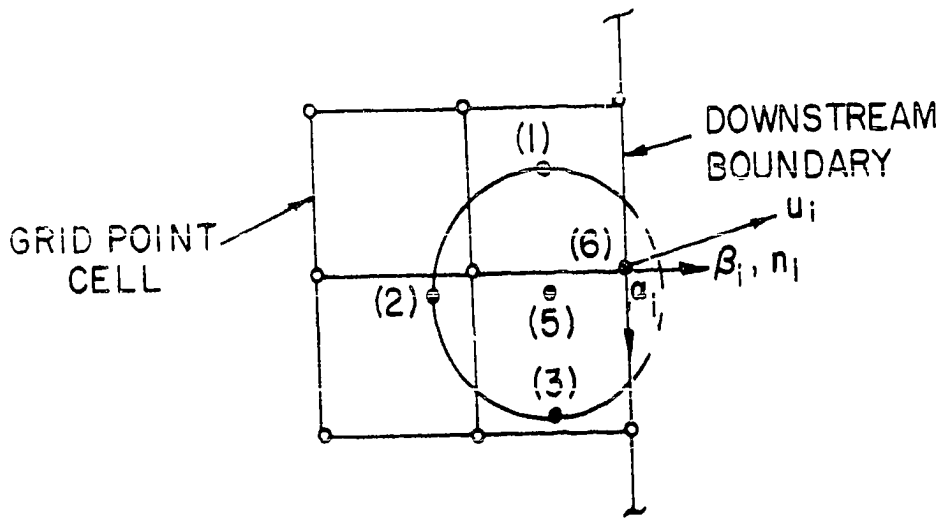

b. Projection onto initial data surface showing differential domain of dependence and grid point cell

Figure 4.4. Downstream boundary point network

$$[\rho(1)\ a(1)\ \alpha_1(1)]\ u_1(6) + [\rho(1)\ a(1)\ \alpha_2(1) - \rho(6)\ a(6)]\ u_2(6)$$

$$+ \rho(6)\ a^2(6)\ \beta_j(6)\ \beta_i(6)\ \frac{\partial u_j(6)}{\partial x_i}\ \Delta t = 2\ [p(1) - p(6)]$$

$$+ [\rho(1)\ a(1)\ \alpha_1(1)]\ u_1(1) + [\rho(1)\ a(1)\ \alpha_2(1) - \rho(6)\ a(6)]\ u_2(1)$$

$$- \rho(1)\ a^2(1)\{\beta_1(1)[\beta_1(1)\ \frac{\partial u_1(1)}{\partial x_1} + \beta_2(1)\ \frac{\partial u_1(1)}{\partial x_2}]$$

$$+ \beta_2(1)[\beta_1(1)\ \frac{\partial u_2(1)}{\partial x_1} + \beta_2(1)\ \frac{\partial u_2(1)}{\partial x_2}]\}\Delta t \qquad (4.8)$$

$$[\rho(6)\ a(6) + \rho(2)\ a(2)\ \beta_1(2)]\ u_1(6) + [\rho(2)\ a(2)\ \beta_2(2)]\ u_2(6)$$

$$+ \rho(6)\ a^2(6)\ \alpha_j(6)\ \alpha_i(6)\ \frac{\partial u_j(6)}{\partial x_i}\ \Delta t = 2\ [p(2) - p(6)]$$

$$+ [\rho(6)\ a(6) + \rho(2)\ a(2)\ \beta_1(2)]\ u_1(2) + [\rho(2)\ a(2)\ \beta_2(2)]\ u_2(2)$$

$$- \rho(2)\ a^2(2)\{\alpha_1(2)[\alpha_1(2)\ \frac{\partial u_1(2)}{\partial x_i} + \alpha_2(2)\ \frac{\partial u_1(2)}{\partial x_2}]$$

$$+ \alpha_2(2)[\alpha_1(2)\ \frac{\partial u_2(2)}{\partial x_1} + \alpha_2(2)\ \frac{\partial u_2(2)}{\partial x_2}]\}\ \Delta t \qquad (4.9)$$

$$- [\rho(3)\ a(3)\ \alpha_1(3)]\ u_1(6) - [\rho(3)\ a(3)\ \alpha_2(3) - \rho(6)\ a(6)]\ u_2(6)$$

$$+ \rho(6)\ a^2(6)\ \beta_j(6)\ \beta_i(6)\ \frac{\partial u_j(6)}{\partial x_i}\ \Delta t = 2\ [p(3) - p(6)]$$

$$- [\rho(3)\ a(3)\ \alpha_1(3)]\ u_1(3) - [\rho(3)\ a(3)\ \alpha_2(3) - \rho(6)\ a(6)]\ u_2(3)$$

$$- \rho(3)\ a^2(3)\{\beta_1(3)\ [\beta_1(3)\ \frac{\partial u_1(3)}{\partial x_1} + \beta_2(3)\ \frac{\partial u_1(3)}{\partial x_2}]$$

$$+ \beta_2(3)\ [\beta_1(3)\ \frac{\partial u_2(3)}{\partial x_1} + \beta_2(3)\ \frac{\partial u_2(3)}{\partial x_2}]\}\ \Delta t \qquad (4.10)$$

Equation 3.28 becomes

$$\rho(6)\ a^2(6)\ \alpha_j(6)\ \alpha_i(6)\ \frac{\partial u_j(6)}{\partial x_i}\ \Delta t$$

$$+ \rho(6)\ a^2(6)\ \beta_j(6)\ \beta_i(6)\ \frac{\partial u_j(6)}{\partial x_i}\ \Delta t$$

$$= 2\ [p(5) - p(6)] - \rho(5)\ a^2(5)\ [\frac{\partial u_1(5)}{\partial x_1} + \frac{\partial u_2(5)}{\partial x_2}] \qquad (4.11)$$

The system of Eqs. 4.8-4.11 rewritten as a matrix equation, again similar to Eq. 3.29, is

$$\begin{bmatrix} B_1 & C_1 & 0 & 1 \\ B_2 & C_2 & 1 & 0 \\ B_3 & C_3 & 0 & 1 \\ 0 & 0 & 1 & 1 \end{bmatrix} \begin{bmatrix} u_1(6) \\ u_2(6) \\ \rho(6)\ a^2(6)\ \alpha_j(6)\ \alpha_i(6)\ \dfrac{\partial u_j(6)}{\partial x_i}\ \Delta t \\ \rho(6)\ a^2(6)\ \beta_j(6)\ \beta_i(6)\ \dfrac{\partial u_j(6)}{\partial x_i}\ \Delta t \end{bmatrix} = \begin{bmatrix} F_1 \\ F_2 \\ F_3 \\ F_5 \end{bmatrix} \tag{4.12}$$

Two equations can be obtained from Eq. 4.12

$$\begin{bmatrix} B_1-B_3 & C_1-C_3 \\ B_1+2B_2+B_3 & C_1+2C_2+C_3 \end{bmatrix} \begin{bmatrix} u_1(6) \\ u_2(6) \end{bmatrix} = \begin{bmatrix} F_1-F_3 \\ F_1+2F_2+F_3-2F_5 \end{bmatrix} \tag{4.13}$$

which can be easily solved for $u_1(6)$, $u_2(6)$. Density $\rho(6)$ is found from Eq. 3.31.

In the case of supersonic exit flow with supersonic axial velocity component u_1, the domain of dependence lies entirely upstream of the downstream boundary. Hence, the distribution of static pressure cannot be specified, and the downstream boundary point calculation becomes simply the interior point calculation.

E. Trailing Edge Boundary Point Calculation

The role of viscosity cannot be ignored in the solution of cascade flows. In the real flow, boundary layers grow along the pressure and suction surfaces of the blades and coalesce at

the trailing edge to form the blade wakes. It is precisely the shedding of the blade surface boundary layers at the trailing edge that sets the circulation and thus the loading on the blades. A steady, inviscid flow analysis in which no accounting is made for the real flow effects at the trailing edge would yield simply the zero lift solution.

The classical criterion used to set the steady circulation on lifting blades or airfoils is the Kutta condition (see ref. 64). The Kutta condition, developed from experimental observations, states that the circulation for the flow past an airfoil is of strength just sufficient to cause the flow to leave the airfoil smoothly at the trailing edge. For the academic case of blades with cusped trailing edges, the Kutta condition requires the velocities on the pressure and suction surfaces to be equal at the trailing edge point. For real blade profiles with rounded trailing edges, the Kutta condition is generally imposed by setting the position of the stagnation point on the blade surface in the trailing edge region according to some additional criteria (see ref. 65). Unfortunately, no accepted method based on a universal model or correlation of the trailing edge flow is available to determine the location of the stagnation point.

The following discussion outlines the blade trailing edge calculation used in the present method. The scheme is based on an approximate model of the blade wake in steady flow. As noted

before, the trailing edge point (points E and F in Figure 4.1) is located at the intersection of the blade mean camber line and the trailing edge plane of the cascade. This particular location was selected since it approximates the midpoint of the wake in the trailing edge plane. The flow direction at this point is taken as the direction of the blade mean camber line at the trailing edge, as shown in Figure 4.5.

The blade trailing edge point calculation is similar to the body point scheme. The difference network, shown in Figure 4.5, involves three bicharacteristics with base points (1), (2), (3) and the particle path with base point (5). The reference vectors $\alpha_i(6)$, $\beta_i(6)$ are oriented with $\alpha_i(6)$ directed along the trailing edge plane of the cascade. With this particular orientation of the reference vectors, the solution at point (6) depends on initial data on both sides of the blade surface as indicated by the locations of the bicharacteristic base points in Figure 4.5. The system of difference equations for the dependent variables $u_1(6)$, $u_2(6)$, $p(6)$ is given in Eq. 4.3 where now the vector $n_i(6)$ satisfying Eq. 4.1, and shown in Figure 4.5, is the unit normal to the blade mean camber line at the trailing edge. Density $\rho(6)$ is obtained from Eq. 3.31.

In the wake model, it is assumed that the flow separates from the blade at the points of tangency of the blade pressure and suction surfaces and the trailing edge circle. The flow

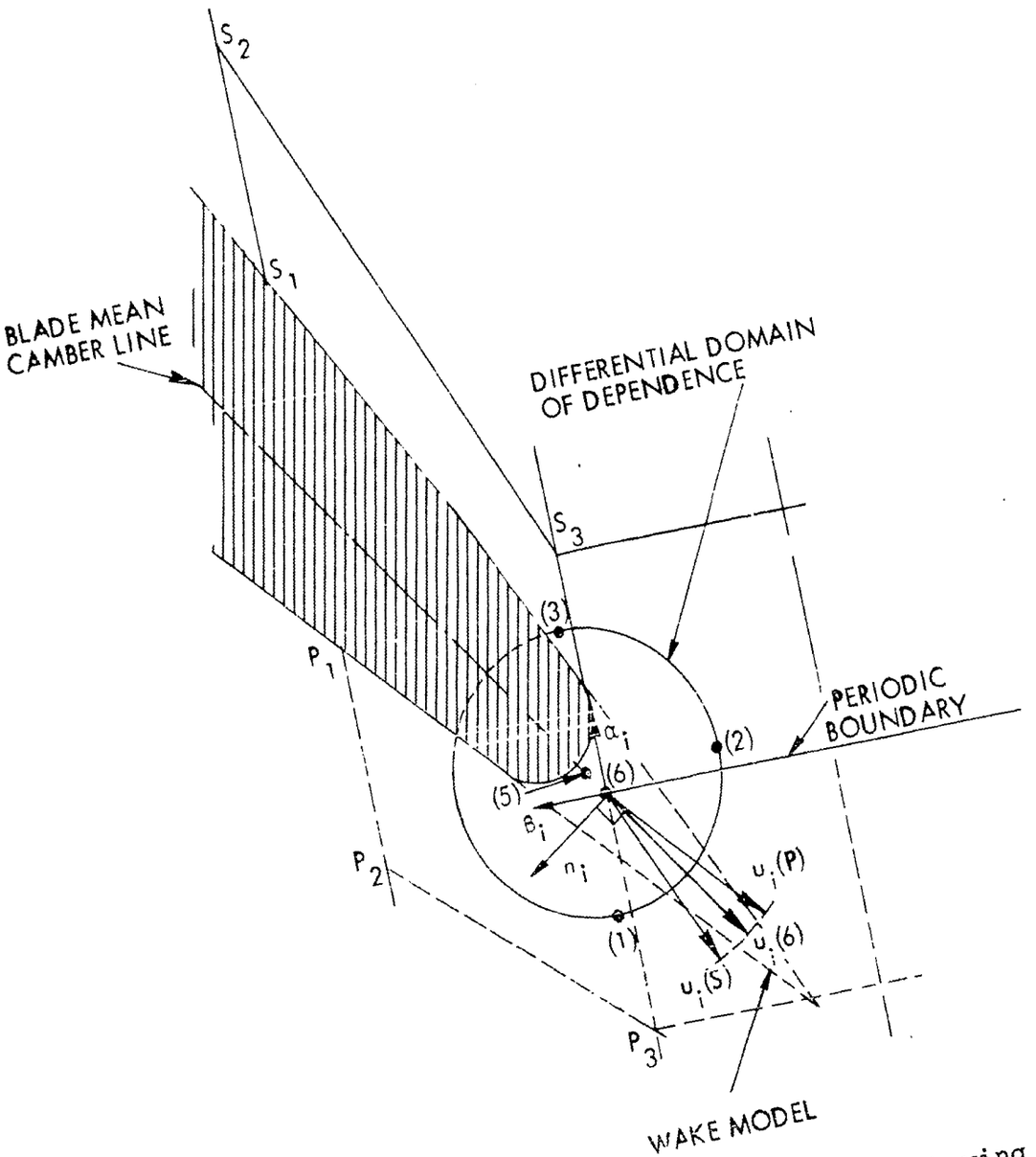

Figure 4.5. Blade trailing-edge point network showing differential domain of dependence, wake model, and periodic boundary

directions at these points, shown as dashed lines in Figure 4.5, are tangent to the blade surfaces. It is also assumed that the pressure, density, and magnitude of velocity do not vary across the wake in the trailing edge plane. The variation of velocity across the wake is shown in Figure 4.5 with $u_i(P)$ the velocity on the pressure side, and $u_i(S)$ the velocity on the suction side. Following the solution at point (6), the velocity vectors $u_i(P)$ and $u_i(S)$ are obtained by simply rotating $u_i(6)$, as shown in Figure 4.5. Next, the finite thickness of the wake is neglected, and the vectors $u_i(6)$, $u_i(P)$, and $u_i(S)$ are assumed to pass through point (6). The variation in flow angle through the wake is accounted for only in the flow solutions at points S_1, S_2, S_3, P_1, P_2, P_3, shown in Figure 4.5. The solution data $p(6)$ and $\rho(6)$ along with $u_i(S)$ or $u_i(P)$ are used in the initial data plane for the solutions at the points just noted. That is, the interpolation polynomials in the flow solutions at points S_1, S_2, and S_3 incorporate $u_i(S)$ at point (6) in the grid point cells; the interpolation polynomials in the flow solutions at points P_1, P_2, and P_3 incorporate $u_i(P)$ at point (6) in the grid point cells.

F. Closure

The body point, upstream boundary point, and downstream boundary point calculations were tested using simple one-

dimensional unsteady flow examples. Three examples of transient duct flows were solved, and the results of these solutions are presented in Appendix F. Where available, the results of other solution methods were used for comparison. The comparisons with the computed results indicate that the boundary point schemes yield accurate transient and asymptotic steady state solutions.

V. OVERALL NUMERICAL ALGORITHM FOR SOLUTION OF CASCADE FLOWS

Essential aspects of the overall numerical algorithm for solution of steady cascade flows are discussed. The overall algorithm consists of the repetitive application of the interior and boundary point calculations in successive time planes over the cascade grid, with the solution starting from prescribed data at grid points in the initial data plane. The solution is advanced in time with the steady state boundary conditions imposed until the asymptotic steady state solution is obtained.

A. Normalized Variables

Steady cascade flows are computed by applying steady inlet stagnation property and whirl velocity distributions along the upstream boundary of the cascade solution grid, and steady discharge static pressure distributions along the downstream boundary. If, in addition, the imposed distributions of stagnation pressure and density are uniform along the upstream boundary, it is convenient to define normalized (primed) dependent variables

$$u_1' = \frac{u_1}{\left[\frac{p_{01}}{\rho_{01}}\right]^{\frac{1}{2}}} \tag{5.1}$$

$$u_2' = \frac{u_2}{\left[\frac{p_{01}}{\rho_{01}}\right]^{\frac{1}{2}}} \tag{5.2}$$

$$p' = \frac{p}{p_{01}} \tag{5.3}$$

$$\rho' = \frac{\rho}{\rho_{01}} \tag{5.4}$$

where p_{01} and ρ_{01} are the upstream stagnation pressure and density, respectively. Use of the normalized variables yields steady state solutions independent of the values of the upstream stagnation state properties. Also, the upstream stagnation pressure and density become simply

$$p_{01}' = 1.0 \tag{5.5}$$

$$\rho_{01}' = 1.0 \tag{5.6}$$

B. Initial Conditions

The values of the four dependent variables u_1', u_2', p' and ρ' must be specified at all grid points in the initial data plane. For this purpose, any reasonable distributions of the variables consistent with the blade surface tangent flow condition may be used. In the cascade flow solutions reported in Chapter VI, zero upstream whirl velocity component was

specified. In this case it was convenient to specify the upstream stagnation conditions throughout the flow field, i.e.

$$u_1' = 0.0 \tag{5.7}$$

$$u_2' = 0.0 \tag{5.8}$$

$$p' = 1.0 \tag{5.9}$$

$$\rho' = 1.0 \tag{5.10}$$

and to start the flow by imposing uniform steady downstream pressure, p_2', along the downstream boundary. The resulting transient solution is similar to the physical situation in which a valve is instantaneously opened downstream of the cascade.

C. Initial Data Cells

Bivariate interpolating polynomials (see Appendix H) are used to determine initial data (u_1', u_2', p', ρ') at base points in the interior and boundary point characteristic networks. The polynomials locally fit the initial data at nine grid points consisting of the solution point on the initial data plane and eight neighboring points. Thus, a cell of nine points is assigned to each grid point for construction of interpolating polynomials. Typical cells are shown in Figure 5.1.

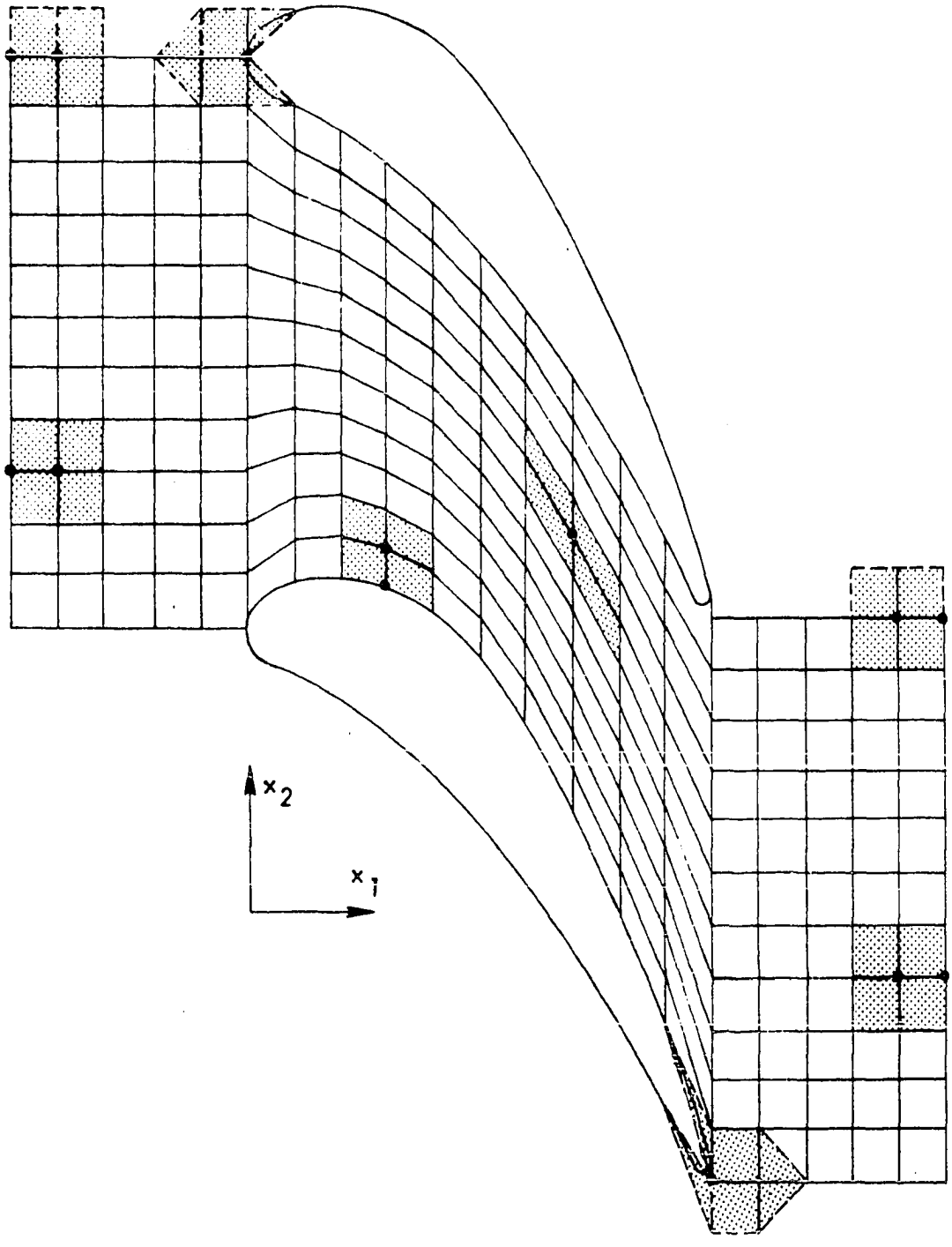

Figure 5.1. Cascade solution grid showing typical grid point cells

The assignment of cell points is based on the order of points in a rectangular grid point stencil. Each point in the solution grid is identified by indices I, J, with I taking successive integer values for constant-x_1 panels starting with I = 1 on the upstream boundary. The index J takes values corresponding to the point number along each constant-x_1 panel starting with J = 1 on the lower boundary of the cascade grid.

The nine point cell for an interior grid point consists of the point and eight neighboring points in the grid point stencil (I,J). Interior point cells are illustrated in Figure 5.1 where dots indicate the interior grid points considered, and the shaded areas cover the corresponding cells. As shown in Figure 5.1, this scheme results in distorted cells within the blade passage. This distortion of the cells was found to have negligible effect on the accuracy of the interpolating polynomials.

Boundary points along the upstream and downstream boundaries are assigned the same cells as the adjacent interior points along constant-x_2 panels, again as indicated in Figure 5.1. Also, as can be seen, blade surface boundary points (excluding the leading and trailing edge points) are assigned the same cells as the adjacent interior points along constant-x_1 panels.

The periodic flow requirement for points upstream and downstream of the cascade is enforced along the bounding constant-x_2 panels (periodic boundaries) by proper assignment

of cell points and initial data. As indicated in Figure 5.1, a panel of pseudo grid points is added outside the solution space along the periodic boundaries. These pseudo points are located one mesh spacing Δx_2 from the periodic boundaries. The grid point cells for points along the periodic boundaries (excluding the endpoints of the boundaries) consist of the point on the boundary and the eight nearest neighbors. Also, for cell construction at the leading and trailing edge points, pseudo blade surface points are added outside the solution space along the first constant-x_1 panel inside the blade passage. The cells for the leading and trailing edge points are constructed as shown in Figure 5.1 with three of the nine points on the blade surface.

Data at all pseudo points are set equal to the corresponding data at grid points lying one blade pitch from the points in the x_2 direction.

D. Time Step Regulation

The time increment between successive solution planes is regulated such that the Courant-Fredrichs-Lewy (CFL) stability criterion is satisfied at all grid points. According to Equation 13.3 the maximum allowable time step at each point is a function of the local velocity and acoustic speed and the minimum distance to the convex hull of the difference scheme. Equation 13.3 is used to calculate a maximum time step at each

mesh point, and the minimum of these values is taken as the integration step size. Following the solution for the new time plane, the maximum allowable time step is recalculated at all points from Equation 13.3 using the solution plane data. The minimum of these values, $\Delta t'$, is compared with the integration step size. If $\Delta t'$ exceeds the integration step size, the solution plane is recalculated with the integration step size set equal to $\Delta t'$.

E. Convergence Criterion

The criterion used for determining convergence of the transient solution to the steady state solution is based on the fact that stagnation pressure is constant in steady isentropic flow fields. The definition of total pressure, written in terms of the normalized variables, is

$$p_0' = p' \left[1 + \frac{\gamma - 1}{2} \left(\frac{u_1'^2 + u_2'^2}{a'^2} \right) \right]^{\gamma/\gamma-1} \tag{5.11}$$

where a' is the normalized acoustic speed, obtained from the perfect gas relation

$$a' = \left[\frac{\gamma p'}{\rho'} \right]^{\frac{1}{2}} \tag{5.12}$$

The values of total pressure are calculated at all grid points on each solution plane from Equation 5.11. When values at all grid points agree with the inlet total pressure, $p'_{01} = 1.0$, to within a specified tolerance, the solution is assumed to be converged.

VI. CASCADE FLOW EXAMPLES

The computed results for two cases of steady flow through a turbine cascade are presented. These solutions were obtained as limit solutions at large time of the transient flow analysis.

The first case presented involves subsonic flow throughout the cascade. The second example involves subsonic inlet and discharge flows, but with transonic flow over a portion of the cascade passage. In both cases, the results are compared with experimental cascade data given by Huffman et al. (66).

A. Cascade Geometry and Solution Grid

The turbine cascade is shown in Figure 4.1. The blade profiles shown are representative of turbine nozzles in current aircraft engine designs. The geometry data for the cascade are tabulated in Table 6.1, and associated nomenclature is described in Figure 6.1.

The cascade solution grid in Figure 4.1 consists of 41 uniformly spaced constant-x_1 panels with 12 points along each panel. The distances from the cascade to the upstream and downstream boundaries are one-half the axial blade chord, C_x. Twenty-one constant-x_1 panels are located from the leading edge to the trailing edge of the blades, and 10 constant-x_1 panels are located upstream and downstream of the cascade.

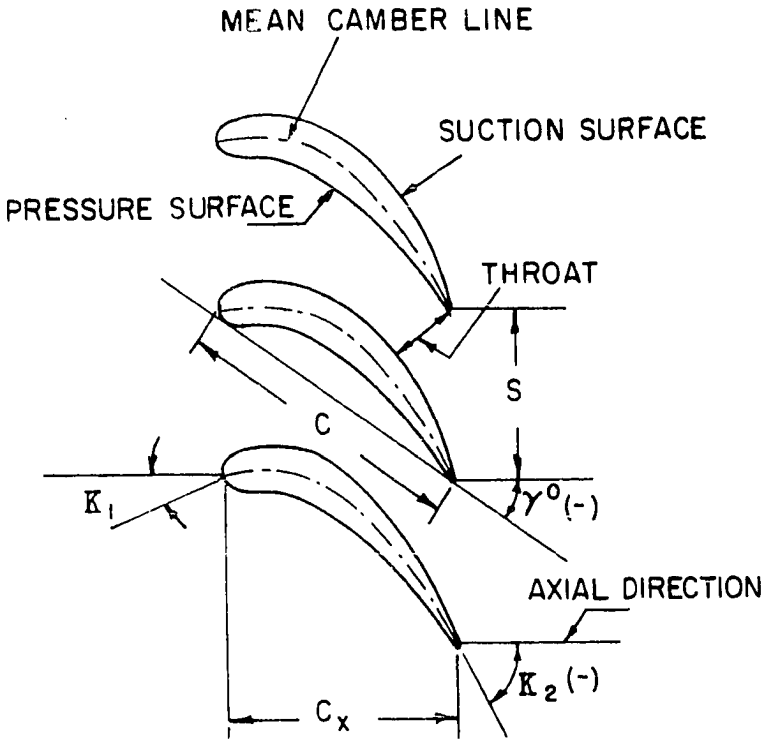

Figure 6.1. Cascade nomenclature

Table 6.1. Cascade geometry data

Blade spacing, S	1.356 in.
Blade chord, C	1.800 in.
Axial chord, C_x	1.200 in.
Axial distance from leading edge to throat location on suction surface	0.790 in.
Stagger angle, γ°	-49.85 deg.
Blade leading edge mean camber angle, κ_1	0.00 deg.
Blade trailing edge mean camber angle, κ_2	-65.00 deg.

B. Subsonic Flow Case

In this example, the steady state boundary conditions were prescribed as; (1) zero whirl velocity component along the upstream boundary, and (2) uniform normalized static pressure $p_2' = 0.685$ along the downstream boundary. The initial data at all grid points were set equal to the stagnation state conditions (i.e., $u_1' = 0.0$, $u_2' = 0.0$, $p' = 1.0$, $\rho' = 1.0$). Approximately 1400 time steps were required to obtain the steady state solution. The computed steady flow results are presented in Figures 6.2-6.5.

In Figure 6.2, the computed values of blade surface static pressure p' are plotted versus normalized distance along the blade, x/C_x. Also presented are the experimental cascade data. Good agreement between the numerical solution and the experimental data is shown. In both the computed and test data, the lowest value of pressure occurs on the blade suction surface near the throat location ($x/C_x = 0.59$). The pressure distribution on the blade pressure surface indicates approximately uniform flow for $x/C_x < 0.5$, followed by accelerated flow to the trailing edge. On the blade suction surface the reverse is true; that is, accelerated flow is indicated upstream of the throat, with nearly uniform flow downstream of the throat.

Velocity vectors at every other point in the solution grid are shown in Figure 6.3. Large velocity gradients are observed upstream of the passage throat, while downstream of

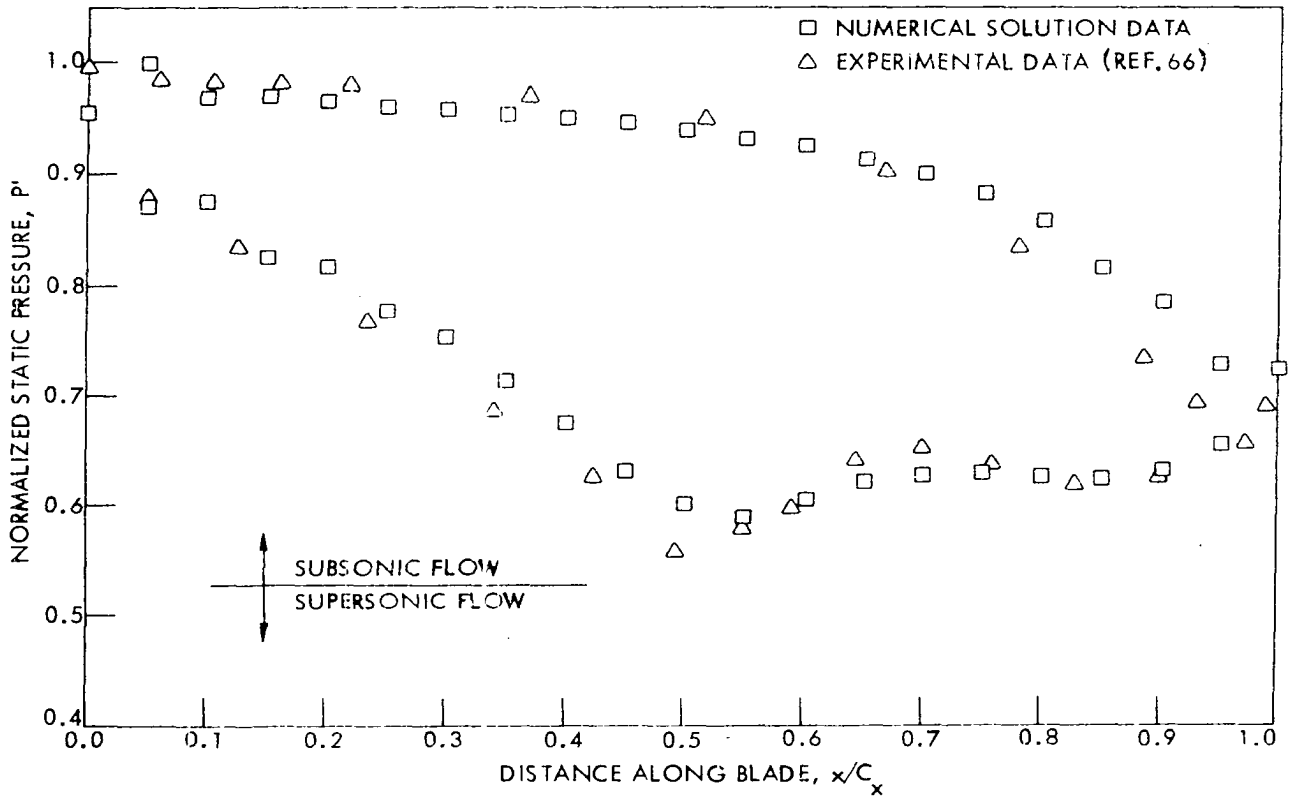

Figure 6.2. Blade surface static pressure distribution, p'

Subsonic flow case; $p'_2 = 0.685$

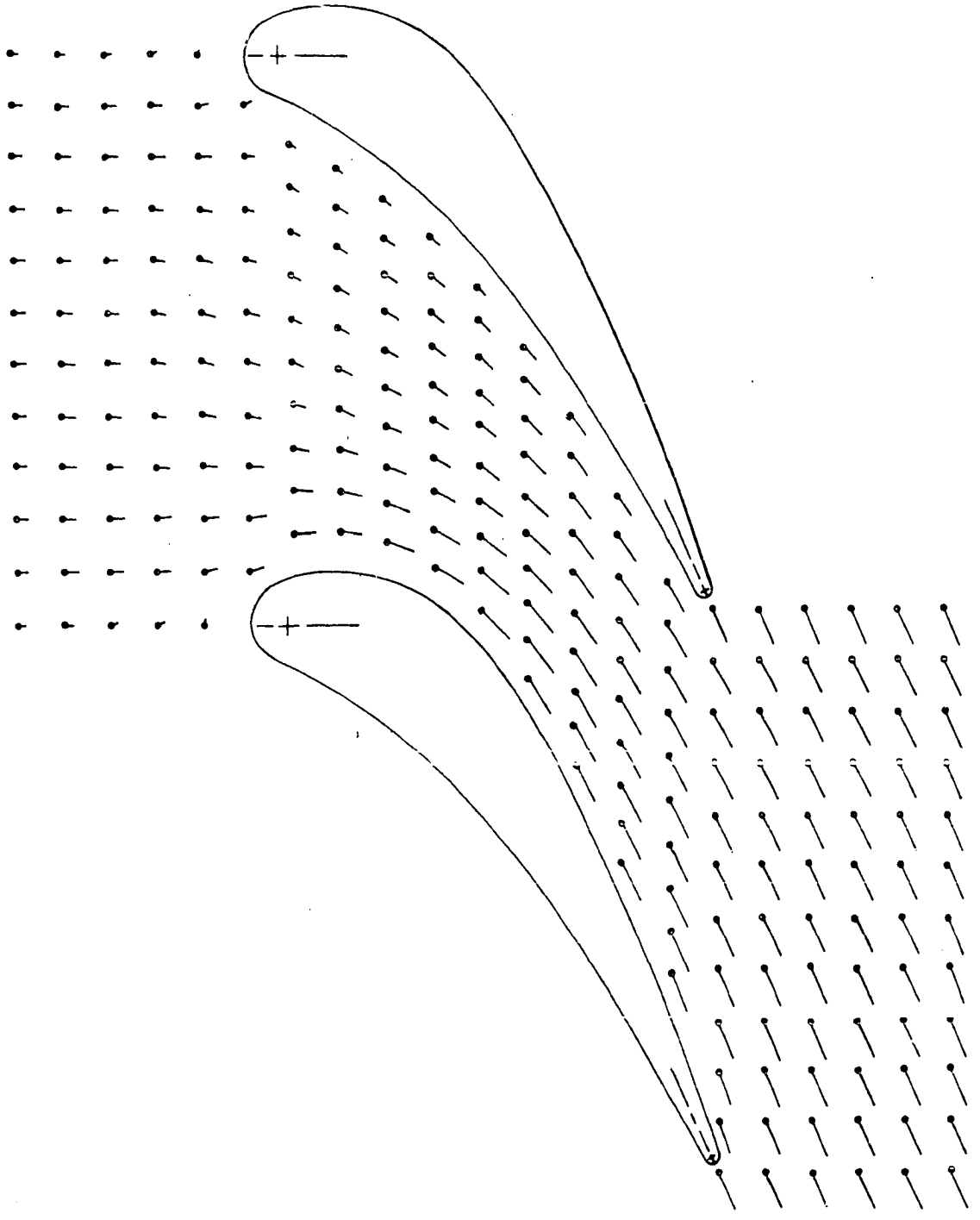

Figure 6.3. Velocity vector field

Subsonic flow case; $p_2' = 0.685$

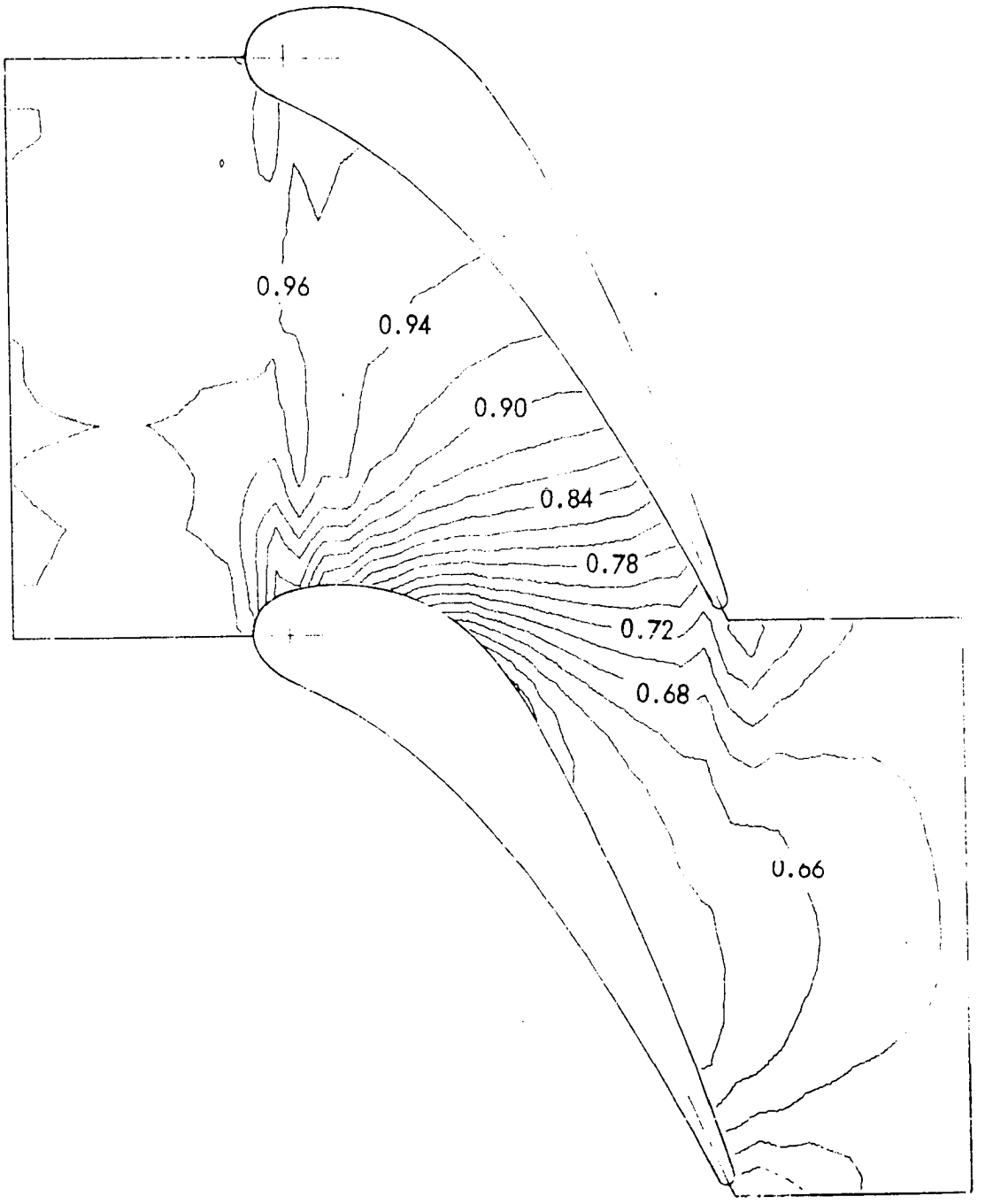

Figure 6.4. Contours of static pressure p'

Subsonic flow case; $p_2' = 0.685$

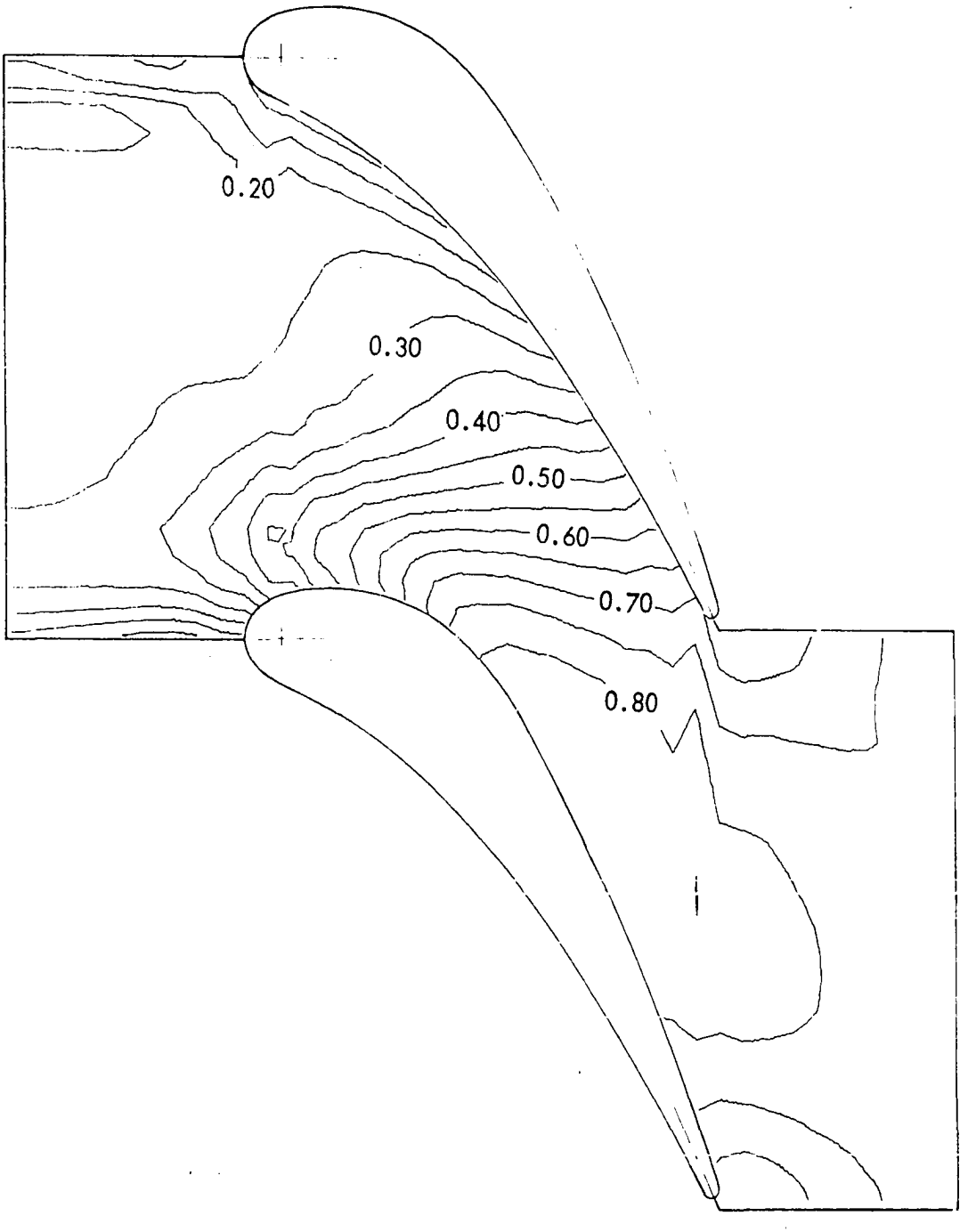

Figure 6.5. Contours of Mach number

Subsonic flow case; $p_2' = 0.685$

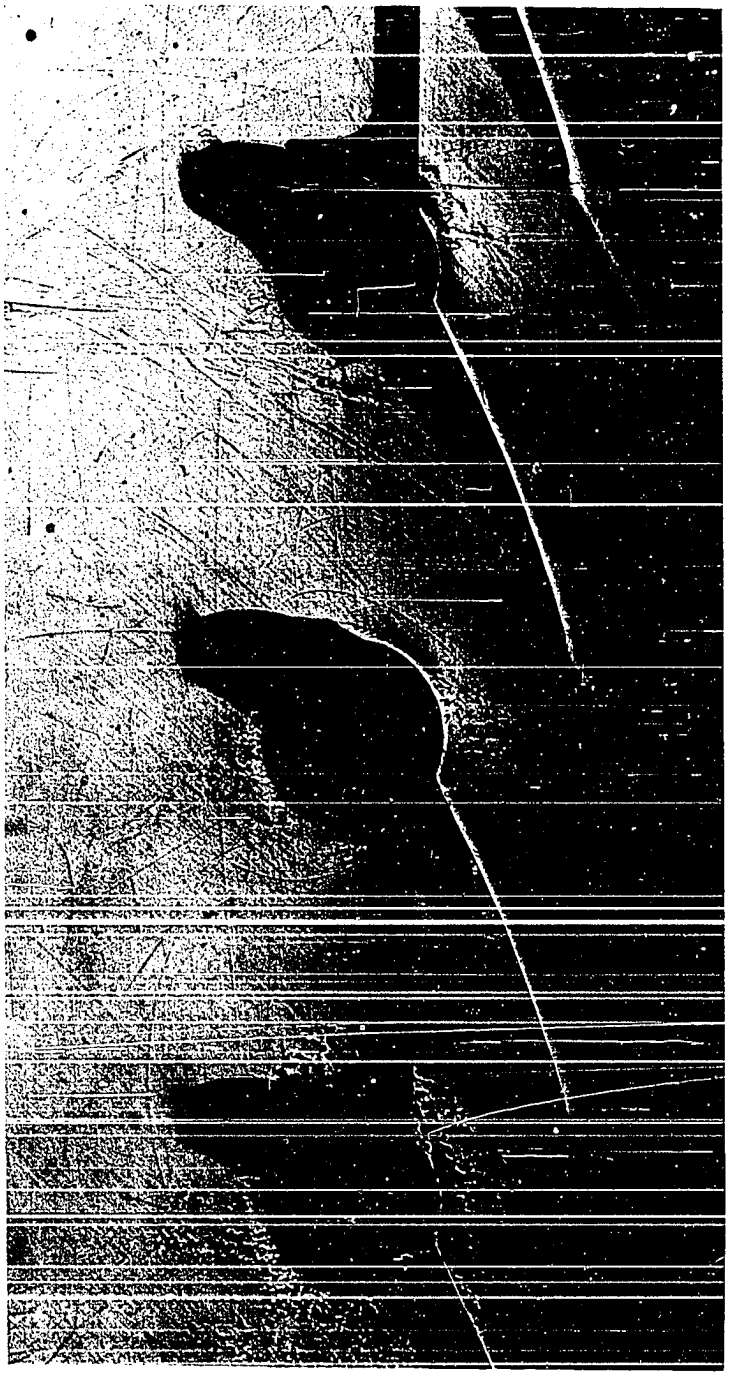

Figure 6.6. Schlieren photograph of cascade flow field

Subsonic flow case; $p_2' = 0.685$

the throat an approximately uniform distribution of velocity can be seen. The velocity distribution around the leading edge of the blade indicates that the stagnation point is located on the pressure surface of the blade. In the region of the upstream boundary the velocity gradient in the axial direction is approximately zero. This tends to support the assumption of uniform whirl velocity distribution along the upstream boundary. The nonuniform distribution of axial velocity component along the upstream boundary is due to the influence of the blades on the upstream flow.

A contour plot of computed normalized static pressure, p', over the flow field is presented in Figure 6.4. The highly two-dimensional character of the flow is indicated. The maximum pressure gradients occur near the passage throat, with the minimum pressure occurring on the blade suction surface near the throat location. Upstream of the cascade a nearly uniform pressure distribution is shown. At the downstream boundary the axial pressure gradients are approximately zero. This supports the assumption made of uniform static pressure along the downstream boundary.

Lines of constant Mach number in the flow field are shown in Figure 6.5. The contours indicate rapidly accelerating flow around the blade leading edge on the suction surface, and relatively uniform flow on the pressure surface near the leading edge. Also, an approximately uniform distribution of

Mach number is shown downstream of the throat on the blade suction surface. At the upstream boundary, the contour lines are nearly horizontal, indicating essentially zero Mach number gradient in the axial direction near the boundary. The Mach number gradient shown along the upstream boundary, however, is substantial, and, as stated previously, is due to the finite location of the boundary. A nearly uniform distribution of Mach number is indicated in the region of the downstream boundary.

A schlieren photograph of the cascade flow field is presented in Figure 6.6. In this photograph, the mean flow angle in the blade wake is approximately equal to the blade mean camber angle at the trailing edge which was the assumption made in the blade trailing edge calculation. The general agreement of the numerical solution and experimental data presented in Figure 6.2 indicates the blade wake model was adequate.

C. Transonic Flow Case

The boundary conditions for this cascade flow example were the same as in the subsonic flow case except that the downstream normalized pressure, p_2', was reduced to 0.578. In this case the flow accelerates to the transonic regime in the blade passage, thus providing a test for the numerical solution method regarding mixed flow prediction capability. The initial

data for the transient solution were taken from the steady state solution in the subsonic flow case. Approximately 1000 time steps were required to obtain the steady flow solution at the new downstream pressure. The computed steady flow results are presented in Figures 6.7-6.10.

The computed blade surface pressure distribution is compared in Figure 6.7 with the experimental cascade data. Agreement between the computed results and the experimental data is good over most of the blade surface. However, on the blade suction surface for $x/C_x > 0.5$ the numerical solution predicts a much smoother pressure distribution than the experimental data shows. The discrepancy in pressure distributions is likely due to the close proximity of the cascade to the imposed uniform pressure distribution along the downstream boundary in the numerical solution. In support of this contention, it can be seen from the pressure contour plot in Figure 6.9 that a large axial pressure gradient exists along the downstream boundary. McDonald (9) determined that with uniform specification of downstream pressure in high Mach number flows it is necessary to maintain a minimum distance equal to the axial blade chord between the cascade and the downstream boundary. As shown in Figure 6.7, the pressure level on the blade suction surface indicates supersonic flow downstream of the throat. Also, the minimum blade surface pressure does not occur at the blade throat as in the subsonic

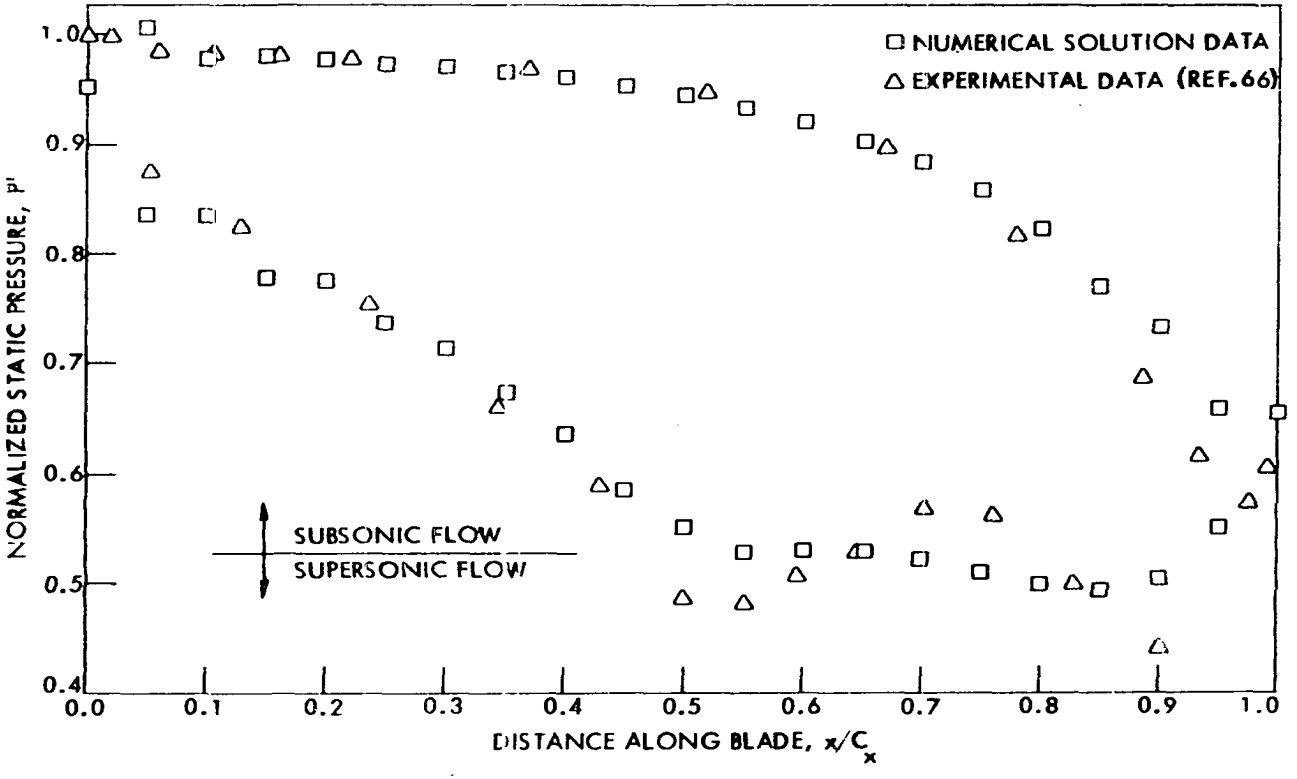

Figure 6.7. Blade surface static pressure distribution, p'

Transonic flow case; $p'_2 = 0.578$

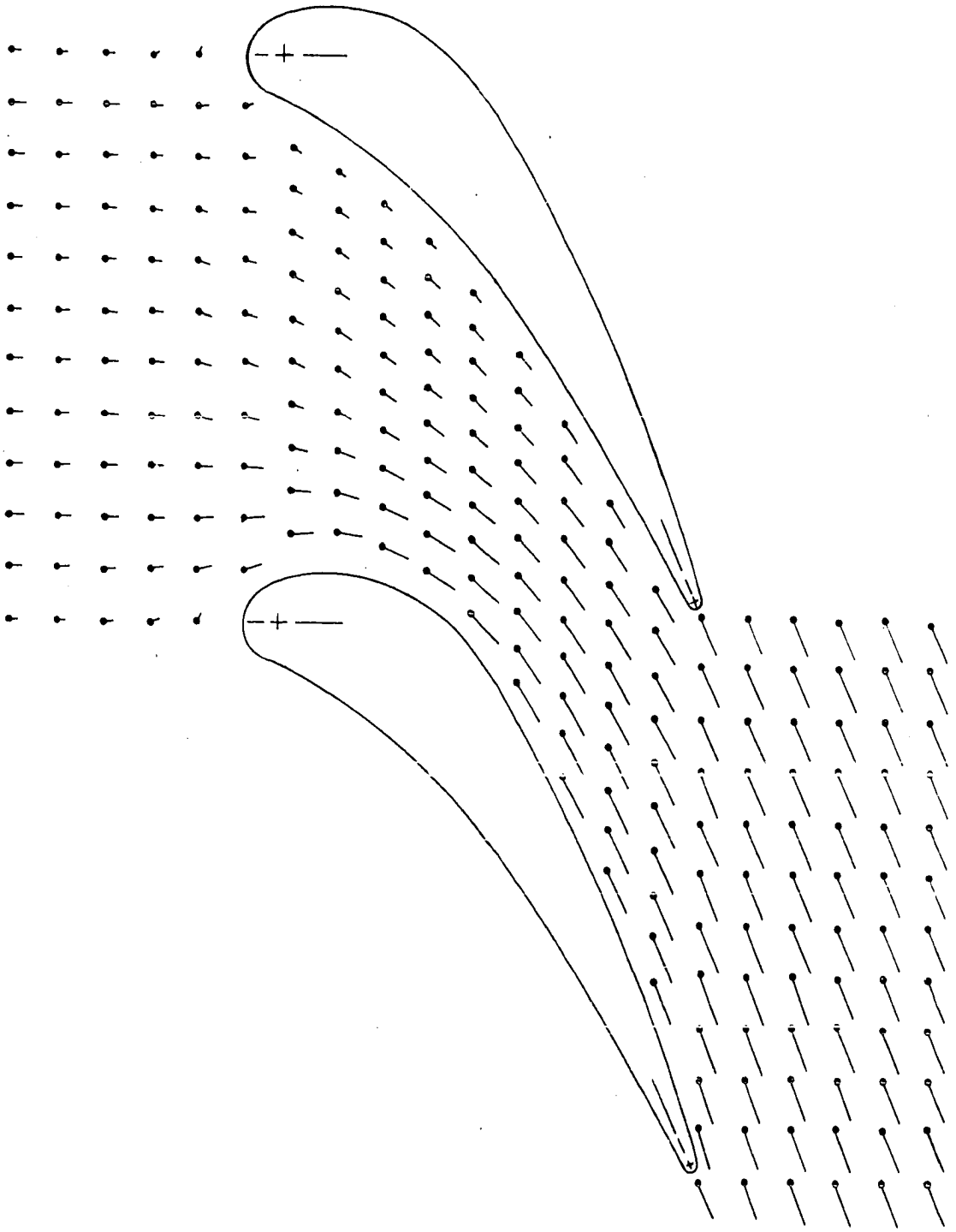

Figure 6.8. Velocity vector field

Transonic flow case; $p_2' = 0.578$

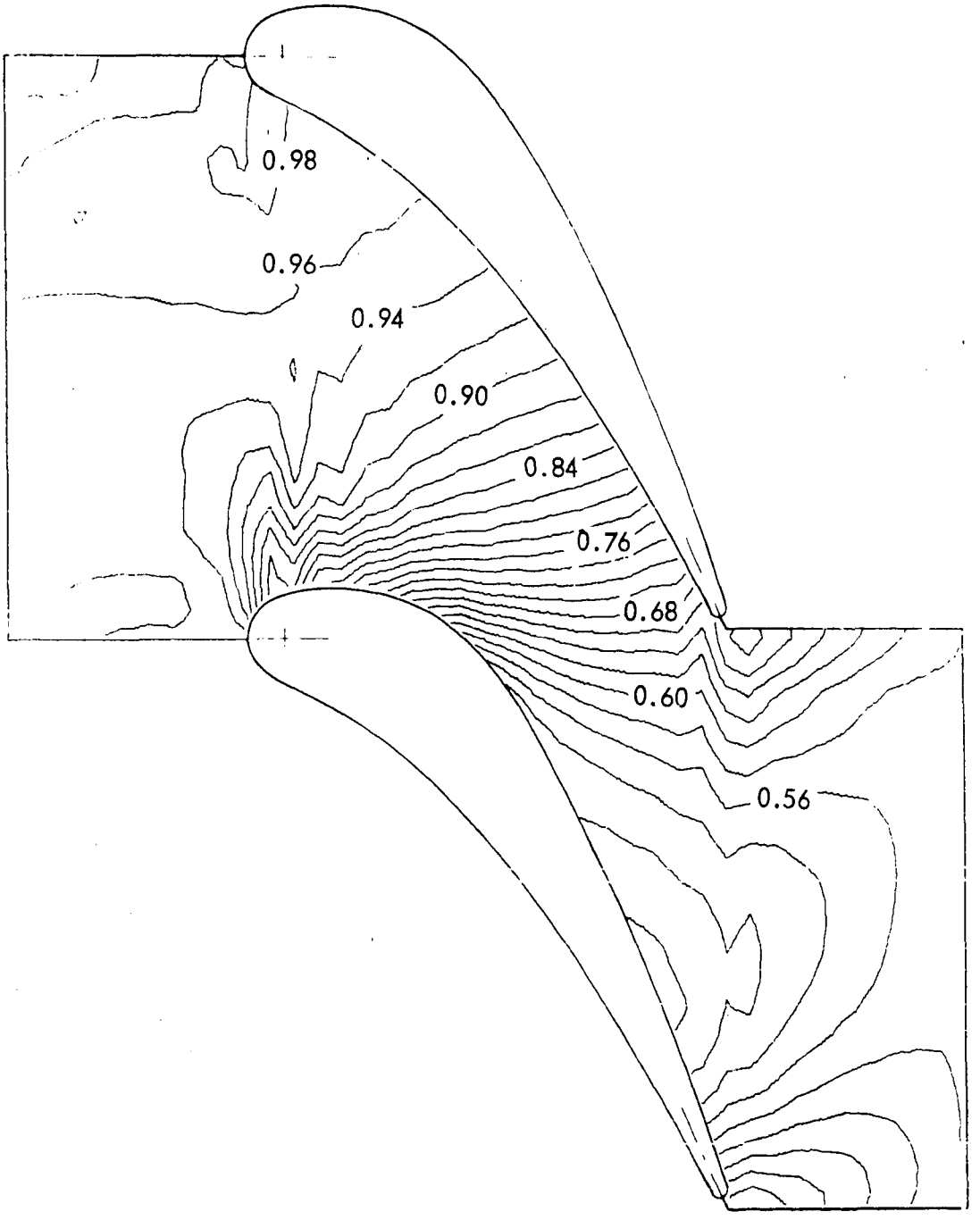

Figure 6.9. Contours of static pressure p'

Transonic flow case; $p_2' = 0.578$

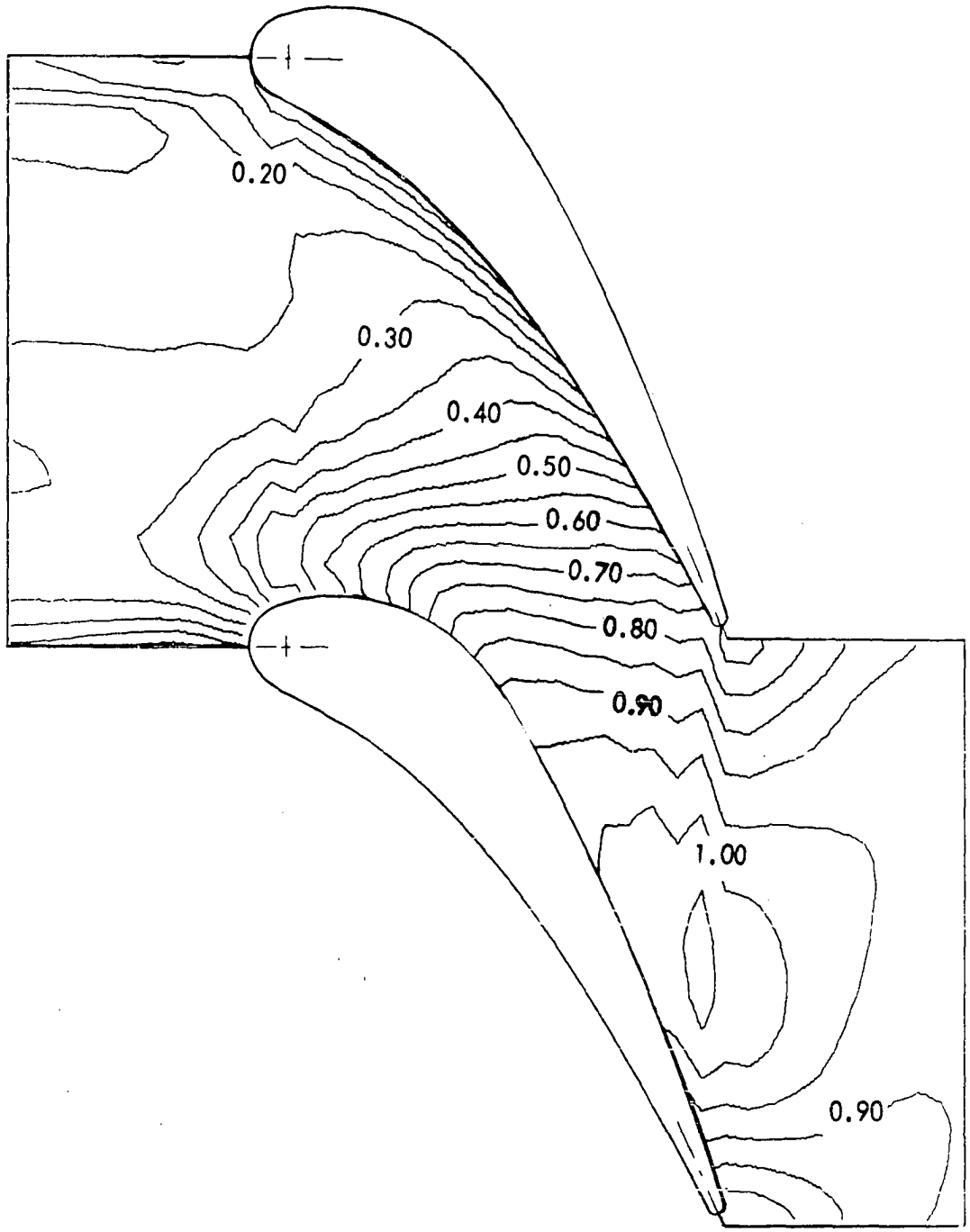

Figure 6.10. Contours of Mach number

Transonic flow case; $p_2' = 0.578$

Figure 6.11. Schlieren photograph of cascade flow field

Transonic flow case; $p_2^{\prime} = 0.578$

flow case (see Figure 6.2), but further downstream at the location $x/C_x = 0.9$. This movement of the minimum pressure point downstream of the throat is indicative of the fact that supersonic flow has been established. Comparison of Figure 6.7 with Figure 6.2 for the subsonic flow case shows substantially higher blade loading in the transonic flow case, with the majority of the loading increase occurring on the rear half of the blade.

The velocity vector field for this example is presented in Figure 6.8. These results resemble those presented in Figure 6.3 for the subsonic flow case. The influence of the blades on the upstream velocity distribution is again evident. Also the leading edge stagnation point appears to be located in approximately the same location as in the subsonic flow case. One difference that can be seen is the increased velocity level which exists downstream of the throat.

The contour plot of normalized static pressure, p', is presented in Figure 6.9. As in the subsonic flow case (see Figure 6.4), a nearly uniform distribution of static pressure exists upstream of the cascade. The contour line distributions in Figures 6.4 and 6.9 are very nearly the same upstream of the passage throat indicating that both flow cases are close to the choked condition. Much higher pressure gradients are shown downstream of the passage throat in the transonic flow case. Also, as stated above, the minimum pressure point location has moved downstream to a point near the blade trailing edge on the

suction surface.

Lines of constant Mach number in the flow field are shown in Figure 6.10. The supersonic flow region is located on the blade suction surface near the trailing edge. Again, the contour line distribution upstream of the throat is nearly the same as that in Figure 6.4 for the subsonic flow case.

In the schlieren photograph presented in Figure 6.11, a weak normal shock is shown on the blade suction surface near the trailing edge. Evidence of this shock wave is also shown in the experimental blade surface pressure distribution presented in Figure 6.7 where a rapid rise in pressure exists on the suction surface downstream of the location $x/C_x = 0.9$. This shock wave has been smeared out in the numerical solution, as indicated in the contour plots presented in Figures 6.9 and 6.10.

VII. CONCLUSIONS AND RECOMMENDATIONS

A method of characteristics numerical integration scheme having second-order accuracy has been developed for solution of two-dimensional unsteady flows in gas dynamics. The method has been applied to steady transonic flow analysis in turbine cascades with the steady state solution computed as the asymptotic limit in time of a transient solution.

Computed results of the cascade analysis are in good agreement with experimental data. The results indicate that the present numerical method lends itself to accurate treatment of cascade boundary conditions and yields accurate mixed-flow solutions. It is concluded that the added complexity involved in the formulation and programming tasks with the method of characteristics over finite-difference methods is justified. The developed analysis method provides a useful and effective tool for the turbomachinery aerodynamicist in the design of high Mach number blading.

The success of the present method in solution of blade-to-blade flows in turbine cascades suggests that the method could be applied as well to other steady or unsteady two-dimensional flow problems. Flows in two-dimensional nozzles and diffusers could be solved by an essentially straightforward application of the method. Also, axisymmetric internal flows could be handled with only minor modifications. Furthermore, the method could be extended for solution of blade-to-blade and hub-to-tip

flows on arbitrary stream surfaces in rotating blade rows. Although no effort was made to consider flows with strong shocks, it appears that shock wave tracing capability could be added to the overall algorithm. Application to supersonic flows in compressor cascades, including entrance region and through-flow analyses, would require the addition of such shock wave tracing procedures.

The following recommendations for further study on the present numerical method are made:

(1) It was found that the bicharacteristic tangency condition was not needed to maintain second-order accuracy in the flow solutions considered, and the reference vectors at bicharacteristic base points could be simply assigned their directions at the solution point. Cline and Hoffman (57) came to the same conclusion in applying Butler's scheme to three-dimensional steady supersonic flows. It should be noted, however, that this observation concerning the bicharacteristic tangency condition is based solely upon numerical experience with the method and has not been verified analytically. Further study is needed to substantiate this finding.

(2) Maximum errors in the computed stagnation pressures in the steady flow cascade solutions occurred at the boundaries of the cascade flow field. These errors

may be due to the fact that the solution points at the boundaries were located at the edges of the corresponding grid point cells where maximum error in least square interpolations would occur. The interpolation error may be reduced by introducing higher terms into the least square interpolating polynomials for the boundary points. Other interpolation procedures for the boundary points should also be investigated.

VIII. BIBLIOGRAPHY

1. Dorodnitsyn, A. A. "On the Numerical Solution of Certain Problems in Aero-Hydrodynamics." Transactions of the Third All Union Mathematical Congress 2, 1956.

2. Wilkinson, D. H. "Calculation of Blade-to-Blade Flow in a Turbomachine by Streamline Curvature." Aeronautical Research Council, Reports and Memoranda No. 3704, December 1970.

3. Katsanis, T. "Fortran Program for Calculating Transonic Velocities on a Blade-to-Blade Stream Surface of a Turbomachine." NASA TN D-5427, September 1969.

4. Lax, P. D., and Wendroff, B. "Systems of Conservation Laws." Communications on Pure and Applied Mathematics 13 (1960): 217-237.

5. Lax, P. D., and Wendroff, B. "Difference Schemes with High Order Accuracy for Solving Hyperbolic Equations." Communications on Pure and Applied Mathematics 17 (1964): 381.

6. Gopalakrishnan, S., and Bozzola, R. "A Numerical Technique for the Calculation of Transonic Flows in Turbomachinery Cascades." ASME Paper No. 71-GT-42, 1971.

7. Gopalakrishnan, S., and Bozzola, R. "Computation of Shocked Flows in Compressor Cascades." ASME Paper No. 72-GT-31, 1972.

8. MacCormack, R. W. "The Effect of Viscosity on Hypervelocity Impact Cratering." AIAA Paper No. 69-345, May 1969.

9. McDonald, P. W. "The Computation of Transonic Flow Through Two-Dimensional Gas Turbine Cascades." ASME Paper No. 71-GT-89, 1971.

10. Fowell, L. R. "Flow Field Analysis for Lifting Re-Entry Configurations by the Method of Characteristics." Institute of Aerospace Sciences, Paper No. 61-208-1902, June 1961.

11. Chushkin, P. I. "Numerical Method of Characteristics for Three-Dimensional Supersonic Flows." Chapter 2. Progress in Aeronautical Sciences, Vol. 9, Edited by P. Kuchemann. New York: Pergamon Press, 1968.

12. Sauerwein, H. "The Calculation of Two- and Three-Dimensional Inviscid Unsteady flows by the Method of Characteristics." Ph.D. Thesis, Massachusetts Institute of Technology, June 1964.

13. Strom, C. R. "The Method of Characteristics for Three-Dimensional Steady and Unsteady Reacting Gas Flows." Ph.D. Thesis, University of Illinois, January 1965.

14. Ransom, V. H. "A Second-Order Numerical Method of Characteristics for Three-Dimensional Supersonic Flow." Ph.D. Thesis, Purdue University, January 1970.

15. Richtmyer, R. D., and Morton, K. W. Difference Methods for Initial Value Problems. Second Edition. New York: Interscience Publishers, 1967.

16. Courant, R., Friedrichs, K. O., and Lewy, H. "Uber die Partiellen Differenzialgleichungen der Mathematischen Physik." Math. Ann. 100 (1928): 32-74.

17. Butler, D. S. "The Numerical Solution of Hyperbolic Systems of Partial Differential Equations in Three Independent Variables." Proceedings of the Royal Society of London 255A (1960): 232-252.

18. Chu, C. W. "Compatibility Relations and a Generalized Finite Difference Approximation for Three-Dimensional Steady Supersonic Flow." AIAA Journal 5, No. 3 (March 1967): 493-501.

19. Pridmore Brown, B. N., and Franks, W. J. "A Method of Characteristics Solution in Three Independent Variables." Aerospace Research Laboratories Report, ARL 65-124, June 1965.

20. Powers, S. A., Niemann, A. F., Jr., and Der, J., Jr. "A Numerical Procedure for Determining the Combined Vicid-Inviscid Flow Fields over Generalized Three-Dimensional Bodies." Vol. I. Discussion of Methods and Results, and Instructions for Use of Computer Program, AFFDL-TR-67-124, December 1967.

21. Chu, C. W. "A New Algorithm for Three-Dimensional Method of Characteristics." AIAA Journal 10, No. 11 (November 1972): 1548-1550.

22. Sauerwein, H. "Numerical Calculations of Arbitrary Multidimensional and Unsteady Flows by the Method of Characteristics." AIAA Paper No. 66-412, June 1966.

23. Ferrari, C. "Interference Between Wing and Body at Supersonic Speeds - Analysis by the Method of Characteristics." Journal of Aeronautical Sciences 16, No. 7 (July 1949): 411-434.

24. Moeckel, W. E. "Use of Characteristic Surfaces for Unsymmetrical Supersonic Flow Problems." NACA Technical Note No. 1849, March 1949.

25. Sauer, R. "Dreidimensionale Probleme der Characteristikentheorie partieller Differentialgleichungen." Zeitschrift fur angewandte Mathematik und Mechanik 30 (November-December 1950): 347-356.

26. Holt, M. "The Method of Characteristics for Steady Supersonic Rotational Flow in Three Dimensions." Journal of Fluid Mechanics 1 (1956): 409-423.

27. Coburn, N. and Dolph, C. L. "The Method of Characteristics in the Three-Dimensional Stationary Supersonic Flow of a Compressible Gas." Proceedings of the First Symposium on Applied Mathematics, American Mathematical Society, 1949.

28. Titt, E. "An Initial-Value Problem for all Hyperbolic Partial Differential Equations of Second-Order with Three Independent Variables." Annals of Mathematics 40, No. 4 (October 1939): 862-891.

29. Heie, H., and Leigh, P. D. "Numerical Stability of Hyperbolic Equations in Three Independent Variables." AIAA Journal 3, No. 6 (June 1965): 1099-1103.

30. Sauer, R. "Practical Numerical Methods of Three-Dimensional Supersonic Flow." Technical (Final) Report, Contract No. AF 61-(052)-377, June 1961.

31. Holt, M. "The Method of Near Characteristics for Unsteady Flow Problems in Two Space Variables." Institute of Engineering Research, University of California, Berkeley, Report No. AS-63-2, June 1963.

32. Moretti, G. "Three-Dimensional Supersonic Flow Computations." AIAA Journal 1, No. 9 (September 1963): 2192-2193.

33. Moretti, G., Sanlorenzo, E. A., Magnus, D. E., and Weilerstein, G. "Flow Field Analysis of Reentry Configurations by a General Three-Dimensional Method of Characteristics." Air Force Systems Command, Aeronautical Systems Division, TR-61-727, Vol. III, February 1962.

34. Rakich, J. V. "A Method of Characteristics for Steady Three Dimensional Supersonic Flow with Application to Inclined Bodies of Revolution." NASA TN D-5341, October 1969.

35. Rakich, J. V., and Cleary, J. W. "Theoretical and Experimental Study of Supersonic Steady Flow around Inclined Bodies of Revolution." AIAA Paper No. 69-187, January 1969.

36. Katskova, O. N., and Chushkin, P. I. "Numerical Calculation of a Supersonic Flow Past Ducted Bodies at an Angle of Attack." Academy of Sciences, USSR, Bulletin, Fluid and Gas Mechanics, No. 3 (1967): 12-130. (Translation by A. E. Schidlovsky, Johns Hopkins University, Applied Physics Laboratory, Translation No. 2149, June 1968.)

37. Moretti, G., and Abbett, M. "A Time-Dependent Calculational Method for Blunt Body Flows." AIAA Journal 4, No. 12 (December 1966): 2136-2141.

38. D'Souza, N., Molder, S., and Moretti, G. "Numerical Method for Hypersonic Internal Flow Over Blunt Leading Edges and Two Blunt Bodies." AIAA Journal 10, No. 5 (May 1972): 617-622.

39. Serra, R. A. "The Determination of Internal Gas Flows by a Transient Numerical Technique." Ph.D. Thesis, Rensselaer Polytechnic Institute, 1970.

40. Serra, R. A. "Determination of Internal Gas Flows by a Transient Numerical Technique." AIAA Journal 10, No. 5 (May 1972): 603-611.

41. Kentzer, C. P. "Discretization of Boundary Conditions on Moving Boundaries." Proceedings of the Second International Conference on Numerical Methods in Fluid Mechanics, Edited by M. Holt, Springer Verlag, Berlin, 1971, pp. 108-113.

42. Porter, R. W., and Coakley, J. C. "Use of Characteristics for Boundaries in Time Dependent Finite Difference Analysis of Multi-dimensional Gas Dynamics." International Journal for Numerical Methods in Engineering 5 (1972): 91-101.

43. Gopalakrishnan, S., and Bozzola, R. "Numerical Representation of Inlet and Exit Boundary Conditions in Transient Cascade Flow." ASME Paper No. 73-GT-55, 1973.

44. Thornhill, C. K. "The Numerical Method of Characteristics for Hyperbolic Problems in Three Independent Variables." ARC Reports and Memoranda No. 2615, September 1948.

45. Tsung, C. C. "Study of Three-Dimensional Supersonic Flow Problems by a Numerical Method of Characteristics (Specially Adapted for Use of High Speed Electronic Digital Computers)." Ph.D. Thesis, University of Illinois, January 1961.

46. Reed, V. L. "Characteristic Relations of Compressible Flow with Three Independent Variables." Brown Engineering Company, Inc., Technical Note R-40, March 1963.

47. Reed, V. L. "The Numerical Analysis of Three Independent Variable Characteristic Formulations of Compressible Flow Problems." Research Laboratories of Brown Engineering Company, Inc., Huntsville, Alabama, May 1964, Contract NAS8-5289.

48. Reed, V. L. "Generalized Three Independent Variable Characteristics Computer Program." Brown Engineering Company, Inc., Huntsville, Alabama, TR R-66-2, Vol. 3, January 1966.

49. Chu, C. W., Powers, S. A., and Ziegler, H. "On the Impingement of a Supersonic Jet on a Flat Plate." Zeitschrift fur angewandte Mathematik und Physik 20 (1969): 15-18.

50. Chu, C. W., Niemann, A. F., Jr., Powers, S. A., Ziegler, A. "Interaction of Two Cylindrical Jets." AIAA Journal 5, No. 2 (February 1967): 375-376.

51. Talbot, G. P. "Application of the Numerical Method of Characteristics in Three Independent Variables to Shock-Thermal Layer Interaction Problems." Royal Armament Research and Development Establishment, Report (B) 11/63, August 1963.

52. Elliott, L. A. "Shock Fronts in Two-Dimensional Flow." Proceedings of the Royal Society of London A267 (1962): 558-565.

53. Richardson, D. J. "The Solution of Two-Dimensional Hydrodynamic Equations by the Method of Characteristics," pages 295-318. In Methods in Computational Physics, Vol. 3, Edited by B. Alder. New York: Academic Press, 1964.

54. Ransom, V. H., Thompson, H. D., and Hoffman, J. D. "Analysis of Three-Dimensional Scramjet Exhaust Nozzle Flow Fields by a New Second-Order Method of Characteristics." AIAA Paper No. 69-5, January 1969.

55. Ransom, V. H., Thompson, H. D., and Hoffman, J. D. "Three Dimensional Supersonic Nozzle Flow Field Calculations." AIAA Paper No. 69-463, June 1969.

56. Ransom, V. H., Hoffman, J. D., and Thompson, H. D. "A Second-Order Bicharacteristics Method for Three-Dimensional, Steady Supersonic Flow." AIAA Journal 10, No. 12 (December 1972): 1573-1581.

57. Cline, M. C., and Hoffman, J. D. "The Analysis of Nonequilibrium Chemically Reacting, Supersonic Flow in Three Dimensions." Vol. 1. Theoretical Development and Results, Report AFAPL-TR-71-73, Air Force Propulsion Laboratory, Wright-Patterson Air Force Base, Ohio, August 1971.

58. Cline, M. C., and Hoffman, J. D. "Comparison of Characteristic Schemes for Three-Dimensional, Steady, Isentropic Flow." AIAA Journal 10, No. 11 (November 1972): 1452-1458.

59. Courant, R., and Hilbert, D. Methods of Mathematical Physics. Vol. II, New York: Interscience Publishers, 1962.

60. Delaney, R. A., and Kavanagh, P. "Entrance Region Flows in Supersonic Axial-Flow Compressor Cascades with Subsonic Inlet Axial Velocity Component, 'General Method of Characteristics for Unsteady Flow'." Iowa State University, Engineering Research Institute, Report No. ERI-73076, February 1973.

61. Hildebrand, F. B. Introduction to Numerical Analysis. Second Edition, New York: McGraw-Hill, Inc., 1974.

62. Glassman, A. J., ed. Turbine Design and Application. Vol. III. NASA SP-290, 1972.

63. Ferri, A. "The Supersonic Compressor, 'Aerodynamic Properties of Supersonic Compressors'," Chapter 2. In Aerodynamics of Turbines and Compressors, Vol. 10. High Speed Aerodynamics and Jet Propulsion, Princeton, 1964.

64. Karamcheti, K. Principles of Ideal-Fluid Aerodynamics. New York: John Wiley & Sons, Inc., 1966.

65. Miller, M. J. "Some Aspects of Deviation Angle Estimation for Axial-Flow Compressors." Ph.D. Thesis, Iowa State University, 1973.

66. Huffman, G. D., McClure, R. B., Holtman, R. L., and Sinnet, G. T. "Results of a Two-Dimensional Turbine Cascade (AACE II) Test." Detroit Diesel Allison Div., General Motors Corp., Indianapolis, Indiana, Research Note 71-47, July 1971.

67. Rusonov, V. V. "The Characteristics of General Equations of Gas Dynamics." Zhurnal vychislitel'noi mathematiki mathematicheskoi fiziki 3, No. 3 (1963): 508-527. (Translation by K. N. Trirogoff, Literature Research Group, Aerospace Library Services, Aerospace Corp., San Bernadino, Calif., LRG-65-T-38, October 1965).

68. Roache, P. J. Computational Fluid Dynamics. Albuquerque, New Mexico: Hermosa Publishers, 1972.

69. Hahn, S. G. "Stability Criteria for Difference Schemes." Communications on Pure and Applied Mathematics 2 (1958): 243-255.

70. Lax, P. D., and Richtmyer, R. D. "Survey of the Stability of Linear Finite Difference Equations." Communications on Pure and Applied Mathematics 9 (1956): 267-293.

71. Henrici, P. Elements of Numerical Analysis. New York: John Wiley & Sons, 1964.

72. Owczarek, J. A. Fundamentals of Gas Dynamics. Scranton, Pennsylvania: International Textbook Co., 1964.

73. McConnell, A. J. Applications of Tensor Analysis. New York: Dover Publications, Inc., 1957.

IX. ACKNOWLEDGEMENTS

Thanks are expressed to Professors Patrick Kavanagh, Robert J. Lambert, George K. Serovy, Donald F. Young, and Harry J. Weiss for serving on the author's graduate study committee.

The author expresses his sincere appreciation to Professor Patrick Kavanagh for encouragement and advice received in the course of this investigation and in the preceding graduate study program.

This investigation was cosponsored by the Detroit Diesel Allison Division of General Motors Corporation and the Iowa State University Engineering Research Institute. This financial support is gratefully acknowledged.

Financial assistance received from the Iowa State University Graduate College is also gratefully acknowledged.

X. APPENDIX A: GENERAL THEORY OF QUASI-LINEAR HYPERBOLIC PARTIAL DIFFERENTIAL EQUATIONS

The general theory of hyperbolic systems of partial differential equations as needed in the development of the general numerical method (Appendix B) is presented. Also presented is supporting theory for the development of characteristic relations previously used in Chapter II for plane two-dimensional unsteady flow. The theory and its development is that due to Rusonov (67) and Ransom (14).

A. Characteristic Surfaces

Consider a general system of n quasi-linear, hyperbolic, partial differential equations in n dependent variables u_ν and three independent variables x_i

$$a_{\mu\nu i} \frac{\partial u_\nu}{\partial x_i} = b_\mu \quad (\mu,\nu = 1,2,\ldots n) \tag{10.1}$$

where $a_{\mu\nu i}$ and b_μ are known functions of u_ν and x_i. The summation convention is used with repeated subscripts unless otherwise stated. Greek subscripts run over the range 1 to n, while Latin subscripts have the range 1 to 3. The system of equations, Eq. 10.1, is a complete set, i.e., n equations having n dependent variables.

If the independent variables are considered as coordinate axes in a three-dimensional space, then any set of real numbers $\{a_1, a_2, a_3\}$ represent components of a vector a_i in the space. The directional differential of any arbitrary function $f(x_i)$ along a_i, denoted by $d_a f$, is

$$d_a f = a_i \frac{\partial f}{\partial x_i} d\tau \tag{10.2}$$

where τ is a parameter increasing in the direction of a_i, and has magnitude $1/|a_i|$.

Consider next a linear combination of the equations of the system formed by taking the scalar product of Eq. 10.1 and the left eigenvector w_μ $(\mu = 1,2,\ldots,n)$

$$w_\mu a_{\mu\nu i} \frac{\partial u_\nu}{\partial x_i} = w_\mu b_\mu \quad (\mu,\nu = 1,2,\ldots,n) \tag{10.3}$$

If we let

$$W_{\nu i} = w_\mu a_{\mu\nu i} \tag{10.4}$$

and

$$B = w_\mu b_\mu \tag{10.5}$$

then Eq. 10.3 can be written in directional differential notation as

$$d_{W_\nu} u_\nu = B \, d\tau \tag{10.6}$$

According to Eq. 10.4 there are n vectors $W_{\nu i}$, and their orientation in space depends on the elements of w_μ.

The hyperbolic character of the original system of equations is revealed by posing the following question: is it possible to choose the elements of w_μ such that the resulting vectors $W_{\nu i}$ are linearly dependent or, in other words, such that the vectors $W_{\nu i}$ lie in a plane? For hyperbolic systems of equations such values for the elements of w_μ exist. The plane containing the vectors $W_{\nu i}$ is called a characteristic plane, and its normal N_i is called a characteristic normal. A surface in space which is everywhere tangent to a characteristic plane is called a characteristic surface. The values of the dependent variables cannot be arbitrarily specified on a characteristic surface since they must satisfy a compatibility relation, Eq. 10.6, written on this surface.

If N_i is a characteristic normal, then the condition that all vectors $W_{\nu i}$ lie in the characteristic plane corresponding to N_i is

$$N_i \, W_{\nu i} = 0 \quad (\nu = 1,2,\ldots,n) \tag{10.7}$$

or, making use of Eq. 10.4

$$N_i \, w_\mu \, a_{\mu\nu i} = (a_{\mu\nu i} N_i) w_\mu = 0 \tag{10.8}$$

where N_i and w_μ are to be determined. Equation 10.8 is a system of linear homogeneous equations for the elements of the left eigenvector. If a nontrivial solution for w_μ exists,

then the determinant of the coefficient matrix with elements $a_{\mu\nu i}N_i$ must vanish, i.e.,

$$\det \{a_{\mu\nu i}N_i\} = 0 \tag{10.9}$$

which is an nth order polynomial in the components of N_i. Equation 10.9 is called the characteristic equation of the original system of partial differential equations, and it yields a condition that must be satisfied by any characteristic normal.

B. Characteristic Surface Geometry in Gas Dynamics

Two-dimensional unsteady flows, and three-dimensional steady supersonic flows in gas dynamics, are governed by systems of quasi-linear hyperbolic partial differential equations in three independent variables. In both cases the characteristic equation factors as follows into a repeated linear factor and a symmetric quadratic factor

$$(U_k N_k)^{n-2} A_{ij} N_i N_j = 0 \tag{10.10}$$

where n is the order of the original system of equations. The vanishing of either factor in Eq. 10.10 satisfies the equation and, therefore, two different types of characteristic surfaces exist.

1. Characteristic flow surfaces

Characteristic flow surface normals, N_i, satisfy the equation obtained by setting the first factor in Eq. 10.10 to zero, i.e.,

$$U_i N_i = 0 \tag{10.11}$$

where U_i is a function of the dependent variables u_ν (ν = 1,2,...,n). According to Eq. 10.11, at a point in space the normal N_i is any one of the infinite family of vectors which lie in a plane orthogonal to the vector U_i. Thus, characteristic flow surfaces are locally tangent to the vector U_i as shown in Figure 10.1a. The envelope of all characteristic flow surfaces is a curve locally tangent to U_i. In two-dimensional unsteady flow this curve is the particle path, while in three-dimensional steady flow it is the streamline.

2. Characteristic wave surfaces

The normal N_i to a characteristic wave surface satisfies the vanishing of the second factor in Eq. 10.10, i.e.,

$$A_{ij} N_i N_j = 0 \tag{10.12}$$

where $A_{ij} = A_{ji}$ are functions of the dependent variables u_ν (ν = 1,2,...,n). Equation 10.12 is a quadratic equation of a cone with the normals N_i directed along the cone generators (see Appendix G on quadric cone geometry). At a point in space there exist an infinite number of characteristic

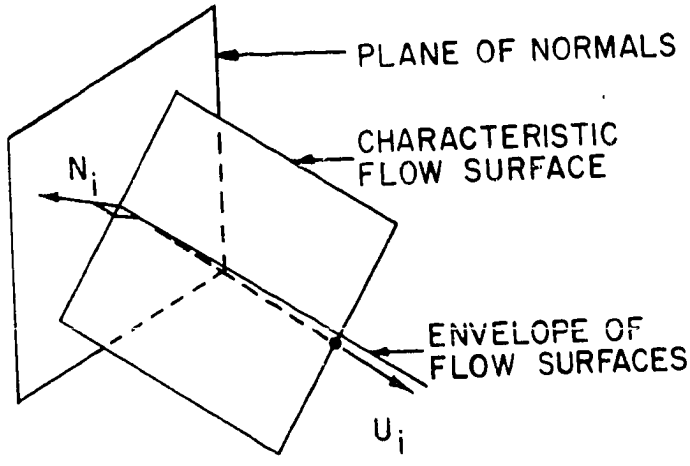

a. Flow surface geometry

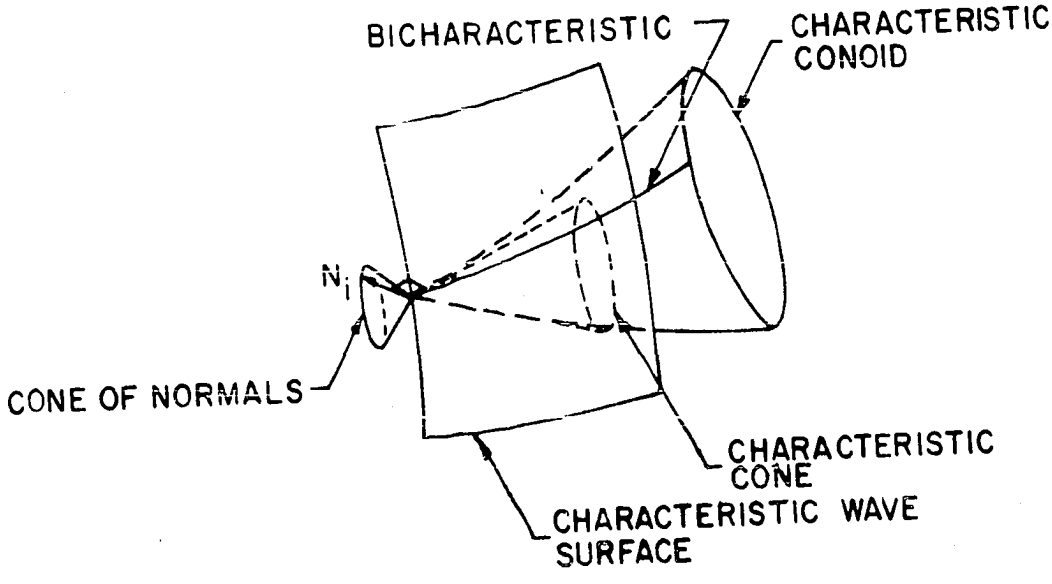

b. Wave surface geometry

Figure 10.1. Characteristic surface geometry for flow problems in gas dynamics

surfaces corresponding to the infinite number of normals which satisfy Eq. 10.12. The envelope of these surfaces is called the characteristic conoid, shown in Figure 10.1b. The reciprocal cone to the cone of normals is called the characteristic cone and is locally tangent to the characteristic conoid. The curves of contact between the characteristic wave surfaces and the characteristic conoid are called bicharacteristics. In three-dimensional steady supersonic flows, the characteristic cone is the right-circular Mach cone, while in two-dimensional unsteady flows the characteristic cone is the oblique-circular sonic cone. In both flow cases, the local tangent vector to the envelope of characteristic flow surfaces, U_i, lies along the axis of the characteristic cone.

The equation of the characteristic cone, or equivalently, the equation of the reciprocal cone to the cone of normals is, according to Eq. 16.32

$$A_{ij}^{-1} x_i x_j = 0 \tag{10.13}$$

where A_{ij}^{-1} are the elements of the inverse matrix to A_{ij}. The vectors x_i satisfying Eq. 10.13, lie along generators of the characteristic cone. This cone is locally tangent to a differential element of the characteristic conoid whose equation is

$$A_{ij}^{-1} dx_i dx_j = 0 \tag{10.14}$$

in which the vectors dx_i are locally tangent to the

bicharacteristics.

C. Compatibility Relations

The compatibility relation, Eq. 10.6, is an interior operator on a characteristic surface; thus, the equation can be written in terms of derivatives in only two independent variables. Consider the transformation from coordinates x_i to a new system x_i', where x_3' = constant is a characteristic surface. Choose the components of N_i such that

$$\frac{\partial x_3'}{\partial x_i} = N_i \tag{10.15}$$

The original system of equations, Eq. 10.1, under this transformation becomes

$$a'_{\mu\nu i} \frac{\partial u_\nu}{\partial x_i'} = b_\mu \qquad (\mu,\nu = 1,2,\ldots,n) \tag{10.16}$$

where

$$a'_{\mu\nu i} = a_{\mu\nu j} \frac{\partial x_i'}{\partial x_j} \tag{10.17}$$

If Eq. 10.16 is multiplied by the left eigenvector defined by Eq. 10.8, then an equivalent form of Eq. 10.3, is

$$w_\mu a'_{\mu\nu i} \frac{\partial u_\nu}{\partial x_i'} = w_\mu b_\mu \tag{10.18}$$

According to Eqs. 10.8 and 10.15 we have

$$w_\mu \, a_{\mu\nu i} \, N_i = w_\mu \, a_{\mu\nu i} \, \frac{\partial x_3'}{\partial x_i} = w_\mu \, a'_{\mu\nu 3} = 0 \qquad (10.19)$$

Thus, Eq. 10.18 becomes

$$w_\mu \, a'_{\mu\nu 1} \, \frac{\partial u_\nu}{\partial x_1'} + w_\mu \, a'_{\mu\nu 2} \, \frac{\partial u_\nu}{\partial x_2'} = w_\mu b_\mu \qquad (10.20)$$

Equation 10.20 is the general form of the compatibility relation which must be satisfied by the dependent variables, u_ν, on a characteristic surface corresponding to eigenvector w_μ. Equation 10.20 can be more simply expressed as

$$E_\nu \, \frac{\partial u_\nu}{\partial x_1'} + F_\nu \, \frac{\partial u_\nu}{\partial x_2'} = D \qquad (10.21)$$

where the coefficients E_ν and F_ν depend on the particular choice of the x_1' and x_2' directions.

D. Interdependence of the Compatibility Relations

The number of independent solutions for the left eigenvector w_μ in Eq. 10.8 corresponding to a particular normal N_i is determined by the rank of the coefficient matrix. If p is the rank of the matrix and n is the order of the system, then the number of linearly independent solutions s for w_μ is

$$s = n - p \qquad (10.22)$$

Thus, there are s independent compatibility relations for each normal which, according to Eq. 10.6, have the form

$$\underset{W_\nu^j}{d}\, u_\nu = B^j\, d\tau \quad (j = 1,2,\ldots,s) \tag{10.23}$$

Here

$$W^j_{\nu i} = w^j_\mu\, a_{\mu\nu i} \tag{10.24}$$

where w^j_μ, $(j = 1,2,\ldots,s)$ are the linearly independent solutions of Eq. 10.8.

Since any compatibility relation is a linear combination of the n original equations, Eq. 10.1, the number of independent relations corresponding to one or several characteristic normals N_i cannot exceed n. The dependency of the various compatibility relations can be determined by constructing the matrix w^j_μ $(j = 1,2,\ldots,n)$ whose rows are the left eigenvectors for each the relations considered. The rank of the matrix yields the number of independent relations and the rows of the highest order nonzero determinant show which relations are independent.

XI. APPENDIX B:

THE GENERAL NUMERICAL METHOD

The general numerical method utilizing the infinite family of bicharacteristics passing through a point and having second-order accuracy is presented in this section. The method was originally developed by Butler (17) and later extended by Ransom (14); the summary given below closely follows Ransom's work.

Butler's scheme applies to problems in which the characteristic equation factors into a repeated linear factor and a symmetric quadratic factor (as presented in the general theory in Appendix A). Such problems are not restricted to those in gas dynamics; however, the discussion here is directed to problems in gas dynamics.

A. Parametric Representation of Bicharacteristics

A differential element of the characteristic conoid, corresponding to the quadratic factor in the characteristic equation, is represented by the quadratic equation [Eq. 10.14]

$$A_{ij}^{-1}\, dx_i\, dx_j = 0 \tag{11.1}$$

where $A_{ij}^{-1} = A_{ji}^{-1}$. The differential vectors satisfying Eq. 11.1 lie along the bicharacteristics of the conoid. Butler (17) introduced the following parametric representation for the

infinite family of bicharacteristics passing through a point

$$dx_i = (\lambda_i + \mu_i \cos\theta + \nu_i \sin\theta)\, d\tau, \qquad (i = 1,2,3) \qquad (11.2)$$

where θ is a parameter corresponding to a particular bicharacteristic and has the range $0 \leq \theta < 2\pi$. The reference vectors set $\{\lambda_i, \mu_i, \nu_i\}$ of the parameterization must satisfy the equation of the differential conoid, Eq. 11.1. Substitution of Eq. 11.2 into Eq. 11.1 for dx_i yields the condition

$$A_{ij}^{-1} (\lambda_i\lambda_j + \mu_i\mu_j \cos^2\theta + \nu_i\nu_j \sin^2\theta + 2\lambda_i\mu_j \cos\theta + 2\lambda_i\mu_j \sin\theta + 2\mu_i\nu_j \cos\theta \sin\theta) = 0 \qquad (11.3)$$

which is identically satisfied if λ_i, μ_i and ν_i are selected such that

$$-A_{ij}^{-1} \lambda_i\lambda_j = A_{ij}^{-1} \mu_i\mu_j = A_{ij}^{-1} \nu_i\nu_j \qquad (11.4)$$

and

$$A_{ij}^{-1} \lambda_i\mu_j = A_{ij}^{-1} \lambda_i\nu_j = A_{ij}^{-1} \mu_i\nu_j = 0 \qquad (11.5)$$

The condition expressed by Eq. 11.5 is that the reference vectors are mutual conjugate diameters of the cone (see Appendix G). Equation 11.4 is a "normalization condition" on the lengths of the reference vectors.

Consider a transformation of coordinates from the coordinates x_i to a new system $\bar{x}_i$ with λ_i, μ_i and ν_i as basis

vectors. The equations of this transformation can be expressed as

$$dx_i = \lambda_i \, d\bar{x}_1 + \mu_i \, d\bar{x}_2 + \nu_i \, d\bar{x}_3, \quad (i = 1,2,3) \tag{11.6}$$

where the endpoints of the basis vectors λ_i, μ_i and ν_i are unit points on the coordinate axes $\bar{x}_1$, $\bar{x}_2$ and $\bar{x}_3$, respectively. The equation of the cone in the new basis, obtained by substitution of Eq. 11.6 into Eq. 11.1, is

$$\begin{aligned} &A^{-1}_{ij} \lambda_i\lambda_j \, (d\bar{x}_1)^2 + A^{-1}_{ij} \mu_i\mu_j \, (d\bar{x}_2)^2 + A^{-1}_{ij} \nu_i\nu_j \, (d\bar{x}_3)^2 \\ &+ 2A^{-1}_{ij} \lambda_i\mu_j \, d\bar{x}_1 d\bar{x}_2 + 2A^{-1}_{ij} \lambda_i\nu_j \, d\bar{x}_1 d\bar{x}_3 + 2A^{-1}_{ij} \mu_i\nu_j \, d\bar{x}_2 d\bar{x}_3 = 0 \end{aligned} \tag{11.7}$$

This reduces to the canonical form

$$\bar{A}^{-1}_{11} \, (d\bar{x}_1)^2 + \bar{A}^{-1}_{22} \, (d\bar{x}_2)^2 + \bar{A}^{-1}_{33} \, (d\bar{x}_3)^2 = 0 \tag{11.8}$$

if the basis vectors are mutually conjugate diameters of the cone [Eq. 11.5]. The normalization condition expressed by Eq. 11.4 renders a particularly simple form of the transformed quadric equation, i.e.,

$$-(d\bar{x}_1)^2 + (d\bar{x}_2)^2 + (d\bar{x}_3)^2 = 0 \tag{11.9}$$

which is the equation of a real cone completely enclosing the $\bar{x}_1$ axis. Thus the normalization condition also ensures that the vector λ_i lies interior to the cone. There is a double

infinity of transformations which reduce the equation of the cone to canonical form corresponding to the double infinity of sets of mutual conjugate diameters of a cone (see Appendix G, Section E).

B. Bicharacteristic Tangency Condition

In Section E, one degree of freedom in the choice of the reference vectors λ_i, μ_i, and ν_i is removed by requiring λ_i to lie along a particular direction interior to the differential conoid throughout the (x_1, x_2, x_3) space.

The remaining degree of freedom in the choice of orientation of μ_i and ν_i in the polar plane of λ_i is used to satisfy the requirement that the integrals

$$x_i - x_i^0 = \int_0^\tau (\lambda_i + \mu_i \cos\theta + \nu_i \sin\theta)\, d\tau, \quad (i = 1,2,3) \qquad (11.10)$$

for constant value of θ define a bicharacteristic. The vertex of the conoid, point 0 in Figure 11.1, has coordinates x_i^0. The vectors λ_i, μ_i, and ν_i satisfy Eqs. 11.4 and 11.5 for the differential conoid throughout the space and, in general, are functions of the coordinates θ and τ on the conoid surface. Since the equation of the conoid, Eq. 11.10, can be expressed as $x_i = x_i(\theta,\tau)$, the differential vector dx_i tangent to the conoid at any point is given by the equations

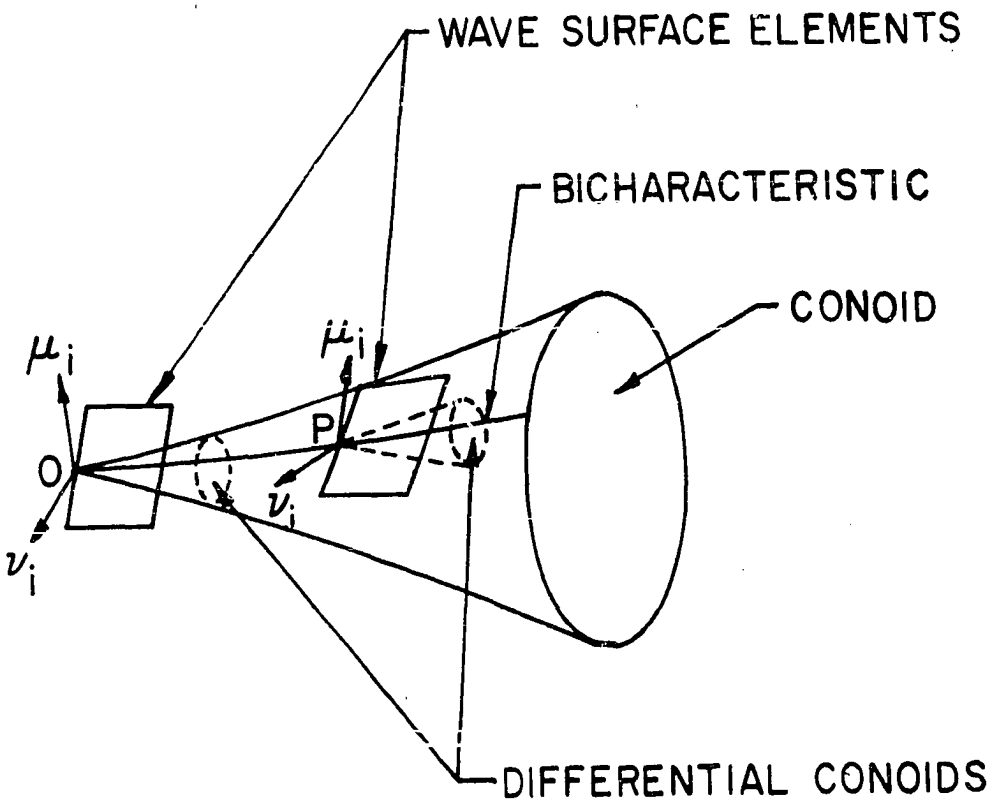

Figure 11.1. Orientation of reference vectors μ_i and ν_i along a bicharacteristic of a characteristic conoid

$$dx_i = \frac{\partial x_i}{\partial \theta} d\theta + \frac{\partial x_i}{\partial \tau} d\tau \qquad (11.11)$$

The second term in Eq. 11.11 is obtained by differentiating Eq. 11.10 with respect to τ, i.e.,

$$\frac{\partial x_i}{\partial \tau} = \lambda_i + \mu_i \cos\theta + \nu_i \sin\theta \qquad (11.12)$$

which is a vector everywhere tangent to the bicharacteristic corresponding to θ. The differential conoid whose vertex is at a point P in Figure 11.1 touches the conoid along the bicharacteristic. The equation of a surface element tangent to this differential conoid (Appendix G, Section C) along the direction $\lambda_i + \mu_i \cos\theta + \nu_i \sin\theta$ is

$$A_{ij}^{-1} (\lambda_j + \mu_j \cos\theta + \nu_j \sin\theta)\, dx_i = 0 \qquad (11.13)$$

This surface element is also tangent to the conoid surface at P. Therefore, Eq. 11.11 must satisfy Eq. 11.13; that is,

$$A_{ij}^{-1} (\lambda_j + \mu_j \cos\theta + \nu_j \sin\theta) \frac{\partial x_i}{\partial \theta} d\theta$$

$$+ A_{ij}^{-1} (\lambda_j + \mu_j \cos\theta + \nu_j \sin\theta) \frac{\partial x_i}{\partial \tau} d\tau = 0 \qquad (11.14)$$

If $\frac{\partial x_i}{\partial \tau}$ from Eq. 11.12 is substituted into this equation and the conditions on the reference vector set $\{\lambda_i, \mu_i, \nu_i\}$, Eqs. 11.4

and 11.5, are employed, then the second term in Eq. 11.14 vanishes identically. Hence, Eq. 11.14 becomes

$$A_{ij}^{-1} (\lambda_j + \mu_j \cos\theta + \nu_j \sin\theta) \frac{\partial x_i}{\partial \theta} = 0 \qquad (11.15)$$

This equation is sufficient to determine the orientation of the vectors μ_i and ν_i along the bicharacteristics relative to a fixed reference at the vertex of the conoid.

C. General Form of the Wave Surface Compatibility Relation

The general form of the compatibility relation, Eq. 10.21, can now be written for the characteristic wave surfaces in terms of the bicharacteristic parameter θ. The equation of a differential element of the wave surface, tangent to the characteristic conoid along the bicharacteristic lirection $\lambda_i + \mu_i \cos\theta + \nu_i \sin\theta$, is obtained from the equation of the conoid, Eq. 11.1, and has the form

$$A_{ij}^{-1} (\lambda_i + \mu_i \cos\theta + \nu_i \sin\theta)\, dx_j = 0 \qquad (11.16)$$

where the differential vector dx_j lies in the wave surface. From this result, the wave surface normal, N_i, can be expressed as

$$N_i = A_{ij}^{-1} (\lambda_j + \mu_j \cos\theta + \nu_j \sin\theta) \quad (i = 1,2,3) \qquad (11.17)$$

The bicharacteristic direction lies in the wave surface and is chosen as one of the two directions of differentiation in the general form of the compatibility relation, Eq. 10.21. The second direction, M_i,

$$M_i = \nu_i \cos\theta - \mu_i \sin\theta \tag{11.18}$$

is picked to yield a particular form for the compatibility relation. The orthogonality of M_i and the wave surface normal N_i can be verified by taking their scalar product and using Eqs. 11.4 and 11.5.

The general form of the wave surface compatibility relation is now written in terms of the bicharacteristic and M_i directions as

$$A_\nu \, (\lambda_i + \mu_i \cos\theta + \nu_i \sin\theta) \, \frac{\partial u_\nu}{\partial x_i}$$

$$= B + C_\nu \, (\nu_i \cos\theta - \mu_i \sin\theta) \, \frac{\partial u_\nu}{\partial x_i} \tag{11.19}$$

where the coefficient A_ν, B, and C_ν are functions of θ, x_i and u_ν.

The dependence of the coefficients A_ν, B, and C_ν on θ in Eq. 11.19 is determined by considering the wave surface compatibility relations for the case n = 3 (i.e., a system of three equations in three dependent variables, u_ν). Equation

11.19, written for $\theta = 0,\ \pi/2,\ \pi,$ and $\frac{3\pi}{2}$, yields

$$A_\nu(0)\ (\lambda_i + \mu_i)\ \frac{\partial u_\nu}{\partial x_i} = B(0) + C_\nu(0)\nu_i\ \frac{\partial u_\nu}{\partial x_i} \tag{11.20}$$

$$A_\nu(\pi/2)\ (\lambda_i + \nu_i)\ \frac{\partial u_\nu}{\partial x_i} = B(\pi/2) - C_\nu(\pi/2)\ \mu_i\ \frac{\partial u_\nu}{\partial x_i} \tag{11.21}$$

$$A_\nu(\pi)\ (\lambda_i - \mu_i)\ \frac{\partial u_\nu}{\partial x_i} = B(\pi) - C_\nu(\pi)\ \nu_i\ \frac{\partial u_\nu}{\partial x_i} \tag{11.22}$$

$$A_\nu(\tfrac{3\pi}{2})(\lambda_i - \nu_i)\ \frac{\partial u_\nu}{\partial x_i} = B\ (\tfrac{3\pi}{2}) + C_\nu(\tfrac{3\pi}{2})\ \mu_i\ \frac{\partial u_\nu}{\partial x_i} \tag{11.23}$$

Each of these four equations can be considered as linear combinations of the original three equations. Therefore, Eqs. 11.20 - 11.23 are not linearly independent, and there exists a linear combination of these equations which yields an identity. Assume that α, β, γ, δ are scalar multipliers of Eqs. 11.20-11.23, respectively, in the linear combination. Since the vectors λ_i, μ_i, and ν_i are independent, the coefficients of the derivatives $\lambda_i \frac{\partial u_\nu}{\partial x_i}$, $\mu_i \frac{\partial u_\nu}{\partial x_i}$, and $\nu_i \frac{\partial u_\nu}{\partial x_i}$ in the linear combination must vanish. This yields the relations

$$\alpha\ A_\nu(0) + \beta\ A_\nu(\tfrac{\pi}{2}) + \gamma\ A_\nu(\pi) + \delta\ A_\nu(\tfrac{3\pi}{2}) = 0 \tag{11.24}$$

$$\alpha A_\nu(0) + \beta C_\nu(\pi/2) - \gamma A_\nu(\pi) - \delta C_\nu(\tfrac{3\pi}{2}) = 0 \qquad (11.25)$$

$$-\alpha C_\nu(0) + \beta A_\nu(\pi/2) + \gamma C_\nu(\pi) - \delta A_\nu(\tfrac{3\pi}{2}) = 0 \qquad (11.26)$$

$$\alpha B(0) + \beta B(\pi/2) + \gamma B(\pi) + \delta B(\tfrac{3\pi}{2}) = 0 \qquad (11.27)$$

Also, any three of the equations, Eqs. 11.20 through 11.23, are equivalent to the original system of differential equations and therefore must have the same characteristic surfaces. This condition yields the additional relation

$$\alpha C_\nu(0) + \beta C_\nu(\pi/2) + \gamma C_\nu(\pi) + \delta C_\nu(\tfrac{3\pi}{2}) = 0 \qquad (11.28)$$

Equations 11.24-11.28 are not only conditions on the numbers α, β, γ, and δ but also (as to be shown later) on the dependence of A_ν, B, and C_ν on the parameter θ.

The θ-dependence of the coefficients A_ν, B, and C_ν is obtained by multiplying Eqs. 11.20-11.23 by the factors $\alpha(1 + 2\cos\theta)$, $\beta(-1-2\sin\theta)$, $\gamma(1 - 2\cos\theta)$, and $\delta(-1 + 2\sin\theta)$, respectively, and summing. This particular combination has the property that the correct θ-dependence of the directional derivatives results, and for $\theta = 0, \pi/2, \pi$, and $\frac{3\pi}{2}$, Eqs. 11.20-11.23 are reproduced.

After considerable rearrangement of terms in the summation equation just described and use of Eqs. 11.24 through 11.28, the general form of the wave surface compatibility relation, Eq. 11.9, is obtained in which the coefficients have the following form

$$A_\nu = A_{1\nu} + A_{2\nu} \cos\theta + A_{3\nu} \sin\theta \tag{11.29}$$

$$B = B_1 + B_2 \cos\theta + B_3 \sin\theta \tag{11.30}$$

$$C_\nu = C_{1\nu} + C_{2\nu} \cos\theta + C_{3\nu} \sin\theta \tag{11.31}$$

in which

$$A_{1\nu} = \alpha\, A_\nu(0) - \beta\, A_\nu(\pi/2) + \gamma\, A_\nu(\pi) - \delta\, A_\nu(\tfrac{3\pi}{2}) \tag{11.32}$$

$$A_{2\nu} = 2[\alpha\, A_\nu(0) - \gamma\, A_\nu(\pi)] \tag{11.33}$$

$$A_{3\nu} = -2[\beta\, A_\nu(\pi/2) - \delta\, A_\nu(\tfrac{3\pi}{2})] \tag{11.34}$$

$$C_{1\nu} = 2[\alpha\, C_\nu(0) + \gamma\, C_\nu(\pi)] \tag{11.35}$$

$$C_{2\nu} = -A_{3\nu} \tag{11.36}$$

$$C_{3\nu} = A_{2\nu} \tag{11.37}$$

$$B_1 = \alpha\, B(0) - \beta\, B(\pi/2) + \gamma\, B(\pi) - \delta\, B(\frac{3\pi}{2}) \tag{11.38}$$

$$B_2 = 2[\alpha\, B(0) - \gamma\, B(\pi)] \tag{11.39}$$

$$B_3 = -2[\beta\, B(\pi/2) - \delta\, B(\frac{3\pi}{2})] \tag{11.40}$$

The dependence of the coefficients A_ν, B, and C_ν on θ is shown explicitly in Eqs. 11.29-11.31.

D. The General Form of the Noncharacteristic Relation

In the general numerical method, a noncharacteristic relation formed by taking a particular linear combination of the original differential equations is employed. This equation is obtained by multiplying Eqs. 11.20-11.23 by α, $-\beta$, γ, and $-\delta$, respectively, and summing. After rearrangement and use of Eqs. 11.25 and 11.26, the equation

$$A_{1\nu}{}^{\lambda_i} \frac{\partial u_\nu}{\partial x_i} = B_1 + C_{2\nu}{}^{\nu_i} \frac{\partial u_\nu}{\partial x_i} - C_{3\nu}{}^{\mu_i} \frac{\partial u_\nu}{\partial x_i} \tag{11.41}$$

is obtained, where the coefficients $A_{1\nu}$, B_1, $C_{2\nu}$, and $C_{3\nu}$ are given in the preceding section. This equation is used in the elimination of cross derivatives of the dependent variables u_ν at the solution point in the numerical scheme.

E. The Second-Order Numerical Scheme

In the numerical solution scheme, an inverse network is used in which the solution point with coordinates $x_i = \alpha_i$ is fixed, and the bicharacteristics through the solution point are projected back into the noncharacteristic initial data surface, $f(x_i) = 0$. It is assumed that the base points at the intersection of the bicharacteristics and the initial data surface can be located to second-order accuracy using Eq. 11.2, and that second-order accurate estimates of the dependent variables u_ν can be obtained at these points. Equations 11.19 and 11.41 are then used to determine u_ν correct to second-order accuracy at the solution point α_i.

Equations 11.19 and 11.41 can be written in operator notation as

$$A_\nu d_L u_\nu = [B + C_\nu(\nu_i \cos\theta - \mu_i \sin\theta) \frac{\partial u_\nu}{\partial x_i}] \, d\tau \qquad (11.42)$$

and

$$A_{1\nu} d_\lambda u_\nu = [B_1 + (C_{2\nu}\nu_i - C_{3\nu}\mu_i) \frac{\partial u_\nu}{\partial x_i}] \, d\tau \qquad (11.43)$$

where L denotes the bicharacteristic direction, L_i, and λ the λ_i direction. Bicharacteristics through α_i meet the initial data surface $f(x_i) = 0$ at $\tau = -\tau(\theta)$. Thus Eq. 11.42 written in finite-difference form along the bicharacteristics, using the modified Euler scheme (ref. 61), is

$$\bar{A}_\nu [u_\nu(\alpha) - u_\nu(f)] = \{\bar{B} + \tfrac{1}{2}[S(\alpha) + S(f)]\}\, \tau(\theta) + 0(\tau^3) \quad (11.44)$$

where

$$S = C_\nu (\nu_i \cos\theta - \mu_i \sin\theta) \frac{\partial u_\nu}{\partial x_i} \quad (11.45)$$

$$\bar{A}_\nu = \tfrac{1}{2}[A_\nu(\alpha) + A_\nu(f)] \quad (11.46)$$

$$\bar{B} = \tfrac{1}{2}[B(\alpha) + B(f)] \quad (11.47)$$

The notations $u_\nu(\alpha)$ and $u_\nu(f)$ are used to denote the dependent variables at the solution point α_i, and at the base points on the surface $f(x_i) = 0$, respectively. The quantities $u_\nu(\alpha)$ and $u_\nu(f)$ in Eq. 11.44 have been assumed correct to order τ^2, and $\bar{B}$, $S(\alpha)$, and $S(f)$ to order τ. The quantities $\bar{A}_\nu$ need only be correct to zeroth order in τ.

The direction of λ_i is now chosen such that $C_{1\nu} = 0$ throughout the (x_1, x_2, x_3) space. (This condition is satisfied in two-dimensional unsteady, and three-dimensional steady supersonic flows in gas dynamics with λ_i directed along the axis of the characteristic cone.) The vanishing of this coefficient is required to eliminate the cross derivative terms at the solution point α_i in the numerical scheme. In Eq. 11.44, $S(\alpha)$ is then given by

$$S(\alpha) = (C_{2\nu} \cos\theta + C_{3\nu} \sin\theta)(\nu_i \cos\theta - \mu_i \sin\theta) \frac{\partial u_\nu}{\partial x_i} \quad (11.48)$$

where $C_{2\nu}$, $C_{3\nu}$, $\nu_i \frac{\partial u_\nu}{\partial x_i}$, and $\mu_i \frac{\partial u_\nu}{\partial x_i}$ are evaluated at $x_i = \alpha_i$.

In order to maintain second-order accuracy in the numerical scheme, the cross derivatives, $\nu_i \frac{\partial u_\nu}{\partial x_i}$ and $\mu_i \frac{\partial u_\nu}{\partial x_i}$, appearing in Eq. 11.48 must be evaluated or eliminated. In any explicit scheme these terms cannot be evaluated until after the entire solution surface is solved. Butler (17) eliminated these terms by using weighted integration of the infinite number of wave surface compatibility relations which exist at a point.

Consider Eq. 11.44 weighted first by the factor $f(\alpha)\cos\theta/\tau(\theta)$, and then by $f(\alpha)\sin\theta/\tau(\theta)$; these resultant equations integrated with respect to θ between limits 0 and 2π give

$$u_\nu(\alpha) \int_0^{2\pi} \frac{f(\alpha)\,\bar{A}_\nu \cos\theta}{\tau(\theta)}\,d\theta = \int_0^{2\pi} \frac{f(\alpha)\,u_\nu(f)\,\bar{A}_\nu \cos\theta}{\tau(\theta)}\,d\theta$$

$$+ \tfrac{1}{2} \int_0^{2\pi} f(\alpha)S(f)\cos\theta\,d\theta + \int_0^{2\pi} f(\alpha)\bar{B}\cos\theta\,d\theta + 0(f^3(\alpha)) \quad (11.49)$$

and

$$u_\nu(\alpha) \int_0^{2\pi} \frac{f(\alpha)\ \bar{A}_\nu\ \sin\theta}{\tau(\theta)}\, d\theta = \int_0^{2\pi} \frac{f(\alpha) u_\nu(f)\ \bar{A}_\nu\ \sin\theta}{\tau(\theta)}\, d\theta$$

$$+ \tfrac{1}{2} \int_0^{2\pi} f(\alpha) S(f)\ \sin\theta\ d\theta + \int_0^{2\pi} f(\alpha)\bar{B}\ \sin\theta\ d\theta + 0(f^3(\alpha)) \qquad (11.50)$$

where $f(\alpha)$ is the evaluation of the function $f(x_i)$ at the point $x_i = \alpha_i$.

A third condition on $u_\nu(\alpha)$ is obtained by considering the noncharacteristic relation, Eq. 11.43, written along the curve $dx_i = \lambda_i d\tau$ inside the characteristic conoid. Suppose that the curve $dx_i = \lambda_i d\tau$ through $x_i = \alpha_i$ meets the initial data surface at $\tau = -h$. Let the value of u_ν at this point be denoted by $u_\nu(h)$. Then, using the modified Euler scheme, the difference form of Eq. 11.43 is

$$A^*_{1\nu}[u_\nu(\alpha) - u_\nu(h)] = h \left[B^*_1 + \tfrac{1}{2}\left(C_{2\nu\nu_i} \frac{\partial u_\nu}{\partial x_i} - C_{3\nu\mu_i} \frac{\partial u_\nu}{\partial x_i} \right)_{x_i = \alpha_i} \right.$$

$$\left. + \tfrac{1}{2}\left(C_{2\nu\nu_i} \frac{\partial u_\nu}{\partial x_i} - C_{3\nu\mu_i} \frac{\partial u_\nu}{\partial x_i} \right)_{\tau = -h} \right] + 0(h^3) \qquad (11.51)$$

where

$$A^*_{1\nu} = \tfrac{1}{2}[A_{1\nu}(\alpha) + A_{1\nu}(h)] \qquad (11.52)$$

$$B_1^* = \tfrac{1}{2}[B_1(\alpha) + B_1(h)] \tag{11.53}$$

Equation 11.44 is weighted by the factor h/τ, and integrated with respect to θ from 0 to 2π. Then Eq. 11.51, multiplied by π, is subtracted from the integral of Eq. 11.44 to yield

$$u_\nu(\alpha)\left[\int_0^{2\pi} \frac{h\bar{A}_\nu}{\tau(\theta)}\, d\theta - \pi A_{1\nu}^*\right] = \int_0^{2\pi} \frac{hu_\nu(f)\,\bar{A}_\nu}{\tau(\theta)}\, d\theta - \pi A_{1\nu}^*\, u_\nu(h)$$

$$+ \tfrac{1}{2}\int_0^{2\pi} h\bar{S}(f)\, d\theta - \frac{\pi h}{2}\left[C_{2\nu}{}^{\nu}{}_i \frac{\partial u_\nu}{\partial x_i} - C_{3\nu}{}^{\mu}{}_i \frac{\partial u_\nu}{\partial x_i}\right]_\tau = -h$$

$$+ \int_0^{2\pi} h\bar{B}\, d\theta - \pi h B_1^* + O(h^3) \tag{11.54}$$

Note that Eqs. 11.49, 11.50 and 11.54 do not depend on the derivatives of the dependent variables at the solution point; hence, they provide a basis for an iterative scheme which determines $u_\nu(\alpha)$ correct to $O(h^2)$. Equations 11.49, 11.50, and 11.54 are the necessary three independent equations for the dependent variables, $u_\nu(\alpha)$, when $n = 3$. If $n > 3$, it is assumed that the additional $n - 3$ conditions needed to form a complete system of equations can be obtained from the compatibility relations written on flow surfaces.

In practice, the integrals with respect to θ in Eqs. 11.49, 11.50, and 11.54 are replaced by sums over the four values $\theta = 0$, $\pi/2$, π, and $\frac{3\pi}{2}$. Initial values of u_ν, $\mu_i \frac{\partial u_\nu}{\partial x_i}$ and $\nu_i \frac{\partial u_\nu}{\partial x_i}$ on the surface $f(x_i) = 0$ at the intersections of the four bicharacteristics and the curve $dx_i = \lambda_i d\tau$ are determined by intepolation among sets of known points on the surface. If it is sufficient to obtain a solution correct to $0(h)$, the terms containing $\mu_i \frac{\partial u_\nu}{\partial x_i}$ and $\nu_i \frac{\partial u_\nu}{\partial x_i}$ in Eqs. 11.49, 11.50, and 11.54 can be neglected since these terms are of order h^2 in the finite-difference form of the compatibility relation, Eq. 11.44.

XII. APPENDIX C: FINITE-DIFFERENCE FORM OF THE BICHARACTERISTIC TANGENCY CONDITION

In order to maintain second-order accuracy in the numerical solution scheme (Chapter III), the bicharacteristic tangency condition Eq. 3.9

$$(\alpha_i \cos\theta + \beta_i \sin\theta) \frac{\partial x_i}{\partial \theta} = 0 \quad (i = 1,2) \tag{12.1}$$

must be satisfied to second-order accuracy. The finite-difference approximation of Eq. 12.1, developed in this section, yields conditions on the reference vectors $\alpha_i(k)$, $\beta_i(k)$ $(k = 1,2,3,4)$ at the intersections of the four bicharacteristics corresponding to $\theta = 0, \pi/2, \pi, 3\pi/2$ and the initial data plane. The equations for the reference vector components are written in terms of a fixed reference for $\alpha_i(6)$ and $\beta_i(6)$ at the solution point (6).

The difference approximation for the derivative $\frac{\partial x_i}{\partial \theta}$ in Eq. 12.1 is found by first integrating the bicharacteristic equation, Eq. 3.3, i.e.,

$$x_i(\theta,t) - x_i(6) = \int_o^t (u_i + a\cos\theta\ \alpha_i + a\sin\theta\ \beta_i)dt$$

$$(i = 1,2) \tag{12.2}$$

where t = 0 corresponds to the solution point (6) at the vertex of the conoid. The integral above, correct to $0(t^2)$, is determined using the power series expansions for u_i, α_i, β_i and a about the solution point (6),

$$u_i = u_i(6) + u_i(\theta)t + 0(t^2) \tag{12.3}$$

$$\alpha_i = \alpha_i(6) + \alpha_i(\theta)t + 0(t^2) \tag{12.4}$$

$$\beta_i = \beta_i(6) + \beta_i(\theta)t + 0(t^2) \tag{12.5}$$

$$a = a(6) + a(\theta)t + 0(t^2) \tag{12.6}$$

where numbers in parentheses indicate evaluations of functions at corresponding network points. Also, the simplified notation $u_i(\theta) = \left.\frac{\partial u_i}{\partial t}\right|_{t=0}$, etc. is used for the coefficient of the first-order terms of the expansions. If Eqs. 12.3-12.6 are substituted into Eq. 12.2 and the resulting equation integrated, we get

$$\begin{aligned} x_i(\theta,t) - x_i(6) = {} & \{u_i(6) + a(6)\,[\alpha_i(6)\cos\theta + \beta_i(6)\sin\theta]\}\,t \\ & + \tfrac{1}{2}\{u_i(\theta) + a(\theta)\,[\alpha_i(6)\cos\theta + \beta_i(6)\sin\theta] \\ & + a(6)\,[\alpha_i(\theta)\cos\theta + \beta_i(\theta)\sin\theta]\}\,t^2 \\ & + 0(t^3) \end{aligned} \tag{12.7}$$

An approximate expression for the derivative $\frac{\partial x_i}{\partial \theta}$ obtained by differentiating Eq. 12.7 with respect to θ is

$$\frac{\partial x_i}{\partial \theta} = a(6)\ [\beta_i(6)\ \cos\theta - \alpha_i(6)\ \sin\theta]\ t$$

$$+ \tfrac{1}{2}\ \{u'_i(\theta) + a'(\theta)\ [\alpha_i(6)\ \cos\theta + \beta_i(6)\ \sin\theta]$$

$$+ a(\theta)\ [\beta_i(6)\ \cos\theta - \alpha_i(6)\ \sin\theta]$$

$$+ a(6)\ [\beta_i(\theta)\ \cos\theta - \alpha_i(\theta)\ \sin\theta$$

$$+ \beta_i'(\theta)\ \sin\theta + \alpha_i'(\theta)\ \cos\theta]\}\ t^2$$

$$+ 0(t^3) \qquad (12.8)$$

where the primes denote differentiation with respect to θ.

To complete the numerical approximation of the bicharacteristic tangency condition, the power series expansions for α_i and β_i, Eqs. 12.4 and 12.5, and the approximation for $\frac{\partial x_i}{\partial \theta}$, Eq. 12.8, are substituted into Eq. 12.1. In the resulting equation, products are expanded and terms are collected in powers of t. These terms must vanish for all values of t; therefore, the coefficients of powers of t must vanish individually. In maintaining second-order accuracy only the coefficients of terms up to $0(t^3)$ need be investigated. No zeroth-order terms result since the expression for $\frac{\partial x_i}{\partial \theta}$ is homogeneous in t.

The coefficient of the first-order term in t, equated to zero, yields

$$a(6)[\alpha_i(6)\cos\theta + \beta_i(6)\sin\theta][\beta_i(6)\cos\theta - \alpha_i(6)\sin\theta]=0 \quad (12.9)$$

Substitution of the orthonormal properties

$$\alpha_i\beta_i = 0 \quad (12.10)$$

$$\alpha_i\alpha_i = 1 \quad (12.11)$$

$$\beta_i\beta_i = 1 \quad (12.12)$$

evaluated at (6) into the expanded form of Eq. 12.9 yields an equation which is identically satisfied. Hence, no condition on the reference vector variation along a bicharacteristic is necessary to maintain a first-order approximation of the tangency condition.

The coefficient of the second-order term in t, equated to zero, yields

$$\begin{aligned} & a(6)\ [\alpha_i(\theta)\cos\theta + \beta_i(\theta)\sin\theta][\beta_i(6)\cos\theta - \alpha_i(6)\sin\theta] \\ & \qquad + \tfrac{1}{2}[\alpha_i(6)\cos\theta + \beta_i(6)\sin\theta] \\ & \times \{u_i'(\theta) + a'(\theta)\ [\alpha_i(6)\cos\theta + \beta_i(6)\sin\theta] \\ & \qquad + a(\theta)\ [\beta_i(6)\cos\theta - \alpha_i(6)\sin\theta] \\ & \qquad + a(6)\ [\beta_i(\theta)\cos\theta - \alpha_i(\theta)\sin\theta \\ & \qquad\qquad + \beta_i'(\theta)\sin\theta + \alpha_i'(\theta)\cos\theta]\} = 0 \end{aligned} \quad (12.13)$$

Expansion of Eq. 12.13 and utilization of the orthonormal properties of the reference vectors, Eqs. 12.10 through 12.12, yields

$$a(6)\ [\alpha_i(\theta)\cos\theta + \beta_i(\theta)\sin\theta][\beta_i(6)\cos\theta - \alpha_i(6)\sin\theta]$$

$$+ \tfrac{1}{2}\{u_i'(\theta)\ [\alpha_i(6)\cos\theta + \beta_i(6)\sin\theta] + a'(\theta)$$

$$+ a(6)\ [\alpha_i(6)\cos\theta + \beta_i(6)\sin\theta]$$

$$\times\ [\beta_i(\theta)\cos\theta - \alpha_i(\theta)\sin\theta$$

$$+\ \beta_i'(\theta)\sin\theta + \alpha_i'(\theta)\cos\theta]\} = 0 \qquad (12.14)$$

The power series expansions for α_i and β_i, Eqs. 12.4 and 12.5, and the orthonormal properties, Eqs. 12.10 and 12.12, yield approximate conditions which can be used to further simplify Eq. 12.14. Consider the scalar product $\alpha_i\alpha_i$. In terms of Eq. 12.4, we can write

$$\alpha_i\alpha_i = \alpha_i(6)\ \alpha_i(6) + 2\ \alpha_i(6)\ \alpha_i(\theta)\ t + 0(t^2) \qquad (12.15)$$

or, with substitution of Eq. 12.11

$$1 = 1 + 2\ \alpha_i(6)\ \alpha_i(\theta)\ t + 0(t^2) \qquad (12.16)$$

From this result we get a zeroth-order approximation for the product $\alpha_i(6)\ \alpha_i(\theta)$, i.e.,

$$\alpha_i(6)\ \alpha_i(\theta) = 0 + 0(t) \qquad (12.17)$$

This relation need only be correct to zeroth-order in Eq. 12.14 since Eq. 12.14 is the coefficient of t^2 in the series approximation to Eq. 12.1. Similarly, we can write

$$\beta_i(6)\ \beta_i(\theta) = 0 + 0(t) \tag{12.18}$$

and

$$\alpha_i(6)\ \beta_i(\theta) = -\ \beta_i(6)\ \alpha_i(\theta) + 0(t) \tag{12.19}$$

The derivatives of Eqs. 12.17 through 12.19 with respect to θ are

$$\alpha_i(6)\ \alpha_i'(\theta) = 0 + 0(t) \tag{12.20}$$

$$\beta_i(6)\ \beta_i'(\theta) = 0 + 0(t) \tag{12.21}$$

$$\alpha_i(6)\ \beta_i'(\theta) = -\ \beta_i(6)\ \alpha_i'(\theta) + 0(t) \tag{12.22}$$

Expansion of Eq. 12.14 and substitution of 12.17-12.22 yields

$$a(6)\ \beta_i(6)\ \alpha_i(\theta)$$

$$+ [\alpha_i(6)\ \cos\theta + \beta_i(6)\ \sin\theta]\ u_i'(\theta) + a'(\theta) = 0 \tag{12.23}$$

In order to evaluate the derivatives $u_i'(\theta)$ and $a'(\theta)$ in Eq. 12.23 we again employ the power series expansions. The derivatives of Eqs. 12.3 and 12.6 with respect to θ are

$$u_i'(\theta) = \frac{\partial u_i}{\partial \theta}\left(\frac{1}{t}\right) + 0(t) \tag{12.24}$$

$$a'(\theta) = \frac{\partial a}{\partial \theta}\left(\frac{1}{t}\right) + O(t) \tag{12.25}$$

The derivatives with respect to θ in Eqs. 12.24 and 12.25 can be expressed in terms of spatial derivatives by the chain rule as

$$\frac{\partial u_i}{\partial \theta} = \frac{\partial u_i}{\partial x_j}\frac{\partial x_j}{\partial \theta} \tag{12.26}$$

$$\frac{\partial a}{\partial \theta} = \frac{\partial a}{\partial x_j}\frac{\partial x_j}{\partial \theta} \tag{12.27}$$

According to Eq. 12.8 we can write

$$\frac{\partial x_i}{\partial \theta} = a(6)\ [\beta_i(6)\ \cos\theta - \alpha_i(6)\ \sin\theta]\ t + O(t^2) \tag{12.28}$$

Substitution of Eqs. 12.26-12.28 in Eqs. 12.24 and 12.25 yields

$$u_i'(\theta) = a(6)\ [\beta_j(6)\ \cos\theta - \alpha_j(6)\ \sin\theta]\ \frac{\partial u_i}{\partial x_j} + O(t) \tag{12.29}$$

and

$$a'(\theta) = a(6)\ [\beta_j(6)\ \cos\theta - \alpha_j(6)\ \sin\theta]\ \frac{\partial a}{\partial x_j} + O(t) \tag{12.30}$$

Since the expressions for $u_i'(\theta)$ and $a'(\theta)$ need only be correct to zeroth-order in t in Eq. 12.23, the derivatives $\frac{\partial u_i}{\partial x_i}$ and $\frac{\partial a}{\partial x_j}$ in Eqs. 12.29 and 12.30 are evaluated at the solution point on the initial data surface without affecting the order of the

approximation. Substitution into Eq. 12.23 for $u'(\theta)$ and $a'(\theta)$ from Eqs. 12.29 and 12.30 gives

$$\beta_i(6)\ \alpha_i(\theta) + [\alpha_i(6)\ \cos\theta + \beta_i(6)\ \sin\theta] \times [\beta_j(6)\ \cos\theta - \alpha_j(6)\ \sin\theta]\ \frac{\partial u_i}{\partial x_j} + [\beta_j(6)\ \cos\theta - \alpha_j(6)\ \sin\theta]\ \frac{\partial a}{\partial x_j} = 0 \qquad (12.31)$$

The scalar product of the power series expansion for α_i, Eq. 12.4, and the vector $\beta_i(6)$ yields

$$\beta_i(6)\ \alpha_i = \beta_i(6)\ \alpha_i(6) + \beta_i(6)\ \alpha_i(\theta)\ t \qquad (12.32)$$

where the higher order terms have been dropped. According to Eq. 12.10 the first term of this equation is zero. Hence, we can rewrite Eq. 12.31 as

$$\beta_i(6)\ \alpha_i = -D(\theta)\ t \qquad (12.33)$$

where

$$D(\theta) = [\alpha_i(6)\ \cos\theta + \beta_i(6)\ \sin\theta] \times [\beta_j(6)\ \cos\theta - \alpha_j(6)\ \sin\theta]\ \frac{\partial u_i}{\partial x_j} + [\beta_j(6)\ \cos\theta - \alpha_j(6)\ \sin\theta]\ \frac{\partial a}{\partial x_j} \qquad (12.34)$$

Equation 12.33 is one equation for the two components of α_i. The other relation needed is Eq. 12.11. Elimination of α_2 from Eqs. 12.33 and 12.11 yields a quadratic equation in α_1. The correct solution for α_1 is

$$\alpha_1 = -D(\theta)\ \beta_1(6)\ t + \alpha_1(6)\ [1 - D^2(\theta)\ t^2]^{\frac{1}{2}} \qquad (12.35)$$

This equation can be verified by letting t go to zero since α_1 at the base point must approach $\alpha_1(6)$ in the limit. The other component, α_2, is found by eliminating α_1 between Eqs. 12.33 and 12.35, with the result

$$\alpha_2 = -D(\theta)\ \beta_2(6)\ t + \alpha_2(6)\ [1 - D^2(\theta)\ t^2]^{\frac{1}{2}} \qquad (12.36)$$

After the components $\alpha_i(k)$ $(k = 1,2,3,4)$ are established at the bicharacteristic base points, the components $\beta_i(k)$ are determined using the orthonormal properties Eqs. 12.10 and 12.12.

XIII. APPENDIX D:

NUMERICAL STABILITY ANALYSIS

Stability of the numerical scheme for solution of a system of differential equations is a property of the difference equations which are used as approximations of the differential equations. There does not appear to exist a universal definition for stability, but the most common concept is that of stepwise stability which refers to the boundedness of the numerical solution as $t \to \infty$ for fixed time increment, Δt. Many criteria exist for testing stability, and a good discussion of the methods is given by Roache (68). All stability criteria which presently exist were developed for linear difference equations. For the case of nonlinear equations, the approach taken is to linearize the difference equations and to apply the same criteria locally.

In this section the Courant-Friedrichs-Lewy (CFL) and von Neumann stability criteria are applied to the interior point numerical algorithm developed in Chapter III. The CFL criterion is a necessary condition for stability and states that the differential domain of dependence must lie within the convex hull of the difference scheme. This condition sets an upper limit on the time increment which can be taken in the interior point algorithm. The von Neumann criterion states that a difference scheme is stable only if there is a limit to the extent that every Fourier component of the initial data is

amplified by application of the difference scheme. In application of the von Neumann criterion to the numerical method, all aspects of the scheme including interpolations for initial data must be considered. However, to show the effect of interpolations on the stability characteristics of the scheme, the difference scheme was first analyzed in two parts; (1) the basic scheme (without interpolation and using exact data at base points), and (2) the initial data interpolation scheme alone. The basic scheme was determined to be unstable for all time increments while the interpolation scheme was found to be stable. Finally the difference scheme (with interpolations for initial data) was analyzed and found to be stable when the CFL criterion was satisfied. These results show the stabilizing influence that interpolations have on the scheme.

A. Courant-Friedrichs-Lewy Stability Criterion

The Courant-Friedrichs-Lewy (CFL) stability criterion (ref. 16) states that the domain of dependence of the difference equations, defined as the convex hull of the points in the initial data surface used in the difference scheme, must contain the domain of dependence of the system of differential equations. The convex hull of the difference scheme, shown in Figure 13.1, is the boundary of the union of lines joining all pairs of the nine mesh points used for interpolation in the

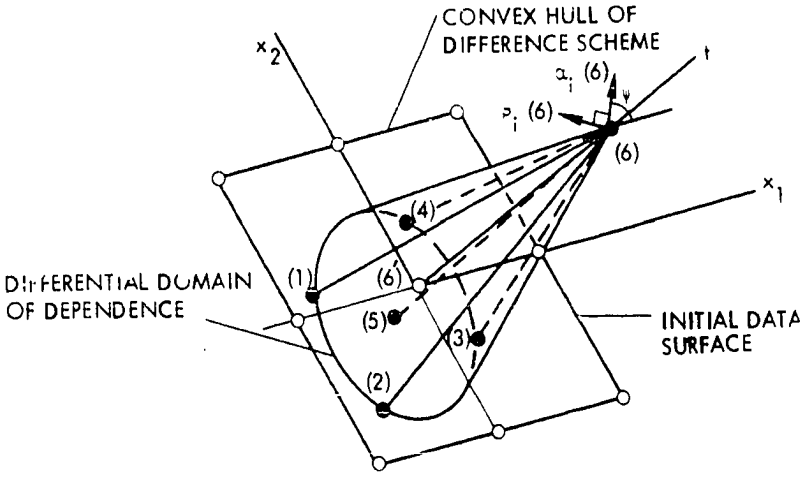

a. View showing bicharacteristics, particle path, and convex hull of difference scheme

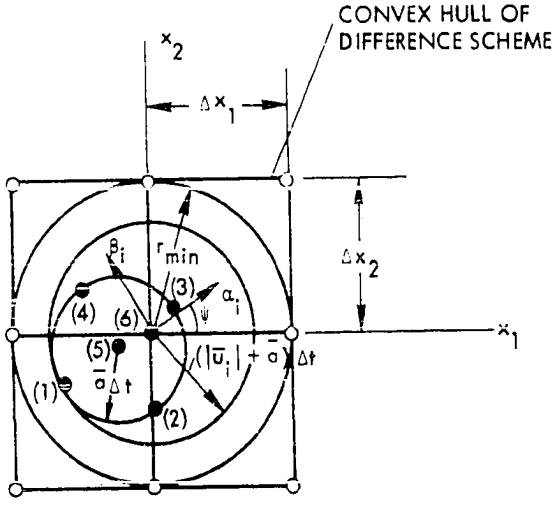

b. Projection onto initial data surface showing differential domain of dependence and convex hull of difference scheme

Figure 13.1. Pentahedral bicharacteristic line network for two-dimensional unsteady flow

initial data surface. The differential domain of dependence is, for the case of steady, uniform flow, a region bounded by a circle of radius $a\Delta t$ concentric about the intersection of the particle path and the initial data surface, point (5) in Figure 13.1.

The CFL criterion will always be satisfied if the maximum distance from the solution point, point (6), to a point on the boundary of the differential domain of dependence, $(|u_i|+a)\ \Delta t$, is made less than or equal to the minimum distance to the convex hull, r_{min} in Figure 13.1. Expressed in terms of the Courant number, C,

$$C = \frac{(|u_i|+a)\ \Delta t}{r_{min}}\ , \tag{13.1}$$

the condition is

$$C \leq 1.0 \tag{13.2}$$

This is a condition on the maximum time step which can be taken in the numerical integration and must be satisfied at all mesh points.

The above analysis was based on steady, uniform flow throughout the region of interest. In the general case, the differential domain of dependence is noncircular due to property variations. Hence, a better estimate of the maximum time step is given by the relation

$$t_{max} = \frac{r_{min}}{(|u_i|+a)_{max}} \tag{13.3}$$

where $(|u_i|+a)_{max}$ is the maximum value of that quantity evaluated at all mesh points of the nine-point cell. After solution for the dependent variables at point (6), Eq. 13.3 is again checked using the data at the solution point. Note that the maximum time step permitted by Eq. 13.3 is a conservative estimate since no accounting is made of the location of the differential domain of dependence within the convex hull (which depends on the flow angle θ).

The CFL stability criterion is a necessary condition for stability. Hahn (69) has determined that the CFL criterion is also a sufficient stability condition for simplicial networks. Networks are termed simplicial if L + 1 bicharacteristic base points are used on an initial data surface of dimension L. For problems in three independent variables, simplicial networks involve three bicharacteristic base points. Thus, the field point network, involving four bicharacteristic base points, is nonsimplicial, and the CFL criterion is not a sufficient condition for stability. Difference schemes based on nonsimplicial networks must satisfy other criteria to ensure stability.

B. von Neumann Stability Criterion

The von Neumann condition (ref. 15) states that a difference scheme is stable only if there is a limit to the extent that every Fourier component of the initial data is amplified by application of the difference scheme. This condition requires that the spectral radii, $\rho(A)$, of the amplification matrix A of the difference equations satisfy the inequality

$$\rho(A) \leq 1 + O(\Delta t) \tag{13.4}$$

for all possible combinations of the Fourier components occurring in a Fourier series solution of the difference equations (ref. 29).

Lax and Richtmyer (70) have shown the von Neumann condition to be a sufficient condition for the stability of linear difference equations only. However, the von Neumann condition has appeared to be sufficient for all nonlinear as well as linear schemes which are known to have been investigated (ref. 29).

1. Linear difference equations

In order to apply the von Neumann condition the differential characteristic relations must be linearized. The system of differential equations for unsteady flow consists of the wave surface compatibility relation, Eq. 3.11, applied along the four bicharacteristics, the noncharacteristic

relation, Eq. 3.22, written along the particle path, and the particle path compatibility relation, Eq. 2.32. However, the particle path compatibility relation is coupled to the remaining equations only through the coefficients, and therefore not needed in the linear analysis. The remaining five equations, written in terms of the directional differential operators, are

$$d_{L_1} p + \rho\, a\, \alpha_j d_{L_1} u_j + \rho\, a^2 \beta_j \beta_i \frac{\partial u_j}{\partial x_i}\, dt = 0 \tag{13.5}$$

$$d_{L_2} p + \rho\, a\, \beta_j d_{L_2} u_j + \rho\, a^2 \alpha_j \alpha_i \frac{\partial u_j}{\partial x_i}\, dt = 0 \tag{13.6}$$

$$d_{L_3} p - \rho\, a\, \alpha_j d_{L_3} u_j + \rho\, a^2 \beta_j \beta_i \frac{\partial u_j}{\partial x_i}\, dt = 0 \tag{13.7}$$

$$d_{L_4} p - \rho\, a\, \beta_j d_{L_4} u_j + \rho\, a^2 \alpha_j \alpha_i \frac{\partial u_j}{\partial x_i}\, dt = 0 \tag{13.8}$$

$$d_U p + \rho\, a^2 (\alpha_j \alpha_i + \beta_j \beta_i) \frac{\partial u_j}{\partial x_i}\, dt = 0 \tag{13.9}$$

where the subscripts L_i ($i = 1,2,3,4$) and U denote the four bicharacteristics and particle path, respectively. Elimination of the terms involving the derivatives $\alpha_j \alpha_i \frac{\partial u_j}{\partial x_i}$ and $\beta_j \beta_i \frac{\partial u_j}{\partial x_i}$ from Eqs. 13.5-13.9 yields the following system of three independent equations:

$$d_{L_1}p - d_{L_3}p + \rho\, a\, \alpha_j (d_{L_1}u_j + d_{L_3}u_j) = 0 \tag{13.10}$$

$$d_{L_2}p - d_{L_4}p + \rho\, a\, \beta_j (d_{L_2}u_j + d_{L_4}u_j) = 0 \tag{13.11}$$

$$d_{L_1}p + d_{L_2}p + d_{L_3}p + d_{L_4}p - 2\, d_U p$$

$$+ \rho\, a\, [\alpha_j (d_{L_1}u_j - d_{L_3}u_j) + \beta_j (d_{L_2}u_j - d_{L_4}u_j)] = 0 \tag{13.12}$$

In the linearization process, the dependent variables are assumed to be represented by

$$u = \bar{u} + \tilde{u} \tag{13.13}$$

where u represents any variable, $\bar{u}$ the mean value (a constant) and $\tilde{u}$ a small perturbation ($\tilde{u} << \bar{u}$). Substitution for the dependent variables in terms of Eq. 13.13 into Eqs. 13.10-13.12 gives

$$d_{L_1}\tilde{p} - d_{L_3}\tilde{p} + \bar{\rho}\, \bar{a}\, \bar{\alpha}_j (d_{L_1}\tilde{u}_j + d_{L_3}\tilde{u}_j) = 0 \tag{13.14}$$

$$d_{L_2}\tilde{p} - d_{L_4}\tilde{p} + \bar{\rho}\, \bar{a}\, \bar{\beta}_j (d_{L_2}\tilde{u}_j + d_{L_4}\tilde{u}_j) = 0 \tag{13.15}$$

$$d_{L_1}\tilde{p} + d_{L_2}\tilde{p} + d_{L_3}\tilde{p} + d_{L_4}\tilde{p} - 2\, d_U\tilde{p}$$

$$+ \bar{\rho}\, \bar{a}[\bar{\alpha}_j (d_{L_1}\tilde{u}_j - d_{L_3}\tilde{u}_j) + \bar{\beta}_j (d_{L_2}\tilde{u}_j - d_{L_4}\tilde{u}_j)] = 0 \tag{13.16}$$

where higher order terms have been neglected. Next, using the

modified Euler scheme, we replace the differentials in Eqs. 13.14-13.16 by differences to obtain

$$\tilde{p}(3) - \tilde{p}(1) + \bar{\rho}\,\bar{a}\,\bar{\alpha}_j[2\,\tilde{u}_j(6) - \tilde{u}_j(1) - \tilde{u}_j(3)] = 0 \quad (13.17)$$

$$\tilde{p}(4) - \tilde{p}(2) + \bar{\rho}\,\bar{a}\,\bar{\beta}_j[2\,\tilde{u}_j(6) - \tilde{u}_j(2) - \tilde{u}_j(4)] = 0 \quad (13.18)$$

$$2\,\tilde{p}(6) + 2\,\tilde{p}(5) - \tilde{p}(1) - \tilde{p}(2) - \tilde{p}(3) - \tilde{p}(4) + \bar{\rho}\,\bar{a}\,\{\bar{\alpha}_j[\tilde{u}_j(3) - \tilde{u}_j(1)] + \bar{\beta}_j[\tilde{u}_j(4) - \tilde{u}_j(2)]\} = 0 \quad (13.19)$$

where the numbers in parentheses denote points in the characteristic network.

2. Stability of the basic difference scheme

The von Neumann stability analysis must include all aspects of the numerical algorithm, including interpolation and the basic difference equations. However, to illustrate the stability characteristics of each of these operations, the basic difference scheme and the interpolation scheme are studied individually. Following these studies, the overall algorithm including both the basic difference scheme and interpolation scheme is analyzed.

Before analyzing the basic difference scheme, it can be seen from Figure 13.2 that the differential domain of dependence extends outside the convex hull of the difference

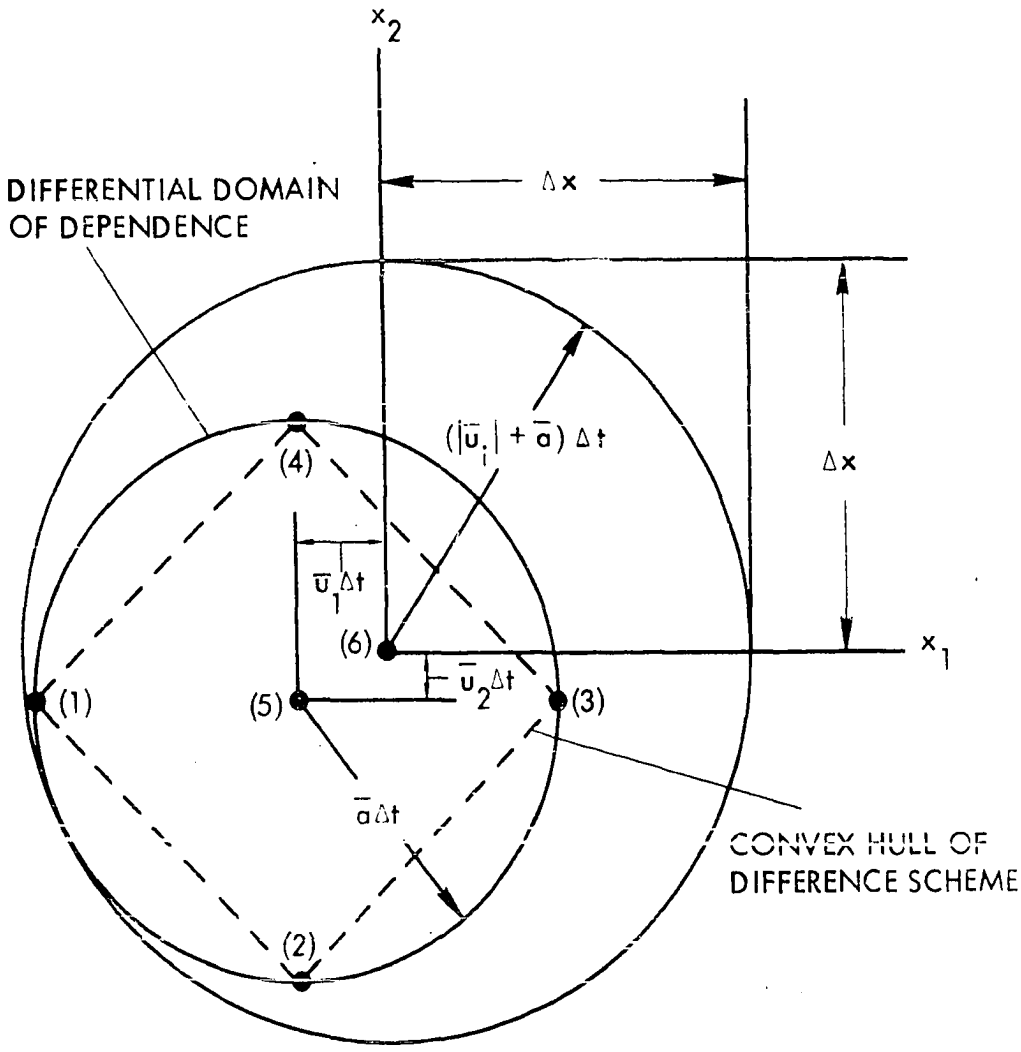

Figure 13.2. Basic difference scheme network in initial data surface. Differential domain of dependence and convex hull of difference scheme

scheme. Hence, according to the CFL stability criterion, an unstable result is expected.

It is assumed that an analytical solution of the system of linear difference equations can be obtained by separation of variables (ref. 29). For the purpose of stability analysis it is sufficient to examine the solution for only one arbitrary component of the Fourier series representation of the initial data. The complete solution is obtained by superposition of all such terms necessary to represent the initial data. The form of a general term is assumed to be

$$\bar{U} = e^{im\pi \frac{x_1}{L}} e^{in\pi \frac{x_2}{L}} \bar{T}(t) \tag{13.20}$$

where

$$\bar{U} = \begin{bmatrix} \tilde{u}_1 \\ \tilde{u}_2 \\ \tilde{p} \end{bmatrix} \qquad \bar{T}(t) = \begin{bmatrix} U_1(t) \\ U_2(t) \\ P(t) \end{bmatrix}$$

The frequency indices m and n are for the particular Fourier components in the x_1 and x_2 directions, respectively, L is a characteristic length such that x_1 and x_2 have the range -L to L, and $\bar{T}(t)$ is a vector function of the variable of integration, t.

To simplify the analysis, the reference vectors $\bar{\alpha}_i$ and $\bar{\beta}_i$ are directed along the coordinate axes, x_1 and x_2, respectively.

With this orientation of $\bar{\alpha}_i$ and $\bar{\beta}_i$, the linearized difference equations, Eqs. 13.17-13.19, become

$$\tilde{p}(3) - \tilde{p}(1) + \bar{\rho}\,\bar{a}[2\,\tilde{u}_1(6) - \tilde{u}_1(1) - \tilde{u}_1(3)] = 0 \qquad (13.21)$$

$$\tilde{p}(4) - \tilde{p}(2) + \bar{\rho}\,\bar{a}[2\,\tilde{u}_2(6) - \tilde{u}_2(2) - \tilde{u}_2(4)] = 0 \qquad (13.22)$$

$$2\,\tilde{p}(6) + 2\,\tilde{p}(5) - \tilde{p}(1) - \tilde{p}(2) - \tilde{p}(3) - \tilde{p}(4)$$
$$+ \bar{\rho}\,\bar{a}[\tilde{u}_1(3) - \tilde{u}_1(1) + \tilde{u}_2(4) - \tilde{u}_2(2)] = 0 \qquad (13.23)$$

The coordinates of the base points may be written relative to the coordinates of point (6) as (see Figure 13.2)

Point (1): $x_1(1) = x_1(6) - (\bar{u}_1 + \bar{a})\,\Delta t$

$x_2(1) = x_2(6) - \bar{u}_2\Delta t$

Point (2): $x_1(2) = x_1(6) - \bar{u}_1\Delta t$

$x_2(2) = x_2(6) - (\bar{u}_2 + \bar{a})\,\Delta t$

Point (3): $x_1(3) = x_1(6) - (\bar{u}_1 - \bar{a})\,\Delta t$

$x_2(3) = x_2(6) - \bar{u}_2\Delta t$

Point (4): $x_1(4) = x_1(6) - \bar{u}_1\Delta t$

$x_2(4) = x_2(6) - (\bar{u}_2 - \bar{a})\,\Delta t$

Point (5): $x_1(5) = x_1(6) - \bar{u}_1\Delta t$

$x_2(5) = x_2(6) - \bar{u}_2\Delta t$

The assumed form of the solution, Eq. 13.20, evaluated at each of these network points yields

$$\bar{U}(1) = e^{im\pi \frac{x_1(6)}{L}} e^{in\pi \frac{x_2(6)}{L}} \left(e^{-\frac{im\pi}{L}(\bar{u}_1+\bar{a})\Delta t} e^{-\frac{in\pi}{L}\bar{u}_2\Delta t}\right)\bar{T}(t(6)-\Delta t) \tag{13.24}$$

$$\bar{U}(2) = e^{im\pi \frac{x_1(6)}{L}} e^{in\pi \frac{x_2(6)}{L}} \left(e^{-\frac{im\pi}{L}\bar{u}_1\Delta t} e^{-\frac{in\pi}{L}(\bar{u}_2+\bar{a})\Delta t}\right)\bar{T}(t(6)-\Delta t) \tag{13.25}$$

$$\bar{U}(3) = e^{im\pi \frac{x_1(6)}{L}} e^{in\pi \frac{x_2(6)}{L}} \left(e^{-\frac{im\pi}{L}(\bar{u}_1-\bar{a})\Delta t} e^{-\frac{in\pi}{L}\bar{u}_2\Delta t}\right)\bar{T}(t(6)-\Delta t) \tag{13.26}$$

$$\bar{U}(4) = e^{im\pi \frac{x_1(6)}{L}} e^{in\pi \frac{x_2(6)}{L}} \left(e^{-\frac{im\pi}{L}\bar{u}_1\Delta t} e^{-\frac{in\pi}{L}(\bar{u}_2-\bar{a})\Delta t}\right)\bar{T}(t(6)-\Delta t) \tag{13.27}$$

$$\bar{U}(5) = e^{im\pi \frac{x_1(6)}{L}} e^{in\pi \frac{x_2(6)}{L}} \left(e^{-\frac{im\pi}{L}\bar{u}_1\Delta t} e^{-\frac{in\pi}{L}\bar{u}_2\Delta t}\right)\bar{T}(t(6)-\Delta t) \tag{13.28}$$

$$\bar{U}(6) = e^{im\pi \frac{x_1(6)}{L}} e^{in\pi \frac{x_2(6)}{L}} \bar{T}(t(6)) \tag{13.29}$$

Equations 13.24-13.29 contain the common factor

$$e^{\frac{im\pi}{L} x_1(6)} \; e^{\frac{in\pi}{L} x_2(6)}$$

and the difference equations, Eqs. 13.21 through 13.23, are homogeneous in the dependent variables; thus the common factor may be eliminated. Substitution for the respective dependent variables from Eqs. 13.24-13.29 into the difference equations Eqs. 13.21-13.23 yields

$$U_1(t(6)) - e^{-i\phi_3} e^{-i\phi_4} [\cos\phi_1 U_1(t(6) - \Delta t)$$

$$-i \frac{1}{\bar{\rho}\,\bar{a}} \sin\phi_1 P(t(6) - \Delta t)] = 0 \qquad (13.30)$$

$$U_2(t(6)) - e^{-i\phi_3} e^{-i\phi_4} [\cos\phi_2 U_2(t(6) - \Delta t)$$

$$-i \frac{1}{\bar{\rho}\,\bar{a}} \sin\phi_2 P(t(6) - \Delta t)] = 0 \qquad (13.31)$$

$$P(t(6)) + e^{-i\phi_3} e^{-i\phi_4} [(1 - \cos\phi_1 - \cos\phi_2) P(t(6) - \Delta t)$$

$$+ i \bar{\rho}\,\bar{a} (\sin\phi_1 U_1(t(6) - \Delta t) + \sin\phi_2 U_2(t(6) - \Delta t))] = 0 \qquad (13.32)$$

where

$$\phi_1 = \frac{m\pi}{L} \bar{a} \Delta t \tag{13.33}$$

$$\phi_2 = \frac{n\pi}{L} \bar{a} \Delta t \tag{13.34}$$

$$\phi_3 = \frac{m\pi}{L} \bar{u}_1 \Delta t \tag{13.35}$$

$$\phi_4 = \frac{n\pi}{L} \bar{u}_2 \Delta t \tag{13.36}$$

In matrix notation, Eqs. 13.30-13.32 can be written as

$$\bar{U}(t(6)) + A\, \bar{U}(t(6) - \Delta t) = 0 \tag{13.37}$$

where the matrix A,

$$A = e^{-i\phi_3} e^{-i\phi_4} \begin{bmatrix} -\cos\phi_1 & 0 & i \frac{1}{\bar{\rho}\,\bar{a}} \sin\phi_1 \\ 0 & -\cos\phi_2 & i \frac{1}{\bar{\rho}\,\bar{a}} \sin\phi_2 \\ i\,\bar{\rho}\,\bar{a} \sin\phi_1 & i\,\bar{\rho}\,\bar{a} \sin\phi_2 & (1-\cos\phi_1 - \cos\phi_2) \end{bmatrix}, \tag{13.38}$$

is called the amplification matrix of the system of difference equations.

The von Neumann stability criterion, Eq. 13.4, requires that the eigenvalues of the amplification matrix satisfy the inequality

$$|\lambda| \leq 1 + 0(\Delta t) \tag{13.39}$$

where λ is any of the three roots of the determinantal equation

$$|A - \lambda I| = 0 \tag{13.40}$$

Expansion of Eq. 13.40 yields the third-order polynomial

$$\sin^2\phi_1(\cos\phi_2 - \lambda') + \sin^2\phi_2(\cos\phi_1 - \lambda')$$

$$+ (\cos\phi_1 + \cos\phi_2 - 1 + \lambda')(\cos\phi_1 + \lambda')(\cos\phi_2 + \lambda') = 0 \tag{13.41}$$

where

$$\lambda' = e^{i\phi_3} e^{i\phi_4} \lambda \tag{13.42}$$

The transformation in Eq. 13.42 does not change the magnitude of the eigenvalues, i.e.,

$$|\lambda'| = |\lambda|$$

Hence, the magnitude of the eigenvalues of the amplification matrix can be obtained directly from Eq. 13.41. If as shown in Figure 13.2,

$$\Delta x = (|\bar{u}_i| + \bar{a})\ \Delta t$$

then the angles ϕ_1 and ϕ_2 in Eq. 13.41 can be reexpressed, according to Eqs. 13.33 and 13.34, as

$$\phi_1 = \frac{m\pi}{M+1} \frac{\Delta x}{L} \tag{13.43}$$

$$\phi_2 = \frac{n\pi}{M+1} \frac{\Delta x}{L} \tag{13.44}$$

where M is the Mach number.

The spectral radii ($|\lambda|_{max}$) of the amplification matrix were calculated from Eq. 13.41 for all combinations of angle sets $\{\phi_1,\phi\}$, $\{\phi,\phi_2\}$ for which $|\phi_1| \leq \phi$, $|\phi_2| \leq \phi$. The results of the eigenvalue calculation are shown in Figure 13.3 with the spectral radii plotted versus the frequency index

$$\frac{I}{M+1}\frac{\Delta x}{L}$$

where

$$I = (M + 1)\frac{L}{\Delta x}\frac{\phi}{\pi} \tag{13.45}$$

The spectral radius, for this case, is an even periodic function of frequency index; hence, only the results of the calculation for the range of $\frac{I}{M+1}\frac{\Delta x}{L}$ from 0.0 to 1.0 are presented.

As expected, the basic difference scheme is unstable by the von Neumann criterion for all values of frequency index. This is due to the direct violation of the necessary CFL stability criterion when the differential domain of dependence is not contained within the convex hull of the difference scheme.

3. Stability of interpolation scheme

The interpolation scheme developed in Appendix H to obtain the dependent variables at base points in the initial data surface must be considered in the overall stability

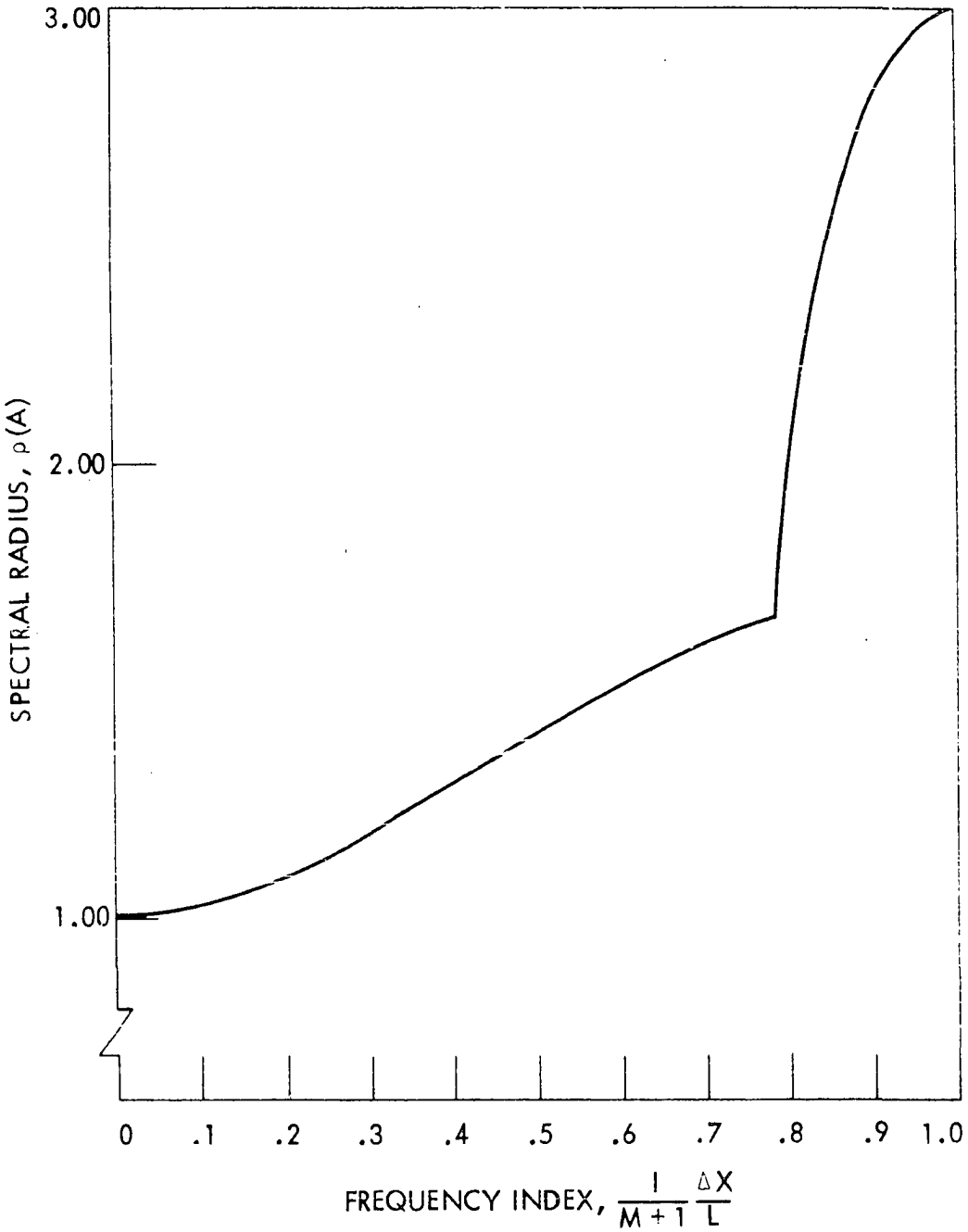

Figure 13.3. Spectral radius of amplification matrix versus frequency index for basic difference scheme

analysis. However, the stability characteristics of the interpolation technique can be determined by treating it separately before coupling it with the difference equations. The approach used here is to consider the interpolation scheme as smoothing process and to analyze the stability of such a scheme.

The analysis is simplified without loss of generality by assuming a square cell of nine points with mesh spacing $\Delta x_1 = \Delta x_2 = \Delta x$ centered about the point (6') which is the solution point (6) for the previous time plane, as shown in Figure 13.1. Point (6'), is taken as the origin of the coordinate system. A general term of the Fourier series representation of the values to be interpolated on the initial data surface is given by Eq. 13.20 as

$$\bar{U}\left(\frac{x_1}{L}, \frac{x_2}{L}, 0\right) = e^{im\pi \frac{x_1}{L}} e^{in\pi \frac{x_2}{L}} \bar{T}(0) \qquad (13.46)$$

The corresponding values of the dependent variables at each of the nine cell points are

$$\bar{U}\left(\frac{\Delta x}{L}, \frac{\Delta x}{L}, 0\right) = \xi \eta \bar{T}(0) \qquad (13.47)$$

$$\bar{U}\left(\frac{\Delta x}{L}, 0, 0\right) = \xi \bar{T}(0) \qquad (13.48)$$

$$\bar{U}\left(\frac{\Delta x}{L}, -\frac{\Delta x}{L}, 0\right) = \xi \eta^{-1} \bar{T}(0) \qquad (13.49)$$

$$\bar{U}\left(0, \frac{\Delta x}{L}, 0\right) = \eta \bar{T}(0) \qquad (13.50)$$

$$\bar{U}(0,\ 0,\ 0) = \bar{T}(0) \tag{13.51}$$

$$\bar{U}(0,\ -\frac{\Delta x}{L},\ 0) = \eta^{-1}\,\bar{T}(0) \tag{13.52}$$

$$\bar{U}(-\frac{\Delta x}{L},\ \frac{\Delta x}{L},\ 0) = \xi^{-1}\,\eta\,\bar{T}(0) \tag{13.53}$$

$$\bar{U}(-\frac{\Delta x}{L},\ 0,\ 0) = \xi^{-1}\,\bar{T}(0) \tag{13.54}$$

$$\bar{U}(-\frac{\Delta x}{L},\ -\frac{\Delta x}{L},\ 0) = \xi^{-1}\eta^{-1}\,\bar{T}(0) \tag{13.55}$$

where

$$\xi = e^{im\pi\,\frac{\Delta x}{L}} \tag{13.56}$$

$$\eta = e^{in\pi\,\frac{\Delta x}{L}} \tag{13.57}$$

The least squares system of equations, in Appendix H, evaluated for this cell of interpolating points is

$$
\begin{bmatrix}
9 & 0 & 0 & 0 & 6\left(\frac{\Delta x}{L}\right)^2 & 6\left(\frac{\Delta x}{L}\right)^2 \\
0 & 6\left(\frac{\Delta x}{L}\right)^2 & 0 & 0 & 0 & 0 \\
0 & 0 & 6\left(\frac{\Delta x}{L}\right)^2 & 0 & 0 & 0 \\
0 & 0 & 0 & 4\left(\frac{\Delta x}{L}\right)^2 & 0 & 0 \\
6\left(\frac{\Delta x}{L}\right)^2 & 0 & 0 & 0 & 6\left(\frac{\Delta x}{L}\right)^4 & 4\left(\frac{\Delta x}{L}\right)^4 \\
6\left(\frac{\Delta x}{L}\right)^2 & 0 & 0 & 0 & 4\left(\frac{\Delta x}{L}\right)^4 & 6\left(\frac{\Delta x}{L}\right)^4
\end{bmatrix}
\begin{bmatrix} a_{1\nu} \\ a_{2\nu} \\ a_{3\nu} \\ a_{4\nu} \\ a_{5\nu} \\ a_{6\nu} \end{bmatrix}
$$

$$
= \begin{bmatrix}
(\xi + \xi^{-1} + 1)(\eta + \eta^{-1} + 1) \\
(\xi - \xi^{-1})(\eta + \eta^{-1} + 1)\left(\frac{\Delta x}{L}\right) \\
(\xi + \xi^{-1} + 1)(\eta - \eta^{-1})\left(\frac{\Delta x}{L}\right) \\
(\xi - \xi^{-1})(\eta - \eta^{-1})\left(\frac{\Delta x}{L}\right)^2 \\
(\xi + \xi^{-1})(\eta + \eta^{-1} + 1)\left(\frac{\Delta x}{L}\right)^2 \\
(\xi + \xi^{-1} + 1)(\eta + \eta^{-1})\left(\frac{\Delta x}{L}\right)^2
\end{bmatrix} T_\nu(0) \quad (\nu = 1,2,3) \qquad (13.58)
$$

Solution for the polynomial coefficients $a_{\mu\nu}$ ($\mu = 1,2,\ldots,6$; $\nu = 1,2,3$) in Eq. (13.58) yields

$$a_{1\nu} = [5/9\ (\xi + \xi^{-1} + 1)(\eta + \eta^{-1} + 1) - 1/3\ (\xi + \xi^{-1})(\eta + \eta^{-1} + 1) - 1/3\ (\xi + \xi^{-1} + 1)(\eta + \eta^{-1})]T_\nu(0) \tag{13.59}$$

$$a_{2\nu} = \frac{L}{\Delta x}\ [1/6\ (\xi - \xi^{-1})(\eta + \eta^{-1} + 1)]T_\nu(0) \tag{13.60}$$

$$a_{3\nu} = \frac{L}{\Delta x}\ [1/6\ (\xi + \xi^{-1} + 1)(\eta - \eta^{-1})]T_\nu(0) \tag{13.61}$$

$$a_{4\nu} = (\frac{L}{\Delta x})^2[1/4\ (\xi - \xi^{-1})(\eta - \eta^{-1})]T_\nu(0) \tag{13.62}$$

$$a_{5\nu} = (\frac{L}{\Delta x})^2[- 1/3\ (\xi + \xi^{-1} + 1)(\eta + \eta^{-1} + 1) + 1/2\ (\xi + \xi^{-1})(\eta + \eta^{-1} + 1)]T_\nu(0) \tag{13.63}$$

$$a_{6\nu} = (\frac{L}{\Delta x})^2[- 1/3\ (\xi + \xi^{-1} + 1)(\eta + \eta^{-1} + 1) + 1/2\ (\xi + \xi^{-1} + 1)(\eta + \eta^{-1})]T_\nu(0) \tag{13.64}$$

Since the coefficients $a_{\mu\nu}$ are homogeneous in $T_\nu(0)$, we can write the least squares polynomial for the dependent variables, denoted $\bar{U}'$, as

$$\bar{U}'\left(\frac{x_1}{L}, \frac{x_2}{L}, 0\right) = \left[a'_1 + a'_2\left(\frac{x_1}{L}\right) + a'_3\left(\frac{x_2}{L}\right) + a'_4\left(\frac{x_1}{L}\right)\left(\frac{x_2}{L}\right)\right.$$

$$\left. + a'_5\left(\frac{x_1}{L}\right)^2 + a'_6\left(\frac{x_2}{L}\right)^2\right]\bar{T}(0) \qquad (13.65)$$

where a'_μ $(\mu = 1,2,\ldots,6)$ are the coefficients of $T_\nu(0)$ in Eqs. 13.59-13.64.

In order to examine the stability characteristics of the interpolation scheme, consider a process in which the new values of the dependent variables at point (6') are calculated from the polynomial, Eq. 13.65, with $x_1 = x_2 = 0$, i.e.,

$$\bar{U}'(6') = a'_1\,\bar{T}(0) \qquad (13.66)$$

The previous values of the dependent variables at point (6') are given by Eq. 13.46 with $x_1 = x_2 = 0$, i.e.

$$\bar{U}(6') = \bar{T}(0) \qquad (13.67)$$

From Eqs. 13.66 and 13.67 we can write

$$\bar{U}'(6') = a'_1\bar{U}(6') \qquad (13.68)$$

Hence, there is only one amplification factor or eigenvalue for this process, i.e.,

$$\lambda = a_1' = [5/9\ (\xi + \xi^{-1} + 1)(\eta + \eta^{-1} + 1)$$

$$- 1/3\ (\xi + \xi^{-1})(\eta + \eta^{-1} + 1)$$

$$- 1/3\ (\xi + \xi^{-1} + 1)(\eta + \eta^{-1})] \qquad (13.69)$$

In terms of the angles ϕ_1 and ϕ_2, defined as

$$\phi_1 = m\pi \frac{\Delta x}{L} \qquad (13.70)$$

$$\phi_2 = n\pi \frac{\Delta x}{L} \qquad (13.71)$$

Eq. 13.69 can be reexpressed as

$$\lambda = 4/9\ [5/4 + (\cos\phi_1 + \cos\phi_2) - \cos\phi_1 \cos\phi_2] \qquad (13.72)$$

The value of λ in Eq. 13.72 was calculated for all combinations of angle sets $\{\phi_1, \phi\}$, $\{\phi, \phi_2\}$ for which $|\phi_1| \leq \phi$, $|\phi_2| \leq \phi$. The magnitude of the maximum eigenvalue is 1.0 for all values of the angle ϕ. Hence, the interpolation scheme is unconditionally stable for all Fourier components of initial data.

4. Stability of difference scheme with interpolation

The linear stability analysis of the overall solution algorithm is made by combining the linearized difference equations with the interpolation procedures for the dependent variables at the base points on the initial data surface. The characteristic point network is shown in Figure 13.1. In the linear analysis, the base points (1) through (4) are equally

spaced around the circumference of a circle of radius $\bar{a}\Delta t$ centered at point (5). These points are located by specification of the acoustic speed, $\bar{a}$, velocity, $\bar{u}_i$, time increment, Δt, and angle ψ in the choice of the reference vectors.

If the assumption is made that the mesh is square with spacing $\Delta x_1 = \Delta x_2 = \Delta x$, then the Courant number in Eq. 13.1 can be expressed as

$$C = \frac{(|\bar{u}_i| + \bar{a})}{\Delta x} \Delta t \tag{13.73}$$

where $C \geq 1.0$ indicates violation of the CFL stability criterion.

The base point coordinates can be written in terms of the Mach number, M (based on average conditions), flow angle, θ, reference vector angle, ψ, Courant number, C, and the relative mesh spacing, $\frac{\Delta x}{L}$, as

Point (1):
$$\frac{x_1(1)}{L} = - \frac{(M \cos\theta + \cos\psi)}{M + 1} \left(C \frac{\Delta x}{L}\right)$$

$$\frac{x_2(1)}{L} = - \frac{(M \sin\theta - \sin\psi)}{M + 1} \left(C \frac{\Delta x}{L}\right)$$

Point (2):
$$\frac{x_1(2)}{L} = - \frac{(M \cos\theta - \sin\psi)}{M + 1} \left(C \frac{\Delta x}{L}\right)$$

$$\frac{x_2(2)}{L} = - \frac{(M \sin\theta + \cos\psi)}{M + 1} \left(C \frac{\Delta x}{L}\right)$$

Point (3): $$\frac{x_1(3)}{L} = -\frac{(M\cos\theta - \cos\psi)}{M+1}\left(C\frac{\Delta x}{L}\right)$$

$$\frac{x_2(3)}{L} = -\frac{(M\sin\theta - \sin\psi)}{M+1}\left(C\frac{\Delta x}{L}\right)$$

Point (4): $$\frac{x_1(4)}{L} = -\frac{(M\cos\theta + \sin\psi)}{M+1}\left(C\frac{\Delta x}{L}\right)$$

$$\frac{x_2(4)}{L} = -\frac{(M\sin\theta - \cos\psi)}{M+1}\left(C\frac{\Delta x}{L}\right)$$

Point (5): $$\frac{x_1(5)}{L} = -\frac{M\cos\theta}{M+1}\left(C\frac{\Delta x}{L}\right)$$

$$\frac{x_2(5)}{L} = -\frac{M\sin\theta}{M+1}\left(C\frac{\Delta x}{L}\right)$$

where the coordinates at the solution point (6) are $x_1(6) = x_2(6) = 0$. The values of the dependent variables at the base points are determined by evaluating the interpolating polynomial, Eq. 13.65, i.e.,

$$\bar{U}(I) = f(I)\,\bar{T}(0) \qquad (I = 1,2,3,4,5) \tag{13.74}$$

where

$$f(I) = a_1' + a_2'\left(\frac{x_1(I)}{L}\right) + a_3'\left(\frac{x_2(I)}{L}\right) + a_4'\left(\frac{x_1(I)}{L}\right)\left(\frac{x_2(I)}{L}\right) + a_5'\left(\frac{x_1(I)}{L}\right)^2 + a_6'\left(\frac{x_2(I)}{L}\right)^2 \tag{13.75}$$

The values of the dependent variables at the solution point (6) are expressed in terms of the assumed exponential form of the solution, Eq. 13.20, evaluated at $x_1(6) = x_2(6) = 0$,

$$\bar{U}(6) = \bar{T}(\Delta t) \tag{13.76}$$

Substitution of $\bar{U}(I)$ $(I = 1,2,\ldots 6)$ from Eqs. 13.74 and 13.76 into the linearized difference equations, Eqs. 13.17-13.19, with $\bar{\alpha}_i = \{\cos\psi, \sin\psi\}$, $\bar{\beta}_i = \{-\sin\psi, \cos\psi\}$ yields

$$\cos\psi\, U_1(\Delta t) + \sin\psi\, U_2(\Delta t) + \frac{1}{2\,\bar{\rho}\,\bar{a}}\,[f(3) - f(1)]\,P(0)$$

$$- 1/2\,[f(1) + f(3)][\cos\psi\, U_1(0) + \sin\psi\, U_2(0)] = 0 \tag{13.77}$$

$$-\sin\psi\, U_1(\Delta t) + \cos\psi\, U_2(\Delta t) + \frac{1}{2\,\bar{\rho}\,\bar{a}}\,[f(4) - f(2)]\,P(0)$$

$$- 1/2\,[f(2) + f(4)][-\sin\psi\, U_1(0) + \cos\psi\, U_2(0)] = 0 \tag{13.78}$$

$$P(\Delta t) + \{f(5) - 1/2\,[f(1) + f(2) + f(3) + f(4)]\}\,P(0)$$

$$+ \frac{\bar{\rho}\,\bar{a}}{2}\{\cos\psi\,[f(3) - f(1)] - \sin\psi\,[f(4) - f(2)]\}\,U_1(0)$$

$$+ \frac{\bar{\rho}\,\bar{a}}{2}\{\sin\psi\,[f(3) - f(1)] + \cos\psi\,[f(4) - f(2)]\}\,U_2(0) = 0 \tag{13.79}$$

This system of equations written in matrix form is

$$\bar{U}(\Delta t) + A\,\bar{U}(0) = 0 \tag{13.80}$$

where A is the amplification matrix

$$A = \begin{bmatrix} A_{11} & A_{12} & A_{13} \\ A_{21} & A_{22} & A_{23} \\ A_{31} & A_{32} & A_{33} \end{bmatrix} \tag{13.81}$$

with elements

$$A_{11} = -1/2 \{\cos^2\psi [f(1) + f(3)] + \sin^2\psi [f(2) + f(4)]\} \tag{13.82}$$

$$A_{12} = -1/2 \sin\psi \cos\psi \{f(1) + f(3) - f(2) - f(4)\} \tag{13.83}$$

$$A_{13} = \frac{1}{2 \bar{\rho} \bar{a}} \{\cos\psi [f(3) - f(1)] - \sin\psi [f(4) - f(2)]\} \tag{13.84}$$

$$A_{21} = -1/2 \sin\psi \cos\psi \{f(1) + f(3) - f(2) - f(4)\} \tag{13.85}$$

$$A_{22} = -1/2 \{\sin^2\psi [f(1) + f(3)] + \cos^2\psi [f(2) + f(4)]\} \tag{13.86}$$

$$A_{23} = \frac{1}{2 \bar{\rho} \bar{a}} \{\sin\psi [f(3) - f(1)] + \cos\psi [f(4) - f(2)]\} \tag{13.87}$$

$$A_{31} = \frac{\bar{\rho} \bar{a}}{2} \{\cos\psi [f(3) - f(1)] - \sin\psi [f(4) - f(2)]\} \tag{13.88}$$

$$A_{32} = \frac{\bar{\rho} \bar{a}}{2} \{\sin\psi [f(3) - f(1)] + \cos\psi [f(4) - f(2)]\} \tag{13.89}$$

$$A_{33} = f(5) - 1/2 [f(1) + f(2) + f(3) + f(4)] \tag{13.90}$$

The elements of A are functions of the angles ϕ_1 and ϕ_2 defined by Eqs. 13.70 and 13.71, respectively.

The spectral radii of the amplification matrix were calculated for all combinations of angle sets $\{\phi_1, \phi\}$, $\{\phi, \phi_2\}$ where $|\phi_1| \leq \phi$, $|\phi_2| \leq \phi$. The results of the stability analysis are presented in Figures 13.4-13.11 with the spectral radii plotted versus the frequency index

$$I \frac{\Delta x}{L}$$

where

$$I = \frac{L}{\Delta x} \frac{\phi}{\pi} \tag{13.91}$$

The spectral radius is an even periodic function of the frequency index, and only the results for the range of $I \frac{\Delta x}{L}$ from 0.0 to 1.0 are presented. The plots illustrate the effect of varying the four free parameters: (1) Mach number, M; (2) flow angle, θ; (3) Courant number, C; and (4) reference vector angle, ψ. For the case $\psi = 0$, shown in Figures 13.4-13.7, the overall scheme is clearly stable ($|\lambda| \leq 1.0$) for the larger values of frequency index. However, for smaller values of frequency index, eigenvalues greater than 1.0 were calculated in all cases. For the case $\psi = 45°$, shown in Figures 13.8 and 13.9, eigenvalues greater than 1.0 were encountered for all values of frequency index for M = 1.0. Figures 13.10 and 13.11 illustrate the unstable character of the method when the CFL stability criterion is violated (C = 1.2). In none

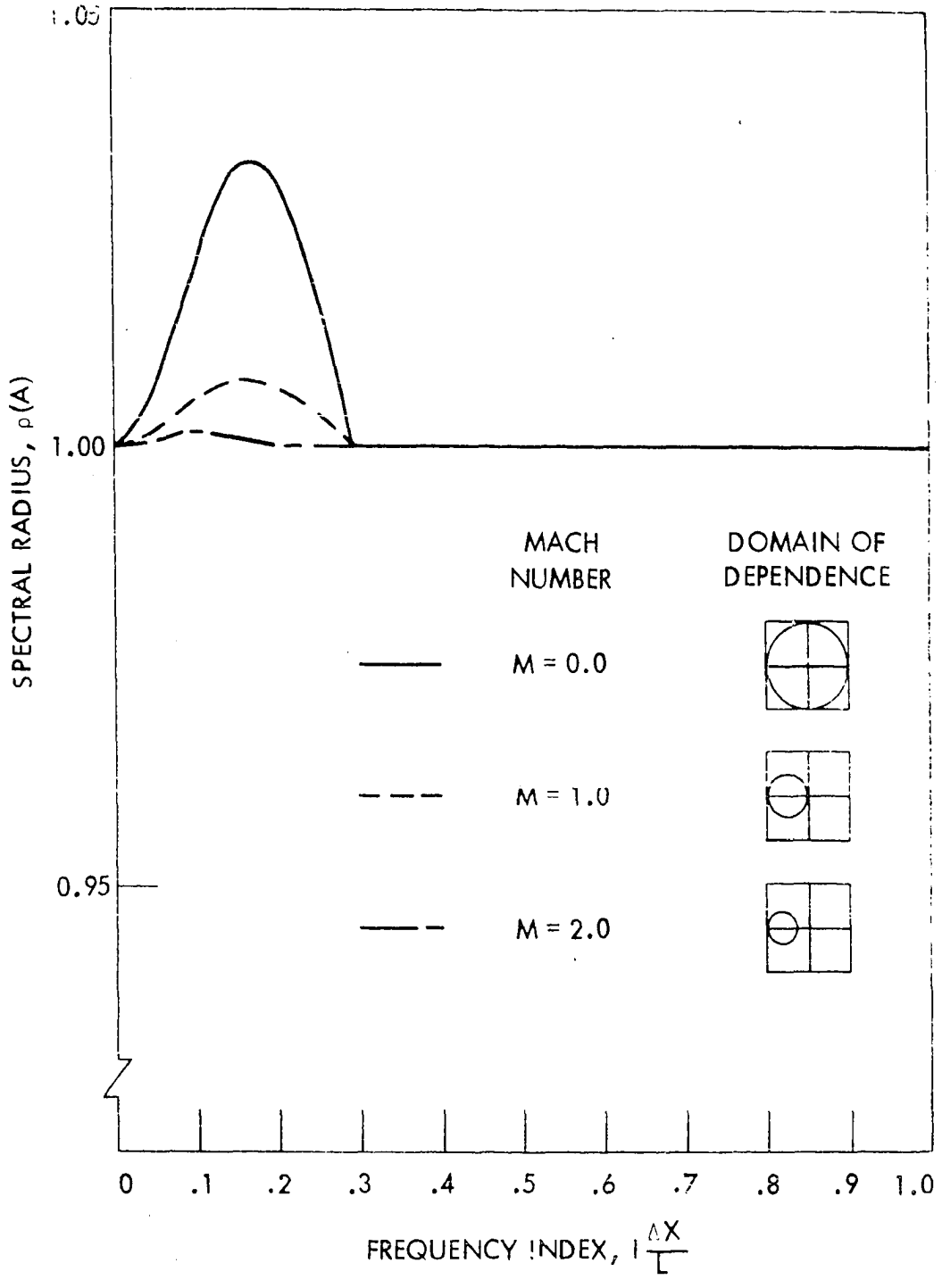

Figure 13.4. Spectral radius of amplification matrix versus frequency index for difference scheme with interpolation; C = 1.0, $\theta = 0°$, $\psi = 0°$

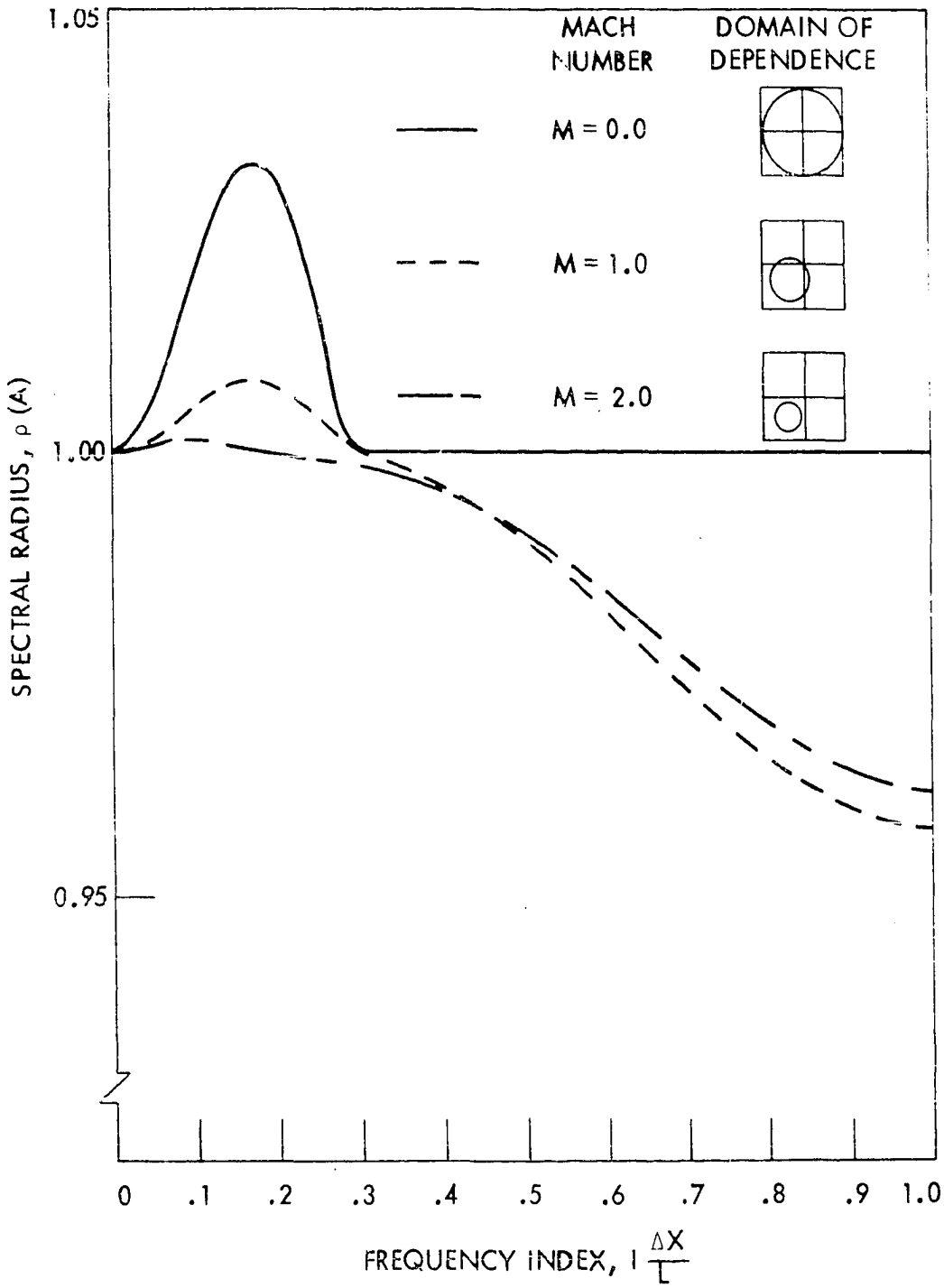

Figure 13.5. Spectral radius of amplification matrix versus frequency index for difference scheme with interpolation; C = 1.0, $\theta = 45°$, $\psi = 0°$

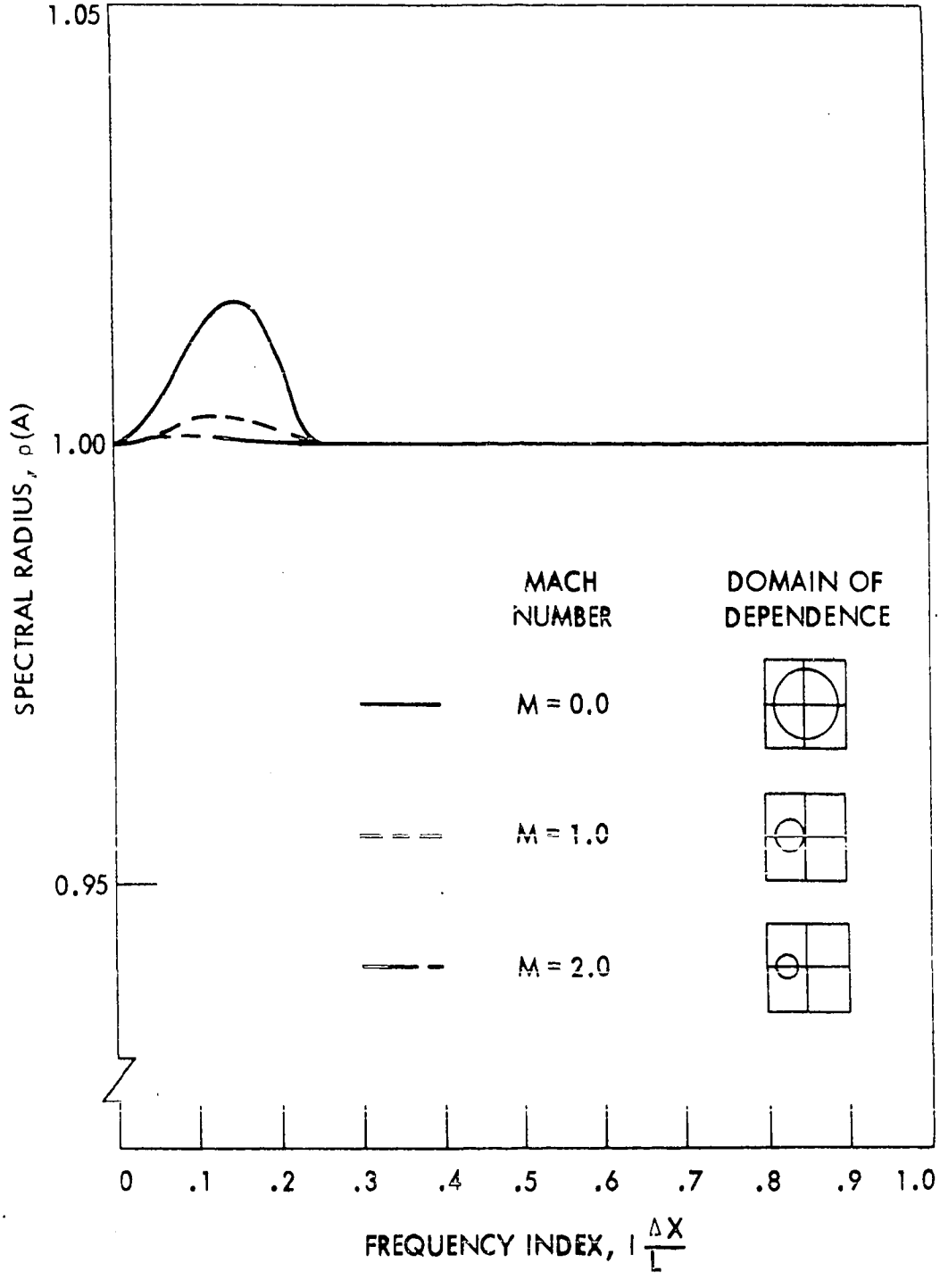

Figure 13.6. Spectral radius of amplification matrix versus frequency index for difference scheme with interpolation; C = 0.8, $\theta = 0°$, $\psi = 0°$

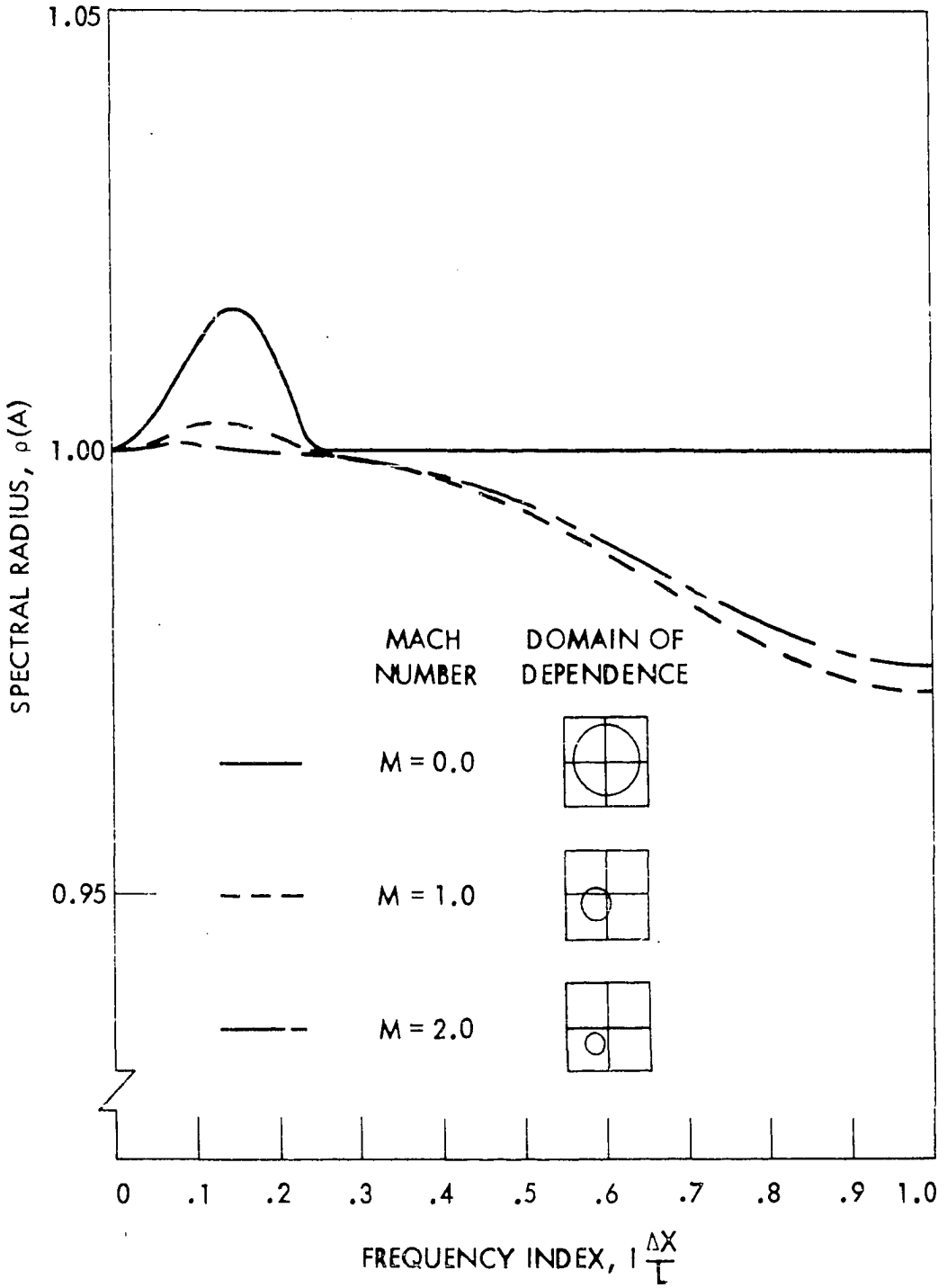

Figure 13.7. Spectral radius of amplification matrix versus frequency index for difference scheme with interpolation; C = 0.8, θ = 45°, ψ = 0°

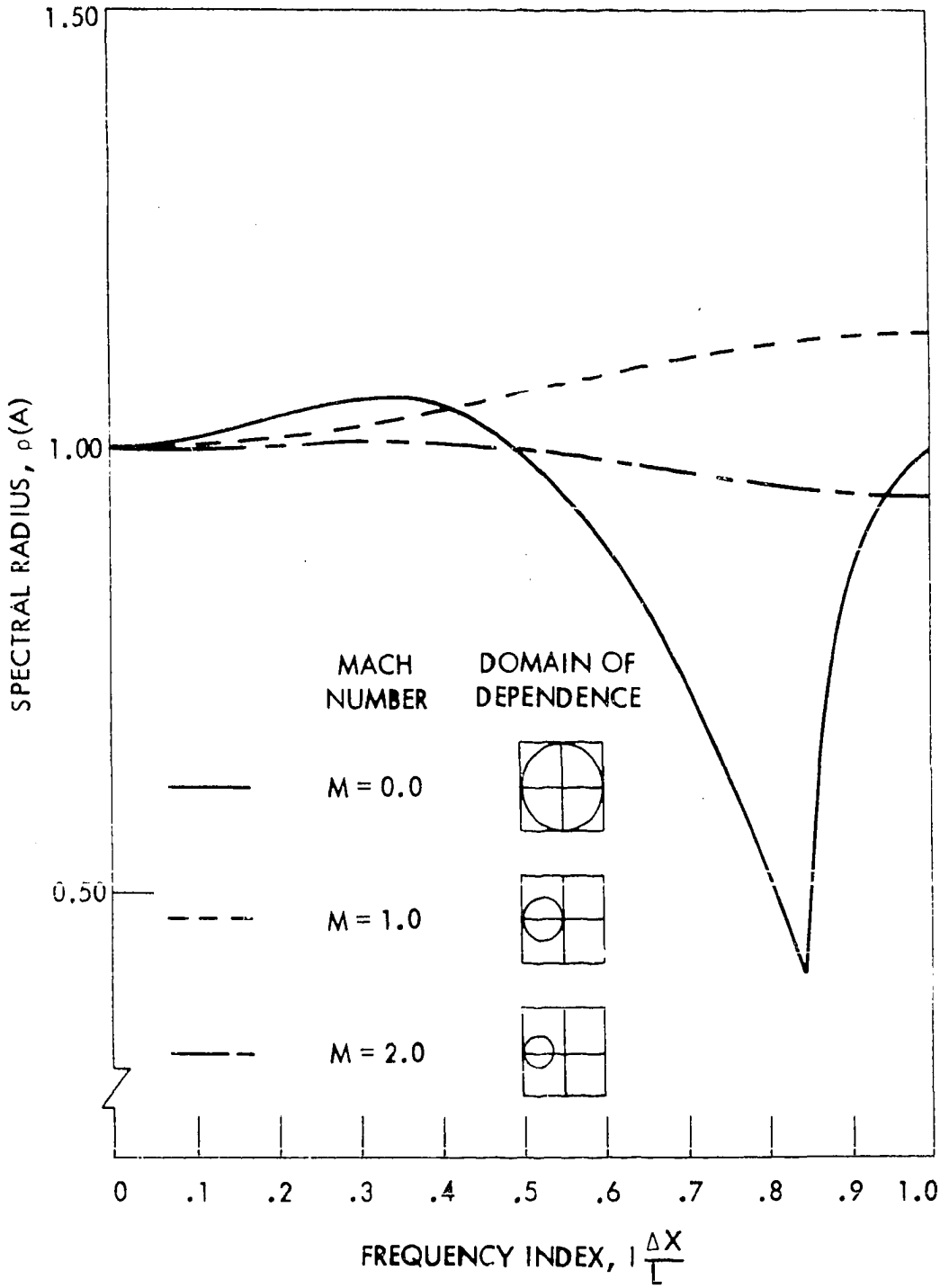

Figure 13.8. Spectral radius of amplification matrix versus frequency index for difference scheme with interpolation; C = 1.0, $\theta = 0°$, $\psi = 45°$

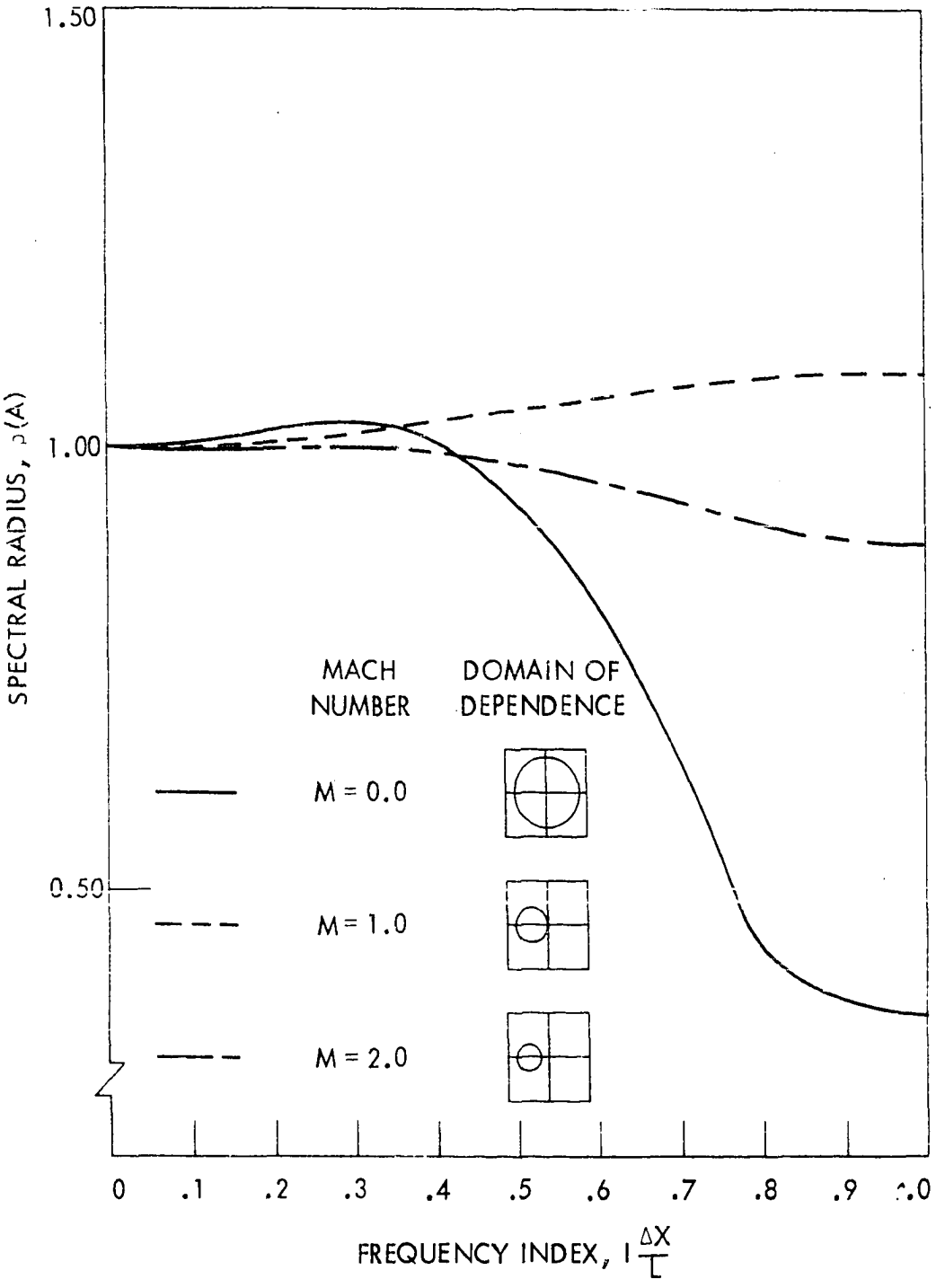

Figure 13.9. Spectral radius of amplification matrix versus frequency index for difference scheme with interpolation; C = 0.8, $\theta = 0°$, $\psi = 45°$

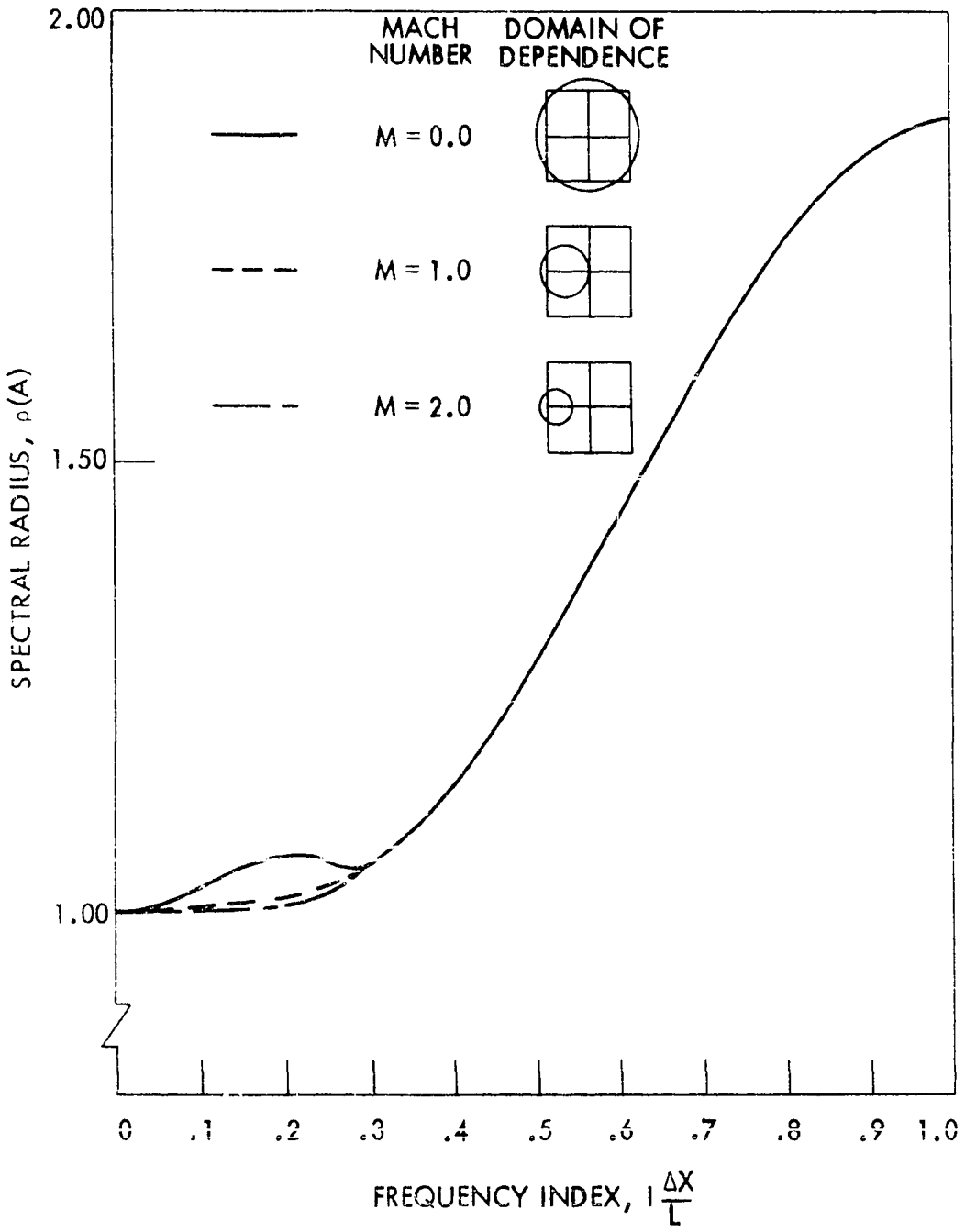

Figure 13.10. Spectral radius of amplification matrix versus frequency index for difference scheme with interpolation; C = 1.2, $\theta = 0°$, $\psi = 0°$

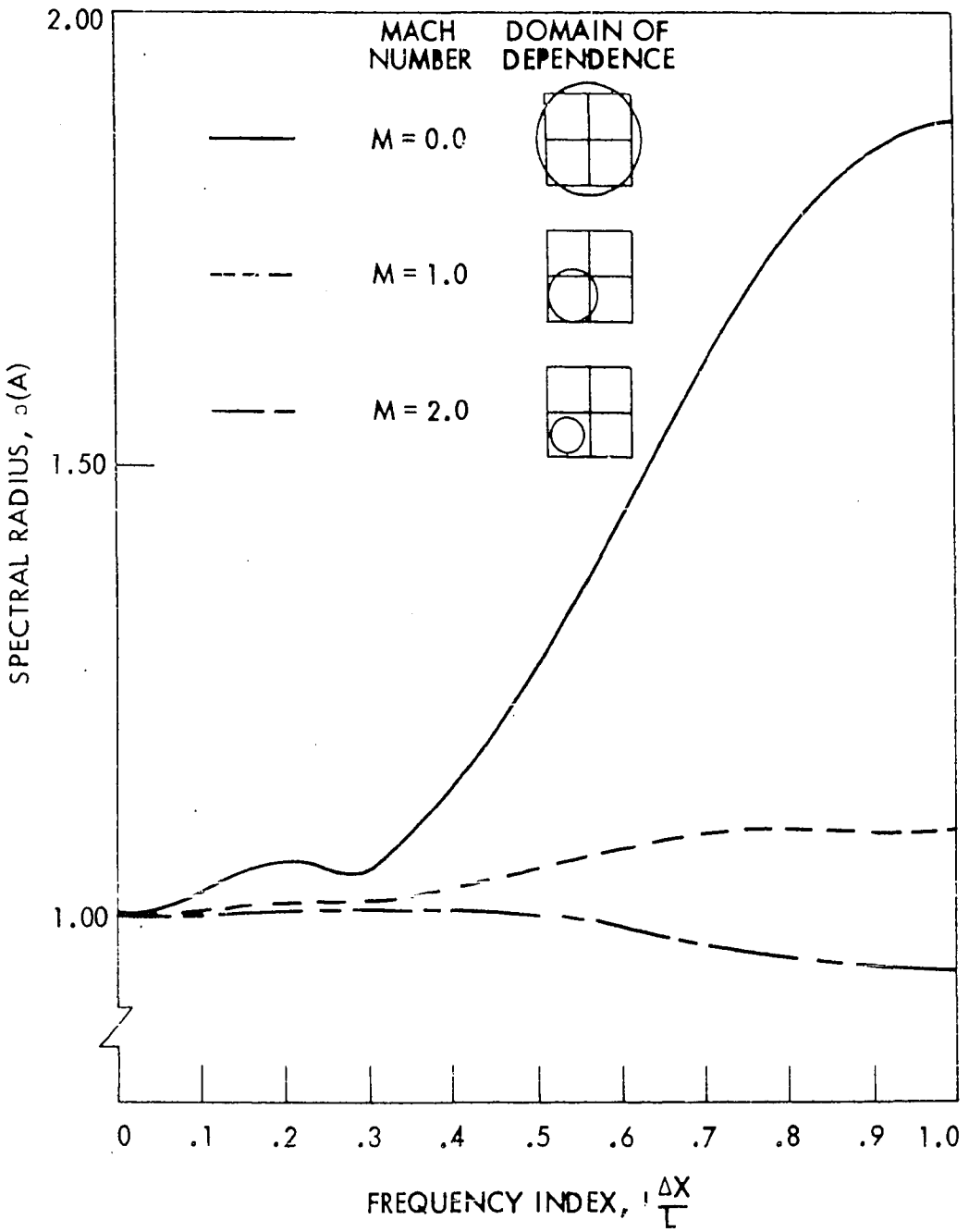

Figure 13.11. Spectral radius of amplification matrix versus frequency index for difference scheme with interpolation; C = 1.2, $\theta = 45°$, $\psi = 0°$

of the cases presented could the scheme be judged unconditionally stable for all values of frequency index if we choose for the criterion $|\lambda| \leq 1.0$. However, in all cases where the CFL criterion is satisfied ($C \leq 1.0$), reductions in Courant number from 1.0 to 0.8 produced corresponding reductions in the amount by which the curves exceed $\lambda = 1.0$. Hence, when the CFL criterion is satisfied, the scheme could be judged stable by the von Neumann criterion which allows maximum eigenvalues somewhat greater than 1.0 ($|\lambda|_{max} \leq 1.0 + 0(\Delta t)$).

To provide another check on the stability characteristics of the overall scheme, an example problem was set up for solution of a square mesh of points with uniform initial data and boundary conditions fixed at the initial conditions. The number of points in each coordinate direction was varied over the range from 5 to 9. Solutions were made for various values of the four free parameters with emphasis placed on the critical cases like those shown in Figures 13.8 and 13.9 at $M = 1.0$. Instabilities were encountered at relatively few time steps (10-20) when the CFL criterion was violated ($C = 1.5$). However, when the CFL criterion was satisfied, no instabilities occurred even after 1000 time steps.

XIV. APPENDIX E:
EXACT COMPARISON SOLUTIONS

The exact comparison solutions used to determine the order of the truncation error of the numerical algorithm were based on; (1) steady source flow, and (2) Prandtl-Meyer flow over a cylinder. Specialized computer programs were developed to compute these solutions at arbitrary points in the flow field. The calculations were made with 16 significant digits with tolerances on iterative portions maintained at 10^{-10}.

The four dependent variables u, v, p, and ρ were calculated at the nine points of the field point initial data cell. Since these flows were steady, the order of the truncation error was determined by comparing the solution from the field point calculation with the exact solution at the midpoint of the initial data cell.

A. Source Flow

Steady source flow is a one-dimensional flow in which the properties vary only with radial distance from the point source. Specification of Mach number at any radial position and any two stagnation state properties completely determines the solution at any point in the flow field. In this analysis, total pressure, p_0, total density, ρ_0 and the Mach number M_1 at radius r_1 as shown in Figure 14.1 were assumed known.

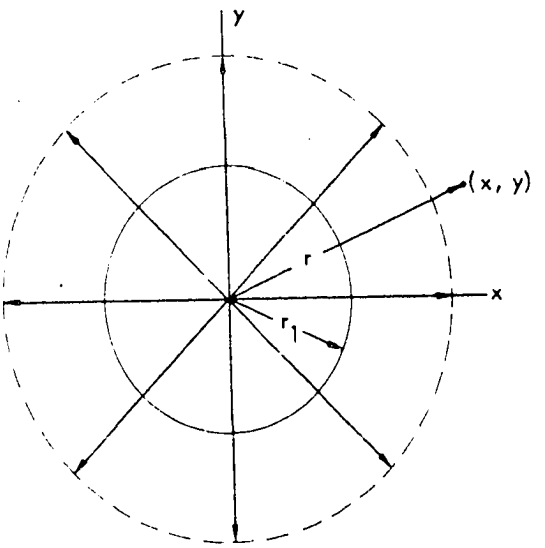

Figure 14.1. Source flow field
Solution point (x,y) and reference radius r_1

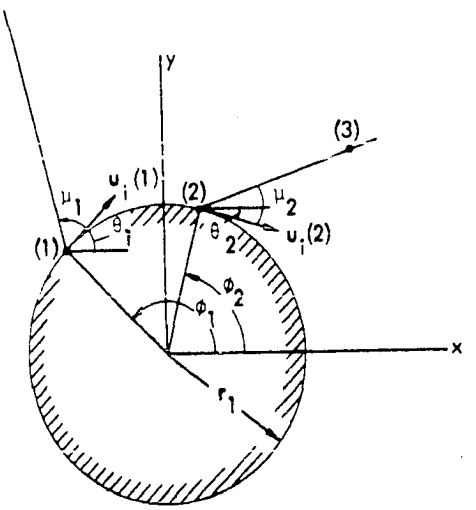

Figure 14.2. Prandtl-Meyer flow over a cylinder
Reference point (1), intermediate point (2), and solution point (3)

The continuity equation, written between the upstream station (1) and any point in the field is

$$\rho_1 r_1 v_{r_1} = \rho r v_r \tag{14.1}$$

where the nonsubscripted variables refer to the solution point, and v_r is the velocity. Substitution of the isentropic flow relations

$$p = p_0 \left(1 + \frac{\gamma-1}{2} M^2\right)^{\frac{\gamma}{\gamma-1}} \tag{14.2}$$

$$\rho = \rho_0 \left(1 + \frac{\gamma-1}{2} M^2\right)^{\frac{\gamma}{\gamma-1}} \tag{14.3}$$

into Eq. 14.1 yields a relation between Mach number and radial location, i.e.,

$$\frac{r}{r_1} = \frac{M_1}{\left(1 + \frac{\gamma-1}{2} M_1^2\right)^{\frac{\gamma+1}{2(\gamma-1)}}} \frac{\left(1 + \frac{\gamma-1}{2} M^2\right)^{\frac{\gamma+1}{2(\gamma-1)}}}{M} \tag{14.4}$$

Solution of Eq. 14.4 for Mach number at the solution point is necessarily iterative. Using Newton's method (ref. 71) we can write

$$M_{i+1} = M_i + \frac{\frac{r}{r_1} - \left(\frac{r}{r_1}\right)_i}{\left[\frac{d\left(\frac{r}{r_1}\right)}{dM}\right]_i} \qquad (i = 0,1\ldots) \tag{14.5}$$

where the subscript i denotes the ith cycle of the iteration.

The derivative $\frac{d(\frac{r}{r_i})}{dM}$ appearing in Eq. 14.5 is found by differentiating Eq. 14.4, the result being

$$\frac{d(\frac{r}{r_1})}{dM} = \frac{M_1}{(1 + \frac{\gamma-1}{2} M_1^2)^{\frac{\gamma+1}{2(\gamma-1)}}} (1 + \frac{\gamma-1}{2} M^2)^{\frac{3-\gamma}{2(\gamma-1)}} (\frac{M^2-1}{M^2}) \quad (14.6)$$

A linear variation of Mach number with radius was assumed to obtain an initial estimate for M in Eq. 14.5.

Following the solution for Mach number, the dependent variables p and ρ were found from Eqs. 14.2 and 14.3. The velocity v_r was determined using the definitions of Mach number and acoustic speed, i.e.,

$$v_r = M \left[\frac{\gamma p}{\rho}\right]^{\frac{1}{2}} \quad (14.7)$$

The velocity components u and v can be expressed in terms of the velocity, v_r, and the flow angle θ as

$$u = v_r \cos\theta \quad (14.8)$$

$$v = v_r \sin\theta \quad (14.9)$$

where the flow angle is equal to the polar angle given by

$$\theta = \tan^{-1}(\frac{y}{x}) \quad (14.10)$$

B. Prandtl-Meyer Flow over a Cylinder

Prandtl-Meyer flow over a cylinder is a simple wave flow in which the flow properties are constant along Mach lines propagating from the cylinder. In this analysis, the air flow over the cylinder was assumed in a clockwise direction so that left-running Mach lines were simple waves as shown in Figure 14.2. Also, it was assumed that the Mach number M_1 at a point upstream on the cylinder (point (1) in Figure 14.2) was known along with stagnation pressure, p_0, and stagnation density, ρ_0. Point (3) in Figure 14.2 represents any solution point in the flow field, and point (2) the intersection of the cylinder and the left-running Mach line through point (3). Hence, the properties at point (3) are the same as those at point (2).

The coordinates of points (2) and (3) are related through the direction equation for a left-running Mach line, i.e.,

$$\frac{dy}{dx} = \tan(\theta + \mu) \tag{14.11}$$

where θ is flow angle, and μ Mach angle. Since the properties are constant along left-running Mach lines, from Eq. 14.11 we can write the exact relation

$$\frac{y_3 - y_2}{x_3 - x_2} = \tan(\theta_2 + \mu_2) \tag{14.12}$$

If trigonometric identities and the relation between the flow angle and the polar angle ϕ for points on the cylinder,

$$\theta = \phi - \pi/2 \tag{14.13}$$

are introduced, Eq. 14.12 can be reexpressed as

$$\frac{y_3 - y_2}{x_3 - x_2} = \frac{\tan\phi_2 \tan\mu_2 - 1}{\tan\phi_2 + \tan\mu_2} \tag{14.14}$$

Next, substitution of the coordinate transformation relation

$$\tan\phi = y/x \tag{14.15}$$

into Eq. 14.14 gives

$$\frac{y_3 - y_2}{x_3 - x_2} = \frac{y_2 \tan\mu_2 - x_2}{y_2 + x_2 \tan\mu_2} \tag{14.16}$$

Finally, elimination of x_3, y_3 and y_2 between Eq. 14.16 and the following geometric relations

$$x_2^2 + y_2^2 = r_1^2 \tag{14.17}$$

$$x_3^2 + y_3^2 = r_3^2 \tag{14.18}$$

$$\tan\phi_3 = y_3/x_3 \tag{14.19}$$

yields (after considerable rearrangement)

$$x_2 = r_1\{\frac{r_1}{r_3}\cos\mu_2\cos(\phi_3 - \mu_2) - \sin(\phi_3 - \mu_2)$$

$$[1 - (\frac{r_2}{r_3})\cos^2\mu_2]^{\frac{1}{2}}\} \qquad (14.20)$$

Equation 14.20 provided a basis for an iterative solution for the coordinates of point (2). The value of μ_2 in Eq. 14.20 was initially estimated as $\mu_2 = \mu_1$, and was corrected as outlined below. Once the solution for x_2 was obtained from Eq. 14.20, y_2 was determined from Eq. 14.17.

Using the estimate for the coordinates at point (2) from the above analysis, the Mach numbers at points (1) and (2) were related through the corresponding Prandtl-Meyer angles by the simple wave relation

$$\nu_2 - \nu_1 = \theta_1 - \theta_2 \qquad (14.21)$$

where the flow angles θ_1 and θ_2 were found from Eq. 14.13. The Mach number M_2 was determined iteratively from the definition of the Prandtl-Meyer angle, i.e.,

$$\nu(M) = \left[\frac{\gamma+1}{\gamma-1}\right]^{\frac{1}{2}}\tan^{-1}\left[\frac{\gamma-1}{\gamma+1}(M^2 - 1)\right]^{\frac{1}{2}} - \tan^{-1}[M^2 - 1]^{\frac{1}{2}} \qquad (14.22)$$

Using Newton's method, we can write the recursive relation

$$M_{i+1} = M_i + \frac{\nu - \nu_i}{\left[\frac{d\nu}{dM}\right]_i} , \qquad (i = 0,1...) \tag{14.23}$$

where the subscript i denotes the ith cycle of the iteration, and where the derivative $\frac{d\nu}{dM}$ was found by differentiating Eq. 14.22, i.e.,

$$\frac{d\nu}{dM} = \frac{(M^2 - 1)^{\frac{1}{2}}}{M}\left(1 + \frac{\gamma-1}{2} M^2\right)^{-1} \tag{14.24}$$

The given Mach number at point (1) was used as the initial estimate for M in Eq. 14.23. To close the iteration for the Mach number M_2 and the coordinates x_2, y_2, the Mach angle μ_2 was determined from the relation

$$\mu = \sin^{-1}\left(\frac{1}{M}\right) \tag{14.25}$$

and substituted back into Eq. 14.20. This process was continued until convergence on μ_2 was achieved.

After the Mach number at point (3) was determined, the pressure p_3 and density ρ_3 were found from the isentropic relations, Eqs. 14.2 and 14.3, respectively. The velocity q_3 was determined from the relation

$$q_3 = M_3 \left[\frac{\gamma p_3}{\rho_3}\right]^{\frac{1}{2}} \tag{14.26}$$

Finally, the velocity components u_3 and v_3 were determined from the relations

$$u_3 = q_3 \cos\theta_3$$

$$v_3 = q_3 \sin\theta_3$$

where the flow angle θ_3 was found from Eq. 14.13 with $\phi = \phi_2$.

XV. APPENDIX F:

ONE-DIMENSIONAL UNSTEADY FLOW EXAMPLES

Three examples of one-dimensional unsteady flows were solved using the field point and boundary point algorithms developed in Chapters III and IV. The results of these solutions are presented in this section. Where available, solutions obtained by the method of characteristics for one-dimensional unsteady flow were used for comparison. These results indicate that the boundary point calculations yield properly posed boundary conditions, and that accurate solutions of transient flows can be obtained using the present method.

In these solutions, a rectangular grid with mesh spacing Δx was overlaid on a straight duct (see Figure 15.1a). The grid had three points along each constant-x panel, which is the minimum number of points needed to incorporate the initial-data interpolation scheme (see Appendix H). Only those points along the center panel on the duct centerline were calculated in the solution. The dependent variables at points along the bounding constant-y panels were set equal to the values of the corresponding dependent variables at each grid point along the duct centerline.

A. Centered Expansion Wave, Semi-Infinite Duct

In this first example, a semi-infinite duct pressurized with air at pressure p_0 is instantaneously opened to the

atmosphere at pressure p_a. A centered expansion wave propagates into the duct as shown in Figure 15.1. The wave accelerates the air from the stagnation state to a uniform state at the ambient pressure. For the unchoked condition ($p_a/p_0 > 0.278$), the transient flow is determined by the stagnation conditions in the duct and the ambient pressure.

In the numerical solution, the semi-infinite duct was approximated by a duct of length L = 1 ft., shown in Figure 15.1a, and the boundary conditions at the upstream end of the duct were fixed at the stagnation state. Field point calculations (Chapter III) were made at interior points, while at the end of the duct the downstream boundary point calculation (Section IV.D.) was employed. Only the transient flow prior to the time the expansion wave reaches the upstream end of the duct was investigated. The solution results for $p_a/p_0 = 0.8$ are shown in Figure 15.2a where pressure ratio is plotted versus time at x = -0.2 ft. for different mesh spacings. Also shown is the exact solution obtained from the method of characteristics for one-dimensional unsteady flow (ref. 72). The results of the present method agree well with the exact solution and also demonstrate the degree of resolution which can be achieved with a relatively fine mesh ($\Delta x = 0.01$ ft.).

As further comparison, results by Serra (39) for this problem using the Lax-Wendroff finite-difference method are presented in Figure 15.2b. The better agreement of the present

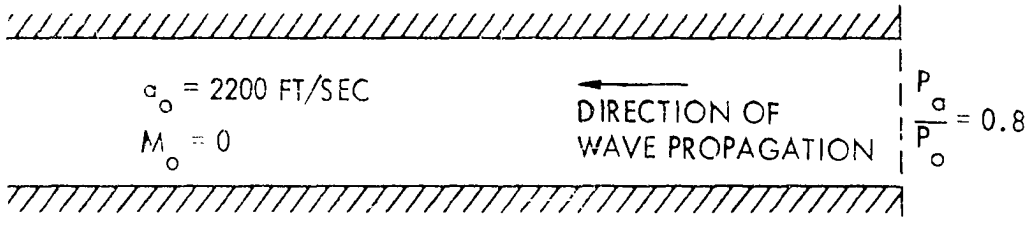

a. Duct geometry

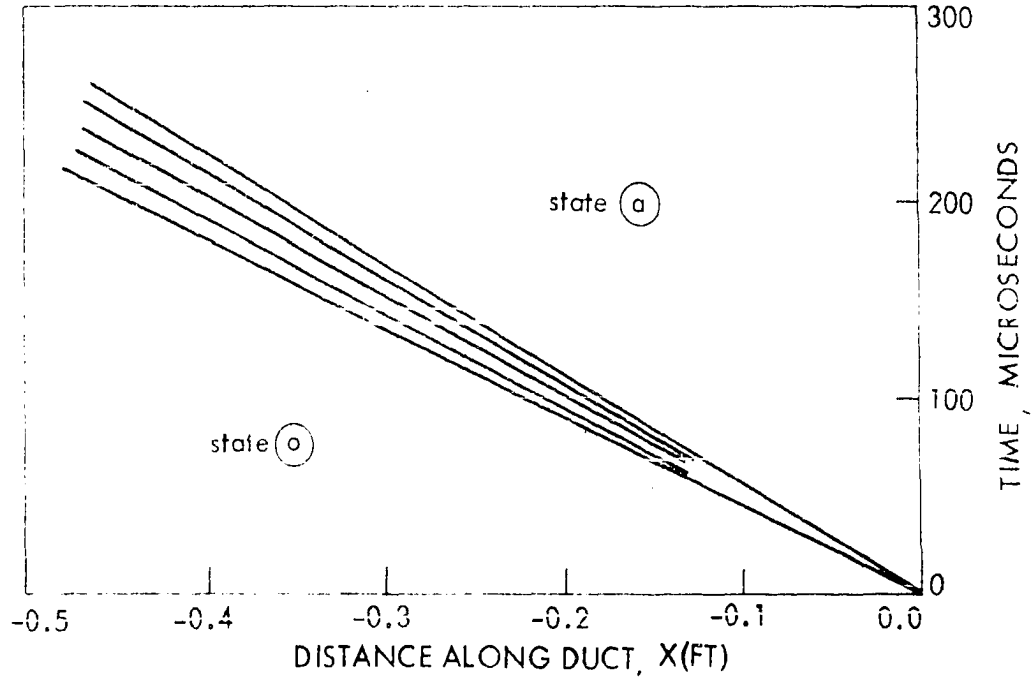

b. Wave diagram

Figure 15.1. Duct geometry and wave diagram for the centered expansion wave, semi-infinite duct problem

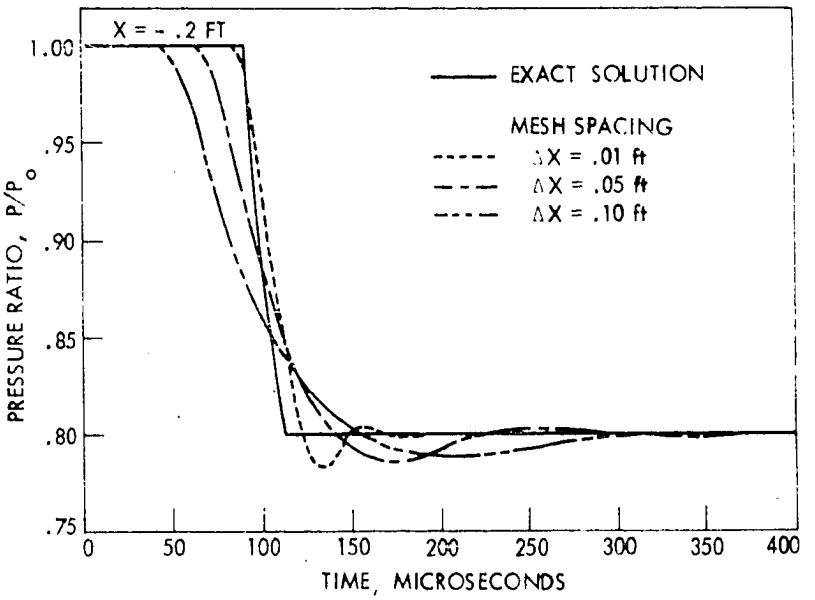

a. Present method solution

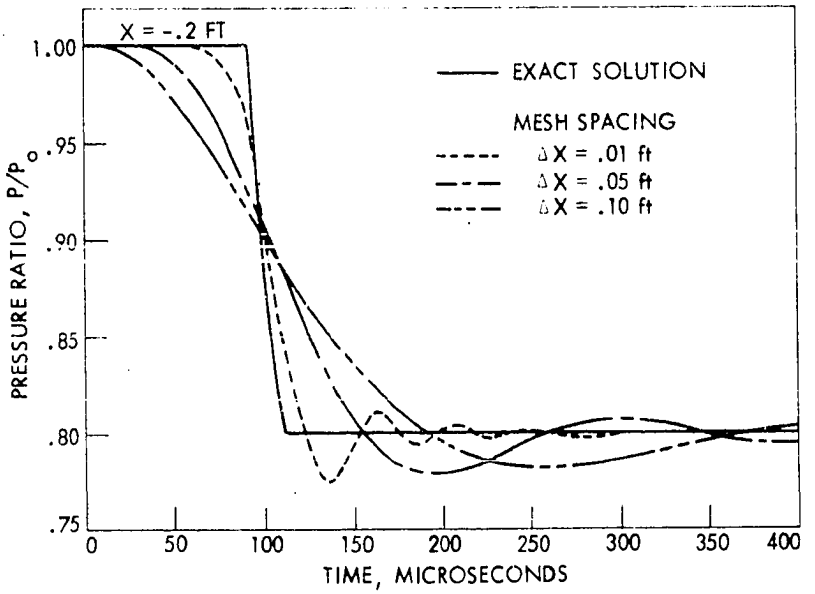

b. Comparison solution (ref. 39)

Figure 15.2. Centered expansion wave, semi-infinite duct problem

Pressure variation with time at position x = -0.2 ft.

method with the exact solution over Serra's method is evident.

B. Centered Expansion Wave, Finite Duct

In this case, a finite duct filled with air is instantaneously opened to the atmosphere where the ratio of ambient pressure to stagnation pressure in the duct, p_a/p_0, was 0.387. A centered expansion wave propagates upstream and reflects in like sense from the closed end of the duct, as shown in Figure 15.3. The region of interaction between the incident and reflected waves is a nonsimple wave region through which the gas overexpands to a uniform state with $p/p_0 = 0.129$ at the closed end of the duct.

In this example, the body point calculation (Section IV.B) was used to compute the solution at the upstream end of the duct at $\frac{x}{L} = -1.0$. The pressure variation with time at this point is shown in Figure 15.4. No exact solution exists for the flow through the non-simple wave region; however, the results of a graphical characteristics solution by Owczarek (72) have been included in Figure 15.4 for comparison. The agreement of results of the present method and the graphical solution is extremely good.

C. Centered Expansion Wave, Subsonic Inflow

This problem is similar to the preceding example, with the exception that a plenum (in which the stagnation state is fixed)

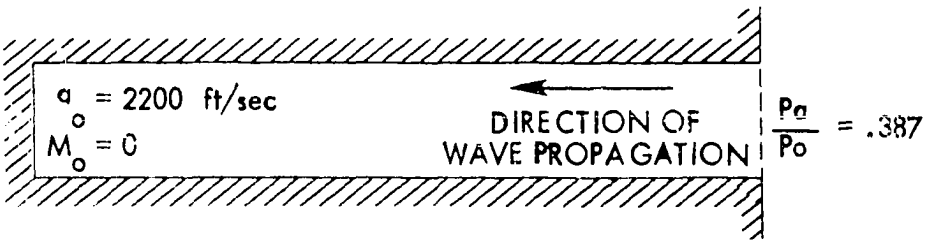

a. Duct geometry

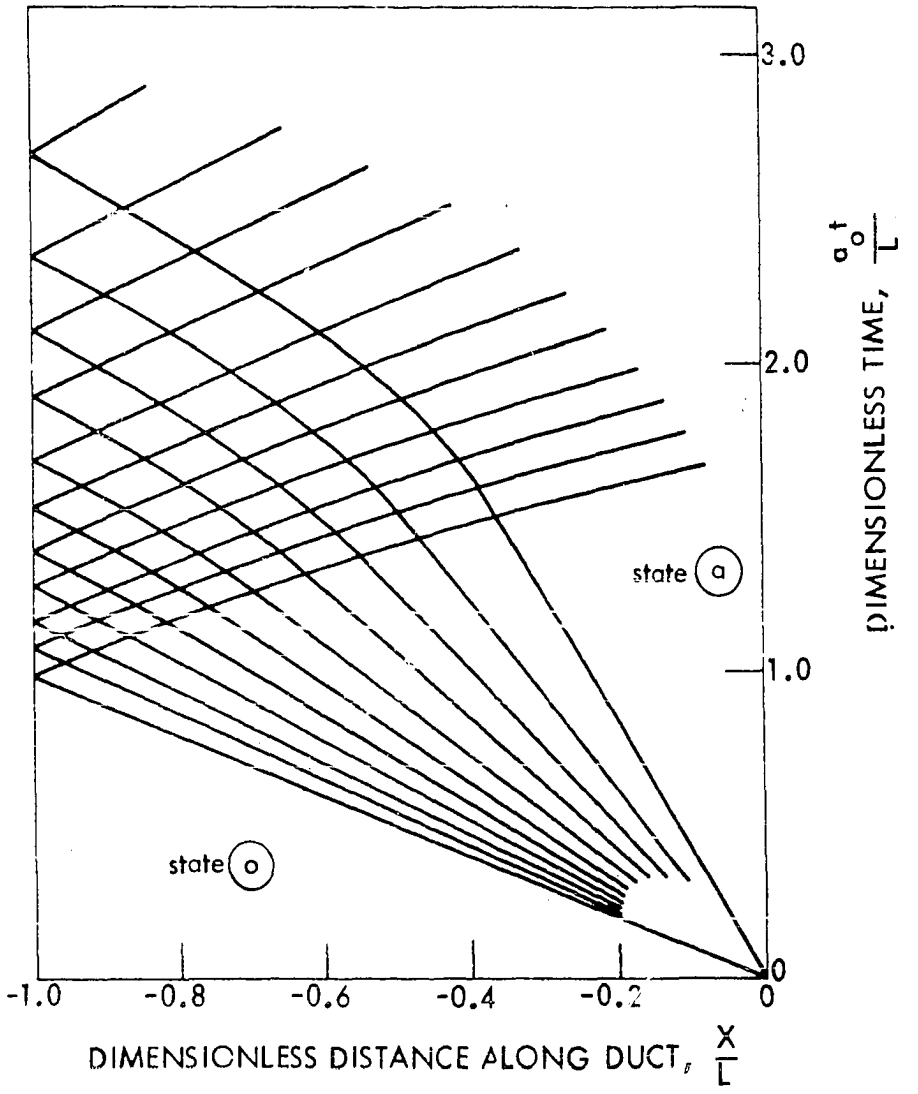

b. Wave diagram

Figure 15.3. Duct geometry and wave diagram for the centered expansion wave, finite duct problem

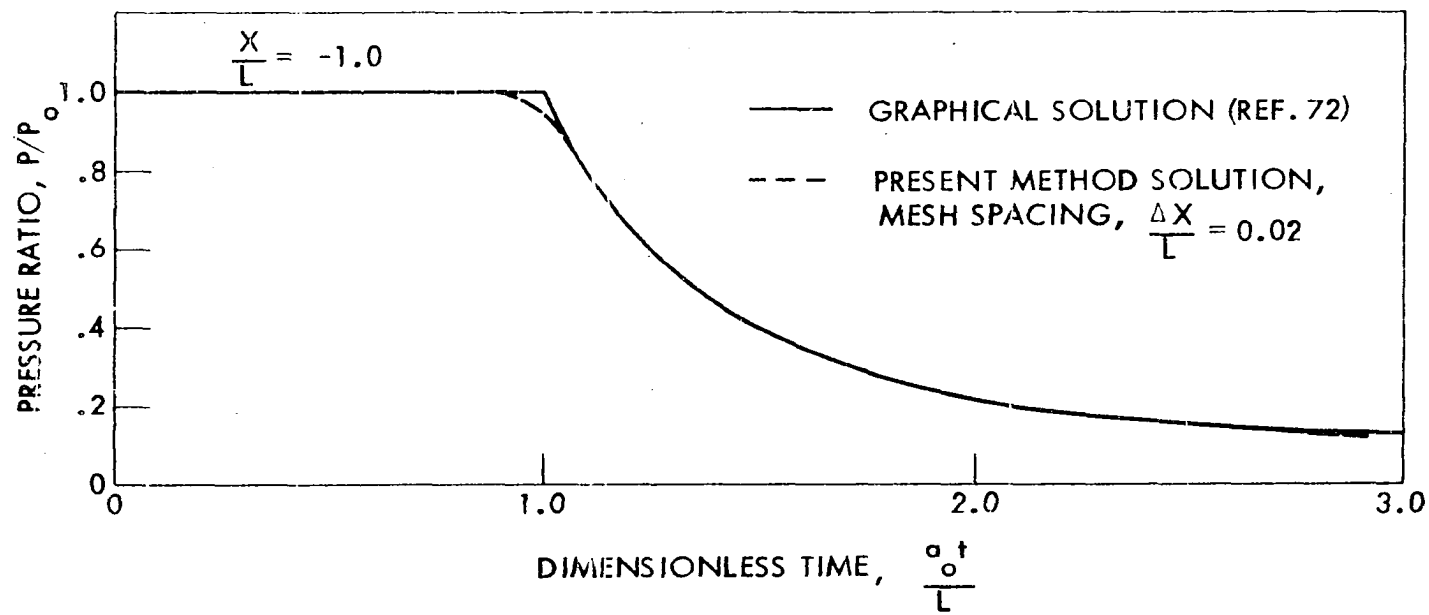

Figure 15.4. Centered expansion wave, finite duct problem
Pressure variation with time at closed end (x/L = -1.0)

is attached to the duct at the upstream boundary ($\frac{x}{L} = -1.0$). In this case, the centered expansion wave propagating upstream reflects at the upstream boundary as a weaker compression wave, as shown in Figure 15.4. The compression wave moves downstream and reflects in opposite sense from the downstream boundary. This process of expansion and compression is repeated until a uniform steady flow corresponding to the constant inlet stagnation state and downstream static pressure is reached throughout the duct.

In this example, the upstream boundary point calculation (Section IV.C) with the velocity component u_2 set to zero was employed at the upstream end of the duct. Pressure variations with time at two points along the duct ($\frac{x}{L} = -1.0$, $\frac{x}{L} = -0.5$) for a sparse grid ($\frac{\Delta x}{L} = 0.1$) are shown in Figure 15.6. It is observed from Figure 15.6 that the steady state solution was reached throughout the duct when $\frac{a_0 t}{L} = 17$. Also, separate expansion and compression waves are discernable at the $\frac{x}{L} = -0.5$ location.

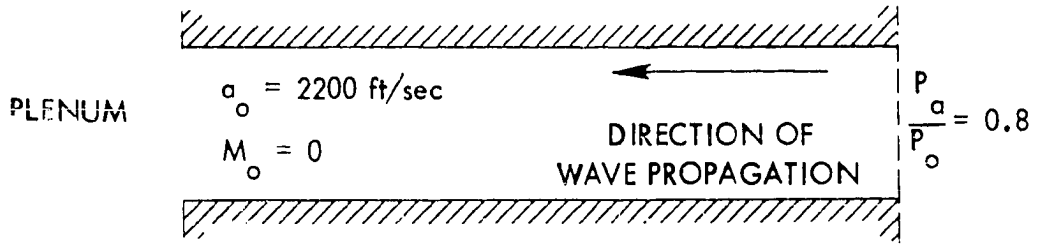

a. Duct geometry

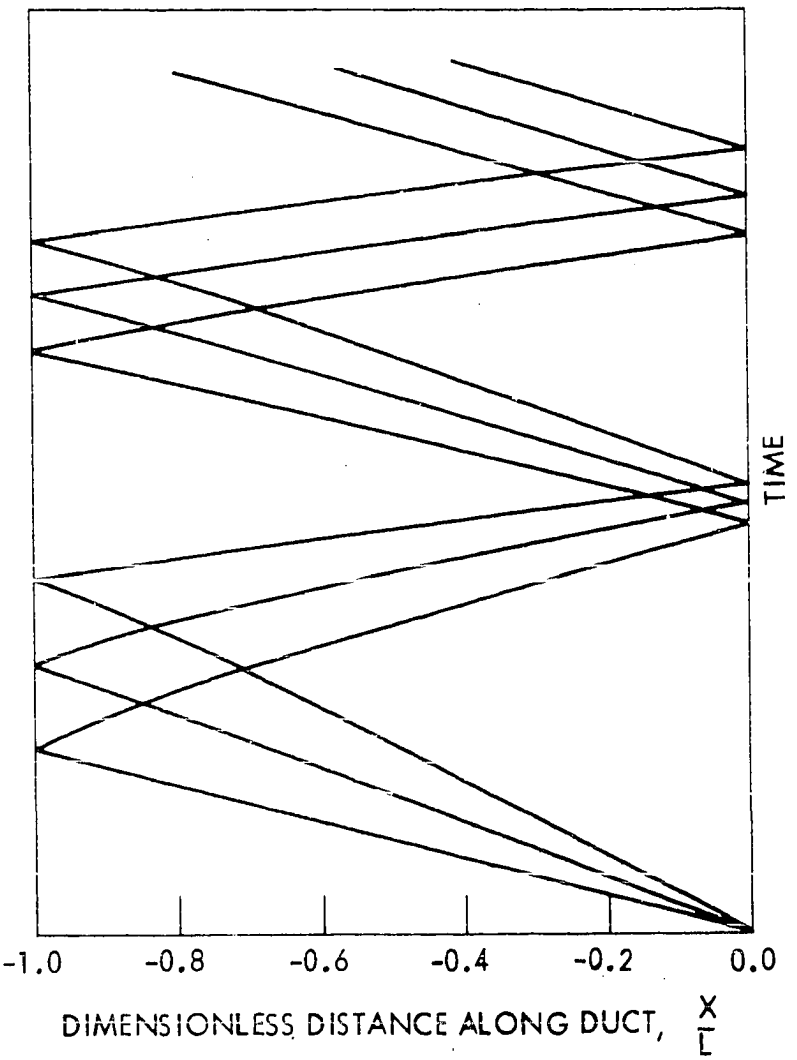

b. Wave diagram

Figure 15.5. Duct geometry and wave diagram representation for the centered expansion wave, subsonic inflow, finite duct problem

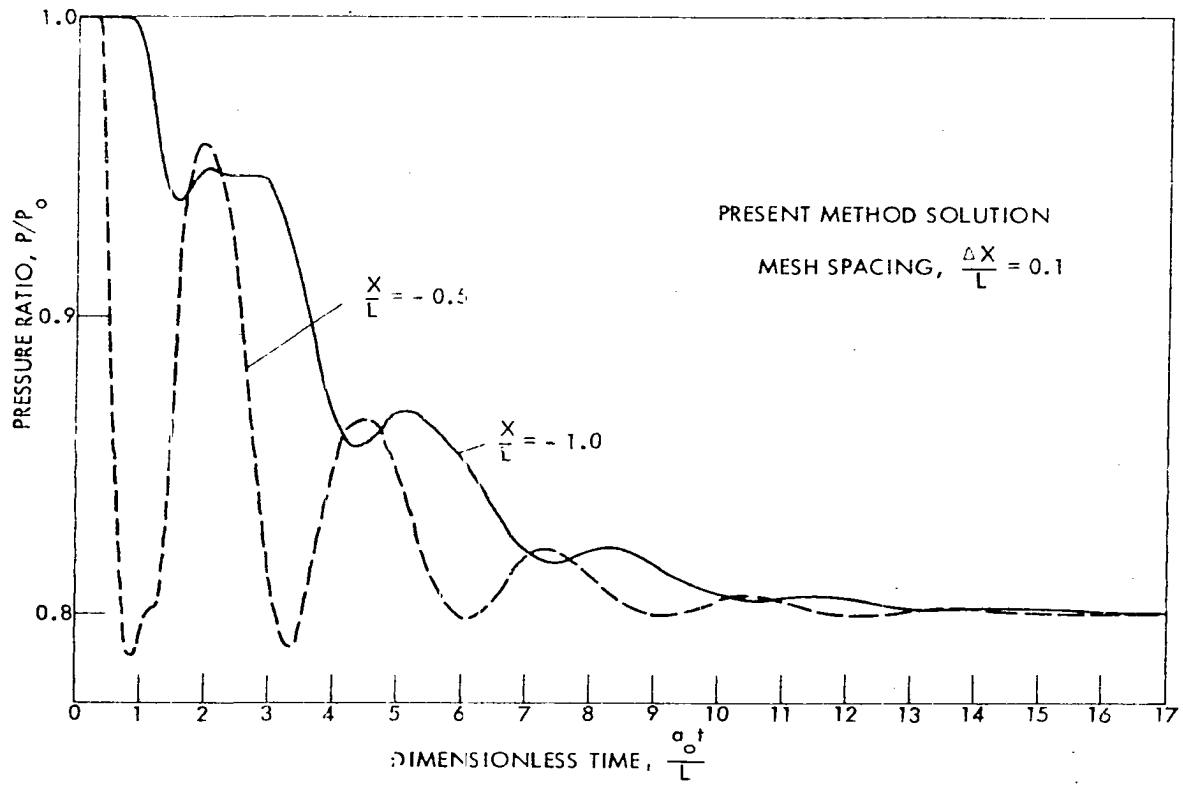

Figure 15.6. Centered expansion wave, subsonic inflow, finite duct problem
Pressure variation with time at locations x/L = -1.0 and x/L = -0.5

XVI. APPENDIX G:

QUADRIC CONE GEOMETRY

The numerical solution of two-dimensional unsteady flows incorporating the method of characteristics involves solution of compatibility relations written on characteristic surfaces in three space. The envelope of characteristic wave surfaces at a point in the space is locally tangent to the characteristic cone which is represented by a quadratic equation in the space coordinates. A discussion of quadric cone geometry, as needed in the mathematical formulation of the method of characteristics and in the numerical solution of the characteristic relations, is presented here. This material is based on the work of McConnell (73).

A. Equation of a Plane

Let P_1, P_2 and P_3 be three points with coordinates x_i^1, x_i^2 and x_i^3, respectively, as shown in Figure 16.1. Here, the notation x_i is used to denote the point coordinates or, equivalently, a vector with components $x_i = \{x_1, x_2, x_3\}$. If the point x_i lies in the plane of points P_1, P_2 and P_3, then the difference vectors $x_i - x_i^1$, $x_i - x_i^2$ and $x_i - x_i^3$ are linearly dependent, i.e.,

$$a\left(x_i - x_i^1\right) + b\left(x_i - x_i^2\right) + c\left(x_i - x_i^3\right) = 0 \qquad (16.1)$$

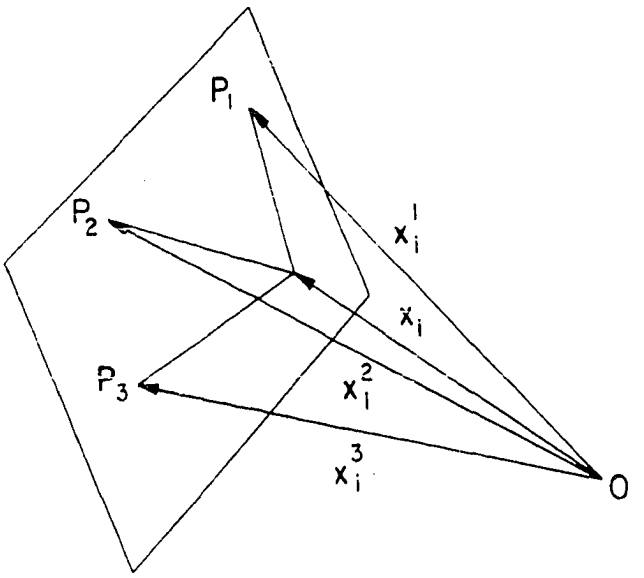

Figure 16.1. Vectors x_i^1, x_i^2, x_i^3 with endpoints P_1, P_2, P_3 lying in a plane

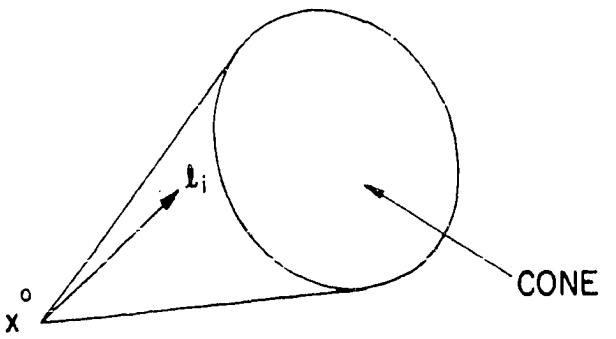

Figure 16.2. Vector ℓ_i lying along a generator of a cone with vertex x_i^o

where a, b and c are scalars. Equation 16.1 can be written in component form as

$$a\left(x_1 - x_1^1\right) + b\left(x_1 - x_1^2\right) + c\left(x_1 - x_1^3\right) = 0$$

$$a\left(x_2 - x_2^1\right) + b\left(x_2 - x_2^2\right) + c\left(x_2 - x_2^3\right) = 0$$

$$a\left(x_3 - x_3^1\right) + b\left(x_3 - x_3^2\right) + c\left(x_3 - x_3^3\right) = 0$$

This system of equations provides three equations for the numbers a, b, and c and can be written in matrix form as

$$\begin{bmatrix} x_1 - x_1^1 & x_1 - x_1^2 & x_1 - x_1^3 \\ x_2 - x_2^1 & x_2 - x_2^2 & x_2 - x_2^3 \\ x_3 - x_3^1 & x_3 - x_3^2 & x_3 - x_3^3 \end{bmatrix} \begin{bmatrix} a \\ b \\ c \end{bmatrix} = 0 \qquad (16.2)$$

If a unique solution for a, b, and c exists, then the determinant of the coefficient matrix in Eq. 16.2 must vanish, i.e.,

$$\begin{vmatrix} x_1 - x_1^1 & x_1 - x_1^2 & x_1 - x_1^3 \\ x_2 - x_2^1 & x_2 - x_2^2 & x_2 - x_2^3 \\ x_3 - x_3^1 & x_3 - x_3^2 & x_3 - x_3^3 \end{vmatrix} = 0 \qquad (16.3)$$

Equation 16.3 can be expressed as the sum of four determinants whose elements involve only one component of the elements of the determinant in Eq. 16.3, i.e.,

$$\begin{vmatrix} x_1 & x_1^1 & x_1^3 \\ x_2 & x_2^2 & x_2^3 \\ x_3 & x_3^2 & x_3^3 \end{vmatrix} + \begin{vmatrix} x_1^1 & x_1 & x_1^3 \\ x_2^1 & x_2 & x_2^3 \\ x_3^1 & x_3 & x_3^3 \end{vmatrix} \tag{16.4}$$

$$+ \begin{vmatrix} x_1^1 & x_1^2 & x_1 \\ x_2^1 & x_2^2 & x_2 \\ x_3^1 & x_3^2 & x_3 \end{vmatrix} = \begin{vmatrix} x_1^1 & x_1^2 & x_1^3 \\ x_2^1 & x_2^2 & x_2^3 \\ x_3^1 & x_3^2 & x_3^3 \end{vmatrix}$$

which is a linear equation in the x_i. Therefore, any linear combination in x_i,

$$A_i x_i = B, \tag{16.5}$$

is the equation of a plane. If any one of the vectors x_i^1, x_i^2, or x_i^3 is a null vector, then the plane passes through the origin and Eq. 16.4 can be written

$$A_i x_i = 0 \tag{16.6}$$

B. Equation of a Quadric Cone

A quadric cone is the locus traced out by a family of lines which all pass through a point x_i^0 and whose unit vectors, ℓ_i, shown in Figure 16.2, satisfy a relation of the form

$$A_{ij}\ell_i\ell_j = 0 \tag{16.7}$$

where A_{ij} is a symmetric second order tensor. The point x_i^0 is called the vertex of the cone and the lines are called the generators of the cone.

If x_i is any point on the cone, then we can write

$$x_i = x_i^0 + c\ell_i \tag{16.8}$$

where c is an arbitrary scalar. Solution for ℓ_i in Eq. 16.8 and substitution into Eq. 16.7 gives

$$A_{ij}\left(x_i - x_i^0\right)\left(x_j - x_j^0\right) = 0 \tag{16.9}$$

which is the equation of the cone. If the vertex of the cone is at the origin, Eq. 16.9 reduces to

$$A_{ij}x_ix_j = 0 \tag{16.10}$$

C. Tangent Plane to a Cone

Consider a point P_1 with coordinates x_i^1 which lies on the line joining the points $P_0(x_i^0)$ and $P(x_i)$. If k is the ratio of the distances a/b shown in Figure 16.3, then the coordinates of

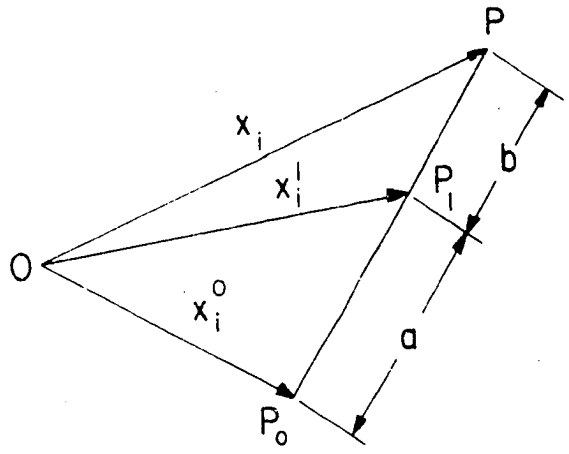

Figure 16.3. Vectors x_i, x_i^0, x_i^1 with endpoints P, P_0, P_1 lying on a straight line

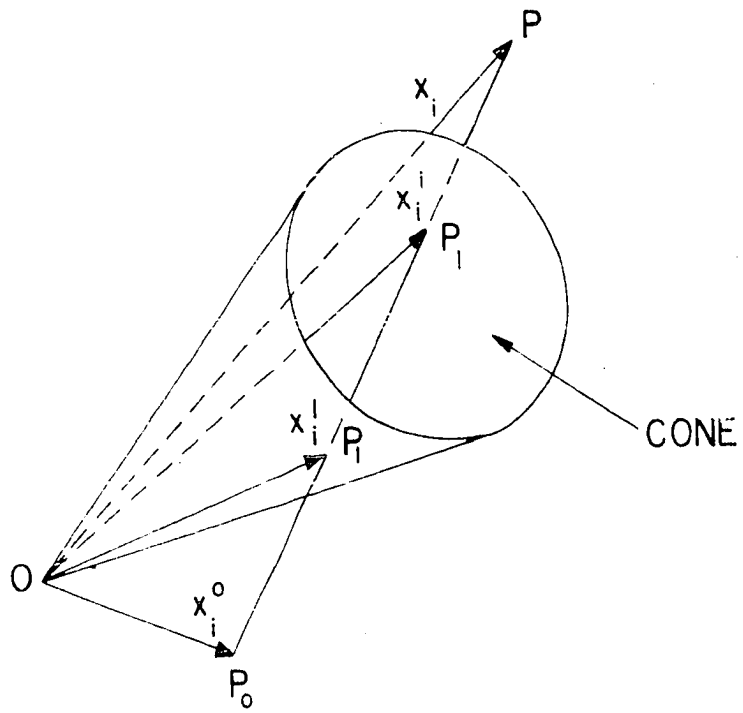

Figure 16.4. Line P_oP intersecting a cone at points P_1

P_1 can be expressed in terms of the coordinates of P_0 and P as

$$x_i^1 = \frac{x_i^0 + kx_i}{1 + k} \tag{16.11}$$

Let the point P_1 lie on a cone, as shown in Figure 16.4, then the coordinates of P_1 satisfy Eq. 16.10, i.e.,

$$A_{ij}x_i^1x_j^1 = 0 \tag{16.12}$$

substitution of x_i^1 from Eq. 16.11 into Eq. 16.12 yields

$$A_{ij}x_i^0x_j^0 + 2kA_{ij}x_i^0x_j + k^2A_{ij}x_ix_j = 0 \tag{16.13}$$

Equation 16.13 is a quadratic equation in k, the roots of which are the ratios in which the two points of intersection of P_0P with the cone divide the line P_0P.

If the point P_0 also lies on the cone, then

$$A_{ij}x_i^0x_j^0 = 0 \tag{16.14}$$

and Eq. 16.13 reduces to the equation

$$k(2A_{ij}x_i^0x_j - kA_{ij}x_ix_j) = 0 \tag{16.15}$$

The root k = 0 in this equation corresponds to the point x_i^0. If the other root is zero the line P_0P just touches the cone at P_0, as shown in Figure 16.5. According to Eq. 16.15, the condition for the vanishing of the second root is

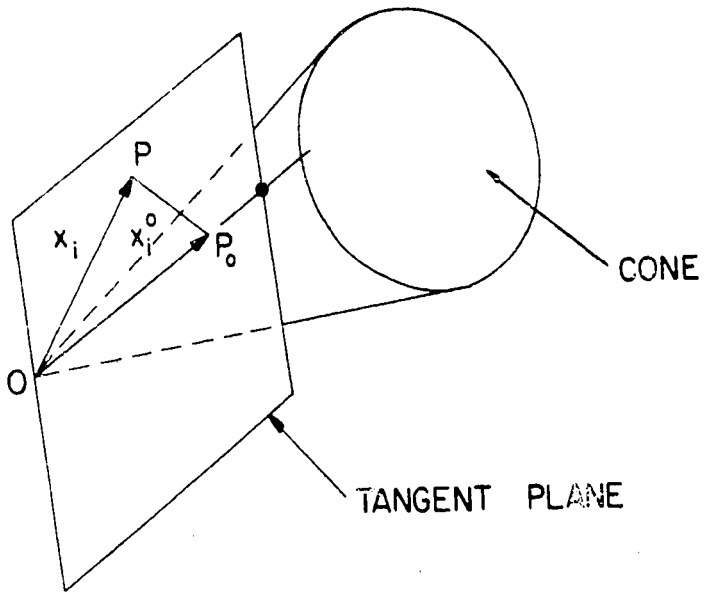

Figure 16.5. Tangent plane to a cone

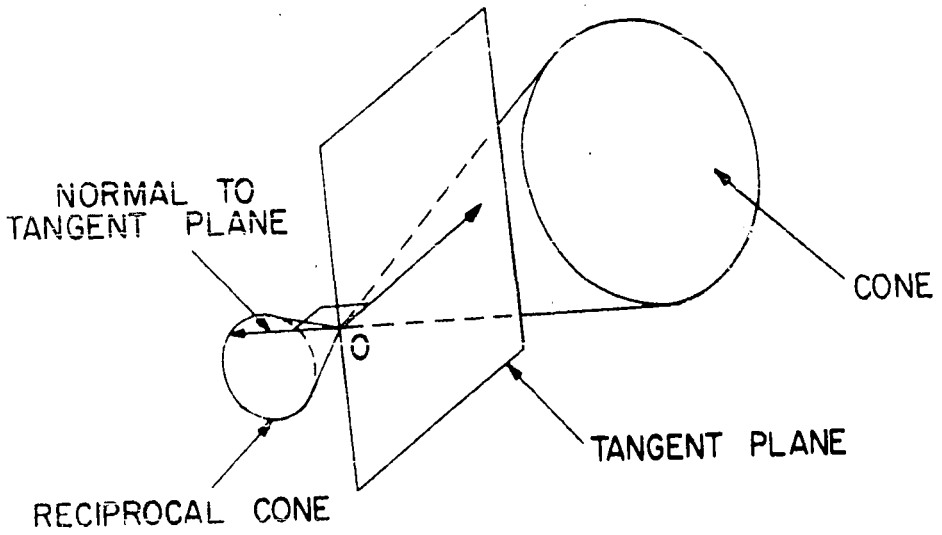

Figure 16.6. Cone and reciprocal cone

$$A_{ij}x_i^0 x_j = 0 \tag{16.16}$$

which is the equation of a plane through the origin [Eq. 16.6]. Any vector which is a scalar multiple of x_i^0 satisfies Eq. 16.16; therefore, x_i^0 lies in the plane and Eq. 16.16 is the equation of a tangent plane to the cone along the generator through x_i^0. The vector x_i is any vector in the tangent plane.

D. Reciprocal Cone

The reciprocal cone is the locus of lines which are perpendicular to the infinite family of tangent planes to a cone, as shown in Figure 16.6.

Consider the equation of a cone whose vertex is at the origin,

$$A_{ij}x_i x_j = 0 \tag{16.17}$$

If x_i^1 is an arbitrary point on the cone, then

$$A_{ij}x_i^1 x_j = 0 \tag{16.18}$$

is the equation of the tangent plant to the cone along the generator through x_i^1. Let

$$C_j = A_{ij}x_i^1 \tag{16.19}$$

then Eq. 16.18 can be written as

$$C_j x_j = 0 \tag{16.20}$$

It is apparent from the form of this equation that the vector C_i is orthogonal to x_i which is any vector in the tangent plane.

The equation of the reciprocal cone can be expressed, in general, as

$$B_{ij}x_i x_j = 0 \tag{16.21}$$

where the coefficients B_{ij} are to be determined. Since the vector C_i is along a generator of the reciprocal cone, it will satisfy Eq. 16.21, i.e.,

$$B_{ij}C_i C_j = 0 \tag{16.22}$$

Substitution of C_i from Eq. 16.19 into Eq. 16.22 yields

$$B_{ij}A_{ki}x^1_k A_{\ell j}x^1_\ell = 0 \tag{16.23}$$

Moreover, x^1_i is an arbitrary point on the cone, therefore, we can write Eq. 16.23, in general, as

$$B_{ij}A_{ki}A_{\ell j}x_k x_\ell = 0 \tag{16.24}$$

Comparison of Eqs. 16.17 and 16.24 yields the equation

$$B_{ij}A_{ki}A_{\ell j} = A_{k\ell} \tag{16.25}$$

for determining the elements B_{ij}.

If A is the matrix of elements A_{ij}, then

$$AA^{-1} = I \tag{16.26}$$

where I is the unit matrix. An equivalent expression of Eq. 16.26 in index notation is

$$A_{ij}A^*_{j\ell} = \delta_{i\ell}|A| \tag{16.27}$$

where A^*_{ij} are the cofactors of A_{ij} and $|A|$ is the determinant of A.

Multiplication of Eq. 16.25 by $A^*_{km}A^*_{\ell n}$ gives

$$B_{ij}\left(A_{ki}A^*_{km}\right)\left(A_{\ell j}A^*_{\ell n}\right) = A^*_{km}\left(A_{k\ell}A^*_{\ell n}\right) \tag{16.28}$$

or, with substitution of Eq. 16.27

$$B_{ij}\delta_{im}\delta_{jn}|A| = A^*_{km}\delta_{kn} \tag{16.29}$$

Hence, it follows that

$$B_{mn}|A| = A^*_{nm} \tag{16.30}$$

Since the elements A_{ij} are symmetric, the cofactors are symmetric and Eq. 16.30 can be written

$$B_{ij} = \frac{A^*_{ij}}{|A|} \equiv A^{-1}_{ij} \tag{16.31}$$

where A^{-1}_{ij} are the elements of the inverse matrix A^{-1}. According to Eqs. 16.21 and 16.31, the equation of the reciprocal cone is

$$A^{-1}_{ij}x_i x_j = 0 \tag{16.32}$$

E. Conjugate Points with Respect to a Cone

Let the line joining the points $P_0(x_i^0)$ and $P(x_i)$ intersect a cone as shown in Figure 16.4. The roots, k, of Eq. 16.13 are the ratios in which the two points of intersection of P_0P with the cone divide the line P_0P. Here the points x_i^0 and x_i do not, in general, lie on the cone.

If the roots of Eq. 16.13 are equal in magnitude but opposite in sign, then the points P_0 and P are called harmonic conjugates with respect to the cone. According to Eq. 16.13, this condition is expressed as

$$A_{ij}x_i^0x_j = 0 \tag{16.33}$$

which, for point P_0 fixed, is the equation of a plane through the origin [Eq. 16.6]. This plane is called the polar plane of P_0 with respect to the cone. Hence, the point P_0 and any point in its polar plane are harmonic conjugates with respect to the cone. The polar plane of the point P_0, lying outside the cone, and the point $P_1(x_i^1)$, lying in the polar plane of P_0 inside the cone, are shown in Figure 16.7. If the point P_0 lies on the cone, its polar plane is the tangent to the cone through P_0 [Eq. 16.16 and Figure 16.5] and the corresponding roots, k, of Eq. 16.13 both vanish.

The equation of the polar plane of a point $P_1(x_i^1)$ is

$$A_{ij}x_i^1x_j = 0 \tag{16.34}$$

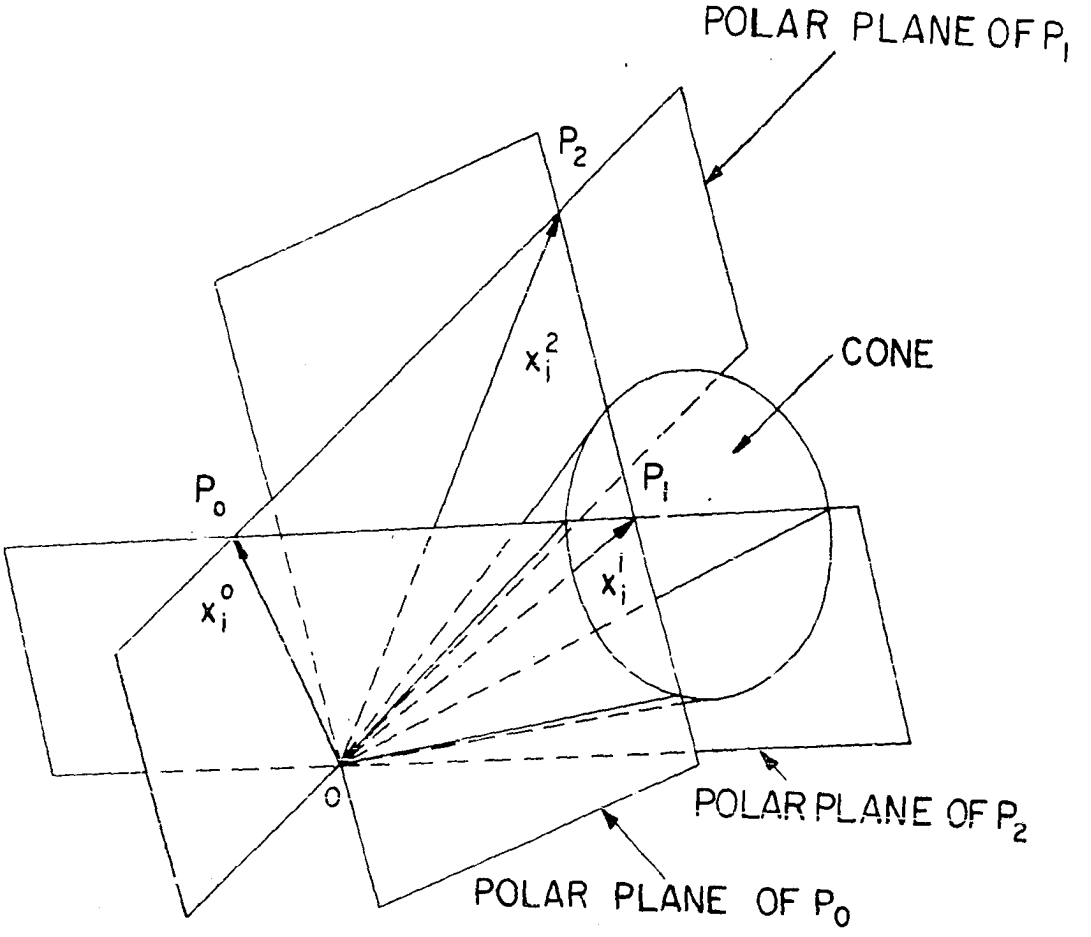

Figure 16.7. Polar planes of points P_0, P_1, P_2 and mutual conjugate diameters OP_0, OP_1, OP_2 of a cone

If P_1 lies in the polar plane of P_0, then the coordinates x_i^1 satisfy Eq. 16.33, i.e.,

$$A_{ij}x_i^0x_j^1 = 0 \tag{16.35}$$

Upon examination of Eqs. 16.34 and 16.35 we see that the polar plane of P_1 passes through P_0, as shown in Figure 16.7. Therefore, a point always lies in the polar plane of its conjugate point.

If ℓ_i^0 is a unit vector in the direction of x_i^0, then

$$x_i^0 = c\ell_i^0 \tag{16.36}$$

where c is a scalar. Substitution for x_i^0 from Eq. 16.36 into Eq. 16.33 we get

$$cA_{ij}\ell_i^0x_j^0 = 0 \tag{16.37}$$

Hence, the polar planes of all points along the line through x_i^0 corresponding to different values of c in Eq. 16.37 coincide and this plane is called the conjugate plane of a given line.

If P_1 and P_0 are conjugate points with respect to a cone then all points along the line through OP_1 are conjugate to all points along the line through OP_0. Two such lines are called conjugate diameters of the cone. Two lines with unit vectors ℓ_i^0 and ℓ_i^1 are conjugate diameters if

$$A_{ij}\ell_i^0\ell_j^1 = 0 \tag{16.38}$$

There exist an infinite number of diameters which are conjugate to a line through the origin, 0, and they are the infinite number of lines through 0 lying in the conjugate plane of the given line.

The polar planes of the points $P_0\left(x_i^0\right)$, $P_1\left(x_i^1\right)$ and $P_2\left(x_j^2\right)$ are given by the equations

$$A_{ij}x_i^0x_j = 0 \tag{16.39}$$

$$A_{ij}x_i^1x_j = 0 \tag{16.40}$$

$$A_{ij}x_i^2x_j = 0, \tag{16.41}$$

respectively. The lines through OP_0, OP_1, OP_2 are called mutual conjugate diameters if

$$A_{ij}x_i^0x_j^1 = 0 \tag{16.42}$$

$$A_{ij}x_i^1x_j^2 = 0 \tag{16.43}$$

$$A_{ij}x_i^2x_j^0 = 0 \tag{16.44}$$

It is apparent from these two sets of equations that two of the points lie in the polar plane of the remaining point, as shown in Figure 16.7. For a given line there exist an infinite number of conjugate diameters lying in its conjugate plane. Hence, there exist a doubly infinite set of mutual conjugate diameters for a cone.

F. Canonical Equation of a Cone

Let the lines along OP_1, OP_2 and OP_3 be mutual conjugate diameters of a cone, then, according to Eqs. 16.42, 16.43 and 16.44, we have

$$A_{ij}x_i^1x_j^2 = A_{ij}x_i^2x_j^3 = A_{ij}x_i^3x_j^1 = 0 \tag{16.45}$$

Let the vectors x_i^1, x_i^2, x_i^3 represent a new system of basis vectors, then in the new basis

$$\bar{x}_i^1 = \delta_{i1} \tag{16.46}$$

$$\bar{x}_i^2 = \delta_{i2} \tag{16.47}$$

$$\bar{x}_i^3 = \delta_{i3} \tag{16.48}$$

where the overbar indicates quantities measured in the new basis. It should be noted that the new coordinate system is not necessarily a cartesian system (uniform scaling along the three axes). The equation of a cone is invariant with respect to coordinate transformations, therefore, from Eqs. 16.45-16.48 we have

$$\bar{A}_{ij}\bar{x}_i^1\bar{x}_j^2 = \bar{A}_{ij}\delta_{i1}\delta_{j2} = \bar{A}_{12} = \bar{A}_{21} = 0 \tag{16.49}$$

$$\bar{A}_{ij}\bar{x}_i^2\bar{x}_j^3 = \bar{A}_{ij}\delta_{i2}\delta_{j3} = \bar{A}_{23} = \bar{A}_{32} = 0 \tag{16.50}$$

$$\bar{A}_{ij}\bar{x}_i^3\bar{x}_j^1 = \bar{A}_{ij}\delta_{i3}\delta_{j1} = \bar{A}_{31} = \bar{A}_{13} = 0 \tag{16.51}$$

Hence, the equation of the cone in the barred system is

$$\bar{A}_{11}(\bar{x}_1)^2 + \bar{A}_{22}(\bar{x}_2)^2 + \bar{A}_{33}(\bar{x}_3)^2 = 0 \qquad (16.52)$$

which is called the canonical form of the equation of the cone. There are an infinite number of coordinate systems in which the equation of the cone can be expressed in canonical form and they correspond to the infinite number of sets of mutual conjugate diameters of the cone. Moreover, we may take any points along the mutual conjugate diameters as unit points and the equation of the cone will still be in canonical form. In particular we may choose the points such that the nonzero coefficients in the canonical form of the equation of the cone may all be plus or minus unity.

XVII. APPENDIX H:

LEAST SQUARES BIVARIATE INTERPOLATION SCHEME

In the numerical integration procedures the values of the four dependent variables and their spatial derivatives are needed on the initial data surface at the intersections of the bicharacteristics and the particle path. Since only discrete data at the grid points are known, interpolation procedures are required.

An interpolation scheme using locally fitted, second-order least squares bivariate polynomials was selected. In this method the polynomials are fit to the given data at nine points by the method of least squares. The points selected are the point whose physical space coordinates are the same as those at the solution point and its eight neighbors in the logical array point stencil shown in Figure 17.1. It should be noted that these neighboring points do not necessarily coincide with the eight nearest neighbors in the physical space. This scheme results in a considerable simplification in accounting procedures over that using the eight nearest neighbors since no metric information is needed in determining the cell points. Numerical studies have shown that the accuracy of both methods are comparable. The global interpolation process consists of the use of overlapping two-dimensional fits.

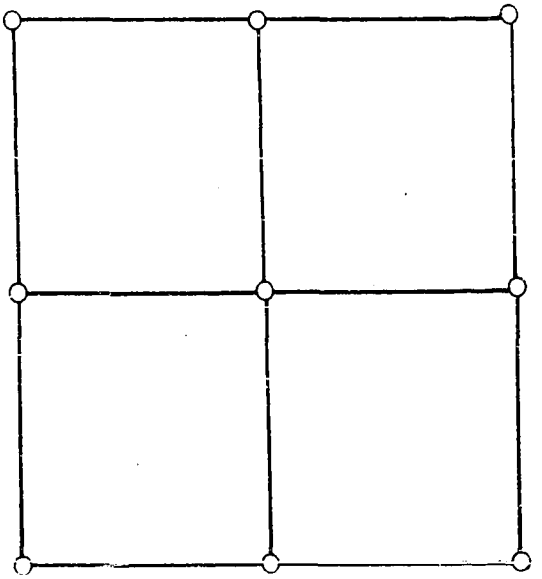

Figure 17.1. Logical array point stencil for bivariate interpolation

The interpolating polynomial has the form

$$u_\nu = a_{1\nu} + a_{2\nu}x + a_{3\nu}y + a_{4\nu}xy + a_{5\nu}x^2 + a_{6\nu}y^2 \qquad (17.1)$$

where u_ν ($\nu = 1,2,3,4$) represent the dependent variables u, v, p and ρ, respectively, x and y are the rectangular cartesian space coordinates and $a_{\mu\nu}$ ($\mu = 1,2,\ldots 6$; $\nu = 1,2,3,4$) are the polynomial coefficients. The coefficients for each dependent variable are obtained by fitting the known data at each point of the nine point cell using the method of least squares. Derivatives of the dependent variables are determined by differentiating the interpolating polynomial.

Collocation at all cell points is achieved only if the minimum number of points corresponding to the number of coefficients in the interpolating polynomial, which is six, is used. However, the loss of accuracy due to the redundancy introduced by using nine points is small and is offset by the advantage of computing ease of both the dependent variables and their derivatives.

The least squares interpolation procedure has an added advantage over the methods in the solution of flows with locally supersonic regions where weak shocks can be expected to occur. Shocks introduce discontinuities in the solution surfaces which cannot be handled by the method of characteristics itself and therefore require the addition of special shock tracing procedures. These procedures involve treating

the shock wave as a boundary, satisfying the Rankine-Hugoniot conditions across the shock and the basic field equations on each side. In addition, independent interpolations are required on both sides of the shock. However, in the case of weak shocks the least squares interpolation method can be expected to smooth out the discontinuity such that special treatment is not required.

Let the known values of the dependent variables at the cell points whose coordinates are x^i, y^i $(i = 1,2,...9)$ be designated by u_ν^i $(i = 1,2,...9)$ where the subscript ν has the range $\nu = 1, 2, 3, 4$ corresponding to the variables u, v, p and ρ, respectively. The values of the dependent variables calculated from the interpolating polynomial at the cell points, denoted by $u_\nu^{i'}$ are

$$u_\nu^{i'} = a_{1\nu} + a_{2\nu}x^i + a_{3\nu}y^i + a_{4\nu}x^iy^i + a_{5\nu}x^{i^2} + a_{6\nu}y^{i^2} \tag{17.2}$$

where the repeated indices do not imply summation. The sum of the squares of the differences between the known values and the values obtained from the interpolating polynomial are given by the equation

$$S_\nu = \sum_{i=1}^{9} (u_\nu^i - u_\nu^{i'})^2 \tag{17.3}$$

or using Eq. 17.2

$$S_\nu = \sum_{i=1}^{9} (u_\nu^i - a_{1\nu} - a_{2\nu}x^i - a_{3\nu}y^i - a_{4\nu}x^iy^i - a_{5\nu}x^{i^2} - a_{6\nu}y^{i^2})^2$$

(17.4)

S_ν is a measure of the error in the interpolating polynomial and is minimized by varying the coefficients $a_{\mu\nu}$ ($\mu = 1,2,\ldots6$) such that

$$\frac{\partial S_\nu}{\partial a_{1\nu}} = \frac{\partial S_\nu}{\partial a_{2\nu}} = \frac{\partial S_\nu}{\partial a_{3\nu}} = \frac{\partial S_\nu}{\partial a_{4\nu}} = \frac{\partial S_\nu}{\partial a_{5\nu}} = \frac{\partial S_\nu}{\partial a_{6\nu}} = 0$$

(17.5)

Equation 17.5 provides six conditions for the coefficients $a_{\mu\nu}$ ($\mu = 1,2,\ldots6$). With the indicated differentiations in Eq. 17.4 performed, these six conditions become

$$9a_{1\nu} + \Sigma x^i a_{2\nu} + \Sigma y^i a_{3\nu} + \Sigma x^i y^i a_{4\nu} + \Sigma x^{i^2} a_{5\nu} + \Sigma y^{i^2} a_{6\nu} = \Sigma u_\nu^i$$

(17.6)

$$\Sigma x^i a_{1\nu} + \Sigma x^{i^2} a_{2\nu} + \Sigma x^i y^i a_{3\nu} + \Sigma x^{i^2} y^i a_{4\nu} + \Sigma x^{i^3} a_{5\nu} + \Sigma x^i y^{i^2} a_{6\nu} = \Sigma u_\nu^i x^i \qquad (17.7)$$

$$\Sigma y^i a_{1\nu} + \Sigma x^i y^i a_{2\nu} + \Sigma y^{i^2} a_{3\nu} + \Sigma x^i y^{i^2} a_{4\nu} + \Sigma x^{i^2} y^i a_{5\nu} + \Sigma y^{i^3} a_{6\nu} = \Sigma u_\nu^i y^i \qquad (17.8)$$

$$\Sigma x^i y^i a_{1\nu} + \Sigma x^{i2} y^i a_{2\nu} + \Sigma x^i y^{i2} a_{3\nu} + \Sigma x^{i2} y^{i2} a_{4\nu} + \Sigma x^{i3} y^i a_{5\nu}$$

$$+ \Sigma x^i y^{i3} a_{6\nu} = \Sigma u_\nu^i x^i y^i \qquad (17.9)$$

$$\Sigma x^{i2} a_{1\nu} + \Sigma x^{i3} a_{2\nu} + \Sigma x^{i2} y^i a_{3\nu} + \Sigma x^{i3} y^i a_{4\nu} + \Sigma x^{i4} a_{5\nu}$$

$$+ \Sigma x^{i2} y^{i2} a_{6\nu} = \Sigma u_\nu^i x^{i2} \qquad (17.10)$$

$$\Sigma y^{i2} a_{1\nu} + \Sigma x^i y^{i2} a_{2\nu} + \Sigma y^{i3} a_{3\nu} + \Sigma x^i y^{i3} a_{4\nu} + \Sigma x^{i2} y^{i2} a_{5\nu}$$

$$+ \Sigma y^{i4} a_{6\nu} = \Sigma u_\nu^i y^{i2} \qquad (17.11)$$

where Σ implies summation on i over the nine cell points. Equations 17.6-17.11 are a system of six linear algebraic equations for the unknowns $a_{\mu\nu}$ ($\mu = 1,2,\ldots 6$). This system can be written in matrix form to include all variables u_ν ($\nu = 1,2,3,4$) as

$$SA = U \qquad (17.12)$$

where

$$S = \begin{bmatrix} 9 & \Sigma x^i & \Sigma y^i & \Sigma x^i y^i & \Sigma x^{i2} & \Sigma y^{i2} \\ \Sigma x^i & \Sigma x^{i2} & \Sigma x^i y^i & \Sigma x^{i2} y^i & \Sigma x^{i3} & \Sigma x^i y^{i2} \\ \Sigma y^i & \Sigma x^i y^i & \Sigma y^{i2} & \Sigma x^i y^{i2} & \Sigma x^{i2} y^i & \Sigma y^{i3} \\ \Sigma x^i y^i & \Sigma x^{i2} y^i & \Sigma x^i y^{i2} & \Sigma x^{i2} y^{i2} & \Sigma x^{i3} y^i & \Sigma x^i y^{i3} \\ \Sigma x^{i2} & \Sigma x^{i3} & \Sigma x^{i2} y^i & \Sigma x^{i3} y^i & \Sigma x^{i4} & \Sigma x^{i2} y^{i2} \\ \Sigma y^{i2} & \Sigma x^i y^{i2} & \Sigma y^{i3} & \Sigma x^i y^{i3} & \Sigma x^{i2} y^{i2} & \Sigma y^{i4} \end{bmatrix} \tag{17.13}$$

$$A = \begin{bmatrix} a_{11} & a_{12} & a_{13} & a_{14} \\ a_{21} & a_{22} & a_{23} & a_{24} \\ a_{31} & a_{32} & a_{33} & a_{34} \\ a_{41} & a_{42} & a_{43} & a_{44} \\ a_{51} & a_{52} & a_{53} & a_{54} \\ a_{61} & a_{62} & a_{63} & a_{64} \end{bmatrix} \tag{17.14}$$

$$U = \begin{bmatrix} \Sigma u_1^i & \Sigma u_2^i & \Sigma u_3^i & \Sigma u_4^i \\ \Sigma u_1^i x^i & \Sigma u_2^i x^i & \Sigma u_3^i x^i & \Sigma u_4^i x^i \\ \Sigma u_1^i y^i & \Sigma y_2^i y^i & \Sigma u_3^i y^i & \Sigma u_4^i y^i \\ \Sigma u_1^i x^i y^i & \Sigma u_2^i x^i y^i & \Sigma u_3^i x^i y^i & \Sigma u_4^i x^i y^i \\ \Sigma u_1^i x^{i\,2} & \Sigma u_2^i x^{i\,2} & \Sigma u_3^i x^{i\,2} & \Sigma u_4^i x^{i\,2} \\ \Sigma u_1^i y^{i\,2} & \Sigma u_2^i y^{i\,2} & \Sigma u_3^i y^{i\,2} & \Sigma u_4^i y^{i\,2} \end{bmatrix} \tag{17.15}$$

The coefficient matrix S in Eq. 17.12 is symmetric and depends only upon the cell point coordinates used in the least squares fit. It is the same for all four variables for all time. Only the nonhomogeneous terms depend on the values of the dependent variables. Thus, it is only necessary to invert the coefficient matrix once in order to determine the polynomial coefficients for all four variables.